GEOLOGICA ULTRAIECTINA

Mededelingen van het
Instituut voor Aardwetenschappen der
Rijksuniversiteit te Utrecht

No. 50

SURFACE WAVE SCATTERING THEORY

WITH APPLICATIONS TO FORWARD AND INVERSE PROBLEMS IN SEISMOLOGY

ROEL SNIEDER

SURFACE WAVE SCATTERING THEORY

WITH APPLICATIONS TO FORWARD AND INVERSE PROBLEMS IN SEISMOLOGY

(met een samenvatting in het Nederlands)

PROEFSCHRIFT

TER VERKRIJGING VAN DE GRAAD VAN DOCTOR AAN
DE RIJKSUNIVERSITEIT TE UTRECHT, OP GEZAG VAN
DE RECTOR MAGNIFICUS PROF. DR. J.A. VAN GINKEL
VOLGENS BESLUIT VAN HET COLLEGE VAN DEKANEN
IN HET OPENBAAR TE VERDEDIGEN OP DONDERDAG
19 NOVEMBER 1987 DES NAMIDDAGS TE 4.15 UUR

DOOR

ROEL SNIEDER

GEBOREN OP 20 MEI 1958 TE LEIDEN

PROMOTOR: PROF. DR. A.M.H. NOLET

If you want to build a factory, or fix a motorcycle, or set a nation right without getting stuck, then classical, structured dualistic subject-object knowledge, although necessary, isn't enough. You have to have some feeling for the quality of the work. You have to have a sense of what's good. *That* is what carries you forward. This sense isn't just something you're born with, although you *are* born with it. It's also something you can develop. It's not just "intuition", not just unexplainable "skill" or "talent". It's the direct result of contact with basic reality, *Quality* , which dualistic reason has in the past tended to conceal.

R.M. Pirsig , Zen and the Art of Motorcycle Maintenance.

The research described in this thesis was carried out at the

Department of Theoretical Geophysics
University of Utrecht
P.O. Box 80.021
3508 TA Utrecht
Netherlands

CIP-data Koninklijke Bibliotheek, Den Haag

Snieder, Roel

Surface wave scattering theory : with applications to
forward and inverse problems in seismology / Roel Snieder.
- [S.l. : s.n.]. - Ill. - (Geologica Ultraiectina ; no. 50)
Thesis Utrecht. - With bibliogr. - With summary in Dutch.
ISBN 90-71577-05-8
SISO 567.2 UDC 550.34(043.3)
Subject heading: seismology.

Contents

Chapter 1

Introduction

Seismological research is concerned with wave propagation in the Earth. An important application of this field is the estimation of ground acceleration, and the related assessment of earthquake hazards. Furthermore, seismologists determine source mechanisms of earthquakes, which are useful indicators of the local stress field. Most efforts in seismology (at least in terms of capital investments) are aimed at constructing images of the Earth's interior using elastic waves. The research presented in this thesis falls in this category, and describes the use of surface waves for probing the Earth's interior.

Even though both exploration seismologists and global seismologists are concerned with probing the Earth's interior with elastic waves, there exists a long standing dichotomy between these groups. In exploration seismics, large scale controlled seismic experiments are performed, leading to extremely large redundant data sets. These data sets are in practice processed with extremely crude methods. In general, the acoustic wave equation is used to describe elastic wave propagation, and virtually all migration schemes consist of linear inversions (often under the guise of names like "the exploding reflector model"). Nevertheless, these methods are very powerful, and they have provided access to the majority of the oil reservoirs that are currently in production.

In global seismology, data are sparse partly because one depends on natural earthquakes and nuclear explosions for the generation of elastic waves, and also because the density of seismic stations is still low. (The oceans are virtually devoid of seismic instruments.) This has forced researchers in global seismology to squeeze the last drop of information out of their valuable data. In general, elastic effects are taken into account and where necessary nonlinear theory is applied. Because of the scarcity of global seismological data, research is in practice aimed at obtaining a detailed insight in restricted information concerning the Earth (e.g. radially symmetric models, the source mechanism of a particular earthquake, etc.)

This situation is changing, however, because the density of digital seismic stations is increasing rapidly, see the PASSCAL and ORFEUS (Nolet et al., 1985) proposals. With large amounts of high quality digital data, it will be possible to perform large scale inversions for the Earth's structure using complete waveforms. Paradoxically, handling these large data sets of complete waveforms on present day computers, calls for more simple minded inversion schemes. In practice, this amounts to making linear approximations to forward and inverse problems that are in reality nonlinear.

In this thesis, linear scattering theory is formulated for surface wave propagation and inversion. This linear theory allows for an efficient waveform inversion of large

sets of surface wave data, using a method reminiscent to Kirchoff migration as used in exploration seismics. In this sense, the work presented here forms an attempt to close the gap between global seismology and exploration seismics.

Up to this point, geometrical optics formed the basis of all surface wave inversion schemes. In the geophysical literature this is formulated as the great circle theorem (Backus, 1964; Jordan, 1978; Dahlen, 1979), or more accurately, the minor arc theorem (Romanowicz, 1987). Using the minor arc theorem one can either perform dispersion measurements (Dziewonski and Hales, 1972; Nolet, 1977; Kovack, 1978), linear waveform fitting surface wave data (Lerner-Lam and Jordan, 1983; Woodhouse and Dziewonski, 1984; Tanimoto, 1987), or nonlinear waveform inversion of fundamental mode (Nolet et al., 1986a) or higher mode (Nolet, 1987) surface wave data.

However, the fact that all these techniques use geometrical optics (the minor arc theorem) limits the application to Earth models that are smooth on a scale of a horizontal wavelength. In practice, this condition is often violated, especially in complex continental areas. A fundamental mode Rayleigh wave of 60 s., has a horizontal wavelength of approximately 240 km., which is of the same order as some of the lateral variations within the continents. In that case, ray theory breaks down, so that scattering and multipathing effects may be operative. One way to attack this problem is to perform finite difference of finite element computations. However, even with present day computers these computations are expensive when applied to three dimensional problems. Furthermore, brute force computational methods may tell us **which** phenomena are occurring, but not **why** they occur.

There clearly was a need for a simple theory for scattering of surface waves in a layered, three dimensional medium with embedded heterogeneities. In chapter 2 such a formalism is presented. (The introduction of chapter 2 contains a historical survey of applications of linear scattering theory in seismology.) The problem with deriving such a scattering theory in the past was that no simple expression for the surface wave Green's function in a layered medium existed. It is shown in chapter 2 that the surface wave Green's function in a flat, layered 3D medium can conveniently be expressed as a dyad of polarization vectors. This facilitates a simple physical interpretation of this Green's function, and allows for a straightforward application of the Born approximation. This leads to a simple expression for the scattered surface waves, where the scattering and mode conversion coefficients are expressed as depth integrals containing the inhomogeneity and the modes under consideration. The resulting expression is simple enough to allow extensive mathematical manipulation. For example, it is shown that surface waves reflected by a continental margin satisfy Snell's law. Furthermore, a holographic method is proposed for the reconstruction of lateral heterogeneity using scattered surface waves.

The derivation of chapter 2 is based on several limiting assumptions. It is assumed that the heterogeneity is weak, that the inhomogeneity is at least several wavelengths away from the source and the receiver (the far field limit), that interactions with body waves can be ignored, and that the heterogeneity is buried. This last restriction is treated in chapter 3, where the effects of topography on surface waves is investigated with the same scattering formalism as in chapter 2.

There exists a close relation between the scattering coefficients for forward scattering of unconverted waves, and the phase velocity perturbations of these waves.

This connection, which turns out to be crucial for large scale inversions (chapter 8 and 9), leads to the same expressions for the phase velocity perturbations as obtained from variational principles, see chapter 3 for details.

Formulating a holographic inversion method for scattered surface waves is one thing, applying this to real data is unfortunately a different issue. In order to test the feasibility of the reconstruction of lateral heterogeneity from scattered surface waves, a field experiment has been performed in 1985 in Zeeland (Netherlands). In this experiment, surface wave data were generated with a simple weight drop source on a tidal flat near a dam (The "Grevelingendam"). The surface waves reflected from this dam have been used successfully to reconstruct the location of this dam. The results of this experiment are reported in chapter 4.

The name "surface wave scattering theory" is deceptive, because this name seems to imply that the Born theory presented in the chapters 2 and 3 only describes truly scattered waves. However, the theory presented in this thesis describes the full first order distortion effects of the wavefield due to the lateral heterogeneity. If the lateral inhomogeneity is abrupt, this implies that scattering effects are operative. Alternatively, if the lateral heterogeneity is smooth (on a scale of a wavelength) and weak, no scattering occurs and the heterogeneity manifests itself through ray geometrical effects such as focusing and phase shifting. The linear theory of the chapters 2 and 3 takes these ray geometrical effects implicitly into account. This is made explicit in chapter 5, where first order ray geometrical solutions are derived from the scattering integral presented in chapter 2. This has implications for the way we deal with surface wave data, because it means that Born theory can also be used to invert the direct surface wave which has been exposed to ray geometrical effects.

In the chapters 2-5, it is assumed that the Earth is flat, which is clearly not the case. For surface waves that propagate over distances of a few thousand kilometers (or more) the sphericity of the Earth might be important. Starting from an expression for the Green's function of the complete Earth in terms of normal modes, a derivation is presented in chapter 6 of the surface wave Green's function on a layered sphere. This Green's function has the same dyadic decomposition as the surface wave Green's function in a flat geometry, only the geometrical spreading is affected. With this Green's function for a layered sphere, the derivation of the scattered surface waves proceeds along the same lines as in chapter 2.

Alternatively, one can give a similar derivation, but with the coupling terms between the Earth's normal modes (Woodhouse, 1980; Woodhouse, 1983) as a starting point. By applying the operator formalism of Romanowicz and Roult (1986) to these expressions, the interactions between the Earth's normal modes are expressed in chapter 7 in the same type of scattering integral as in the chapters 2, 3 and 6. As an additional advantage, the effects of gravitational perturbations, and of interface displacements are obtained. Furthermore, it is shown in chapter 7 that the far field restriction does affect the propagator terms, but not the mode coupling and scattering coefficients. This solves at least part of the problem concerning the far field limitation.

With the formulation of linear theory for the effects of lateral heterogeneity on surface waves, large scale waveform inversions of surface wave data can be formulated as a huge system of linear equations. These equations can only be solved in the least square sense, and it is shown in chapter 8 how this solution can be constructed

iteratively. Several numerical examples are presented of this inversion method. Finally, in chapter 9, application of this scheme is shown for surface wave data recorded with the NARS array (Dost et al., 1984; Nolet et al., 1986b). Both the surface wave coda and the direct surface wave are analyzed with this inversion method. In this way, systematic waveform inversions of large sets of surface wave data are feasible. With the advent of dense networks of digital seismic instruments, combined with a new generation of computers, this technique can provide valuable new insights in the Earth's interior.

References

Backus, G.E., Geographical interpretation of measurements of average phase velocities over great circular and great semi circular paths, *Bull. seism. Soc. Am., 54,* 571-610, 1964.

Dahlen, F.A., The spectra of unresolved split normal mode multiplets, *Geophys. J. R. Astr. Soc., 58,* 1-33, 1979.

Dost, B., A. van Wettum, and G. Nolet, The NARS array, *Geol. Mijnbouw, 63,* 381-386, 1984.

Dziewonski, A.M., and A.L. Hales, Numerical analysis of dispersed seismic waves, in *Methods in computational physics, 11,* edited by B.A. Bolt, pp. 39-85, Academic Press, New York, 1972.

Jordan, T.H., A procedure for estimating lateral variations from low frequency eigenspectra data, *Geophys. J. R. Astr. Soc., 52,* 441-455, 1978.

Kovack, R.L., Seismic surface waves and crustal and upper mantle structure, *Rev. Geophys. Space Phys., 16,* 1-13, 1978.

Lerner-Lam, A.L., and T.J. Jordan, Earth structure from fundamental and higher-mode waveform analysis, *Geophys. J. R. Astron. Soc., 75,* 759-797, 1983.

Nolet, G., The upper mantle under Western-Europe inferred from the dispersion of Rayleigh wave modes, *J. Geophys., 43,* 265-285, 1977.

Nolet, G., Waveform tomography, in *Seismic tomography, with applications in global seismology and exploration geophysics,* edited by G. Nolet, pp. 301-322, Reidel, Dordrecht, 1987.

Nolet, G., B. Romanowicz, R. Kind, and E. Wielandt, ORFEUS, Observatories and Research Facilities for European Seismology, 1985.

Nolet, G., J. van Trier, and R. Huisman, A formalism for nonlinear inversion of seismic surface waves, *Geophys. Res. Lett., 13,* 26-29, 1986a.

Nolet, G., B. Dost, and H. Paulssen, Intermediate wavelength seismology and the NARS experiment, *Ann. Geophys., B4,* 305-314, 1986b.

PASSCAL, Program for Array Studies of the Continental Lithosphere, issued by the Incorporated Research Institute for Seismology, 1984.

Romanowics, B., and G. Roult, First order asymptotics for the eigenfrequencies of the Earth and application to the retrieval of large scale variations of structure, *Geophys. J. R. astr. Soc., 87,* 209-239, 1986.

Romanowicz, B., Multiplet-multiplet coupling due to lateral heterogeneity: asymptotic effects on the amplitude and frequency of the Earth's normal modes, *Geophys. J. R. Astr. Soc., 90,* 75-100, 1987.

Tanimoto, T., The three-dimensional shear wave velocity structure in the mantle by overtone waveform inversion -I: Radial seismogram inversion, *Geophys. J. R. Astron. Soc., 89,* 713-740, 1987.

Woodhouse, J.H., The coupling and attenuation of nearly resonant multiplets in the Earth's free oscillation spectrum, *Geophys. J. R. Astr. Soc., 61,* 261-283, 1980.

Woodhouse, J.H., The joint inversion of seismic waveforms for lateral variations in Earth structure and earthquake source parameters, in *Earthquakes: Observation, Theory and Interpretation, Proc. Int. School Phys. Enrico Fermi, 85,* edited by H. Kanamori and E. Boschi, pp. 366-397, 1983.

Woodhouse, J.H., and A.M. Dziewonski, Mapping the upper mantle: three dimensional modeling of the Earth structure by inversion of seismic waveform, *J. Geophys. Res., 89,* 5953-5986, 1984.

Chapter 2

Basic principles of surface wave scattering

This chapter is published as:

Snieder, R., 3D Linearized scattering of surface waves and a formalism for surface wave holography, *Geophys. J. R. astr. Soc.*, *84*, 581-605, 1986.

3-D linearized scattering of surface waves and a formalism for surface wave holography

Roel Snieder *Department of Theoretical Geophysics, University of Utrecht, Budapestlaan 4, PO Box 80.021, 3508 TA Utrecht, The Netherlands*

Accepted 1985 August 6. Received 1985 August 6; in original form 1985 May 6

Summary. Scattering of surface waves by lateral heterogeneities is analysed in the Born approximation. It is assumed that the background medium is either laterally homogeneous, or smoothly varying in the horizontal direction. A dyadic representation of the Green's function simplifies the theory tremendously. Several examples of the theory are presented. The scattering and mode conversion coefficients are shown for scattering of surface waves by the root of an Alpine-like crustal structure. Furthermore a 'great circle theorem' in a plane geometry is derived. A new proof of Snell's law is given for surface wave scattering by a quarter-space. It is shown how a stationary phase approximation can be used to simplify the Fourier synthesis of the scattered wave in the time domain. Finally a procedure is suggested to do 'surface wave holography'.

Key words: Born, inversion, scattering, seismology, surface waves

1 Introduction

The propagation of surface waves in a laterally homogeneous medium is nowadays well understood (Aki & Richards 1980). Unfortunately there is no exact theory yet for the propagation of surface waves in a three-dimensional laterally varying medium. It is desirable to have such a theory because there are several observations indicating that short-period (< 20 s) surface waves are distorted severely by the lateral heterogeneities in the Earth. Levshin & Berteussen (1979) and Bungum & Capon (1974) give evidence of the scattering of short-period surface waves by lateral inhomogeneities.

The classical approach used in the analysis of surface waves in a laterally inhomogeneous earth is to assume that the surface waves are only influenced by the heterogeneities on the great circle joining the source and the receiver. A theoretical justification for this assumption is given for weak and smooth heterogeneities by Backus (1964), Jordan (1978) or Dahlen (1979). However, the observations of Levshin & Berteussen (1979) and Bungum & Capon (1974) show that in some cases an appreciable fraction of the surface wave energy propagates over non-great circle paths.

The effect of lateral heterogeneities on surface wave propagation in two dimensions has

received considerable interest. Knopoff & Hudson (1964) investigated the transmission of Love waves through a continental margin using a representation theorem. They modelled the continental margin by a vertical interface between two media. Alsop (1966) and Malichewsky (1979) studied the same model by minimizing the stress mismatch or the energy flux mismatch across the continental margin. However, none of these models could handle a non-zero angle of incidence, so that conversions from Love waves to Rayleigh waves could not be described. Hudson (1977a) treated the effect of a heterogeneous strip by using a variational method. All these studies involved some form of approximation. Finally, Kennett (1984a) devised an exact theory for the propagation of surface waves in a 2-D laterally heterogeneous medium.

The 3-D surface wave problem has received considerably less attention. Gregersen & Alsop (1974) and Alsop, Goodman & Gregersen (1974) considered the reflection and the transmission of surface waves in three dimensions by a vertical discontinuity. They did this by decomposing the surface wave in homogeneous and inhomogeneous body waves and using expressions for the reflection and transmission by an infinite discontinuity. However, their solutions did not satisfy the boundary conditions at the surface, so that it is not clear how useful their results are. Recently Its & Yanovskaya (1985) studied the 3-D reflection and transmission of surface waves at a vertical or weakly tilted discontinuity in a more rigorous way.

For 3-D media with a smooth lateral heterogeneity, ray tracing (Babich, Chikhachev & Yamovskaya 1976) or Gaussian beams (Yomogida & Aki 1985) are suitable techniques to describe the propagation of surface waves. However, it is impossible to treat sharp horizontal heterogeneities with these methods. Therefore, the theory for surface wave propagation in 3-D laterally heterogeneous media was restricted to lateral smoothly varying media, and to media consisting of two welded quarter-spaces. This was not very satisfactory since one would like to describe the scattering effects of an arbitrary distribution of scatterers in three dimensions.

The Born approximation is very useful in incorporating these effects. This approximation was first applied to the 2-D surface wave problem by Kennett (1972) who gave a derivation in wavenumber space. Subsequent papers used a similar theory to describe the scattering of body waves, see Hudson (1977b), Malin (1980), Malin & Phinney (1985) or Wu & Aki (1985). Herrera (1964) and Herrera & Mal (1965) used the Born approximation to describe 3-D surface wave scattering, and gave an expression for the scattered surface wave using representation theorems. Their results did not receive much attention because no convenient form of the Green's function was available. Therefore the Born approximation has not been used yet to describe surface wave scattering by organized 3-D heterogeneities. The aim of this paper is to provide such a scattering theory. The theory, as it is presented here, applies to scattering in the far field in a plane geometry.

In order to do this, a dyadic representation of the far field Green's function in a laterally homogeneous medium is presented in Section 2. The representation is similar to the dyadic form of the Green's function derived by Ben-Menahem & Singh (1968) for a homogeneous sphere, but is much easier to interpret. The Green's function for an elastic half-space consists of a surface wave part and a body wave part. In this study the body wave contribution to the Green's function has been neglected throughout. The reason for this is that the theory relies heavily on a dyadic representation of the Green's function. Unfortunately, there is no dyadic representation of the body wave Green's function in a layered medium available. This problem can be overcome in two ways. One alternative is to use a locked mode approximation (Harvey 1981). Another option is to consider an elastic sphere instead of an elastic half-space. In that case both surface waves and body waves can be expressed in normal

modes. The generalization of the theory presented in this paper to a laterally inhomogeneous sphere is presented in Snieder & Nolet (in preparation).

In Sections 3 and 4 the dyadic representation of the surface wave Green's function is used to derive the Born approximation for surface waves in the far field. The theory describes mode conversion in a natural way because the Green's function is a superposition of all surface wave modes. In Section 5 this theory is generalized for the important application of a background medium with smooth lateral variations.

The second half of the paper deals with some examples and illustrations of the theory. These examples by no means exhaust the possibilities of the theory. In Section 6 the interaction terms and the radiation patterns are presented for surface wave scattering by a point scatterer which has a vertical structure similar to the root of the Alps.

The advantage of the formulation using a dyadic representation of the Green's function is that the final expression for the scattered wave is quite simple. This enables one to use the formalism for the scattering of surface waves in realistic situations. Section 7 features two examples of this. Propagation through a band-like structure is discussed. This leads to a 'great circle theorem' in a flat geometry. Furthermore the reflection by a quarter-space is treated as a simple example of scattering by a continental margin.

All the derivations are given in the frequency domain, since surface waves are dispersive. In Section 8 it is shown how a stationary phase approximation leads to an efficient formulation in the time domain, which is useful for calculating synthetic seismograms.

One would like to use scattered surface waves to invert for the location and the structure of the scatterers. This can in principle be done with an inversion scheme similar to the algorithm of Tarantola (1984a, b). It is shown in Section 9 how 'back propagation' of scattered surface waves can be used to invert for the scatterers.

In this paper the summation convention is used unless stated otherwise. Latin indices are used to denote vector components, while Greek indices are used for the mode numbers. The dot product which is used is defined by:

$$[\mathbf{p} \cdot \mathbf{q}] = p_i^* q_i \tag{1}$$

where * denotes complex conjugation. Double contractions are defined by:

$$[A : B] = A_{ij}^* B_{ji}. \tag{2}$$

Finally, in order to see the limitations of the theory the assumptions which are used throughout the paper are listed. It is assumed that:

there is a plane geometry;
the interaction with body waves can be neglected;
the far field approximation can be used;
the heterogeneity is weak;
the scatterers are buried.

2 The dyadic representation of the far field Green's function of a laterally homogeneous medium

The surface wave Green's function in the spectral domain for the excitation of a laterally homogeneous elastic medium with density ρ and elastic parameters λ and μ by a point force is given by Aki & Richards (1980, chapter 7). The Green's function contains a matrix, but this matrix can be rewritten as a dyad. The expressions of Aki & Richards include an azimuth angle φ, which depends on the positions of the source and the receiver. This

azimuth dependence can be interpreted easily by rewriting the Green's function in a dyadic form. Both for Love waves and for Rayleigh waves the far field Green's function can be written as:

$$G_{ij}(\mathbf{r}, \mathbf{r}_s) = p_i^\nu(z, \varphi)\, p_j^{\nu *}(z_s, \varphi) \frac{\exp\,[i(k_\nu X + \pi/4)]}{\sqrt{(\pi/2)\, k_\nu X}}. \tag{3}$$

For Love waves $\mathbf{p}^\nu$ is given by:

$$\mathbf{p}^\nu(z, \varphi) = \begin{pmatrix} -l_1^\nu(z) \sin \varphi \\ l_1^\nu(z) \cos \varphi \\ 0 \end{pmatrix} \tag{4a}$$

while for Rayleigh waves:

$$\mathbf{p}^\nu(z, \varphi) = \begin{pmatrix} r_1^\nu(z) \cos \varphi \\ r_1^\nu(z) \sin \varphi \\ i r_2^\nu(z) \end{pmatrix}. \tag{4b}$$

$\mathbf{p}^\nu$ is called the polarization vector. The index ν refers to the mode number; it should be remembered that modal summation is implied in (3). The functions $l_1^\nu(z)$, $r_1^\nu(z)$ and $r_2^\nu(z)$ are the surface wave eigenfunctions in the notation of Aki & Richards. It is assumed that the eigenfunctions are normalized in such a way that:

$$8 c_\nu U_\nu I_1^\nu = 1 \text{ (no summation)}. \tag{5}$$

Here c_ν and U_ν are the phase velocity and the group velocity of mode ν. The integral I_1^ν is for Love waves defined by:

$$I_1^\nu = \tfrac{1}{2} \int \rho(z)\, l_1^{\nu^2}(z)\, dz \tag{6a}$$

and for Rayleigh waves:

$$I_1^\nu = \tfrac{1}{2} \int \rho(z)\, (r_1^{\nu^2}(z) + r_2^{\nu^2}(z))\, dz. \tag{6b}$$

The polarization vectors can be interpreted by expressing them in the following vector form:

$$\mathbf{p}^\nu(z, \varphi) = l_1^\nu(z)\, \hat{\varphi} \quad \text{for Love waves} \tag{7}$$

$$\mathbf{p}^\nu(z, \varphi) = r_1^\nu(z)\, \hat{\Delta} + i r_2^\nu(z)\, \hat{z} \quad \text{for Rayleigh waves.} \tag{8}$$

(See Fig. 1 for the definition of $\hat{\Delta}$ and $\hat{\varphi}$.) It can now be understood why the $\mathbf{p}$ vectors are called the polarization vectors, since they describe the direction in which the displacement vector oscillates. In the far field, this oscillation is purely transverse for Love waves, while Rayleigh waves oscillate both in the radial and vertical direction.

From this point on, Love and Rayleigh waves are treated in a unified way, and the modal summation involves both Love and Rayleigh waves. Using the representation (3), the displacement excited by a point force $\mathbf{F}$ oscillating with angular frequency ω can be written as:

$$\mathbf{u}^0(\mathbf{r}) = \mathbf{p}^\nu(z, \varphi) \frac{\exp\,[i(k_\nu X + \pi/4)]}{\sqrt{(\pi/2)\, k_\nu X}}\, [\mathbf{p}^\nu(z_s, \varphi) \cdot \mathbf{F}]. \tag{9}$$

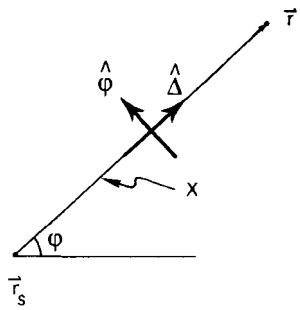

Figure 1. Geometry for the direct wave in a laterally homogeneous medium.

It can be seen explicitly that the displacement oscillations are in the $\mathbf{p}^{\nu}$ direction. The excitation is described by the dot product in the right side of (9). This means that only the projection of the force on the polarization vector contributes to the excitation.

In subsequent sections the gradient of the Green's function is needed. The gradient is derived here in the far field limit, since the Green's function itself is already in the far field limit. The azimuthal derivative in the gradient can be neglected, since it is $0(1/kX)$ compared to the radial derivative. The gradient with respect to the receiver position (index 1), or the source position (index 2) is in the far field limit:

$$\tilde{\nabla}_1 G_{ij}(\mathbf{r}_1, \mathbf{r}_2) = ik_\nu \hat{\Delta} p_i^\nu(z_1, \varphi) p_j^{\nu *}(z_2, \varphi) \frac{\exp[i(k_\nu X + \pi/4)]}{\sqrt{(\pi/2)k_\nu X}} \tag{10a}$$

$$\tilde{\nabla}_2 G_{ij}(\mathbf{r}_1, \mathbf{r}_2) = -ik_\nu \hat{\Delta} p_i^\nu(z_1, \varphi) p_j^{\nu *}(z_2, \varphi) \frac{\exp[i(k_\nu X + \pi/4)]}{\sqrt{(\pi/2)k_\nu X}} \tag{10b}$$

$$\partial_{z_1} G_{ij}(\mathbf{r}_1, \mathbf{r}_2) = (\partial_{z_1} p_i^\nu(z_1, \varphi)) p_j^{\nu *}(z_2, \varphi) \frac{\exp[i(k_\nu X + \pi/4)]}{\sqrt{(\pi/2)k_\nu X}} \tag{10c}$$

$$\partial_{z_2} G_{ij}(\mathbf{r}_1, \mathbf{r}_2) = p_i^\nu(z_1, \varphi)(\partial_{z_2} p_i^{\nu *}(z_2, \varphi)) \frac{\exp[i(k_\nu X + \pi/4)]}{\sqrt{(\pi/2)k_\nu X}}. \tag{10d}$$

In these expressions $\tilde{\nabla}$ is the horizontal gradient operator.

With these expressions the excitation by a moment tensor can be determined. The response to a single couple follows by superposing the response to point force $\mathbf{F}$ at $\mathbf{r}_s + \delta$ to the response to a point force $-\mathbf{F}$ at $\mathbf{r}_s - \delta$. The response to this single couple follows by Taylor expanding the superposition in δ, and using (10a–d) for the gradient. Interchanging the direction of $\mathbf{F}$ and δ and adding the single couple displacement fields leads to the following response to the excitation by a moment tensor:

$$\mathbf{u}^0(\mathbf{r}) = \mathbf{p}^\nu(z, \varphi) \frac{\exp[i(k_\nu X + \pi/4)]}{\sqrt{(\pi/2)k_\nu X}} [(ik_\nu \hat{\Delta} + \hat{z}\partial_{z_s}) \mathbf{p}^\nu(z_s, \varphi) : M] \tag{11}$$

where M is defined as:

$$M = 2(\delta \mathbf{F} + \mathbf{F}\delta). \tag{12}$$

Note that the factor $-i$ coming from the horizontal gradient in the source coordinate is absorbed in the definition of the dot product.

All the following sections deal with the excitation by a point force, but the results can be

generalized everywhere in case of excitation by a double couple by making the following substitution:

$$[\mathbf{p}^{\nu}(z_s,\varphi)\cdot\mathbf{F}] \rightarrow [(ik_{\nu}\hat{\Delta}+\hat{z}\,\partial_{z_s})\,\mathbf{p}^{\nu}(z_s,\varphi) : M]\,. \tag{13}$$

3 The Born approximation

The effect of lateral heterogeneities is treated here in a linearized way by using the Born approximation for the scattered wave. Suppose that the structural parameters in the medium can be written in the following way:

$$\mu(x,y,z) = \mu_0(z) + \epsilon\,\Delta\mu(x,y,z) \tag{14a}$$

$$\lambda(x,y,z) = \lambda_0(z) + \epsilon\,\Delta\lambda(x,y,z) \tag{14b}$$

$$\rho(x,y,z) = \rho_0(z) + \epsilon\,\Delta\rho(x,y,z). \tag{14c}$$

The parameters μ_0, λ_0 and ρ_0 define a laterally homogeneous background medium, which has a Green's function as presented in the last section. The parameter ϵ has been added to indicate that the inhomogeneity is weak, and serves only for bookkeeping purposes.

The equations of motion of the laterally heterogeneous system can be written as:

$$L_{ij}u_j = F_i \tag{15}$$

with

$$L_{ij} = -\delta_{ij}\rho\omega^2 - \partial_i\lambda\,\partial_j - \partial_j\mu\,\partial_i - \delta_{ij}\partial_k\mu\,\partial_k. \tag{16}$$

This operator can be written in the form $L = L^0 + \epsilon L'$ by inserting (14a–c) in (15). The displacement field can be expressed as a perturbation series: $\mathbf{u} = \mathbf{u}^0 + \epsilon\mathbf{u}^1 + 0(\epsilon^2)$. If these expressions are inserted in (15), then the terms of zeroth order and first order in ϵ lead to the relations:

$$L^0\mathbf{u}^0 = \mathbf{F} \tag{17}$$

$$L^0\mathbf{u}^1 = -L^1\mathbf{u}^0\,. \tag{18}$$

If we now assume that the heterogeneity does not affect the boundary conditions (which may be a very debatable assumption in realistic situations), then both (17) and (18) can be solved with the Green's function of the background medium. This leads to the following expression for the direct wave:

$$\mathbf{u}^0 = G\mathbf{F}. \tag{19}$$

While the scattered wave is given by:

$$\mathbf{u}^1 = -GL^1\mathbf{u}^0 = -GL^1G\mathbf{F}. \tag{20}$$

The operator products in (19) and (20) imply both summation over matrix elements as well as integration over space variables of the Green's function. For example, (19) is an abbreviated notation for:

$$u_i^0(\mathbf{r}) = \int d^3r'\,G_{ij}(\mathbf{r},\mathbf{r}')\,F_j(\mathbf{r}'). \tag{21}$$

For the moment we shall only concern ourselves with excitation by a point force in $\mathbf{r}_s$ and

scattering by a point heterogeneity in $\mathbf{r}_0$:

$$\Delta\mu(\mathbf{r}) = \Delta\mu\delta(\mathbf{r} - \mathbf{r}_0) \tag{22a}$$

$$\Delta\lambda(\mathbf{r}) = \Delta\lambda\delta(\mathbf{r} - \mathbf{r}_0) \tag{22b}$$

$$\Delta\rho(\mathbf{r}) = \Delta\rho\delta(\mathbf{r} - \mathbf{r}_0) \tag{22c}$$

$$\mathbf{F}(\mathbf{r}) = \mathbf{F}\delta(\mathbf{r} - \mathbf{r}_s). \tag{22d}$$

Since the theory in this approximation is linear in the heterogeneity, as well as in the excitation, more general situations can be handled by integration over both the heterogeneity and the excitation.

The unperturbed direct wave has been discussed in Section 2. The scattered wave is explicitly:

$$u_i^1(\mathbf{r}) = -\int d^3r' G_{ij}(\mathbf{r}, \mathbf{r}') L_{jk}^1(\mathbf{r}') G_{kl}(\mathbf{r}', \mathbf{r}_s) F_l(\mathbf{r}_s). \tag{23}$$

where the heterogeneity operator is:

$$\begin{aligned} L_{ij}^1(\mathbf{r}') = & -\Delta\rho\omega^2\delta_{ij}\,\delta(\mathbf{r}' - \mathbf{r}_0) && \text{(i)} \\ & -\Delta\lambda\,\partial_i'\,\delta(\mathbf{r}' - \mathbf{r}_0)\,\partial_j' && \text{(ii)} \\ & -\Delta\mu\,\partial_j'\,\delta(\mathbf{r}' - \mathbf{r}_0)\,\partial_i' && \text{(iii)} \\ & -\Delta\mu\delta_{ij}\,\partial_k'\,\delta(\mathbf{r}' - \mathbf{r}_0)\,\partial_k'. && \text{(iv)} \end{aligned} \tag{24}$$

The differentiations are all with respect to the $\mathbf{r}'$ coordinates. Note that the differentiations act both on the delta functions as well as on the Green's function at the right of L^1. The differentiation of the delta functions can be removed with a partial integration. For instance, the contribution of term (ii) to (23) can be rewritten:

$$\begin{aligned} & -\int d^3r' G_{ij}(\mathbf{r}, \mathbf{r}')\partial_j' \left[\Delta\lambda\,\delta(\mathbf{r}' - \mathbf{r}_0)\,\partial_k' G_{kl}(\mathbf{r}', \mathbf{r}_s)\right] F_l \\ & = \int d^3r' \left[\partial_j' G_{ij}(\mathbf{r}, \mathbf{r}')\right] \Delta\lambda\,\delta(\mathbf{r}' - \mathbf{r}_0) \left[\partial_k' G_{kl}(\mathbf{r}', \mathbf{r}_s)\right] F_l \\ & = \Delta\lambda \left[\partial_j^0 G_{ij}(\mathbf{r}, \mathbf{r}_0)\right] \left[\partial_k^0 G_{kl}(\mathbf{r}_0, \mathbf{r}_s)\right] F_l. \end{aligned}$$

The partial integration leads to a surface integral, which is zero for buried scatterers. If partial integration is also applied to the terms (iii) and (iv) the scattered wave takes the following form:

$$\begin{aligned} u_i^1(\mathbf{r}) = & \left[\Delta\rho\omega^2 G_{il}(\mathbf{r}, \mathbf{r}_0) G_{jl}(\mathbf{r}_0, \mathbf{r}_s)\right. && \text{(i)} \\ & -\Delta\lambda(\partial_j^0 G_{ij}(\mathbf{r}, \mathbf{r}_0))\,(\partial_k^0 G_{kl}(\mathbf{r}_0, \mathbf{r}_s)) && \text{(ii)} \\ & -\Delta\mu(\partial_k^0 G_{ij}(\mathbf{r}, \mathbf{r}_0))\,(\partial_j^0 G_{kl}(\mathbf{r}_0, \mathbf{r}_s)) && \text{(iii)} \\ & \left.-\Delta\mu(\partial_k^0 G_{ij}(\mathbf{r}, \mathbf{r}_0))\,(\partial_k^0 G_{jl}(\mathbf{r}_0, \mathbf{r}_s))\right] F_l(\mathbf{r}_s). && \text{(iv)} \end{aligned} \tag{25}$$

This expression is not easy to interpret because of all the gradient terms of the Green's function. However, the expression may be simplified considerably by using the dyadic form for the Green's function (3) and its gradient (10a–d). After some algebra it follows that in

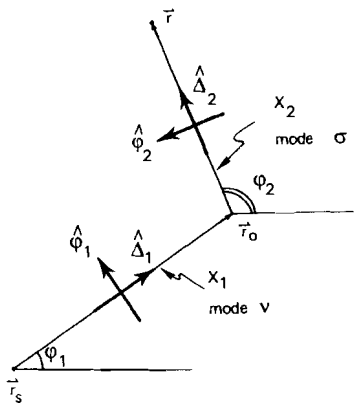

Figure 2. Geometry for the scattered wave in a laterally homogeneous background medium.

the notation of Fig. 2:

$$\mathbf{u}^1(\mathbf{r}) = \mathbf{p}^\sigma(z,\varphi_2)\,\frac{\exp\,[i(k_\sigma X_2 + \pi/4)]}{\sqrt{(\pi/2)k_\sigma X_2^1}}\,V^{\sigma\nu}(\mathbf{r}_0)\,\frac{\exp\,[i(k_\nu X_1 + \pi/4)]}{\sqrt{(\pi/2)k_\nu X_1^1}}\,[\mathbf{p}^\nu(z_s,\varphi_1)\cdot\mathbf{F}] \tag{26}$$

where $V^{\sigma\nu}$ is given by:

$$\begin{aligned}
V^{\sigma\nu}(\mathbf{r}_0) &= \Delta\rho\omega^2\,[\mathbf{p}^\sigma(z_0,\varphi_2)\cdot\mathbf{p}^\nu(z_0,\varphi_1)] && \text{(i)}\\
&- \Delta\lambda\,[\![(-ik_\sigma[\mathbf{p}^\sigma(z_0,\varphi_2)\cdot\hat{\Delta}_2] + [\partial_{z_0}\mathbf{p}^\sigma(z_0,\varphi_2)\cdot\hat{z}])\,(ik_\nu[\hat{\Delta}_1\cdot\mathbf{p}^\nu(z_0,\varphi_1)]\\
&\qquad + [\hat{z}\cdot\partial_{z_0}\mathbf{p}^\nu(z_0,\varphi_1)])]\!] && \text{(ii)}\\
&-\Delta\mu\,[\![k_\sigma k_\nu[\mathbf{p}^\sigma(z_0,\varphi_2)\cdot\hat{\Delta}_1]\,[\hat{\Delta}_2\cdot\mathbf{p}^\nu(z_0,\varphi_1)]\\
&\qquad - ik_\sigma[\mathbf{p}^\sigma(z_0,\varphi_2)\cdot\hat{z}]\,[\hat{\Delta}_2\cdot\partial_{z_0}\mathbf{p}^\nu(z_0,\varphi_1)]\\
&\qquad + ik_\nu[\partial_{z_0}\mathbf{p}^\sigma(z_0,\varphi_2)\cdot\hat{\Delta}_1]\,[\hat{z}\cdot\mathbf{p}^\nu(z_0,\varphi_1)]\\
&\qquad + [\partial_{z_0}\mathbf{p}^\sigma(z_0,\varphi_2)\cdot\hat{z}]\,[\hat{z}\cdot\partial_{z_0}\mathbf{p}^\nu(z_0,\varphi_1)]]\!] && \text{(iii)}\\
&-\Delta\mu\,[\![k_\sigma k_\nu[\hat{\Delta}_2\cdot\hat{\Delta}_1]\,[\mathbf{p}^\sigma(z_0,\varphi_2)\cdot\mathbf{p}^\nu(z_0,\varphi_1)]\\
&\qquad + [\partial_{z_0}\mathbf{p}^\sigma(z_0,\varphi_2)\cdot\partial_{z_0}\mathbf{p}^\nu(z_0,\varphi_1)]]\!]. && \text{(iv)}
\end{aligned} \tag{27}$$

The expression for the scattered wave (26) is now easy to interpret. If one reads (26) from right to left one follows the 'life history' of the scattered wave. The point force excites mode ν. The surface wave then travels to the point of scattering $\mathbf{r}_0$, the phase shift and the geometrical spreading are determined by the propagation term $\exp i(k_\nu X_1 + \pi/4)/\sqrt{(\pi/2)k_\nu X_1}$. Then the wave is scattered by the interaction matrix $V^{\sigma\nu}$. After the scattering, which may include mode conversion since the modes σ and ν can be different, the wave propagates to the receiver. The oscillation at the receiver is finally given by the polarization vector $\mathbf{p}^\sigma(z, \varphi_2)$. Note that (26) implies a summation over all the surface wave modes, and that all the modes in principle interact with each other.

4 Analysis of the interaction matrix

The interaction matrix as given in (27) is very general, but is hard to interpret. However, (27) can be simplified by inserting the expressions (7) and (8) for the polarization vectors of

Love and Rayleigh waves. It turns out that even though the polarization vectors depend on the azimuthal angles φ_1 and φ_2 separately, the interaction matrix depends only on the scattering angle:

$$\varphi = \varphi_2 - \varphi_1 . \tag{28}$$

As an example this is shown for the scattering of Love waves by the density variation:

$$V_{LL}^{\sigma\nu}(\mathrm{i}) = \Delta\rho\omega^2 \, l_1^{\sigma}(z_0) l_1^{\nu}(z_0) [\hat{\varphi}_2 \cdot \hat{\varphi}_1] = \Delta\rho\omega^2 l_1^{\sigma}(z_0) l_1^{\nu}(z_0) \cos\varphi .$$

Similar expressions hold for all the interaction terms.

It can be seen that the λ heterogeneity does not affect the Love waves. The reason for this is that the incoming wave (ν) enters the λ scattering term in the following way:

$$ik_{\nu}[\hat{\Delta}_1 \cdot \mathbf{p}^{\nu}(z_0, \varphi_1)] + \partial_{z_0} p_3^{\nu}(z_0, \varphi_1).$$

For a Love wave the polarization vector has no vertical component, and is perpendicular to the direction of propagation ($\hat{\Delta}_1$). Therefore both terms vanish if the incoming wave is a Love wave. If the outgoing wave (σ) is a Love wave the same holds, so that λ variations do not affect Love waves at all.

If the polarization vectors for Love and Rayleigh waves ((7) and (8)) are inserted in (27) then the following expression for the interaction matrix results:

$$V_{LL}^{\sigma\nu} = [l_1^{\sigma} l_1^{\nu} \Delta\rho\omega^2 - (\partial l_1^{\sigma})(\partial l_1^{\nu}) \Delta\mu] \cos\varphi - k_{\sigma} k_{\nu} l_1^{\sigma} l_1^{\nu} \Delta\mu \cos 2\varphi \tag{29a}$$

$$V_{RL}^{\sigma\nu} = [r_1^{\sigma} l_1^{\nu} \Delta\rho\omega^2 + (k_{\sigma} r_2^{\sigma} - \partial r_1^{\sigma}) \partial l_1^{\nu} \Delta\mu] \sin\varphi - k_{\sigma} k_{\nu} r_1^{\sigma} l_1^{\nu} \Delta\mu \sin 2\varphi \tag{29b}$$

$$V_{LR}^{\sigma\nu} = -V_{RL}^{\nu\sigma} \tag{29c}$$

$$\begin{aligned} V_{RR}^{\sigma\nu} = {} & [r_2^{\sigma} r_2^{\nu} \Delta\rho\omega^2 - (k_{\sigma} r_1^{\sigma} + \partial r_2^{\sigma})(k_{\nu} r_1^{\nu} + \partial r_2^{\nu}) \Delta\lambda - k_{\sigma} k_{\nu} r_1^{\sigma} r_1^{\nu} \Delta\mu - 2(\partial r_2^{\sigma})(\partial r_2^{\nu}) \Delta\mu] \\ & + [r_1^{\sigma} r_1^{\nu} \Delta\rho\omega^2 - (k_{\sigma} r_2^{\sigma} - \partial r_1^{\sigma})(k_{\nu} r_2^{\nu} - \partial r_1^{\nu}) \Delta\mu] \cos\varphi - k_{\sigma} k_{\nu} r_1^{\sigma} r_1^{\nu} \Delta\mu \cos 2\varphi . \end{aligned} \tag{29d}$$

For convenience the z_0 dependence of the eigenfunctions is not shown explicitly. Vertical derivatives are denoted in the following abbreviated form:

$$\partial f = \frac{\partial f}{\partial z_0}(z_0).$$

Observe that the interaction terms depend in a very simple way on the scattering angle. There is no conversion from Love wave to Rayleigh wave or vice versa in the forward direction ($\varphi = 0$), or in the backward direction ($\varphi = \pi$). The interaction terms V_{RL} and V_{LR} differ only in sign, but have the same magnitude.

5 Linearized scattering with a smooth background medium

The theory of the previous sections can be generalized for a smoothly varying background medium with embedded scatterers. 'Smoothly varying' means in this context that the horizontal variations of the background medium are small on a scale of the largest horizontal wavelength under consideration. (There is of course no restriction on the vertical variations of the background medium.)

Bretherton (1968) showed that in this limit the surface wave modes decouple, and Babich *et al.* (1976) derived a ray tracing formalism for surface waves, as well as a condition for the amplitude variations along a ray. Hudson (1981) derived a parabolic approximation for surface waves, which Yomogida (1985) extended to a Gaussian beam formalism for surface waves. We shall proceed here with a derivation of the Green's function for Love waves in a smoothly varying background medium. (The derivation is completely analogous in the case of Rayleigh waves.) Since the surface wave modes are decoupled we will restrict ourselves to one mode, and modal summation is temporarily suppressed.

According to Yomogida the Love wave displacement on a ray (i.e. $n = 0$ in his notation) is in the far field:

$$\mathbf{u}^0 = \frac{\hat{\varphi}(s)\bar{I}_1(s, z)}{\sqrt{q(s)U(s)I_1(s)}} \exp\,[i\theta(s)]\,\phi_L. \tag{30}$$

In this expression $\bar{I}_1$ is defined by the condition $\bar{I}_1(s, 0) = 1$, $\bar{I}_1(s, z)$ is a 'local mode' since the mode varies along the ray. The phase of the Love wave is given by:

$$\theta(s) = \int_0^s \kappa(s')ds' \tag{31}$$

where $k(s)$ is the local wavenumber, and the integral is along the ray. The geometrical spreading factor $q(s)$ follows for a point source from the equations of dynamical ray tracing:

$$\partial_s p = -c^{-2}(s)\partial_{nn}c(s)q$$

$$\partial_s q = c(s)\,p, \tag{32a}$$

with starting values:

$$p(0) = c^{-1}(0), \quad q(0) = 0. \tag{32b}$$

In these expressions ∂_s denotes differentiation along a ray, while ∂_n is the horizontal derivative perpendicular to a ray. Finally ϕ_L represents the excitation of the Love wave. This factor follows from the consideration that the excitation depends only on the local properties of the medium, so that ϕ_L is the same in a smoothly varying medium as in a laterally homogeneous medium with the properties of the source region. For a laterally homogeneous medium (32a, b) can be integrated to give $q(s) = s$, so that in that case:

$$u = \frac{\hat{\varphi}(s)\bar{I}_1(s, z)}{\sqrt{U(s)I_1(s)}} \cdot \frac{\exp\,(iks)}{\sqrt{s}}\,\phi_L. \tag{33}$$

A comparison with (9), (7) and the normalization condition (5) shows that ϕ_L is determined by:

$$\phi_L = \frac{\exp\,(i\pi/4)}{\sqrt{4\pi\omega}} \quad l_1(z, s = 0)[\hat{\varphi}(0) \cdot \mathbf{F}]. \tag{34}$$

If $l_1(z, s)$ in (30) is normalized according to (5), and (34) is used for the excitation factor, then it follows that the Love wave displacement is:

$$\mathbf{u}^0 = l_1(z, s)\,\hat{\varphi}(s) \frac{\exp\,[i(\theta(s) + \pi/4)]}{\sqrt{(\pi/2)k(s)q(s)}} \quad l_1(z_s, s = 0)\,[\hat{\varphi}(s = 0) \cdot \mathbf{F}]. \tag{35}$$

A similar result holds for Rayleigh waves, so that the Green's function for a smoothly varying background medium has the following dyadic form:

$$G_{ij}(\mathbf{r}, \mathbf{r}_s) = p_i^{\nu}\,[z,\ s,\ \varphi(s)]\,\frac{\exp\,[i(\theta_\nu(s) + \pi/4)]}{\sqrt{(\pi/2)k_\nu(s)q_\nu(s)}}\ p_j^{\nu *}\,[z_s, s = 0, \varphi(0)]. \tag{36}$$

It should be stressed that the normalization condition (5) is crucial in obtaining the correct amplitude variations along the ray. The modal summation now includes both Love and Rayleigh waves. Note that quantities like the phase shift $\theta_\nu(s)$ or the geometrical spreading $q_\nu(s)$ are different from mode to mode. Also the ray paths are in general different for different modes, so that ray tracing has to be done for each mode separately.

The expressions for the gradient of the Green's function (10a–d) are unaffected by a smooth horizontal heterogeneity of the background medium, since the horizontal derivatives of the parameters of the medium are by assumption small compared to $k_\nu(s)$. The derivation in Sections 3 and 4 is therefore unaffected by the smooth variations in the background medium. Therefore the expression for the scattered wave is:

$$\mathbf{u}^1(\mathbf{r}) = \mathbf{p}^{\sigma}(z, \varphi_2(s), s)\,\frac{\exp\,[i(\theta_\sigma(s) + \pi/4)]}{\sqrt{(\pi/2)k_\sigma(s)q_\sigma(s)}}\,V^{\sigma\nu}(\mathbf{r}_0)\,\frac{\exp\,[i(\theta_\nu(s) + \pi/4)]}{\sqrt{(\pi/2)k_\nu(s)q_\nu(s)}}\,[\mathbf{p}^{\nu}(z_s, \varphi_1(0), 0) \cdot \mathbf{F}]. \tag{37}$$

See Fig. 3 for the definition of the variables. In principle the length along the ray path (s) depends on the mode number, but this is not shown explicitly. The interaction matrix is given by (27) or (29a–d) with the local polarization vectors. The scattering angle is now determined by the angle between the incoming and the outgoing ray at the scatterer. Therefore the scattering angle for a fixed source receiver pair is in general different for different sets of modes (σ, ν).

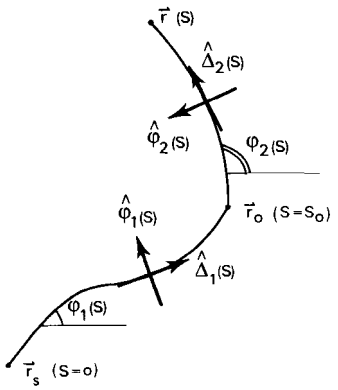

Figure 3. Geometry for the scattered wave in a smoothly varying background medium.

Note that the expression for the scattered wave depends explicitly on the scattering angle. This makes it impossible to use a Gaussian beam formalism in this context, since one has to do the ray tracing from source to scatterer to receiver in order to obtain the scattering angle. This is a time-consuming procedure since it has to be repeated for every new set of modes (σ, ν).

6 The interaction matrix for scattering by a mountain root

In the previous sections the theory of surface wave scattering was developed. The subsequent sections deal with some examples to clarify the theory. In this section the depth integrals of the interaction matrix (29a–d) are presented for the scattering of surface waves by the root of the Alps. The heterogeneity consists of a light, low velocity anomaly between 20 and 50 km, taken from Mueller & Talwani (1971). The M7 model or Nolet (1977) is used as a background medium. Both the background medium and the heterogeneity are shown in Fig. 4.

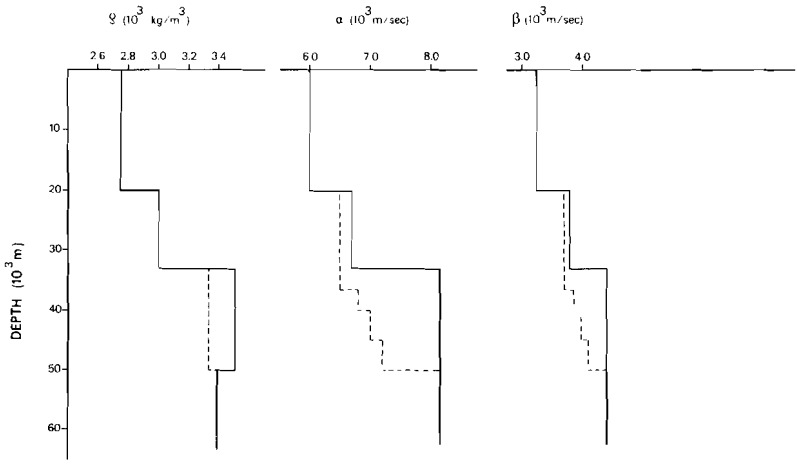

Figure 4. Density, *P*-wave velocity and *S*-wave velocity for the background medium (solid line), and the mountain root model (dashed line) used in the calculations of the interaction matrix of Section 6.

It can be seen from (29a–d) that the interaction matrix for the scattering from Rayleigh wave to Rayleigh wave, or from Love wave to Love wave has the form:

$$V_{\mathrm{RR\ or\ LL}} = V(0) + V(1)\cos\varphi + V(2)\cos 2\varphi.$$

Here φ is the scattering angle. In case a Rayleigh wave is converted to a Love wave, or vice versa, the interaction matrix takes the form:

$$V_{\mathrm{RL\ or\ LR}} = V(1)\sin\varphi + V(2)\sin 2\varphi.$$

In this section the 'sin $n\varphi$' scattering coefficient for the conversion of the νth Love wave to the σth Rayleigh wave is denoted by $V_{R_\sigma \leftarrow L_\nu}(n)$. A similar notation is used for the Love wave–Love wave scattering and the Rayleigh wave–Rayleigh wave scattering.

In Fig. 5 the fundamental mode interaction terms $V_{R_1 \leftarrow R_1}$, $V_{R_1 \leftarrow L_1}$ and $V_{L_1 \leftarrow L_1}$ are shown as a function of frequency. The interaction terms are given per unit area because (29a–d) has only been integrated over z. In order to obtain the strength of the scattered wave one has to multiply by the horizontal area of the scatterer. For a scatterer of 100 × 100 km the scattering coefficient is of order 1. However, surface waves with a period of 20 s have a wavelength of the order of 100 km, so that one cannot consider a scatterer of 100 × 100 km as a point scatterer. In that case one would have to integrate over the horizontal extent of the whole scatterer. In order to circumvent this complication the interaction terms are simply given per unit area.

Note that the three types of fundamental mode scattering are of the same order of magnitude. Also observe that the scattering coefficients are strongly dependent on the

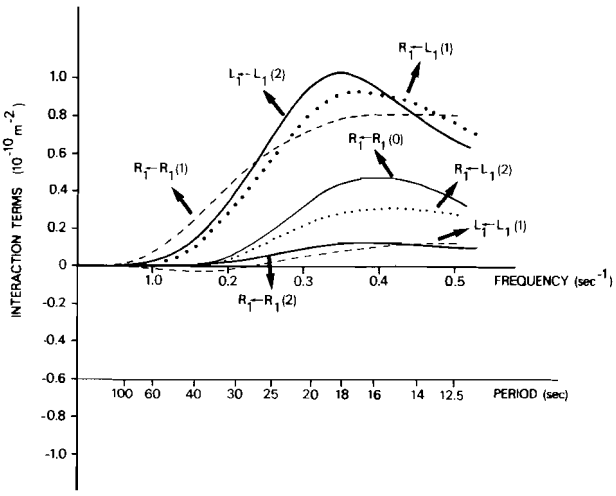

Figure 5. Fundamental mode interaction terms for different azimuth numbers for scattering by the mountain root as a function of frequency.

period. The interaction terms at 20 s are almost an order of magnitude larger than the interaction terms at 40 s. This agrees well with observations of scattered surface waves which show that 20 s Rayleigh waves are much more strongly scattered than 40 s Rayleigh waves (Levshin & Berteussen 1979). The reason for this is that for a period of 40 s the penetration depth of the surface waves is so large that the influence of the shallow scatterer on the propagation of the surface wave is relatively small. Mathematically this is realized by the normalization condition (5).

The interaction terms for $R_1 \leftarrow R_1$ scattering and $R_1 \leftarrow L_1$ conversion decreases for periods shorter than 17 s. The reason for this effect is that for these high frequencies the surface waves are too shallow to be influenced by the heterogeneity.

In order to appreciate the difference in the radiation patterns for the different fundamental mode scattering events, the scattering amplitude is shown in Fig. 6 as a function of

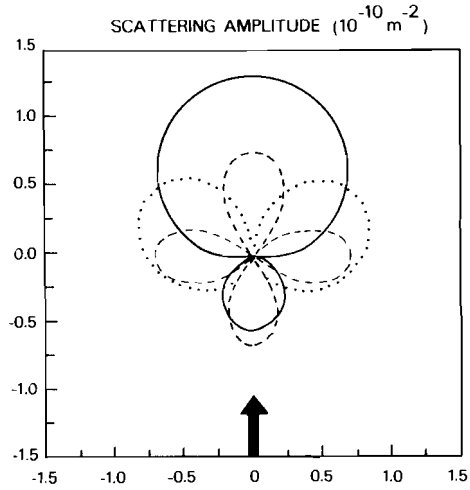

Figure 6. Radiation pattern for the scatterer of Fig. 5. The wave comes in from below. $R_1 \leftarrow R_1$ scattering is shown by a solid line, $L_1 \leftarrow L_1$ scattering by a dashed line and $R_1 \leftarrow L_1$ conversion by a dotted line.

the scattering angle for a period of 21 s. Note that there is no converted wave being radiated in the forward or in the backward direction. The $R_1 \leftarrow R_1$ scattering is much stronger in the forward direction than for backscattering, while $L_1 \leftarrow L_1$ has a much more symmetrical four lobe radiation pattern.

Fig. 5 shows that the different azimuth terms $V(n)$ in general behave in a different way as a function of frequency. Consequently, not only the strength of the radiation pattern depends on frequency, but also the shape of the radiation pattern is frequency dependent. This can be seen in Fig. 7 which shows the $R_1 \leftarrow R_1$ scattering for several periods. For a period of 40 s the scattering is very weak, and forward scattering and backscattering have almost the same strength. For larger periods the radiation pattern loses this symmetry.

For periods larger than 20 s the interaction among the fundamental modes is in general much stronger than the interactions involving higher modes. For shorter periods this does not hold any more, because for these periods the fundamental modes are too shallow to be influenced by the heterogeneity.

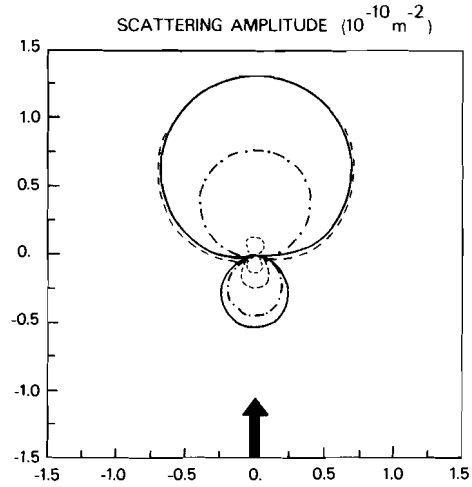

Figure 7. Radiation pattern for $R_1 \leftarrow R_1$ scattering as in Fig. 6 for different periods. The thin dashed line is for $T = 40$ s, the dashed-dotted line for $T = 26$ s, the solid line for $T = 21$ s and the thick dashed line for $T = 14$ s.

As a representative example the interaction terms $V_{R_N \leftarrow R_1}(1)$ and $V_{R_N \leftarrow R_N}(1)$ are shown in Fig. 8(a, b). Note that the coupling of the higher modes with the fundamental mode is stronger than the interaction of the higher modes with themselves. The only exception is the scattering of the first higher mode ($N = 2$) to itself for short periods. This strong scattering is caused by the fact that for periods of 10–14 s the first higher mode behaves like a Stoneley mode on the Moho, and therefore carries most of its energy at the depth of the heterogeneity.

One should be a bit careful with the conclusion that for periods larger than 20 s the higher mode scattering effects are negligible. It is true that this conclusion holds for the interaction terms $V(n)$, but it is not necessarily true for all scattering angles since for some scattering angles the fundamental mode interaction terms vanishes. As an example the Rayleigh wave radiation pattern is shown in Fig. 9 for the coupling of the fundamental mode with itself, as well as with the higher modes. The scattering amplitude for $R_1 \leftarrow R_1$ scattering vanishes for a scattering angle of 106°. This means that for this scattering angle the coupling to the higher modes dominates the $R_1 \leftarrow R_1$ scattering.

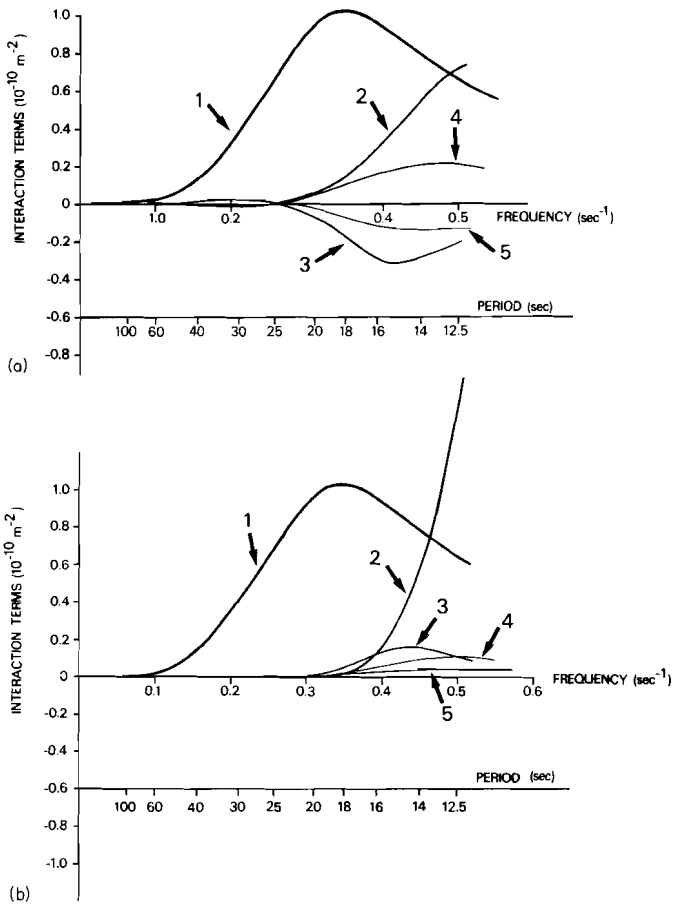

Figure 8. (a) $V_{R_N \leftarrow R_1}(1)$ interaction terms for the mountain root scatterer as a function of frequency. Numbers in figure are mode numbers N. (b) $V_{R_N \leftarrow R_N}(1)$ interaction terms for the mountain root scatterer as a function of frequency. Numbers in figure are mode numbers N.

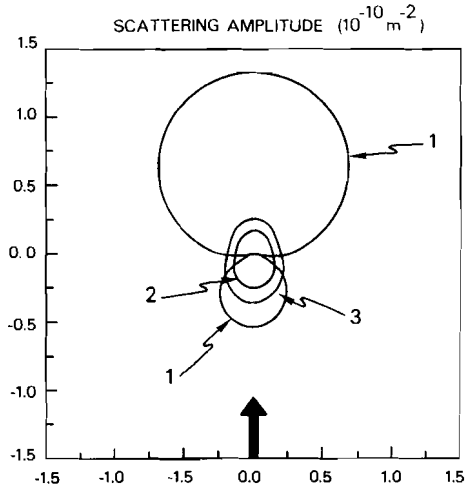

Figure 9. Radiation pattern as in Fig. 6 for $R_N \leftarrow R_1$ scattering for a period of 21 s. Numbers in the figure are mode numbers N.

7 Application of stationary phase principles to the calculation of the scattered wave

The theory presented in Sections 2–5 dealt with surface wave scattering by point scatterers. However, since the theory is linear(ized), more general inhomogeneities can be treated by integrating over the inhomogeneity. This integration can be simplified considerably by using the stationary phase approximation (Bender & Orszag 1978). Two examples are given for a laterally homogeneous background medium.

7.1 PROPAGATION THROUGH A BAND-LIKE HETEROGENEITY

Consider the propagation of surface waves through a band-like inhomogeneity confined between $x = x_L$ and $x = x_R$ (see Fig. 10). This heterogeneity is not unlike the model for the Central Graben in the North Sea, used by Kennett (1984b). The inhomogeneity is assumed to depend on y in a smooth way, compared with the horizontal wavelength of the surface waves. In that case the scattered wave is:

$$\mathbf{u}^1(\mathbf{r}_r) = \int_{X_L}^{X_R} dx \int_{-\infty}^{\infty} dy \int_0^{\infty} dz \exp\left[i(k_\nu X_1 + k_\sigma X_2)\right] \mathbf{f}_{\sigma\nu} \tag{38}$$

with

$$\mathbf{f}_{\sigma\nu} = i\mathbf{p}^\sigma(z_r, \varphi_2) \frac{V^{\sigma\nu}(x, y, z)}{\sqrt{(\pi/2)k_\sigma X_2}\sqrt{(\pi/2)k_\nu X_1}} [\mathbf{p}^\nu(z_s, \varphi_1) \cdot \mathbf{F}]. \tag{39}$$

The y integral can be evaluated with the stationary phase approximation. The point of stationarity is given by $y = 0$ for all x and z, so that the phase function can be approximated by:

$$(k_\nu X_1 + k_\sigma X_2) \approx k_\nu x + k_\sigma(x_r - x) + \tfrac{1}{2}\left(\frac{k_\nu}{x} + \frac{k_\sigma}{x_r - x}\right) y^2.$$

Integration over y then leads to the following approximation for the scattered wave:

$$\mathbf{u}^1(\mathbf{r}_r) \approx 2\sqrt{\frac{2}{\pi}} \frac{\exp\left[i(k_\sigma x_r + 3\pi/4)\right]}{\sqrt{k_\nu k_\sigma}} \int_0^{\infty} dz \int_{X_L}^{X_R} dx \frac{\exp\left[i(k_\nu - k_\sigma)x\right]}{\sqrt{k_\nu(x_r - x) + k_\sigma x}} V^{\sigma\nu}(x, y = 0, z)$$
$$\mathbf{p}^\sigma(z_r, \varphi_2 = 0) [\mathbf{p}^\nu(z_s, \varphi_1 = 0) \cdot \mathbf{F}]. \tag{40}$$

This means that in order to calculate the scattered wave one only needs to integrate over the line joining the source and the receiver. Equation (40) is a restatement of the 'great circle theorem' (Jordan 1978 or Dahlen 1979), but now in a plane geometry. The only difference is that in order to arrive at (40) we did not have to assume smoothness of the heterogeneity along the great circle, but only in the transverse direction.

Equation (40) shows that the interaction matrix is only needed for a scattering angle $\varphi = 0$. This means that mode conversions from a Love wave to a Rayleigh wave (and vice versa) vanish in this limit, since V_{RL} vanishes for $\varphi = 0$. This reflects the fact that appreciable transverse gradients of the inhomogeneity are needed to couple Love waves to Rayleigh waves.

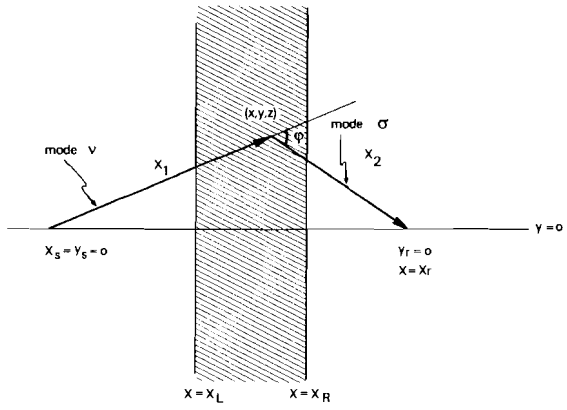

Figure 10. Geometry for surface wave scattering by a band-like heterogeneity.

For Love waves the z integral of the interaction matrix term in (40) is given by:

$$\int_0^\infty V_{LL}^{\sigma\nu}(x, y = 0, z)dz = \int_0^\infty dz\ [(\Delta\rho\omega^2 - k_\sigma k_\nu \Delta\mu) l_1^\sigma(z) l_1^\nu(z) - \Delta\mu(\partial_z l_1^\sigma)(\partial_z l_1^\nu)]. \quad (41)$$

This expression is the linearized form of the interaction terms (2.21) of the 2-D theory of Kennett (1984a). The only difference with Kennett's result is the appearance of the geometrical spreading factor in (40), as well as a phase shift of $\pi/4$. Both differences are caused by the fact that in this theory the surface waves are propagating in two horizontal directions.

7.2 SCATTERING BY A QUARTER-SPACE

In the previous section it was shown that only the heterogeneity on the source–receiver line influences the scattered wave if the inhomogeneity is smooth in the transverse direction. The next example shows what can happen if this condition is violated. Consider the situation shown in Fig. 11. The left half of the (x, y) plane consists of a different medium than the right half of the plane, where the source and the receiver are located. This situation models the scattering of surface waves by a sharp continental margin. The heterogeneity in the left half plane is assumed to be smooth in the horizontal direction (compared to the largest horizontal wavelength under consideration). This means that:

$$|\partial_x(\Delta\mu)| \ll |k\Delta\mu|, \quad |\partial_y(\Delta\mu)| \ll |k\Delta\mu|. \quad (42)$$

(Similar expressions hold for $\Delta\lambda$ and $\Delta\rho$.) Lastly, it is assumed that both the source and the receiver are located many wavelengths away from the continental margin.

Again, the scattered wave can be written as an integral over the inhomogeneity:

$$\mathbf{u}^1(\mathbf{r}_r) = \int_{-\infty}^\infty dx \int_{-\infty}^\infty dy \int_0^\infty dz \exp\ [i(k_\nu X_1 + k_\sigma X_2)]\ \mathbf{f}_{\sigma\nu} H(-x) \quad (43)$$

with $\mathbf{f}$ given by (39), and H is the Heaviside function. After a partial integration in x the

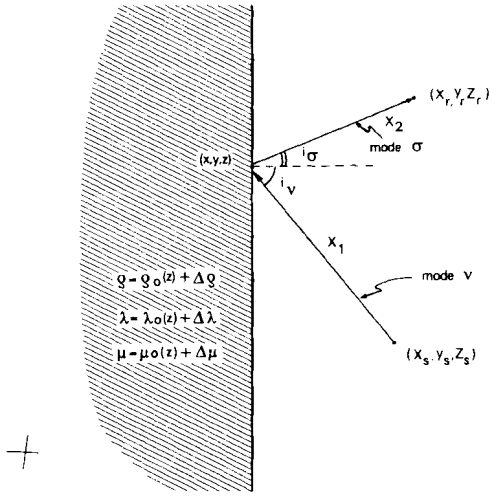

Figure 11. Geometry for surface wave scattering by a quarter-space.

scattered wave can be rewritten as:

$$u^1(r) = \int_{-\infty}^{\infty} dy \int_0^{\infty} dz \left. \frac{\exp\,[i(k_\nu X_1 + k_\sigma X_2)]\,\mathbf{f}_{\sigma\nu} H(-x)}{i[\![k_\nu[(x - x_s)/X_1] + k_\sigma[(x - x_r)/X_2]]\!]} \right|_{x=-\infty}^{x=\infty}$$

$$+ i \int_{-\infty}^{\infty} dx \int_{-\infty}^{\infty} dy \int_0^{\infty} dz\, \partial_x \left[\frac{H(-x)\,\mathbf{f}_{\sigma\nu}}{[\![k_\nu[(x-x_s)/X_1] + k_\sigma[(x-x_r)/X_2]]\!]} \right] \exp[i(k_\nu X_1 + k_\sigma X_2)]$$

The first term on the right side is zero if a small amount of damping is present; this can be realized by giving k_σ and k_ν a (small) positive imaginary component. The x differentiation in the second term produces three kinds of terms. Differentiation of the geometrical factors yields terms of the relative order $0(1/k_\nu X_1,\ 1/k_\sigma(x - x_r)$, etc.) which are negligible in the far field compared to the original expression (43). The contributions of the derivatives of $\Delta\mu$, $\Delta\lambda$ and $\Delta\rho$ (which are contained in $\mathbf{f}$) are also negligible compared to the original expression (43) because of the smoothness we assumed (42). Therefore the dominant contribution comes from the derivative of the Heaviside function. This leads to the following expression for the scattered wave:

$$\mathbf{u}^1(\mathbf{r}_r) = i \int_{-\infty}^{\infty} dy \int_0^{\infty} dz\, \mathbf{f}_{\sigma\nu} \frac{\exp\,[i(k_\nu X_1 + k_\sigma X_2)]}{[k_\nu(x_s/X_1) + k_\sigma(x_r/X_2)]}. \tag{44}$$

The y integral can again be evaluated with a stationary phase approximation. The phase function is:

$$\theta_{\sigma\nu}(y) = k_\nu \sqrt{x_s^2 + (y - y_s)^2} + k_\sigma \sqrt{x_r^2 + (y - y_r)^2}\ . \tag{45}$$

Let the minimum of $\theta_{\sigma\nu}(y)$ be attained for $\hat{y}$, so that:

$$\theta'_{\sigma\nu}(\hat{y}) = k_\nu \frac{\hat{y} - y_s}{X_1} + k_\sigma \frac{\hat{y} - y_r}{X_2} = 0. \tag{46}$$

It then follows from a stationary phase evaluation of the y integral that the scattered wave is given by:

$$\mathbf{u}^{1}(\mathbf{r}_r) = \sqrt{\frac{8}{\pi\,\theta''_{\sigma\nu}(\hat{y})}}\;\frac{\exp\,[i(k_\nu X_1 + k_\sigma X_2 + 3\pi/4)]}{[k_\nu(x_s/X_1) + k_\sigma(x_r/X_2)]\,\sqrt{k_\nu X_1}\,\sqrt{k_\sigma X_2}}\;\mathbf{p}^{\sigma}(z_r, \varphi_2)\;[\mathbf{p}^{\nu}(z_s, \varphi_1)\cdot\mathbf{F}]\Big|_{\substack{x=0\\ y=\hat{y}}}$$

$$\times \int_0^\infty V^{\sigma\nu}(x=0, y=\hat{y}, z)\,dz. \tag{47}$$

Inspection of Fig. 11 shows that the stationary phase condition (46) is just Snell's law for the reflection of surface waves:

$$\frac{\sin i_\nu}{c_\nu} = \frac{\sin i_\sigma}{c_\sigma} \quad \text{(no summation)} \tag{48}$$

where

$$c_\nu = \omega/k_\nu. \tag{49}$$

This means that for every set of modes (ν, σ) scattering by a quarter-space is equivalent to reflection by a point on the boundary between the two quarter-spaces which is determined by Snell's law. This means that the forward problem can be solved very efficiently because the cumbersome integration over the heterogeneity can be avoided. Unlike in Alsop *et al.* (1974) and Gregersen & Alsop (1974) the surface boundary condition is satisfied, since each mode satisfies the surface boundary condition. In contrast to previous studies it is not necessary to calculate the modes in both quarter-spaces in order to find the reflection coefficients.

Unfortunately, it is not possible to consider the transmission of surface waves through a continental margin by locating the receiver in the heterogeneous quarter-space. The reason for this is that in that case the far field approximation cannot be used any more.

The results derived in this section are applicable to a step-like continental margin. A smoother transition between two half-spaces can be treated numerically by dividing the transition zone into many small step discontinuities and by adding the scattered waves (47) from every step discontinuity.

8 The scattered wave in the time domain

Up to this point the theory was presented in the frequency domain. A Fourier transform makes it possible to find the scattered wave in the time domain. A stationary phase approximation of the frequency integral simplifies the final result considerably. In this section scattering by a point scatterer is discussed as an example.

The scattered wave in the time domain is given by:

$$\mathbf{u}^{1}(\mathbf{r}_r, t) = \int_{-\infty}^{\infty} \mathbf{f}_{\sigma\nu}(\omega)\exp\,[i(k_\nu X_1 + k_\sigma X_2 - \omega t)]\,d\omega. \tag{50}$$

Here, $\mathbf{f}$ is defined by (39). The frequency derivative of the phase function vanishes if the following condition is satisfied:

$$\frac{X_1}{U_\nu(\hat{\omega})} + \frac{X_2}{U_\sigma(\hat{\omega})} = t. \tag{51}$$

In this expression U_ν is the group velocity of mode ν. This condition determines a frequency $\hat{\omega}$ for every X_1, X_2 and t. It is possible that (51) has more than one solution $\hat{\omega}$, in which case one can simply sum over the contribution of every stationary frequency. A stationary phase evaluation of the ω integral leads to the following result:

$$\mathbf{u}^1(\mathbf{r}, t) = \sqrt{\frac{8}{\pi}} \frac{1}{\sqrt{(k_\nu''(\hat{\omega})X_1 + k_\sigma''(\hat{\omega})X_2)}} \frac{\exp\left[i(k_\nu(\hat{\omega})X_1 + k_\sigma(\hat{\omega})X_2 - \hat{\omega}t + 3\pi/4)\right]}{\sqrt{k_\nu(\hat{\omega})k_\sigma(\hat{\omega})X_1X_2}}$$

$$\mathbf{p}^\sigma(z, \hat{\omega}, \varphi_2)\, V^{\sigma\nu}(\mathbf{r}_0, \hat{\omega})\, [\mathbf{p}^\nu(z_s, \hat{\omega}, \varphi_1) \cdot \mathbf{F}(\hat{\omega})]\,. \tag{52}$$

The prime denotes differentiation with respect to ω.

It is instructive to investigate the condition (51) in some more detail. If the modes σ and ν have the same group velocity, then (51) describes an ellipse, so that for a fixed time t all the points on the ellipse should be evaluated in (52) with the same frequency $\hat{\omega}$ (see Fig. 12a). If $U_\nu(\hat{\omega}) \neq U_\sigma(\hat{\omega})$, then (51) defines an egg-like curve and, at a given time t, all the points on the egg can be evaluated at the same frequency $\hat{\omega}$ (see Fig. 12b).

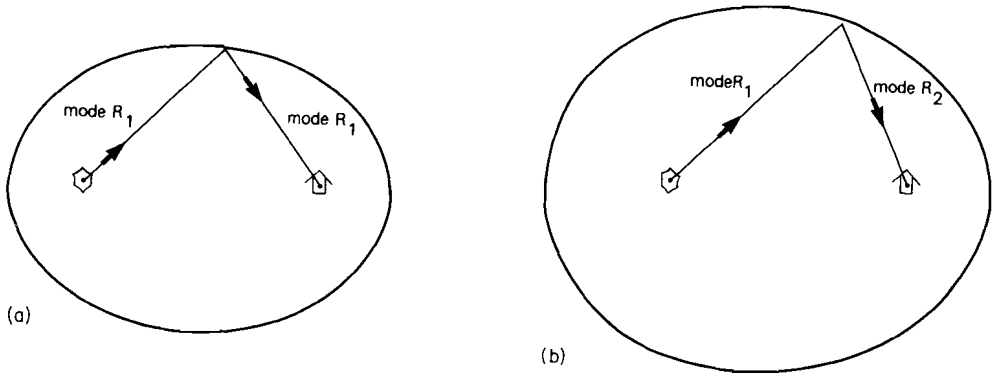

Figure 12. (a) Set of points which satisfy (51) for $R_1 \leftarrow R_1$ scattering for a period of 21 s. (b) Set of points which satisfy (51) for $R_2 \leftarrow R_1$ scattering for a period of 21 s.

9 Least squares inversion of scattered surface wave data

The theory for surface wave scattering is presented here in the Born approximation, so that there is a linear integral relation between the scattered wave (26) and the heterogeneity. (Remember that for a general configuration of scatterers (26) has to be integrated over all the scatterers, so that a r_0 integration should be performed.) This is convenient for solving the inverse problem, since the inversion of (possibly ill-posed) linear integral relations in the presence of noise is well understood. Franklin (1970) showed how to invert a discretized linear relation if the covariances of all variables are prescribed. Tarantola & Valette (1982) pointed out that discretization can be postponed to the moment of numerical implementation. The application of this formalism to the acoustic reflection problem is shown by Tarantola (1984a, b). Here a similar inversion method is presented for surface wave data. We shall assume that the source parameters and the background medium are known. If necessary these properties could be included in a simultaneous inversion with the direct wave and the scattered wave.

In the surface wave inversion problem we try to reconstruct the elastic parameters and the density from surface wave data. This means that we want to find the following model vector (which is a function of the three space variables):

$$\mathbf{m} = \begin{pmatrix} \Delta\mu \\ \Delta\lambda \\ \Delta\rho \end{pmatrix}. \tag{53}$$

The *a priori* knowledge can be incorporated by prescribing the *a priori* value of the model vector, as well as a covariance matrix. It is assumed that the *a priori* knowledge of the heterogeneity is given by:

$$\mathbf{m}_0 = 0. \tag{54}$$

The *a priori* model covariance is given by a matrix (operator) $C_m(\mathbf{r}_1, \mathbf{r}_2)$, which we shall leave unspecified. The data consist of the observations of the scattered wave, which in general consists of a superposition of different modes. It is possible that only one component of the scattered wave is measured, or that more components are measured. In general we will have data from many receivers, possibly also for different sources. We can put all these data in one data vector $\mathbf{d}$:

$$\mathbf{d} = "\mathbf{u}^1_{\text{obs}}". \tag{55}$$

All the different observations are simply put below each other, so that $\mathbf{d}$ can have any dimension. If the inversion is done in the frequency domain the scattered waves for different frequencies are all entered in the data vector (55) as separate data. Here the inversion is presented in the time domain formulation. In that case the data vector consists of the displacement measurements as a function of time, hence the data vector is a function of time. The inversion can be started once the covariance matrix of the data vector (C_d) is specified.

The inversion can be done in one step, since the theory is linear. This means that the stabilized least squares solution is given by (Tarantola 1984a):

$$\mathbf{m} = (I + C_m A^{\mathrm{T}} C_d^{-1} A)^{-1} C_m A^{\mathrm{T}} C_d^{-1} \mathbf{d}. \tag{56}$$

In this expression A is the gradient of the data vector in model space, i.e.

$$A = \begin{pmatrix} \dfrac{\partial \mathbf{u}^1}{\partial \Delta\mu} & \dfrac{\partial \mathbf{u}^1}{\partial \Delta\lambda} & \dfrac{\partial \mathbf{u}^1}{\partial \Delta\rho} \\ \cdot & \cdot & \cdot \\ \cdot & \cdot & \cdot \\ \cdot & \cdot & \cdot \\ \cdot & \cdot & \cdot \end{pmatrix}. \tag{57}$$

(The dots indicate that all the measured displacements are put on top of each other.) Note that A is a function of time, since $\mathbf{u}^1$ is a function of time.

The first step in the inversion entails weighting of the displacement components. The weighted data vector is defined by:

$$\tilde{u}(t) = C_d^{-1} \mathbf{d}(t). \tag{58}$$

If one now inserts the time-dependent version of the scattered wave in (57), one obtains the following result for $A^{\mathrm{T}}\tilde{u}$:

$$A^{\mathrm{T}}\tilde{u}(\mathbf{r}_0) = \sum_{r,s} \int \begin{pmatrix} \dfrac{\partial V^{\sigma\nu}(\mathbf{r}_0)}{\partial \Delta\mu} \\ \dfrac{\partial V^{\sigma\nu}(\mathbf{r}_0)}{\partial \Delta\lambda} \\ \dfrac{\partial V^{\sigma\nu}(\mathbf{r}_0)}{\partial \Delta\rho} \end{pmatrix} g_{\sigma\nu}(\hat{\omega}, X_1, X_2)$$

$$[F_s(\hat{\omega}) \cdot \mathbf{p}^{\nu}(z_s, \hat{\omega}, \varphi_1)] \frac{\exp\,[-i(k_\nu(\hat{\omega})X_1 - \hat{\omega}t + 3\pi/4)]}{\sqrt{(\pi/2)k_\nu(\hat{\omega})X_1}} \frac{\exp\,[-ik_\sigma(\hat{\omega})X_2]}{\sqrt{(\pi/2)\,k_\sigma(\hat{\omega})X_2}}$$

$$\times\, [\mathbf{p}^{\sigma}(z_r, \hat{\omega}, \varphi_2) \cdot \tilde{u}(t)]\, dt \tag{59}$$

where

$$g_{\sigma\nu}(\hat{\omega}, X_1, X_2) = \sqrt{2\pi/(k_\nu''(\hat{\omega})X_1 + k_\sigma''(\hat{\omega})X_2)}\ . \tag{60}$$

The integration over time in (59) is performed because both A and $\tilde{u}$ are functions of time, and a contraction over the time variable is implied by the operator product. All variables have the same meaning as in Fig. 2, for the appropriate sources and receivers. The symbol $\sum_{r,s}$ indicates that a summation over all the sources and receivers is performed. For each source–receiver pair and each value of t the value of $\hat{\omega}$ is determined by (51). If (51) has more than one solution one should sum over these solutions. The derivatives of $V^{\sigma\nu}$ can easily be obtained from (29a–d).

Just as in Tarantola (1984a) the inversion consists of a back propagation, as well as a correlation with the source function. This can be seen in (59) because this expression is the temporal correlation of a surface wave propagating back from the source to the scatterer with a surface wave propagating from the receiver to the scatterer. Equation (59) therefore implies a summation in the horizontal plane over the ellipses or egg-curves of Fig. 12. The weight factor in this summation is determined by the geometrical spreading factors, the projection of the observed scattered wave on the appropriate polarization vector, and the source characteristics.

In order to do the back propagation correctly the different modes have to be separated. In practice this is hard to realize. However, often the fundamental mode contributions are dominant, and higher mode scattering is relatively weak. Moreover, the fundamental mode wavetrain is usually separated in time from the higher mode contributions. In that case time windowing can be used to separate the fundamental modes from the higher modes, and the inversion can be done with the fundamental modes only. The fundamental Love wave and the fundamental Rayleigh wave are separated by projecting the displacement vector on the polarization vector (see (59)).

At this point only qualitative statements about the resolution can be made. The horizontal resolution and the vertical resolution are controlled by different factors. The horizontal resolution is mainly dependent on the number of sources and receivers that are available, since this determines how well the scattered wave energy can be focused on the scatterer. The vertical resolution depends mostly on the bandwidth of the signal. Synthetic

examples, or scattering data from a well-known distribution of scatterers are needed to make these statements more quantitative.

The inversion presented here can be called 'surface wave holography' because the surface waves which are scattered and reflected by the heterogeneity (the object) are projected back in space and are correlated with the source signal (the illumination) to give an image of the heterogeneity.

10 Conclusions

The scattering of surface waves has been treated in this paper in the Born approximation. This means that a linearization in the scattering effects is performed, so that the theory is only applicable for inhomogeneities which are weak enough. (See Hudson & Heritage (1982) for the validity of the Born approximation in seismic problems.) However, even if the heterogeneity is not weak, one might hope that the theory still gives a qualitative understanding of the scattering and mode conversion phenomena.

For simplicity it is assumed in this study that the surface boundary conditions are not perturbed by the heterogeneity, so that the heterogeneity is assumed to be buried. This means that this theory cannot be applied to the important case of surface wave scattering by variations in the topography without making some modifications.

The far field condition restricts the application of the theory. Because of this restriction it is impossible to consider scatterers close to the source or the receivers. This means that the theory cannot be applied if either the source or the receiver is located in a heterogeneous region. Moreover, the far field condition also makes it impossible to calculate higher order corrections to the Born approximation, since these corrections contain near field terms.

The dyadic form of the far field Green's function for either a laterally homogeneous medium or a laterally smoothly varying medium shows that the polarization vectors play a crucial role. The polarization vector determines not only the depth dependence and the displacement direction of the elastic waves; the excitation is also conveniently expressed in terms of the polarization vectors.

In the Born approximation the scattered waves are characterized by an excitation at the source, followed by an undisturbed propagation to the scatterer. Here scattering and mode conversion occur. These effects are described by the interaction matrix. After the scattering an undisturbed propagation to the receiver occurs. The 'undisturbed propagation' can be either in a laterally homogeneous medium, or in a laterally smoothly varying background medium.

Stationary phase theorems are very useful in simplifying the resulting integrals over the heterogeneity. It is shown that if the inhomogeneity is smooth in the transverse direction, then only the heterogeneity on the source–receiver line influences the scattered wave. This is the analogy of the 'great circle theorem' in a plane geometry.

The same principle holds for scattering by a quarter-space. It is shown that in the far field limit for each pair of incoming and outgoing modes the scattering is determined by a reflection point on the interface between the two quarter-spaces. The phase speeds of the incoming and the reflected surface wave determine this point by means of Snell's law.

The linearized scattering theory can be used in conjunction with the inversion algorithm of Tarantola (1984a). The inversion is formulated in a way which is reminiscent of holography techniques used in optics. This kind of inversion will be tested with data from the NARS array (Nolet & Vlaar 1982 and Dost, Van Wettum & Nolet 1984), but only a limited resolution can be expected with a small number of stations and a few source positions. A

dense network, as is presented in the PASSCAL proposal (1984), would be ideal for an accurate reconstruction of lateral heterogeneities with surface wave holography.

Acknowledgment

I thank Guust Nolet not only for his help and advice, but most importantly for creating a stimulating environment for doing seismological research.

References

Aki, K. & Richards, P. G., 1980. *Quantitative Seismology*, volume 1, Freeman, San Francisco.

Alsop, L. E., 1966. Transmission and reflection of Love waves at a vertical discontinuity, *J. geophys. Res.*, **71**, 3969–3984.

Alsop, L. E., Goodman, A. S. & Gregersen, S., 1974. Reflection and transmission of inhomogeneous waves with particular application to Rayleigh waves, *Bull. seism. Soc. Am.*, **64**, 1635–1652.

Babich, V. M., Chikhachev, B. A. & Yanovskaya, T. B., 1976. Surface waves in a vertically inhomogeneous elastic halfspace with a weak horizontal inhomogeneity, *Izv Phys. Earth*, **12**, 242–245.

Backus, G. E., 1964. Geographical interpretation of measurements of average phase velocities of surface waves over great circular and great semi circular paths, *Bull. seism. Soc. Am.*, **54**, 571–610.

Bender, C. M. & Orszag, S. A., 1978. *Advanced Mathematical Methods for Scientists and Engineers*, McGraw-Hill, New York.

Ben-Menahem, A. & Singh, S. J., 1968. Eigenvector dyads with application to geophysical theory, *Geophys. J. R. astr. Soc.*, **16**, 417–452.

Bretherton, F. P., 1968. Propagation in slowly varying waveguides, *Proc. R. Soc., A*, **302**, 555–576.

Bungum, H. & Capon, J., 1974. Coda pattern and multipathing propagation of Raleigh waves at NORSAR, *Phys. Earth planet. Int.*, **9**, 111–127.

Dahlen, F. A., 1979. The spectra of unresolved split normal mode multiplets, *Geophys. J. R. astr. Soc.*, **58**, 1–33.

Dost, B., Van Wettum, A. & Nolet, G., 1984. The NARS array, *Geologie Mijnb.*, **63**, 381–386.

Franklin, J. N., 1970. Well posed stochastic extensions of ill-posed linear problems, *J. Math. Analysis Applic.*, **31**, 682–716.

Gregersen, S. & Alsop, L. E., 1974. Amplitudes of horizontally refracted Love waves, *Bull. seism. Soc. Am.*, **64**, 535–553.

Harvey, D. J., 1981. Seismogram synthesis using normal mode superposition: the locked mode approximation, *Geophys. J. R. astr. Soc.*, **66**, 37–70.

Herrera, I., 1964. A perturbation method for elastic wave propagation, *J. geophys. Res.*, **69**, 3845–3851.

Herrera, I. & Mal, A. K., 1965. A perturbation method for elastic wave propagation 2. Small inhomogeneities, *J. geophys. Res.*, **70**, 871–883.

Hudson, J. A., 1977a. The passage of elastic waves through an anomalous region – IV. Transmission of Love waves through a laterally varying structure, *Geophys. J. R. astr. Soc.*, **49**, 645–654.

Hudson, J. A., 1977b. Scattered waves in the coda of *P*, *J. Geophys.*, **43**, 359–374.

Hudson, J. A., 1981. A parabolic approximation for surface waves, *Geophys. J. R. astr. Soc.*, 67, 755–770.

Hudson, J. A. & Heritage, J. R., 1982. The use of the Born approximation in seismic scattering problems, *Geophys. J. R. astr. Soc.*, **66**, 221–240.

Its, E. & Yanovskaya, T. B., 1985. Propagation of surface waves in a half space with vertical, inclined or curved interfaces, *Wave Motion*, 7, 79–94.

Jordan, T. H., 1978. A procedure for estimating lateral variations from low frequency eigenspectra data, *Geophys. J. R. astr. Soc.*, **52**, 441–455.

Kennett, B. L. N., 1972. Seismic waves in laterally inhomogeneous media, *Geophys. J. R. astr. Soc.*, 27, 301–325.

Kennett, B. L. N., 1984a. Guided wave propagation in laterally varying media – I. Theoretical development, *Geophys. J. R. astr. Soc.*, 79, 235–255.

Kennett, B. L. N., 1984b. Guided wave propagation in laterally varying media – II. *Lg* waves in northwestern Europe, *Geophys. J. R. astr. Soc.*, 79, 256–267.

Knopoff, L. & Hudson, J. A., 1964. Transmission for Love waves past a continental margin, *J. geophys. Res.*, **69**, 1649–1653.

Levshin, A. & Berteussen, K. A., 1979. Anomalous propagation of surface waves in the Barentz Sea as inferred from NORSAR recordings, *Geophys. J. R. astr. Soc.*, **56**, 97–118.

Malichewsky, P., 1979. Eine Verbesserung von Alsops Methode zur Bestimmung der Reflexions- und Transmissionskoeffizienten von Oberflachwellen, *Pure appl. Geophys.*, **117**, 1045–1049.

Malin, P. E., 1980. A first order scattering solution for modelling elastic wave codas – I. The acoustic case, *Geophys. J. R. astr. Soc.*, **63**, 361–380.

Malin, P. E. & Phinney, R. A., 1985. On the relative scattering of *P*- and *S*-waves, *Geophys. J. R. astr. Soc.*, **80**, 603–618.

Mueller, S. & Talwani, M., 1971. A crustal section across the Eastern Alps based on gravity and seismic refraction data, *Pure appl. Geophys.*, **85**, 226.

Nolet, G., 1977. The upper mantle under Western Europe inferred from the dispersion of Raleigh modes, *J. Geophys.*, **43**, 265–285.

Nolet, G. & Vlaar, N. J., 1982. The NARS project: probing the Earth's interior with a large seismic antenna, *Terra Cognita*, **2**, 17–25.

PASSCAL, 1984. Program for Array Seismic Studies of the Continental Lithosphere, issued by the Incorporated Research Institute for Seismology.

Tarantola, A., 1984a. Inversion of seismic reflection data in the acoustic approximation, *Geophysics*, **49**, 1259–1266.

Tarantola, A., 1984b. Linearized inversion of seismic reflection data, *Geophys. Prospect.*, **32**, 998–1015.

Tarantola, A. & Valette, B., 1982. Generalized nonlinear inverse problems solved using the least squares criterion, *Rev. Geophys. Space Phys.*, **20**, 219–232.

Wu, R. & Aki, K., 1985. Scattering characteristics of elastic waves by an elastic heterogeneity, *Geophysics*, **50**, 582–595.

Yomogida, K., 1985. Gaussian beams for surface waves in laterally slowly-varying media, *Geophys. J. R. astr. Soc.*, **82**, 511–534.

Yomogida, K. & Aki, K., 1985. Total waveform synthesis of surface waves in laterally heterogeneous earth by Gaussian beam method, *J. geophys. Res.*, **90**, 7665–7688.

Chapter 3

Surface wave scattering by surface topography

This chapter is published as:

Snieder, R., The influence of topography on the propagation and scattering of surface waves, *Phys. Earth. Plan. Int.*, *44*, 226-241, 1986

The influence of topography on the propagation and scattering of surface waves

Roel Snieder

Department of Theoretical Geophysics, University of Utrecht, Budapestlaan 4, P.O. Box 80.021, 3508 TA Utrecht (The Netherlands)

(Received January 31, 1986; accepted March 28, 1986)

Snieder, R., 1986. The influence of topography on the propagation and scattering of surface waves. Phys. Earth Planet. Inter., 44: 226–241.

The effects of topography on three dimensional surface-wave scattering and surface-wave conversions is treated in the Born approximation. Surface-wave scattering by topography is compared with surface-wave scattering by a mountain root model. The interference effects between surface waves scattered by different parts of a heterogeneity are analysed by considering Fraunhofer diffraction for surface waves. For a smooth heterogeneity a relation is established between the interaction terms and the phase speed derivatives. The partial derivatives of the phase speed c with respect to the topography height h for Love (L) and Rayleigh (R) waves are

$$\left[\frac{1\partial c}{c\partial h}\right]^{L} = \frac{-1}{4cUI_1}\rho^0 1_1^2\left(c^2-\beta^2\right) \quad (z=0)$$

$$\left[\frac{1\partial c}{c\partial h}\right]^{R} = \frac{-1}{4cUI_1}\rho^0\left[r_2^2c^2+r_1^2\left(c^2-4\left(1-\frac{\beta^2}{\alpha^2}\right)\beta^2\right)\right] \quad (z=0)$$

Phase speed perturbations due to topography can amount to 1–2% and cannot be ignored in surface-wave studies.

1. Introduction

Observations of teleseismic surface waves demonstrate that surface-wave scattering is an important process. Levshin and Berteussen (1979), and Bungum and Capon (1974) showed, using observations from NORSAR, that distinct multipathing of surface waves occurs for periods below 40 s. A formalism to describe the three-dimensional scattering of surface waves by buried heterogeneities was presented in Snieder (1986). (This is referred to as paper 1.)

There is, however, no reason to assume that surface waves are scattered by buried heterogeneities only, since topography variations also cause surface-wave scattering. Even for very idealised models the effects of topography turn out to be very complicated. Asymptotic results for a narrow mountain ridge on a homogeneous two-dimensional half-space are given by Sabina and Willis (1975, 1977). A survey of numerical methods which have been used to study the effects of topography on seismic waves is given by Sanchez-Sesma (1983). Bullit and Toksoz (1985) used ultrasonic Rayleigh waves in an aluminum model to investigate the effects of topography on three-dimensional surface waves. Because of the complexity of the problem this paper is restricted to topography variations that are weak enough to render the Born approximation valid.

The linearised scattering of elastic waves by surface heterogeneities has received considerable interest. The basic theory for this is outlined in Gilbert and Knopoff (1960) for a homogeneous

0031-9201/86/$03.50

half-space, and by Herrera (1964) for a layered medium. Hudson (1977) applied the theory to the generation of the P-wave Coda, while Woodhouse and Dahlen (1978) considered the effect of topography on the free oscillations of the Earth. A completely different approach was used by Steg and Klemens (1974) who analysed Rayleigh waves in solid materials, which they treated as a lattice instead of a continuum.

This paper provides an explicit formalism to analyse three-dimensional surface-wave scattering by topography in a continuous elastic medium. A formalism for the linearised scattering of three-dimensional elastic waves is presented in section 2. It is shown in section 3 how surface-wave scattering by topography can be accommodated in the theory of paper 1. (An appendix is added with a proof that the theory of paper 1 is unaffected if the heterogeneity is nonzero at the surface.) Because of the linearisations these results are only approximations. The validity of the Born approximation is discussed in Hudson and Heritage (1982). In the treatment of the scattering by topography the stress is assumed to behave linearly with depth over the topography. This imposes another restriction on the validity of the results presented here, which is discussed in section 4. The interaction terms due to the topography are analysed in section 5, where they are quantitatively compared with the surface-wave scattering by a mountain-root structure.

The expressions for the scattered surface waves contain integrals over the heterogeneity. Interference effects make the analytic evaluation of these integrals complicated, even for idealised scatterers. In section 6 a formalism is derived for Fraunhofer diffraction by surface waves, which is applied in section 7 to a Gaussian mountain.

It is well known that smooth heterogeneities do not cause surface-wave scattering (Bretherton, 1968), but they do cause variations in the phase speed and the amplitude. In section 8 a heuristic argument is used for the relation between the interaction terms and the phase speed variations. It is shown in section 9 that this leads to the partial derivatives of the phase speed with respect to the density, P-wave speed and S-wave speed as obtained from variational principles (Aki and Richards, 1980). Furthermore, the partial derivatives of the phase speed with respect to the topography are derived.

The results presented here are valid under certain restrictions. Firstly, the heterogeneity must be weak enough to make the Born approximation valid (Hudson and Heritage, 1982), and to allow a linearisation of the stress over the topography height. Secondly, the far field limit is used throughout. Thirdly, a plane geometry is assumed, it is shown in Snieder and Nolet (in preparation) that this condition can easily be relaxed. Fourthly, the slope of the topography has to be small. Lastly, it is assumed that the interaction with the body-wave part of the Green's function can be ignored. Body waves and surface waves are shown to be coupled by strong topography variations in Hudson (1967), Greenfield (1971), Hudson and Boore (1980) or Baumgardt (1985). The locked mode approximation (Harvey, 1981) can in principle be used to take this coupling into account, without using the body-wave Green's function.

Throughout this paper the summation convention is used both for vector or tensor indices, as well as for mode numbers. Vector and tensor components are denoted by Roman subscripts, while Greek indices are used for the mode numbers. The dot product which is used is defined by

$$[\bar{p} \cdot \bar{q}] = p_i^* q_i \tag{1.1}$$

where * denotes complex conjugation.

2. Derivation of the equations for the scattered wave

The equation of motion combined with the elasticity relations can be written as

$$L_{ij} u_j = F_i \tag{2.1}$$

In this expression u_i is the i-th component of the displacement, and F_i is the force which excites the wavefield. The (differential) operator L is defined by

$$L_{ij} = -\rho\omega^2 \delta_{ij} - \partial_n c_{inmj} \partial_m \tag{2.2}$$

where $\bar{c}$ is the elasticity tensor. The surface boundary condition is given by

$$n_i \tau_{ij} = 0 \quad \text{at the surface} \tag{2.3}$$

$\bar{n}$ is the normal vector pointing outwards from the medium, and τ_{ij} is the stress tensor

$$\tau_{ij} = c_{ijkl}\partial_k u_l \tag{2.4}$$

It is well known how surface-wave solutions can be obtained from (2.1) and (2.3) if the medium is laterally homogeneous and the surface is flat. Aki and Richards (chapter 7, 1980) treated this problem in great detail. They showed that in that case the solution was given by

$$\bar{u}^0 = G\bar{F} \tag{2.5}$$

which is an abbreviated notation for

$$u_i^0(\bar{r}) = \int G_{ij}(\bar{r}, \bar{r}')F_j(\bar{r}')d^3r' \tag{2.6}$$

The Green's function (G) satisfies

$$L_{ij}^0 G_{jk}(\bar{r}, \bar{r}') = \delta_{ik}\delta(\bar{r} - \bar{r}') \tag{2.7}$$

In this expression L^0 is the operator L for a laterally homogeneous medium.

If lateral heterogeneities are present, or if the surface is not flat, scattering of elastic waves occurs. These scattering effects are treated here in a linearised way, i.e., it is assumed that both the lateral inhomogeneities of the medium, and the topography variations are small. In that case the density and the elasticity tensor can be written as

$$\rho(x, y, z) = \rho^0(z) + \epsilon\rho^1(x, y, z) \tag{2.8}$$

$$\bar{c}(x, y, z) = \bar{c}^0(z) + \epsilon c^{-1}(x, y, z) \tag{2.9}$$

The (small) parameter ϵ is added to make explicit that the perturbations are small. Let the topography be given by

$$z = -\epsilon h(x, y) \tag{2.10}$$

The $-$ sign has been added because z is counted positively downward, and h is the topography height above $z = 0$. The functions $\bar{c}^0$ and ρ^0 define together with a zero stress boundary condition at $z = 0$ a laterally homogeneous background medium, which is perturbed by the heterogeneities $\bar{c}^1$ and ρ^1. Since the perturbations are small the wave field can be written as a perturbation series in ϵ

$$\bar{u} = \bar{u}^0 + \epsilon\bar{u}^1 + 0(\epsilon^2) \tag{2.11}$$

In this expression $\bar{u}^1$ denotes the Born approximation to the scattered wave.

Hudson (1977) derived expressions for the scattered wave in the Born approximation. He showed that the wave scattered by the medium heterogeneities (ρ^1 and $\bar{c}^1$), and the topography variation is given by

$$\begin{aligned} u_i^1(\bar{r}) = \Big\{ &+ \int G_{ij}(\bar{r}, \bar{r}')\rho^1(\bar{r}')\omega^2 G_{jl}(\bar{r}', \bar{r}_s)\mathrm{d}V' \\ &- \int \big(\partial_m G_{ij}(\bar{r}, \bar{r}')\big)c_{jmnk}^1(\bar{r}') \\ &\times \big(\partial_n G_{kl}(\bar{r}', \bar{r}_s)\big)\mathrm{d}V' \\ &+ \int G_{ij}(\bar{r}, \bar{r}')h(\bar{r}')\rho^0(\bar{r}')\omega^2 G_{jl}(\bar{r}', \bar{r}_s)\mathrm{d}S' \\ &- \int \big(\partial_m G_{ij}(\bar{r}, \bar{r}')\big)h(\bar{r}')c_{jmnk}^0(\bar{r}') \\ &\times \big(\partial_n G_{kl}(\bar{r}', \bar{r}_s)\mathrm{d}S'\big)\Big\} F_l(\bar{r}_s) \end{aligned} \tag{2.12}$$

The volume integrals are over the volume of the reference medium ($z > 0$), while the surface integrals are to be evaluated at the surface of the reference medium ($z = 0$). The differentiations are taken with respect to the $\bar{r}'$-coordinates. Hudson (1977) derived this result in the time domain, (2.12) is the same expression in the frequency domain. It has been assumed here that the wave field is excited by a point force $\bar{F}$ in $\bar{r}_s$. A more general excitation can be treated by superposition. It is shown in paper 1 how a moment-tensor excitation can be incorporated.

To derive this result three assumptions have to be made:

(1) the heterogeneity is so weak that multiple scattering can be ignored, i.e., that the Born approximation is valid.

(2) The slope of the heterogeneity has to be small, since in Hudson's derivation it is assumed that $(\nabla h) = 0(\epsilon)$.

(3) The stress should behave linearly over the mountain height, i.e., it is assumed that

$$\tau(-h) = \tau(0) - h\partial_z\tau(0) \tag{2.13}$$

is a good approximation.

Using the Dirac δ-function, we can rewrite (2.12) as

$$u_i^1(\bar{r}) = \int G_{ij}(\bar{r}, \bar{r}')\left[\rho^1 + h\rho^0\delta(z')\right] \times \omega^2 G_{jl}(\bar{r}', \bar{r}_s) F_l(\bar{r}_s)\mathrm{d}V' - \int \left(\partial_m G_{ij}(\bar{r}, \bar{r}')\right)\left[c^1_{jmnk} + hc^0_{jmnk}\delta(z')\right] \times (\partial_n G_{kl}(\bar{r}', \bar{r}_s)) F_l(\bar{r}_s)\mathrm{d}V' \qquad (2.14)$$

The upshot of this calculation is that topography variations in this approximation act on the scattered waves as if both the mass of the mountain ($h\rho^0$), and the total elasticity of the mountain ($h\bar{c}^0$) are compressed to a δ-function at the surface of the reference medium. For the mass term this is intuitively clear, because for surface waves which penetrate much deeper than the mountain height the precise mass distribution is not very important. For the elasticity term this is less obvious, because it is not clear what the implications are of 'compressing' the total elasticity of the mountain in a δ-function.

3. A formalism for surface wave scattering

Up to this point the theory was developed for an arbitrary elastic medium, and for the complete Green's function. This means that all sorts of complex scattering phenomena can be dealt with. (For example (2.14) could be used to describe the scattering of body waves by anisotropic regions, etc.)

From this point on we restrict ourselves to the surface wave part of the Green's function in an isotropic medium. It is shown in paper 1 that the far field Green's function can conveniently be expressed as a dyad of polarisation vectors. Using

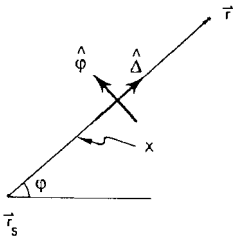

Fig. 1a. Geometry for the direct wave.

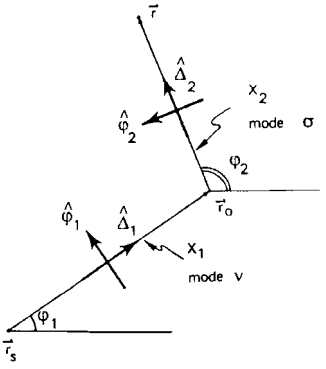

Fig. 1b. Geometry for the scattered wave.

these polarisation vectors we can show that the direct wave is given by

$$\bar{u}^0(\bar{r}) = \bar{p}^\nu(z, \phi)\frac{e^{i(k_\nu X + \pi/4)}}{\left(\frac{\pi}{2}k_\nu X\right)^{1/2}}\left[\bar{p}^\nu(z_s, \phi).\bar{F}\right] \qquad (3.1)$$

and the scattered wave is for an arbitrary distribution of scatterers

$$\bar{u}^1(\bar{r}) = \int\int \bar{p}^\sigma(z, \phi_2)\frac{e^{i(k_\sigma X_2 + \pi/4)}}{\left(\frac{\pi}{2}k_\sigma X_2\right)^{1/2}} \times V^{\sigma\nu}(x_o, y_o)\frac{e^{i(k_\nu X_1 + \pi/4)}}{\left(\frac{\pi}{2}k_\nu X_1\right)^{1/2}} \times \left[\bar{p}^\nu(z_s, \phi_1).\bar{F}\right]\mathrm{d}x_o\mathrm{d}y_o \qquad (3.2)$$

See Fig. (1a,b) for the definition of variables. Because of the summation convention a double sum over excited modes (ν), and scattered modes (σ) must be applied. The modes are coupled by the interaction matrix $V^{\sigma\nu}$. The only difference with the results in paper 1 is that the depth integrals over the heterogeneity are included in the interaction terms $V^{\sigma\nu}$.

The polarisation vector for Love waves is

$$\bar{p}^\nu(z, \phi) = l_1^\nu(z)\,\hat{\phi} \qquad (3.3a)$$

and for Rayleigh waves

$$\bar{p}^{\nu}(z, \phi) = r_1^{\nu}(z)\hat{\Delta} + ir_2^{\nu}(z)\hat{z} \tag{3.3b}$$

Where l_1, r_1 and r_2 are the surface-wave eigenfunctions defined in Aki and Richards (1980). These eigenfunctions are assumed to be normalised according to

$$8c_{\nu}U_{\nu}I_1^{\nu} = 1 \quad \text{(no summation)} \tag{3.4}$$

In this expression I_1^{ν} is the kinetic energy integral. For Love waves

$$I_1 = 1/2\int \rho l_1^2 \mathrm{d}z \tag{3.5a}$$

and for Rayleigh waves

$$I_1 = 1/2\int \rho(r_1^2 + r_2^2)\mathrm{d}z \tag{3.5b}$$

It was shown in the previous section how surface irregularities could be treated as a δ-function heterogeneity at $z = 0$. Therefore the expression for the interaction coefficients ($V^{\sigma\nu}$) of paper 1 can be used. (In paper 1, (3.2) was derived for buried scatterers. An appendix is added to this paper with a proof that perturbations at the surface do not affect this result.)

Since the scattered wave (2.14) consists of a contribution of the perturbation of the medium parameters, and of a contribution of topography variations, the interaction terms ($V^{\sigma\nu}$) can be decomposed in the following way

$$V^{\sigma\nu} = B^{\sigma\nu} + S^{\sigma\nu} \tag{3.6}$$

$B^{\sigma\nu}$ describes the interaction terms due to the ρ^1 and $\bar{c}^1$ heterogeneity, while $S^{\sigma\nu}$ describes the scattering due to the surface irregularities. The $B^{\sigma\nu}$ terms can be expressed in the surface-wave eigenfunctions l_1, r_1 and r_2. $B^{\sigma\nu}_{\mathrm{RL}}$ is used to denote the scattering from the ν-th Love wave to the σ-th Rayleigh wave by $\bar{c}^1$ and ρ^1, and a similar notation is used for other pairs of interacting modes. It was shown in paper 1 that in this notation the interaction terms for an isotropic medium are given by

$$B^{\sigma\nu}_{\mathrm{LL}} = \int\left[l_1^{\sigma}l_1^{\nu}\rho^1\omega^2 - (\partial_z l_1^{\sigma})(\partial_z l_1^{\nu})\mu^1\right]\mathrm{d}z\cos\phi - k_{\sigma}k_{\nu}\int l_1^{\sigma}l_1^{\nu}\mu^1\mathrm{d}z\cos 2\phi \tag{3.7a}$$

$$B^{\sigma\nu}_{\mathrm{RL}} = \int\left[r_1^{\sigma}l_1^{\nu}\rho^1\omega^2 + (k_{\sigma}r_2^{\sigma} - \partial_z r_1^{\sigma})(\partial_z l_1^{\nu})\mu^1\right]\mathrm{d}z\sin\phi - k_{\sigma}k_{\nu}\int r_1^{\sigma}l_1^{\nu}\mu^1\mathrm{d}z\sin 2\phi \tag{3.7b}$$

$$B^{\sigma\nu}_{\mathrm{LR}} = -B^{\nu\sigma}_{\mathrm{RL}} \tag{3.7c}$$

$$B^{\sigma\nu}_{RR} = \int\left[r_2^{\sigma}r_2^{\nu}\rho^1\omega^2 - (k_{\sigma}r_1^{\sigma} + \partial_z r_2^{\sigma})(k_{\nu}r_1^{\nu} + \partial_z r_2^{\nu})\lambda^1 - k_{\sigma}k_{\nu}r_1^{\sigma}r_1^{\nu}\mu^1 - 2(\partial_z r_2^{\sigma})(\partial_z r_2^{\nu})\mu^1\right]\mathrm{d}z + \int\left[r_1^{\sigma}r_1^{\nu}\rho^1\omega^2 - (k_{\sigma}r_2^{\sigma} - \partial_z r_1^{\sigma}) \times (k_{\nu}r_2^{\nu} - \partial_z r_1^{\nu})\mu^1\right]\mathrm{d}z\cos\phi - k_{\sigma}k_{\nu}\int r_1^{\sigma}r_1^{\nu}\mu^1\mathrm{d}z\cos 2\phi \tag{3.7d}$$

In these expressions ∂_z denotes the depth derivative, and ϕ is the scattering angle (Fig. 1b)

$$\phi = \phi_2 - \phi_1 \tag{3.8}$$

Since these relations hold for an isotropic medium the interaction terms are expressed in the perturbations of the Lame parameters (λ^1 and μ^1).

The expressions (3.7a–d) can be used for the calculation of the interaction terms due to topography by substituting

$$\rho^1(x, y, z) \dashrightarrow h(x, y)\rho^0(z)\delta(z)$$

and making the same substitution for λ and μ. In the depth integrals in (3.7a–d) the surface-wave modes then only have to be evaluated at $z = 0$. At that point the vertical derivatives take a particularly simple form. Aki and Richards (1980) showed that at $z = 0$

$$\begin{aligned}\partial_z l_1 &= 0\\ \partial_z r_1 &= kr_2\\ \partial_z r_2 &= \frac{-k\lambda^0}{\lambda^0 + 2\mu^0}r_1\end{aligned} \tag{3.9}$$

Using this, the topography interaction terms are given by

$$S^{\sigma\nu}_{\mathrm{LL}} = h\left(l_1^{\sigma}l_1^{\nu}\rho^0\omega^2\cos\phi - k_{\sigma}k_{\nu}l_1^{\sigma}l_1^{\nu}\mu^0\cos 2\phi\right) \tag{3.10a}$$

$$S^{\sigma\nu}_{\mathrm{RL}} = h\left(r_1^{\sigma}l_1^{\nu}\rho^0\omega^2\sin\phi - k_{\sigma}k_{\nu}r_1^{\sigma}l_1^{\nu}\mu^0\sin 2\phi\right) \tag{3.10b}$$

$$S^{\sigma\nu}_{LR} = -S^{\nu\sigma}_{RL} \tag{3.10c}$$

$$S^{\sigma\nu}_{RR} = h\Big(r_2^{\sigma} r_2^{\nu} \rho^0 \omega^2 - k_\sigma k_\nu \mu^0 \frac{3\lambda^0 + 2\mu^0}{\lambda^0 + 2\mu^0} r_1^{\sigma} r_1^{r} + r_1^{\sigma} r_1^{\nu} \rho^0 \omega^2 \cos\phi - k_\sigma k_\nu r_1^{\sigma} r_1^{r} \mu^0 \cos 2\phi \Big) \tag{3.10d}$$

where all quantities have to be evaluated at the surface of the reference medium ($z = 0$).

4. An error analysis of the stress linearisation

The linearisation in the topography in the derivation of Hudson entails two approximations. The Born approximation requires that the scattered wave is sufficiently weak, this is discussed in Hudson and Heritage (1982). The other approximation which is made requires that the stress behaves linearly over the topography height (2.13). An impression of the magnitude of this error can be obtained by verifying this condition for the unperturbed Love waves and Rayleigh waves. This of course gives only a necessary condition for the validity of the stress linearisation, and not a sufficient condition, because the stress in the perturbed medium may behave differently. The error made by the linearisation is defined here as

$$e_i = \frac{\tau_{3i}(z=-h) - (-h)\partial_z \tau_{3i}(z=0)}{\tau_{3i}(z=-h)} \times 100\% \tag{4.1}$$

The eigenfunctions are calculated for the M7 model of Nolet (1977). As a representative example, the error made by linearising τ_{zz} for the fundamental mode as a function of period is shown in Fig. 2 for several values of the topography. The other stress components, and the error for the higher modes behaves similarly. It is quite arbitrary to decide how large an error is acceptable. A relative error of 20% is used here as a maximum since the error made by the stress linearisation is only part of the total error. With this criterium it follows that for a mountain height of 2 km the error is unacceptably large for periods shorter than 12 s. In general, for realistic values of the large scale topography, the linearisation of the stress poses no problems for periods larger than 15 s.

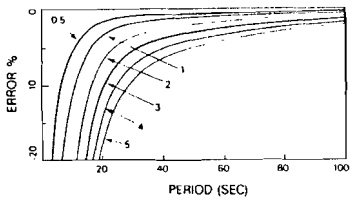

Fig. 2. Relative error for τ_{zz} (defined in (4.1)) for the fundamental Rayleigh mode for several values of the topography height (given in kilometers).

5. The topography interaction terms

In this section the topography interaction terms per unit area ($S^{\sigma\nu}$) are shown for a point topography with a height of 1 km. Since the topography interaction terms are linear in the mountain height (3.10a–d), results for a mountain of arbitrary height can be found by rescaling. The M7 model of Nolet (1977) was used again as a reference medium. The topography interaction terms are a simple function of the scattering angle, and the same convention as in paper 1 is used to de-

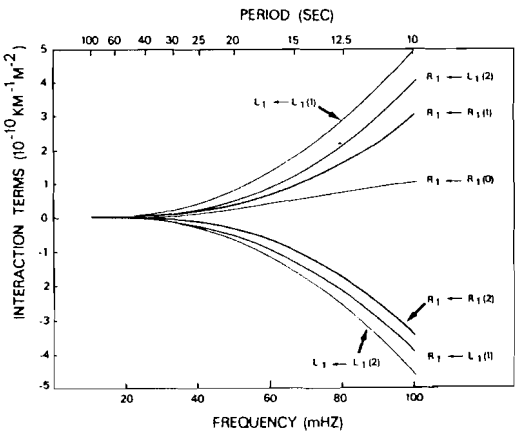

Fig. 3. Topography fundamental mode interaction terms for a mountain height of 1 km.

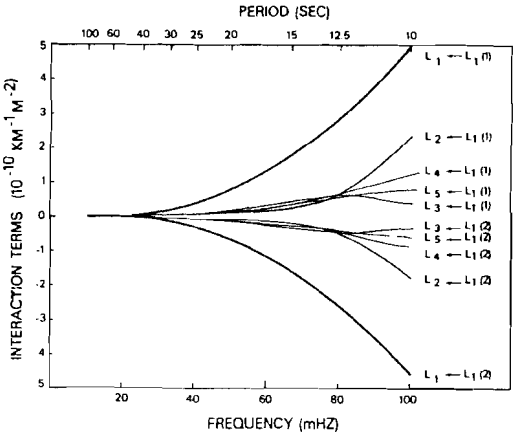

Fig. 4. Topography Love wave interaction terms for a mountain height of 1 km.

note the different azimuth terms. For example, $S_{R_2 \leftarrow L_1}$ (1) denotes the sin ϕ coefficient for the conversion from the fundamental Love mode to the first higher Rayleigh mode, $S_{R_1 \leftarrow R_1}$ (0) indicates the isotropic part of the scattering of the fundamental Rayleigh mode to itself, etc.

Figure 3 shows the different azimuth components of the fundamental mode topography interaction terms. These terms all rapidly increase with frequency. The interaction terms are given in units of (m^{-2}), and should be integrated in (3.2) over the surface of the topography to give the total scattering coefficients.

Just as with surface-wave scattering by a mountain root model (paper 1), the fundamental mode interactions dominate the interactions involving higher modes. As a representative example, the $L_N \leftarrow L_1$ interaction terms are shown in Fig. 4.

It can be seen in Fig. 3 that $S_{L_1 \leftarrow L_1}$ (1) $\approx -S_{L_1 \leftarrow L_1}$ (2), the same holds for the $R_1 \leftarrow R_1$ interactions, and for the $R_1 \leftarrow L_1$ conversion. It turns out that a similar property holds for the interactions with higher modes too. This can be verified in Fig. 4 which shows the $L_N \leftarrow L_1$ topography interaction terms. Therefore, for each conversion $L_N \leftarrow L_1$ the 'cos ϕ' coefficient is almost opposite to the 'cos 2ϕ' coefficient. The reason for this can be seen by rewriting (3.10a–d) in the following way

$$S_{LL}^{\sigma\nu} = hk_\sigma k_\nu l_1^\sigma l_1^\nu \rho^0 \left(c_\sigma c_\nu \cos\phi - \beta^2 \cos 2\phi\right) \tag{5.1a}$$

$$S_{RL}^{\sigma\nu} = hk_\sigma k_\nu r_1^\sigma l_1^\nu \rho^0 \left(c_\sigma c_\nu \sin\phi - \beta^2 \sin 2\phi\right) \tag{5.1b}$$

$$S_{RR}^{\sigma\nu} = S_{RR}^{\sigma\nu}(0) + hk_\sigma k_\nu r_1^\sigma r_1^\nu \rho^0 \left(c_\sigma c_\nu \cos\phi - \beta^2 \cos 2\phi\right) \tag{5.1c}$$

In these expressions c_ν is the phase speed of mode ν, and β is the shear-wave velocity at the surface of the reference medium. For deep modes (long periods) the topography interaction terms are small (Fig. 4), while for shallower modes (shorter periods) the phase speed of both Love and Rayleigh waves is close to the shear-wave velocity in the top layer. This explains that for all cases of importance

$$S(1) \approx -S(2) \tag{5.2}$$

This implies for Love waves

$$S_{LL}^{\sigma\nu} \approx S_{LL}^{\sigma\nu}(1)(\cos\phi - \cos 2\phi) \tag{5.3}$$

which means that the L ← L radiation pattern has zero's approximately for

$$\phi \approx 0° \quad \text{and} \quad \phi \approx \pm 120° \tag{5.4}$$

so that the scattering in the forward direction is weak, and back-scattering is favoured.

For R ← L topography scattering, (5.2) implies that

$$S_{RL}^{\sigma\nu} \approx S_{RL}^{\sigma\nu}(1)\sin\phi(1 - 2\cos\phi) \tag{5.5}$$

which means that the radiation pattern for R ← L conversion by topography has zero's for

$$\phi = 0°, \quad \phi \approx \pm 60° \quad \text{and} \quad \phi = 180° \tag{5.6}$$

For Rayleigh waves a similar analysis cannot be made because of the isotropic term $S_{RR}^{\sigma\nu}(0)$. However, it can be seen in Fig. 3 that (at least for the fundamental mode) this term is relatively small, so that the radiation pattern due to the topography for $R_1 \leftarrow R_1$ scattering is not too different from $L_1 \leftarrow L_1$ scattering.

That this is indeed the case can be verified in

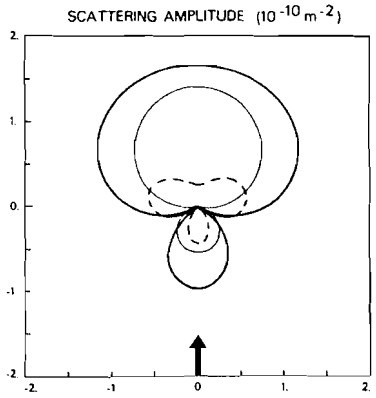

Fig. 5a. Radiation pattern for $R_1 \leftarrow R_1$ scattering for a period of 20 s. Dashed line is scattering by topography of 1 km height, thin line is scattering by a mountain root, thick line is the sum. The direction of the incoming wave is shown by an arrow.

Fig. 5a–c, where the dashed line shows the radiation patterns for the fundamental mode interactions by topography for a period of 20 s. Note that the $L_1 \leftarrow L_1$ topography scattering and the $R_1 \leftarrow R_1$ topography scattering is very weak in the forward direction. The $L_1 \leftarrow L_1$ topography radiation pattern has a zero near $\phi = 120°$, while the $R_1 \leftarrow L_1$ topography radiation pattern has a node near $\phi = 60°$. Observe that the $R_1 \leftarrow R_1$ topography radiation pattern differs mostly from the $L_1 \leftarrow L_1$ pattern in the weaker back-scattering. For other periods the topography radiation patterns are very similar because the different azimuth terms behave similarly as a function of frequency.

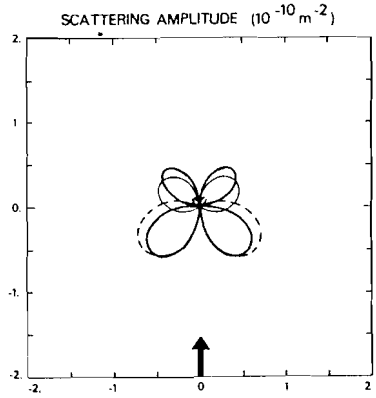

Fig. 5b. Radiation pattern for $L_1 \leftarrow R_1$ scattering for a period of 20 s. Lines defined as in Fig. 5a.

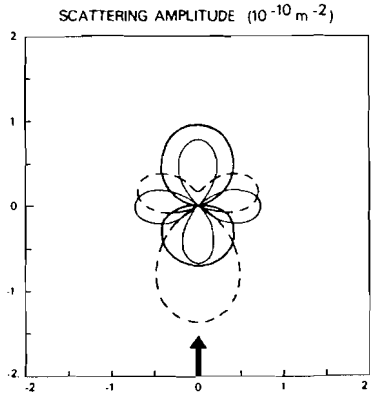

Fig. 5c. Radiation pattern for $L_1 \leftarrow L_1$ scattering for a period of 20 s. Lines defined as in Fig. 5a.

Figure 5a–c shows the relative importance of scattering by topography to the scattering by buried heterogeneities for a period of 20 s. These figures of course depend strongly on the type of heterogeneity which is considered, on the mountain height, and on frequency. Therefore these figures are only a rough indication of the relative importance in general. In this case a mountain height of 1 km is used, and the mountain root model shown in paper 1 is used for the buried scatterer. (The mountain root model is taken from Mueller and Talwani (1971), and consists of a light, low velocity heterogeneity between 30 and 50 km depth, perturbing the medium in that region with approximately 10%. The structure of a mountain root depends in general both on the height of the mountain, as well as on the horizontal extent. This dependence is ignored here by using the same mountain root model, irrespective of the topography.)

In all three fundamental mode interactions the topography scattering is of the same order of magnitude as the scattering by the mountain root. For periods shorter than 20 s the surface waves

are so shallow that the topography scattering tends to dominate. It can be seen in Fig. 5a–c that usually the topography interaction (S), and the mountain root interaction (B) are of the same sign, because the sum of the two terms is larger than each term separately. (The only exception is $L_1 \leftarrow L_1$ scattering at a right angle.) It turns out that this is also the case for the radiation patterns involving higher modes.

That the topography scattering and the scattering by the mountain root enhance each other is caused by the fact that both the topography and the presence of the mountain root give rise to a thickening of the waveguide (the crust). Therefore, these effects are in a sense similar. The difference is that the mountain root heterogeneity results in a perturbation of the medium itself, while the topography affects the surface boundary condition. This gives rise to the different shapes of the radiation patterns, and shows that one should be careful in modelling subsurface heterogeneities with variations of the free surface, as suggested by Bullit and Toksoz (1985).

6. Fraunhofer diffraction of surface waves

The interaction terms which were calculated in the previous section were given per unit area. To obtain the scattered wave (3.2), an integration over the heterogeneity should be performed. A crude estimate of the strength of the scattered wave can be obtained by multiplying the interaction terms with the horizontal extent of the inhomogeneity. This will, however, overestimate the strength of the scattered wave because this procedure ignores interference effects which tend to reduce the scattered wave.

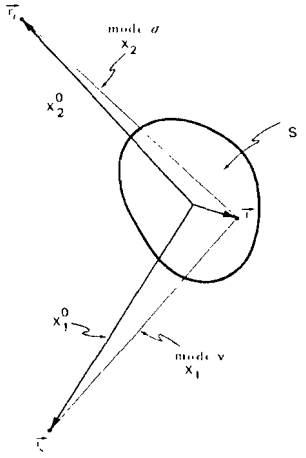

Fig. 6. Geometry for Fraunhofer diffraction.

To incorporate these interference effects, let us consider a localized scatterer which has a horizontal extension which is small compared to the source–scatterer distance, and the scatterer–receiver distance. This means that in the notation of Fig. 6

$$|\bar{r}| \ll X_1^0 \text{ and } |\bar{r}| \ll X_2^0 \tag{6.1}$$

In that case the phase of the integrand in (3.2) can be linearised in $|\bar{r}|$. Furthermore, the variation of the geometrical spreading factors over the scatterer can be ignored, because these variations are of relative order $|\bar{r}|/X^0_{1\text{ or }2}$. In that case the scattered wave can be written as

$$\bar{u}^1(\bar{r}_r) = \bar{p}^\sigma(z_r, \phi_2)\frac{e^{i(k_\sigma X_2^0 + \pi/4)}}{\left(\frac{\pi}{2}k_\sigma X_2^0\right)^{1/2}} T^{\sigma\nu} \frac{e^{i(k_\nu X_1^0 + \pi/4)}}{\left(\frac{\pi}{2}k_\nu X_1^0\right)^{1/2}} \times [\bar{p}^\nu(z_s, \phi_1).\bar{F}] \tag{6.2}$$

where $T_{\sigma\nu}$ is the total interaction coefficient

$$T^{\sigma\nu} = \int_S e^{-i((k_\sigma \hat{r}_r + k_\nu \hat{r}_i).\bar{r})} V^{\sigma\nu}(\bar{r}) \mathrm{d}S \tag{6.3}$$

This means that the total interaction term is given by the two-dimensional Fourier transform of the heterogeneity.

The wavenumber of the incoming wave is given by

$$\bar{k}_\nu^{\text{in}} = -\hat{r}_s k_\nu \tag{6.4}$$

and the scattered wave has wavenumber

$$\bar{k}_\sigma^{\text{out}} = \hat{r}_r k_\sigma \tag{6.5}$$

Therefore the Fourier transform (6.3) is to be evaluated at the wavenumber corresponding to the wavenumber change in the scattering event

$$(\Delta\bar{k})^{\sigma\nu} = \bar{k}_\sigma^{\text{out}} - \bar{k}_\nu^{\text{in}} \tag{6.6}$$

The magnitude of this wavenumber can easily be

expressed in the scattering angle ϕ

$$\Delta k^{\sigma\nu} = \left(k_\sigma^2 + k_\nu^2 - 2k_\sigma k_\nu \cos\phi\right)^{1/2} \tag{6.7}$$

If the scatterer exhibits cylinder symmetry, the azimuth integration in the Fourier integral can be performed. If one uses the integral representation of the Bessel function it follows that

$$T^{\sigma\nu} = 2\pi \int_0^\infty r J_0(\Delta k^{\sigma\nu} r) V^{\sigma\nu}(r) \mathrm{d}r \tag{6.8}$$

So that for a scatterer with cylinder symmetry the total scattering coefficient is just the Fourier–Bessel transform of the heterogeneity.

7. Application to a Gaussian mountain

In this section Fraunhofer diffraction by an idealised Gaussian shaped mountain is considered. This means that it is assumed here that

$$V^{\sigma\nu}(\bar{r}) = V^{\sigma\nu} \exp -r^2/L^2 \tag{7.1}$$

Of course a Gaussian mountain cannot satisfy the conditions (6.1). However, the tail of the scatterer contributes little to the integral, and this error is simply ignored. For a Gaussian mountain the integral (6.8) can be performed analytically. Abramowitz and Stegun (1970) gave an expression for the Fourier–Bessel transform of a Gaussian. Using this result one finds

$$T^{\sigma\nu} = \pi L^2 V^{\sigma\nu} \times \exp\left[-\tfrac{1}{4}\left(k_\sigma^2 + k_\nu^2 - 2k_\sigma k_\nu \cos\phi\right) L^2\right] \tag{7.2}$$

The term $\pi L^2 V^{\sigma\nu}$ is the integral of the heterogeneity over the volume of the scatterer. The exponent term describes the interference effects of different parts of the scatterer. For interactions of the fundamental mode with the higher modes, k_σ and k_ν are different so that the exponent is always negative. This term therefore leads to a weakening of the interactions of the fundamental mode with the higher modes.

It is interesting to consider this interference term in some more detail for unconverted waves

$$k_\sigma \approx k_\nu = k \tag{7.3}$$

(This condition is almost satisfied for the interaction of the fundamental Love mode with the fundamental Rayleigh mode, since their wavenumbers are usually not too different.) In that case the interference term is given by

$$\exp\left[-\tfrac{1}{4}(kL)^2(1-\cos\phi)\right]$$

If the scatterer is wide compared to the wavelength of the surface wave (i.e., $kL \gg 1$), this term is very small except for $\phi = 0$, so that the radiation pattern is strongly peaked in the forward direction. This effect is known in the theory of scattering of electromagnetic waves as the Mie-effect (Born and Wolf, 1959). In Fig. 7 this effect is shown for $R_1 \leftarrow R_1$ scattering by topography at a period of 20 s. To appreciate the dependence of the shape of the radiation pattern on the width of the mountain, the radiation patterns are normalised. For a small mountain ($L = 0$), the forward scattering is comparable to the back-scattering. As the width of the mountain ($2L$) increases to values comparable to the wavelength of the Rayleigh wave (70 km), the radiation pattern has only one narrow lobe in the forward direction.

The strength of the scattered wave for $R_1 \leftarrow R_1$ scattering at a period of 20 s by topography of 1 km height can be seen in Fig. 8. This figure includes the topography only, the contribution from the mountain root is not taken into account,

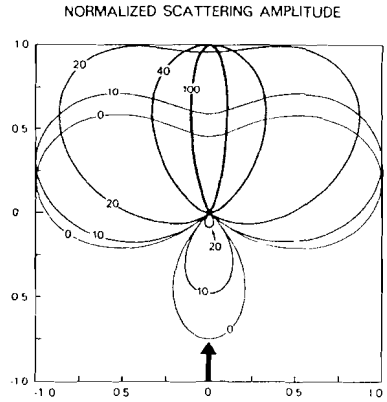

Fig. 7. Normalised topography scattering amplitude $T_{R_1 \leftarrow R_1}$ for a Gaussian mountain for a period of 20 s. Half width L is indicated in kilometers. Incoming wave is shown by an arrow.

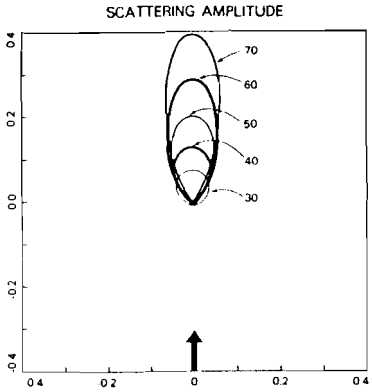

Fig. 8. Topography scattering amplitude $T_{R_1 \leftarrow R_1}$ for a Gaussian mountain of 1 km height at a period of 20 s. Half width L is indicated in kilometers. Incoming wave is shown by an arrow.

because the degree of compensation depends on the size of the mountain too. One should therefore be careful with the interpretation of this figure, since the presence of a mountain root affects the forward scattering drastically (Fig. 5a–c). Furthermore, the strength of the topography scattering depends on the mountain height.

For this particular example it can be concluded that for mountains with a half width less than 30 km the $R_1 \leftarrow R_1$ scattering at 20 s is extremely weak. However, for larger mountains the forward scattering increases rapidly with the mountain size. For mountains with a half width larger than 70 km the total topography interaction coefficient is larger than 0.4. This means that the scattered wave (as it follows from this calculation) is not small compared to the direct wave, which signals the breakdown of the Born approximation. This confirms the NORSAR observations that surface waves with a period shorter than 20 s are strongly scattered (Bungum and Capon, 1974). It will be clear that a mountain complex like the Alps, which has a half width much larger than 70 km, and which has a pronounced root (Mueller and Talwani, 1971) will severely distort the propagation of surface waves with a period shorter than 20 s.

8. Scattering by a band heterogeneity revisited

The perturbation theory derived in this paper and in paper 1 is valid for 'weak inhomogeneities'. The inhomogeneity has to be weak because of the requirement that the scattered waves are small compared to the direct wave. Now suppose we want to apply the theory to a weak and smooth heterogeneity with a large horizontal extent. Smooth means in this context that

$$|\partial_H \mu^1| \ll |k\mu^1| \tag{8.1}$$

where ∂_H is a horizontal derivative, and k is the horizontal wavenumber of the mode under consideration. A similar condition is assumed to hold for λ^1, ρ^1 and h. This condition implies that the heterogeneity varies little on a scale of a horizontal wavelength.

For a heterogeneity with a large horizontal extent, the integrals for the scattered wave may diverge with the size of the heterogeneity, even if the inhomogeneity is relatively weak. This divergence is an effect of the truncation of the perturbation series (Nayfeh, 1973), since the sum of all orders is necessarily finite. Physically this can be understood in the following way. If a wave propagates through a region with a weak and smooth heterogeneity, the only effect of the inhomogeneity is to perturb the local wavenumber. Instead of a solution $\exp(ik_0 x)$ for a laterally homogeneous medium, the laterally heterogeneous

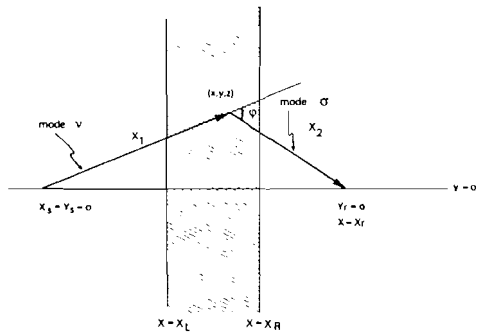

Fig. 9. Geometry for surface wave scattering by a band heterogeneity.

medium has a solution $\exp if^{x}(k_0 + \delta k)\mathrm{d}x$. In that case it can be shown with WKBJ theory that reflections and wave conversions are negligible (Bretherton, 1968; Woodhouse, 1974). This means that the Born approximation, which splits the total wave in a direct wave and a scattered wave, does not make much sense physically because in reality there is just one phase shifted transmitted wave.

We discuss this for the band heterogeneity model shown in Fig. 9. It was shown in paper 1 that the total wave in case of propagation through a band heterogeneity is given by

$$\bar{u}(\bar{r}_r) = \sum_{\nu} \bar{p}^{\nu}(z_r) \frac{e^{i(k_\nu x_r + \pi/4)}}{\left(\frac{\pi}{2} k_\nu x_r\right)^{1/2}} [\bar{p}^{\nu}(0).\bar{F}] \times \left[1 + \frac{2i\epsilon}{k_\nu} \int_{x_L}^{x_R} V^{\nu\nu}(x)\mathrm{d}x\right] + \sum_{\nu \neq \sigma} 2i\epsilon \bar{p}^{\sigma}(z_r) \frac{e^{i(k_\sigma x_r + \pi/4)}}{\left(\frac{\pi}{2} k_\nu k_\sigma\right)^{1/2}} [\bar{p}^{\nu}(0).\bar{F}] \times \int_{x_L}^{x_R} \frac{e^{i(k_\nu - k_\sigma)x}}{(k_\nu(x_r - x) + k_\sigma x)^{1/2}} V^{\sigma\nu}(x)\mathrm{d}x \tag{8.2}$$

Figure 9 defines the geometric variables in this expression. For convenience the modal summation has for once been made explicit. The unconverted waves are taken together with the direct wave. The last term in (8.2) describes the converted waves. The interaction terms are to be evaluated in the forward direction ($\phi = 0$).

From this point on we shall only concern ourselves with the unconverted wave, since the last integral in (8.2) is negligible for a smooth heterogeneity. (This is because of the oscillation of the exponent term in the integrand.) For simplicity the index ν will be suppressed, but it should be kept in mind that a sum over all unconverted modes is implied.

If the heterogeneity is weak, and not too wide, we can approximate

$$1 + \frac{2i\epsilon}{k} \int V(x)\mathrm{d}x = \exp \frac{2i\epsilon}{k} \int V(x)\mathrm{d}x \tag{8.3}$$

so that the only effect of the heterogeneity is a phase shift of the transmitted wave.

If the heterogeneity is weak and smooth, but wide, the interval (x_L, x_R) can be divided in thin subintervals. By increasing the number of these subintervals they can be made arbitrarily thin, so that (8.3) can be used for each subinterval. However, the transmission coefficient of a combination of subintervals is in general not related in a simple way to the transmission coefficients of the subintervals.

Rayleigh (1917) addressed this problem by considering the reflection and transmission in a medium consisting of many layers with equal reflection and transmission coefficients. Let r_n and t_n denote the reflection and transmission coefficient of n of these layers. Rayleigh (1917) showed that in that case

$$t_{n+m} = \frac{t_n t_m}{1 - r_n r_m} \tag{8.4}$$

Therefore the transmission coefficient of the combination of two substacks is the product of the transmission coefficient of each substack, provided the reflection coefficients are small.

For a smooth heterogeneity the reflection coefficients are indeed small (Bretherton, 1968), so that the transmission coefficient of a stack of subintervals is the product of the transmission coefficients of each subinterval. Therefore the phase shifts introduced by each subinterval should be added.

This means that, under the restriction that the heterogeneity is smooth, the (divergent) Born approximation should be replaced by

$$1 + \frac{2i\epsilon}{k} \int_{x_1}^{x_R} V(x)\mathrm{d}x \dashrightarrow \exp \frac{2i\epsilon}{k} \int_{x_1}^{x_R} V(x)\mathrm{d}x \tag{8.5}$$

This renormalisation procedure yields a finite result for a wide and smooth heterogeneity, and is consistent with results from WKBJ theory (Bretherton, 1968). Morse and Feshbach (1953) gave in paragraph 9.3 a rigorous proof of (8.5) for scattering by a potential in the 1-D Schrodinger equation.

9. The partial derivatives of the phase speed with respect to topography

If the expressions (8.2) and (8.5) are combined, the following expression results for the uncon-

verted wave

$$\bar{u}_{\text{unc}}(\bar{r}_r) = \bar{p}(z_r)\frac{\exp i\left[kX + \frac{\pi}{4} + \frac{2}{k}\int_{x_L}^{x_R} V(x)\mathrm{d}x\right]}{\left(\frac{\pi}{2}kx_r\right)^{1/2}} \times [\bar{p}(0).\bar{F}] \qquad (9.1)$$

(The modal summation is not made explicit, and the parameter ϵ is suppressed.) It follows from this expression that the interaction terms V are closely related to the wavenumber perturbation due to the heterogeneity

$$\delta k = \frac{2}{k}V(x) \qquad (9.2)$$

and the relative phase speed perturbation is given by

$$\left[\frac{\delta c}{c}\right] = -\frac{2}{k^2}V(x) \qquad (9.3)$$

These results are derived for a smooth band heterogeneity. However, since the phase speed depends only on the local properties of the medium, these results can be used for an arbitrary medium with heterogeneities which vary smoothly in the horizontal direction.

The interaction terms V contain a contribution of the buried heterogeneities and a contribution of the topography variations. As an example, consider the phase speed perturbation for Rayleigh waves by a buried heterogeneity. In that case V in (9.3) follows from (3.7d) with $\phi = 0$.

$$\left[\frac{\delta c}{c}\right]^R = \frac{1}{4cUI_1}\int \mathrm{d}z\left[-\rho^1\omega^2(r_1^2 + r_2^2) + (kr_1 + \partial_z r_2)^2\lambda^1 + \left(2k^2 r_1^2 + 2(\partial_z r_2)^2 + (kr_2 - \partial_z r_1)^2\right)\mu^1\right] \qquad (9.4)$$

The factor $4cUI_1$ could be added because of the normalisation condition (3.4). Equation 9.4 is equal to expression (7.78) of Aki and Richards (1980), where the Rayleigh-wave phase speed perturbations are calculated with a variational principle. The scattering theory thus produces the same result in a roundabout way, confirming that small variations in the phase speed are treated correctly. For Love waves a similar result can be derived from (3.7a).

Since the interaction terms for topography scattering are known, the partial derivatives of the phase speed with respect to the topography height (h) can be calculated too. For Love waves one finds by inserting (3.10a) (with $\phi = 0$) in (9.3) that

$$\left[\frac{\delta c}{c}\right]^L = -2\rho^0 l_1^2(c^2 - \beta^2)h \qquad (9.5a)$$

while (3.10d) yields for Rayleigh waves

$$\left[\frac{\delta c}{c}\right]^R = -2\rho^0\left[r_2^2c^2 + r_1^2\left(c^2 - 4\left(1 - \frac{\beta^2}{\alpha^2}\right)\beta^2\right)\right]h \qquad (9.5b)$$

In these expressions all variables are to be evaluated at the surface. With the normalisation condition (3.4), this finally gives the partial derivatives of the phase speed with respect of the topography height. For Love waves this leads to

$$\left[\frac{1\partial c}{c\partial h}\right]^L = \frac{-1}{4cUI_1}\rho^0 l_1^2(c^2 - \beta^2) \quad (z = 0) \qquad (9.6a)$$

and for Rayleigh waves

$$\left[\frac{1\partial c}{c\partial h}\right]^R = \frac{-1}{4cUI_1}\rho^0\left[r_2^2c^2 + r_1^2\left(c^2 - 4\left(1 - \frac{\beta^2}{\alpha^2}\right)\beta^2\right)\right] \quad (z = 0) \qquad (9.6b)$$

The partial derivatives of the phase speed with respect to topography height are shown in Fig. 10 for the fundamental modes, calculated with the

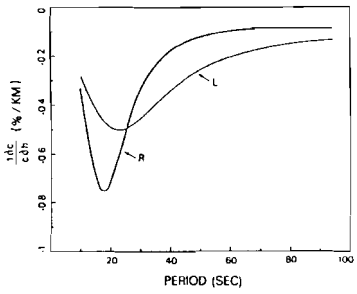

Fig. 10. Phase speed derivative with respect to topography for the fundamental Love mode (L) and for the fundamental Rayleigh mode (R).

M7 model of Nolet (1977). It can be seen that the effect of topography on the phase speed is largest for periods of about 20 s. For large periods the penetration depth of the surface waves is so large that the topography has little effect. For short periods the surface waves only sample the top layer. In that case, a thickening of the top layer by topography does not influence the phase speed.

The relative phase speed perturbation for a topography of 1 km is of the order of 0.5%. This means that for realistic values of the topography (up to several kilometers) this effect cannot be ignored. Since the topography is in general well known, this effect can easily be taken into account in inversions using phase speed observations (Nolet, 1977; Cara et al., 1980; Panza et al., 1980).

10. Summary

Surface-wave scattering by topography can be incorporated in the linearised surface-wave scattering formalism of paper 1. An error analysis shows, however, that for realistic values of the large scale topography (1–5 km) the theory breaks down for periods shorter than 15 s. Furthermore, steep slopes cannot be handled by the theory.

The radiation pattern for scattering by topography shows that the scattering in the forward direction is relatively weak. A comparison with the radiation pattern for a 'mountain root model' shows that scattering by topography, and scattering by a mountain root in general enhance each other. The reason for this is that both effects lead to a thickening of the crustal waveguide.

For scattering by an extended heterogeneity, interference effects between waves radiated from different parts of the scatterer lead to an enhancement of the forward scattering (Mie effect). Furthermore, these interference effects lead to a relative weakening of the interaction of the fundamental mode with the higher modes, compared to the interactions among the fundamental modes.

For a heterogeneity which is smooth in the horizontal direction a relation is established between the interaction terms and the variations in the phase speed. The partial derivatives of the phase speed with respect to the medium parameters, as they are known from variational principles, can be obtained from the scattering theory too. In an analogous way the partial derivatives of the phase speed with respect to topography are obtained.

This is important for the efficient calculation of surface-wave seismograms, and for applying travel-time corrections for the topography. Furthermore, the phase-speed variations due to topography could cause surface-wave focussing and defocussing effects. Ray-tracing techniques, as developed by Gjevik (1974), Babich et al. (1976) or Gaussian beams (Yomogida and Aki, 1985), could be used to investigate this.

The equivalence between topography and surface perturbations of the medium parameters shows that (in this approximation) the inverse problem has a non-unique solution. This poses no problems for the holographic inversion scheme presented in paper 1, since the topography is in general well known. Therefore the surface waves scattered by the topography can be calculated, and subtracted from the recorded surface waves. The remaining scattered surface waves are scattered by the heterogeneity under the topography, so that given enough data the inversion scheme of paper 1 could be used to map the heterogeneity under the topography.

Acknowledgement

I thank Guust Nolet both for providing the context for this research, and for his help and advice.

Appendix

Surface perturbations of medium parameters

Suppose that the density and the elastic parameters are perturbed all the way up to the surface, but that there is a flat topography ($h = 0$). As shown in paper 1 the scattered wave satisfies in the interior

$$L^0\bar{u}^1 = -L^1\bar{u}^0 \qquad \text{(A1)}$$

Linearising the boundary condition (2.3-4) yields for the perturbed quantities at $z = 0$

$$n_i c^0_{ijkl} \partial_k u^1_l = -n_i c^1_{ijkl} \partial_k u^0_l \qquad \text{(A2)}$$

The r.h.s. of (A1) can be considered as a surface traction exciting the scattered wave. With a representation theorem (Aki and Richards, 1980), (A1) and (A2) can be solved for $\bar{u}^1$

$$u^1_i(\bar{r}) = -\int G_{ij}(\bar{r}, \bar{r}') L^1_{jk}(\bar{r}') u^0_k(\bar{r}') \mathrm{d}V' - \int G_{ij}(\bar{r}, \bar{r}') n^0_m c^1_{mjnk}(\bar{r}') \partial_n u^0_k(\bar{r}') \mathrm{d}S' \qquad \text{(A3)}$$

Using the representation (2.2) for L^1, (2.6) for the direct wave, and applying a partial integration leads to

$$\begin{aligned} u^1_i(\bar{r}) = & \int G_{ij}(\bar{r}, \bar{r}') \rho^1(\bar{r}') \omega^2 G_{jl}(\bar{r}', \bar{r}_s) F_l(\bar{r}_s) \mathrm{d}V' \\ & - \int \left(\partial_m G_{ij}(\bar{r}, \bar{r}')\right) c^1_{jmnk}(\bar{r}') \\ & \times \left(\partial_n G_{kl}(\bar{r}', \bar{r}_s)\right) F_l(\bar{r}_s) \mathrm{d}V' \\ & + \int n^0_m G_{ij}(\bar{r}, \bar{r}') c^1_{jmnk}(\bar{r}') \\ & \times \left(\partial_n G_{kl}(\bar{r}', \bar{r}_s)\right) F_l(\bar{r}_s) \mathrm{d}S' \\ & - \int n^0_m G_{ij}(\bar{r}, \bar{r}') c^1_{mjnk}(\bar{r}') \\ & \times \left(\partial_n G_{kl}(\bar{r}', \bar{r}_s)\right) F_l(\bar{r}_s) \mathrm{d}S' \end{aligned} \qquad \text{(A4)}$$

The third term denotes the 'surface terms' which have been suppressed in paper 1 by considering only buried scatterers. As it turns out, this term is cancelled by the last term in (A4), which is the contribution to the scattered wave from the perturbed boundary conditions (A2). (This follows from the symmetry properties of the elasticity tensor: $c_{jmnk} = c_{mjnk}$.) Therefore only the volume terms in (A4) contribute, and surface perturbations of the medium can be allowed without any modification.

References

Abramowitz, M. and Stegun, I.A., 1970. Handbook of Mathematical Functions. Dover Publications, New York.

Aki, K. and Richards, P.G., 1980. Quantitative Seismology, volume 1. Freeman, San Francisco.

Babich, V.M., Chikhachev, B.A. and Yanovskaya, T.B., 1976. Surface waves in a vertically inhomogeneous halfspace with a weak horizontal inhomogeneity. IZV Phys. Earth, 12: 242-245.

Baumgardt, D.R., 1985. Comparative analysis of teleseismic P-Coda and Lg waves from underground nuclear explosions in Eurasia. Bull. Seismol. Soc. Am., 74: 1087-1104.

Born, M. and Wolf, E., 1959. Principles of Optics. Pergamon Press, New York.

Bretherton, F.B., 1968. Propagation in slowly varying waveguides. Proc. R. Soc., A302: 555-576.

Bullit, J.T. and Toksoz, M.N., 1985. Three dimensional ultrasonic modeling of Rayleigh wave propagation. Bull. Seismol. Soc. Am., 74: 1087-1104.

Bungum, H. and Capon, J., 1974. Coda pattern and multipathing propagation of Rayleigh waves at NORSAR. Phys. Earth Planet. Inter., 9: 111-127.

Cara, M., Nercessian, A. and Nolet, G., 1980. New inferences from higher mode data in western Europe and northern Asia. Geophys. J.R. Astron. Soc., 61: 459-478.

Gilbert, F. and Knopoff, L., 1960. Seismic scattering from Topographic irregularities. J. Geophys. Res., 65: 3437-3444.

Gjevik, B., 1974. Ray tracing for seismic surface waves. Geophys. J.R. Astron. Soc., 39: 29-39.

Greenfield, R.J., 1971. Short-period P-wave generation by Rayleigh-wave scattering at Novaya Zemlya. J. Geophys. Res., 76: 7988-8002.

Harvey, D.J., 1981. Seismogram synthesis using normal mode superposition: the locked mode approximation. Geophys. J.R. Astron. Soc., 66: 37-70.

Herrera, I., 1964. A perturbation method for elastic wave propagation. J. Geophys. Res., 69: 3845-3851.

Hudson, J.A., 1967. Scattered surface waves from a surface obstacle. Geophys. J.R. Astron. Soc., 13: 441-458.

Hudson, J.A., 1977. Scattered waves in the Coda of P. J. Geophys., 43: 359-374.

Hudson, J.A. and Boore, D.M., 1980. Comments on 'Scattered surface waves from a surface obstacle' by J.A. Hudson. Geophys. J.R. Astron. Soc., 60: 123-127.

Hudson, J.A. and Heritage, J.R., 1982. The use of the Born approximation in seismic scattering problems. Geophys. J.R. Astron. Soc., 66: 221-240.

Levshin, A. and Berteussen, K.A., 1979. Anomalous propagation of surface waves in the Barentz Sea as inferred from NORSAR recordings. Geophys. J.R. Astron. Soc., 56: 97-118.

Morse, P.M. and Feshbach, H., 1953. Methods of Theoretical Physics. McGraw-Hill, New York.

Mueller, S. and Talwani, M., 1971. A crustal section across the Eastern Alps based on gravity and seismic refraction data. Pure Appl. Geophys., 85: 226-239.

Nayfeh, A.H., 1973. Perturbation Methods. Wiley, New York.

Nolet, G., 1977. The upper mantle under western Europe inferred from the dispersion of Rayleigh modes. J. Geophys., 43: 265-285.

Panza, G.F., Mueller, S. and Colcognile, G., 1980. The gross features of the Lithosphere–Asthenosphere system in Europe from seismic surface waves and body waves. Pure Appl. Geophys., 118: 1209–1213.

Rayleigh, Lord, 1917. On the reflection of light from a regularly stratified medium. Proc. R. Soc. London, A93: 565–577.

Sabina, F.J. and Willis, J.R., 1975. Scattering of SH waves by a rough half-space of arbitrary slope. Geophys. J.R. Astron. Soc., 42: 685–703.

Sabina, F.J. and Willis, J.R., 1977. Scattering of Rayleigh waves by a ridge. Geophys. J.R. Astron. Soc., 42: 685–703.

Sanchez-Sesma, F.J., 1983. Diffraction of elastic waves by three-dimensional surface irregularities. Bull. Seismol. Soc. Am., 73: 1621–1636.

Snieder, R., 1986. 3D Linearized scattering of surface waves and a formalism for surface wave holography. Geophys. J.R. Astron. Soc., 84: 581–605.

Snieder, R. and Nolet, G. Linearized scattering of elastic waves on a laterally inhomogeneous sphere, in preparation.

Steg, R.G. and Klemens, P.G., 1974. Scattering of Rayleigh waves by surface defects. J. Appl. Phys., 45: 23–29.

Woodhouse, J.H., 1974. Surface waves in a laterally varying layered structure. Geophys. J.R. Astron. Soc., 37: 461–490.

Woodhouse, J.H. and Dahlen, F.A., 1978. The effect of a general aspherical perturbation on the free oscillations of the Earth. Geophys. J. R. Astron. Soc., 53: 335–354.

Yomogida, K. and Aki, K., 1985. Waveform synthesis of surface waves in a laterally heterogeneous Earth by Gaussian beam method. J. Geophys. Res., B9: 7665–7689.

Chapter 4

A field experiment for image reconstruction

This chapter is published as:

Snieder, R., Surface wave holography, in *Seismic tomography, with applications in global seismology and exploration geophysics,* edited by G. Nolet, pp. 323-337, Reidel, Dordrecht, 1987.

Chapter 14

Surface wave holography

R. Snieder

1. Introduction

Surface waves have proven to be very useful in determining the properties of the Earth's crust and mantle. The traditional surface wave analysis consists of two steps. First, from surface wave recordings, dispersion data (phase velocities or group velocities) are retrieved for each source receiver pair (Dziewonski and Hales, 1972; Nolet, 1977). Next, the information for different frequencies and many source receiver pairs is combined to yield an image of the Earth's interior (e.g. Woodhouse and Dziewonski, 1984; Montagner, 1986; Nataf et al., 1986). These methods implicitly use ray theory by resorting to the "great circle theorem" (Backus, 1964; Jordan, 1978; Dahlen, 1979). This theorem states that for a sufficiently smooth medium the surface wave data are only influenced by the structure under the great circle joining the source and the receiver. The great circle theorem is acceptable provided the inhomogeneity varies little on the scale of the wavelength of the surface waves.

It turns out, however, that this condition is often violated in realistic situations. A Rayleigh wave with a period of 20 seconds has a horizontal wavelength of about 70 kilometers. It is well known that, especially in continents, the lateral heterogeneity on this scale can be considerable. In fact, the models constructed from surface wave data using the great circle theorem sometimes vary strongly on a distance of one wavelength (Panza et al., 1980). In that case the constructed model is inconsistent with the ray theory used for producing the model. It is clear that in these situations one has to resort to a more complete wave theory which takes surface wave scattering and reflection into account. Since these effects are most sensitive to the horizontal *gradient* in the Earth's structure, scattered

G. Nolet (ed.), Seismic Tomography, 323–337.

surface waves could provide valuable independent information on the structure of the Earth.

Surface wave scattering and reflection can be treated analytically in two dimensions (Kennett, 1984), but for three dimensional surface wave scattering no analytical solutions are available. In that case one either has to use numerical methods, or make some simplifying assumptions. The Born approximation has been used successfully for describing surface wave scattering in three dimensions (Snieder, 1986ab). A brief outline of this theory is presented in section 2. The Born approximation gives a linear relation between the scattered waves and the heterogeneity. This situation is closely analogous to the wave theories forming the basis of modern migration schemes in exploration geophysics (Clayton and Stolt, 1981; Tarantola, 1984ab; Bleistein et al., 1985; Bleistein and Gray, 1985; Ikelle et al., 1986).

It is therefore not surprising that an inversion scheme using scattered surface waves can be formulated along similar lines. In section 3 it is shown that this scheme can be derived using a least squares criterion, as in Tarantola (1984ab). Without making additional simplifying assumptions the resulting inversion scheme isn't very manageable. It is shown in section 4 how some simplifications result in a workable scheme for reconstructing an inhomogeneity using scattered surface waves. The resulting reconstruction method is similar to holographic techniques used in optics.

In order to check if the method works with real data, a field experiment was conducted on a tidal flat, where surface waves were reflected by a dam. The results for this inversion are presented in section 5. A field experiment, as presented here, is an ideal tool for testing the feasibility of abstract mathematical inversion schemes.

In this chapter the summation convention is used throughout for vector and tensor indices. The dot product which is used is defined by

$$[\mathbf{p}.\mathbf{q}] \equiv p_i^* q_i . \tag{1.1}$$

2. Linearized theory for surface wave scattering

The equation of motion combined with the equations for linear elasticity lead to the following expression for the displacement field in the frequency domain

$$L_{ij} u_j = F_i \tag{2.1}$$

where the differential operator L is defined by

$$L_{ij} = -\rho\omega^2 \delta_{ij} - \partial_n c_{inmj} \partial_m \tag{2.2}$$

and **F** is the point force which excites the wavefield.

Now suppose that the elastic medium (i.e., the density and the elasticity tensor) can be decomposed as follows:

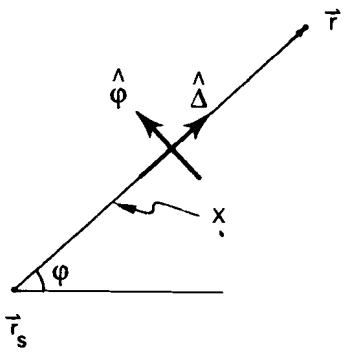

Figure 1 Definition of the geometric variables for the direct wave.

$$\rho(x,y,z) = \rho^0(z) + \rho^1(x,y,z) \tag{2.3.a}$$

$$\underline{c}(x,y,z) = \underline{c}^0(z) + \underline{c}^1(x,y,z). \tag{2.3.b}$$

This means that the medium is viewed here as a laterally homogeneous reference medium, with heterogeneities superposed on it. This decomposition suggests the following decomposition of the displacement

$$\mathbf{u} = \mathbf{u}^0 + \mathbf{u}^1. \tag{2.4}$$

$\mathbf{u}^0$ is the displacement in the laterally homogeneous reference medium, this term is usually called the direct wave. $\mathbf{u}^1$ describes the effect of inhomogeneities, this term is usually labelled the scattered wave.

In order to derive expressions for $\mathbf{u}^0$ and $\mathbf{u}^1$ it is convenient to introduce the surface wave polarization vectors. For Love waves the polarization vector is

$$\mathbf{p}^\nu(z,\phi) = l_1^\nu(z)\,\hat{\phi} \tag{2.5.a}$$

and for Rayleigh waves

$$\mathbf{p}^\nu(z,\phi) = r_1^\nu(z)\,\hat{\Delta} + i r_2^\nu(z)\,\hat{\mathbf{z}}. \tag{2.5.b}$$

In this chapter Greek indices are used to label the surface wave modes. A summation over these indices indicates a summation over both Love waves and Rayleigh waves, thus treating both kinds of waves in an unified way. The unit vectors $\hat{\Delta}$, $\hat{\phi}$ and $\hat{\mathbf{z}}$ point respectively in the radial, transverse and down direction, see figure 1. The functions $l_1^\nu(z)$, $r_1^\nu(z)$ and $r_2^\nu(z)$ are the surface wave eigenfunctions as defined in Aki and Richards (1980). These eigenfunctions are assumed to be normalized according to:

$$8 c_\nu U_\nu I_1^\nu = 1 \tag{2.6}$$

U_ν and c_ν are the group and phase velocity of the mode under consideration, and I_1^ν is the kinetic energy integral (Aki and Richards, 1980).

The far field surface wave Green's function of the laterally homogeneous reference medium can conveniently be expressed as a dyad of the polarization vectors. As shown in

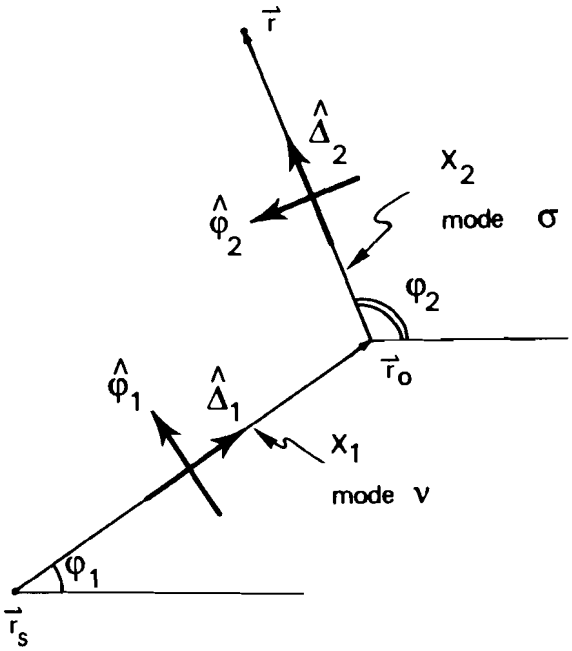

Figure 2. Definition of the geometric variables for the scattered wave.

Snieder (1986a), this leads to the following far field expression for the direct wave in the frequency domain

$$\mathbf{u}^0(\mathbf{r}) = \sum_\nu \mathbf{p}^\nu(z,\phi) \frac{\exp i(k_\nu X + \frac{\pi}{4})}{(\frac{\pi}{2} k_\nu X)^{1/2}} [\mathbf{p}^\nu(z_s,\phi).\mathbf{F}] \tag{2.7}$$

see figure 1 for the definition of the geometric variables. It is assumed here that the wavefield is excited by a point force $\mathbf{F}$ at location $\mathbf{r}_s$. Note that the direct wave is written as a superposition of modes (Love waves and Rayleigh waves), and that the modes don't interact with each other. Using the Born approximation, one can show that for sufficiently weak scatterers the scattered wave in the frequency domain is given by

$$\mathbf{u}^1(\mathbf{r}) = \sum_{\sigma,\nu} \iint \mathbf{p}^\sigma(z,\phi_2) \frac{\exp i(k_\sigma X_2 + \frac{\pi}{4})}{(\frac{\pi}{2} k_\sigma X_2)^{1/2}} V^{\sigma\nu}(x_0,y_0) \frac{\exp i(k_\nu X_1 + \frac{\pi}{4})}{(\frac{\pi}{2} k_\nu X_1)^{1/2}} [\mathbf{p}^\nu(z_s,\phi_1).\mathbf{F}]\, dx_0 dy_0 \tag{2.8}$$

see figure 2 for the definition of geometric variables. This expression is derived in Snieder (1986a) for buried scatterers in an isotropic medium. It is shown in Snieder (1986b) that scattering due to surface topography can also be described by (2.8). Reading (2.8) from right to left, one follows the "life history" of the scattered wave. At the source (in $\mathbf{r}_s$), mode

ν is excited by the projection of the point force $\mathbf{F}$ on the polarization vector $\mathbf{p}^{\nu}$. Then, a propagation to the scatterer occurs. This gives a phase shift and amplitude decay due to geometrical spreading, described by the term $\exp i(k_{\nu}X_1+\frac{\pi}{4})/(\frac{\pi}{2}k_{\nu}X_1)^{1/2}$. At the scatterer (in $\mathbf{r}_0$), scattering and mode conversion occurs. This is described by the interaction terms $V^{\sigma\nu}$. This term gives the coupling between the incoming mode ν, and the outgoing mode σ. After this, the mode σ propagates to the receiver, which is shown by another propagator term. Finally, the oscillation at the receiver (in $\mathbf{r}$) is described by the polarization vector $\mathbf{p}^{\sigma}$. An integration over the scatterer, and a summation over all outgoing and incoming modes (σ,ν) superposes the different parts of the scattered waves $\mathbf{u}^1$.

The interaction terms $V^{\sigma\nu}$ are a linear function of the perturbations in the density (ρ^1), the Lame parameters (λ^1 and μ^1), and the surface topography h. It can explicitly be seen that in (2.8) a single scattering approximation is used, since the interaction terms appear only once. For buried inhomogeneities the interaction terms are given in Snieder (1986a), while the interaction terms due to surface topography are derived in Snieder (1986b). For example, the Love wave-Love wave interaction for buried heterogeneities is given by

$$V_{LL}^{\sigma\nu} = \int \left[(l_1^{\sigma} l_1^{\nu} \rho^1 \omega^2 - (\partial_z l_1^{\sigma})(\partial_z l_1^{\nu})\mu^1) \cos\phi - k_{\sigma} k_{\nu} l_1^{\sigma} l_1^{\nu} \mu^1 \cos 2\phi \right] dz. \qquad (2.9)$$

In this expression $\phi=\phi_2-\phi_1$ is the scattering angle, and k_{ν} is the wavenumber of mode ν. The interaction terms are a very simple function of the scattering angle ϕ.

At this point we can already conclude that in inversions using scattered surface waves, we can only obtain information of the scatterers through the interaction terms $V^{\sigma\nu}$. Information at different frequencies (and possibly different modes) is needed to obtain the depth dependence of the inhomogeneities. The dependence of $V^{\sigma\nu}$ on the scattering angle can in principle be used to unravel the contributions from the density and the Lame parameters.

The theory is presented here for a point force excitation in a plane geometry. The excitation by a moment tensor is discussed in Snieder (1986a), and the formulation of this theory in a spherical geometry is shown in Snieder and Nolet (1987). In both cases only minor changes in the theory have to be made.

3. A formalism for surface wave holography

Scattered surface waves can be used to map the inhomogeneities in the Earth. The theory in the previous section is linear(ized), therefore least squares inversion techniques can conveniently be used for this. Least squares inversion for variables depending continuously on one or more space variables has been discussed in detail by Tarantola and Valette (1982). Suppose we want to find the following model vector

$$\mathbf{m}(\mathbf{r}) = \begin{bmatrix} \rho^1(\mathbf{r}) \\ \lambda^1(\mathbf{r}) \\ \mu^1(\mathbf{r}) \end{bmatrix} \qquad (3.1)$$

and suppose we describe the a-priori knowledge of the heterogeneity with the vector $\mathbf{m}_0(\mathbf{r})$.

Let the vector **u** denote all available data in the time domain. With "data" we mean here the difference between the recorded signals, and the synthetics produced by the a-priori model $\mathbf{m}_0(\mathbf{r})$. We shall assume here that the a-priori model is zero ($\mathbf{m}_0(\mathbf{r})=0$). This means that the data (**u**) consist of the difference between the recorded signals, and the synthetic seismograms of the laterally homogeneous reference medium.

The inversion scheme of Tarantola and Valette (1982) requires the a-priori covariances of the model ($C_m(\mathbf{r},\mathbf{r}')$), and of the data ($C_u$). If the a-priori cross covariances between the model and the data (C_{um}) are assumed to vanish, the least squares solution of the model is given by (Tarantola, 1984a):

$$\mathbf{m} = \mathbf{M}^{-1}\, \mathbf{C}_m\, \mathbf{G}^T\, \mathbf{C}_u^{-1}\, \mathbf{u} \tag{3.2}$$

with

$$\mathbf{M} = \mathbf{C}_m\, \mathbf{G}^T\, \mathbf{C}_u^{-1}\, \mathbf{G} + \mathbf{I} \tag{3.3}$$

and G is the gradient of the data with respect to the model parameters.

In principle, (3.2) can be used to compute the model $\mathbf{m}(\mathbf{r})$ at every point in three dimensional space. In practice one shouldn't be too optimistic about a straightforward use of (3.2), since three different kinds of inversion are implied in (3.2):

[1] The surface wave energy should be focussed in the horizontal directions on the scatterers.

[2] The contribution of the three parameters ρ^1, μ^1 and λ^1 should be unraveled.

[3] The depth dependence of these parameters should be reconstructed.

It shall be clear that with band limited, noisy data for a limited range of scattering angles, the goals [2] and [3] can never be fully reached. As a simplification it is therefore appropriate to expand the depth dependence of ρ^1, μ^1 and λ^1 in a suitably chosen set of basis functions $\mathbf{b}_p(z)$. The subscripts p and q are used throughout this chapter to denote these basisfunctions. The basisfunctions are used to parameterize the depth dependence of the heterogeneity, and to separate the contributions from ρ^1, μ^1 and λ^1. From now on, we assume that the inhomogeneity can be decomposed as follows

$$\mathbf{m}(\mathbf{r}) = \sum_p h_p(\mathbf{x})\, \mathbf{b}_p(z) \tag{3.4}$$

and the aim of the inversion is to reconstruct the fields $h_p(\mathbf{x})$. The vector **x** shall be used to denote the horizontal components of **r** ($\mathbf{x}\equiv\mathbf{r}-(\mathbf{r}.\hat{\mathbf{z}})\hat{\mathbf{z}}$) this convention will be followed throughout this chapter.

In order to obtain a workable formalism, more notation needs to be introduced. A superscript "rs" shall be used to denote the source receiver pair which is considered, thus $u^{rs}(t)$ is the time signal of the recorded scattered surface wave for source "s" and receiver "r". Furthermore, let the synthetic seismogram for source receiver pair "rs", basis function $\mathbf{b}_p(z)$ and a scatterer at location **x** be denoted by $s_p^{rs}(\mathbf{x},t)$. Since the theory is linear, this synthetic seismogram is precisely the contribution of source receiver pair "rs" to the gradient (G) of the data at location **x** and basisfunction p.

Now let us assume that the data are uncorrelated, but that the autocorrelation of different seismograms may be different

$$C_u^{rs,r's'}(t,t') = \delta_{r,r'}\delta_{s,s'}\delta(t-t')\sigma_{rs}^2 \tag{3.5}$$

Inserting this in (3.2-3), and working out the implied operator products yields

$$h_p(\mathbf{x}) = \sum_{p_1,p_2} \int d^2x_1 \int d^2x_2\, M_{pp_1}^{-1}(\mathbf{x},\mathbf{x}_1)\, C_{m,p_1p_2}(\mathbf{x}_1,\mathbf{x}_2)\, H_{p_2}(\mathbf{x}_2) \tag{3.6}$$

where

$$H_p(\mathbf{x}) = \sum_{rs} \frac{1}{\sigma_{rs}^2} \int s_p^{rs}(\mathbf{x},t)\, u^{rs}(t)\, dt \tag{3.7}$$

and

$$M_{pq}(\mathbf{x},\mathbf{x}') = \sum_{p_1} \int d^2x_1\, C_{m,pp_1}(\mathbf{x},\mathbf{x}_1) \sum_{rs} \frac{1}{\sigma_{rs}^2} \int s_{p_1}^{rs}(\mathbf{x}_1,t)\, s_q^{rs}(\mathbf{x}',t)\, dt + \delta_{pq}\delta(\mathbf{x}-\mathbf{x}'). \tag{3.8}$$

It can be seen from (3.6) that the inversion consist of three steps. The data ($u^{rs}(t)$) enter the inversion through the "holography term" $H_p(\mathbf{x})$. After this, an integration with the model covariance (C_m) is performed. Finally, a contraction with the inverse operator M^{-1} completes the inversion. Now let us focus on the holography term (3.7).

This term can be interpreted most easily by converting (3.7) to a frequency integral using Parseval's theorem (Butkov, 1968). Inserting (2.8) for the synthetic seismogram $s_p^{rs}(\mathbf{x},\omega)$ we get

$$H_p(\mathbf{x}) = \frac{1}{2\pi} \sum_{rs} \int d\omega \sum_{\sigma,\nu} [\mathbf{u}^{rs}.\mathbf{p}^{\sigma}(z_r)] \frac{\exp i(k_\sigma X_2 + \frac{\pi}{4})}{(\frac{\pi}{2} k_\sigma X_2)^{1/2}} V_p^{\sigma\nu}(\mathbf{x}) \frac{\exp i(k_\nu X_1 + \frac{\pi}{4})}{(\frac{\pi}{2} k_\nu X_1)^{1/2}} [\mathbf{p}^{\nu}(z_s)\cdot\mathbf{F}] \tag{3.9}$$

It is understood that all quantities at the right hand side are evaluated in the frequency domain, and that the geometric variables are to be considered for each source receiver pair separately. The interaction terms $V_p^{\sigma\nu}(\mathbf{x})$ are for scattering (and conversion) by basis function $\mathbf{b}_p(z)$ at location $\mathbf{x}$. Equation (3.9) can be interpreted by considering the terms on the left and on the right of the interaction matrix. The term $\exp i(k_\nu X_1 + \frac{\pi}{4})/(\frac{\pi}{2} k_\nu X_1)^{1/2}\ [\mathbf{p}^{\nu}(z_s).\mathbf{F}]$ describes the waves excited by the point force $\mathbf{F}$, which travel to the scatterer. In optics this term would be called "the illumination", since this term describes how much energy emanating from the source reaches the scatterer. The term $[\mathbf{u}^{rs}.\mathbf{p}^{\sigma}(z_r)]\ \exp i(k_\sigma X_2 + \frac{\pi}{4})/(\frac{\pi}{2} k_\sigma X_2)^{1/2}$ can be interpreted as the backpropagation of the data $\mathbf{u}^{rs}$, into the medium. This can most easily be understood by noting the symmetry in (3.9) in the excitation $\mathbf{F}$ and the data $\mathbf{u}^{rs}$. The holographic term (3.9) depends on the correlation between the illumination and the backpropagated signal. A summation over all source receiver pairs completes this term. This procedure is similar to holographic techniques in optics, where an image is reconstructed using the interference between the

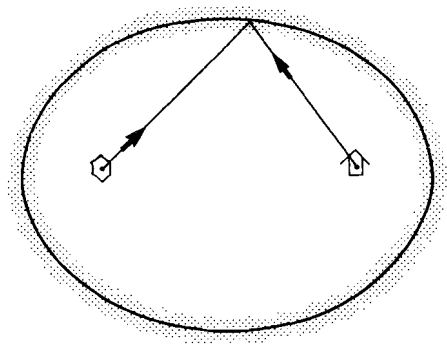

Figure 3. Ellipsoidal area over which the contribution of one source-receiver pair to the holographic term (3.7) is spread out in the absence of mode conversions.

illumination, and the light which has (back)propagated from the hologram to the area of reconstruction.

This holographic reconstruction procedure amounts to smearing out the recorded scattered energy over ellipses, or egg shaped curves in the medium. For instance, if mode conversions are absent, the recorded scattered wave for one source receiver pair is smeared out over an ellipse with the source and the receiver as focal points (figure 3). Using many different source receiver pairs, these ellipses are superposed to reconstruct the heterogeneity. Virtually all migration schemes used in exploration seismics use the same principle (either explicitly or implicitly). Insufficient data, or an inadequate reference model for the propagation leads to an imperfect reconstruction, producing the characteristic "smiles" in migrated seismic sections (Berkhout, 1984, chapter 5).

After applying the holographic operator in (3.6), an integration with the model covariance C_m is to be applied. This covariance operator makes it possible to impose a-priori knowledge on the spatial scale of variation in the medium. The integration over $\mathbf{x}_2$ with this operator implies a smoothing of the holographic image. One should be careful not to apply too much smoothing. The reason for this is that the scattering effects are most sensitive to the horizontal gradients of the inhomogeneities. Smoothing scatterers over one wavelength of the surface waves eliminates virtually all scattering effects. Therefore it is crucial to allow sufficiently horizontal abrupt variations of the inhomogeneities.

The last step in the inversion (3.6) entails the inversion of the operator M (3.8). After discretizing the model in cells, this inversion amounts to inverting a huge matrix. The matrix is in general very large, since the cell size should be much smaller than a wavelength. In order to do an inversion on a continental scale using surface waves with periods less than 100 seconds, several thousands of cells are required. A direct inversion of such a matrix is not feasible, but iterative techniques such as steepest descent, or conjugate gradients can be used for this, see chapter 1.2. Alternatively, one can complete the reconstruction (3.6) by making strongly restricting assumptions on the matrix M, which allows for a more convenient, but less accurate inversion of this matrix.

4. A simplified reconstruction procedure

In this section a simplified version of the reconstruction (3.6) is proposed. It is assumed that the heterogeneity can be described by one basisfunction $\mathbf{b}_p(z)$ and the subscript "p" is therefore dropped. Furthermore, it is assumed that the heterogeneity has a zero correlation length

$$C_m(\mathbf{x},\mathbf{x}') = \sigma_m^2\, \delta(\mathbf{x}-\mathbf{x}') \tag{4.1}$$

and that all data have the same covariance σ_u^2. Lastly, and this is the most restricting assumption, we ignore the off-diagonal elements of the operator $M(\mathbf{x},\mathbf{x}')$. In this approximation

$$h(\mathbf{x}) = M^{-1}(\mathbf{x},\mathbf{x})\, H(\mathbf{x}) \tag{4.2}$$

with

$$M(\mathbf{x},\mathbf{x}) = 1 + \frac{\sigma_m^2}{\sigma_u^2} \sum_{rs} \int s^{rs}(\mathbf{x},t)^2\, dt. \tag{4.3}$$

Assuming the operator M to be diagonal means that one assumes that for each point $\mathbf{x}$, all the scattered waves for all source receiver pairs are generated by a single scatterer at location $\mathbf{x}$. This assumption clearly breaks down when different scatterers collectively generate scattered waves for all source receiver pairs. In that case (4.2-3) cannot be expected to give results which are quantitatively correct. However, it is shown in section 5 that this simplifying assumption is able to produce qualitatively meaningful results. In fact, many migration schemes used in exploration geophysics implicitly use this assumption. (As an alternative, the system (3.2-3) could be solved iteratively, as shown in Tarantola (1984ab). In that case the substitution (4.3) specifies a preconditioning parameter for the iterative inversion (Tarantola, 1984c), and the final model is insensitive to the choice of this parameter. An explicit inversion of the operator M can then be avoided.)

Combining (3.7) and (4.2-3) the image reconstruction is in this approximation

$$h(\mathbf{x}) = \frac{\sum_{rs} \int s^{rs}(\mathbf{x},t)\, u^{rs}(t)\, dt}{\frac{\sigma_u^2}{\sigma_m^2} + \sum_{rs} \int s^{rs}(\mathbf{x},t)^2\, dt} \tag{4.4}$$

The numerator is simply the holographic term. The denominator contains two terms. The autocorrelation of the synthetic seismograms in the denominator serves to normalize the reconstructed heterogeneity. The σ_u^2/σ_m^2 term serves to suppress the contaminating influence of noise.

It is shown in Snieder (1986ab) that the radiation pattern for surface wave scattering usually has one or more nodes. For one source receiver pair, near a node of the radiation pattern, the autocorrelation of the synthetic seismograms in the denominator approaches zero faster than crosscorrelation in the numerator. This might lead to a numerical instability. The regularization term σ_u^2/σ_m^2 damps this instability.

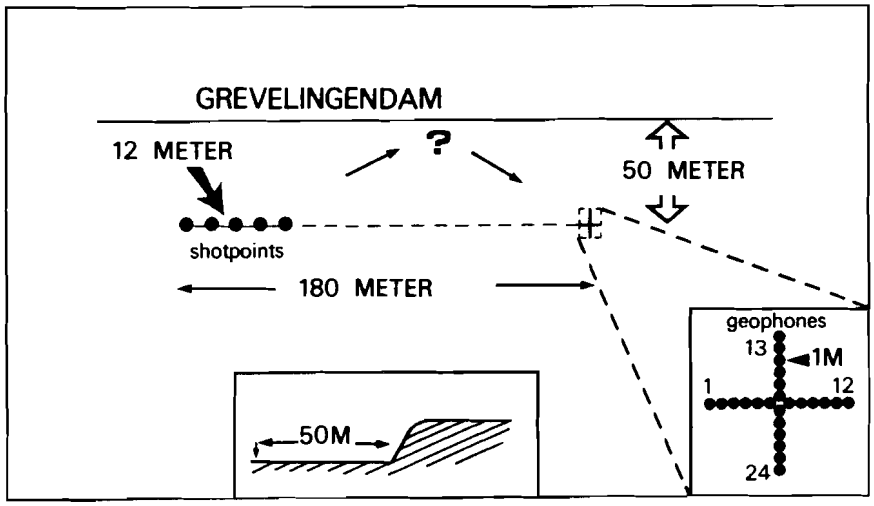

Figure 4. Layout of the field experiment.

5. A field experiment for image reconstruction with scattered surface waves

A field experiment was carried out in order the test the feasibility of surface wave holography. Surface wave measurements were done on a tidal flat in the Netherlands. A cross shaped array of 24 (10 Hz.) geophones was placed 50 meters from a concrete dam (the "Grevelingendam"). A weight drop source (of 30 kg.) was used to generate surface waves at several locations 50 meters from the dam, see figure 4. A description of the field equipment is given by Doornenbal and Helbig (1983). The reference model $(\rho_0(z), \mu_0(z), \lambda_0(z))$ used in the inversion was determined using standard surface wave dispersion analysis, using the fundamental Rayleigh modes and five higher modes (Gabriels et al., 1987).

An example of the geophone records for one shotpoint is shown in figure 5. Note the relatively strong higher mode signal before the arrival of the fundamental mode. It can be seen that the direct fundamental mode arrives simultaneously at the geophones on the transverse leg of the array (geophone 13-24), confirming that this wave propagates parallel to the dam. After this, the scattered fundamental mode arrives. On both the parallel (geophone 1-12), and the transverse (geophone 13-24) leg of the array this wave has a slanted lineup, indicating that this part of the signal comes from the direction of the dam. In this inversion the signal was muted until just after the arrival of the direct fundamental mode, so that only the scattered fundamental Rayleigh mode was used in the inversion.

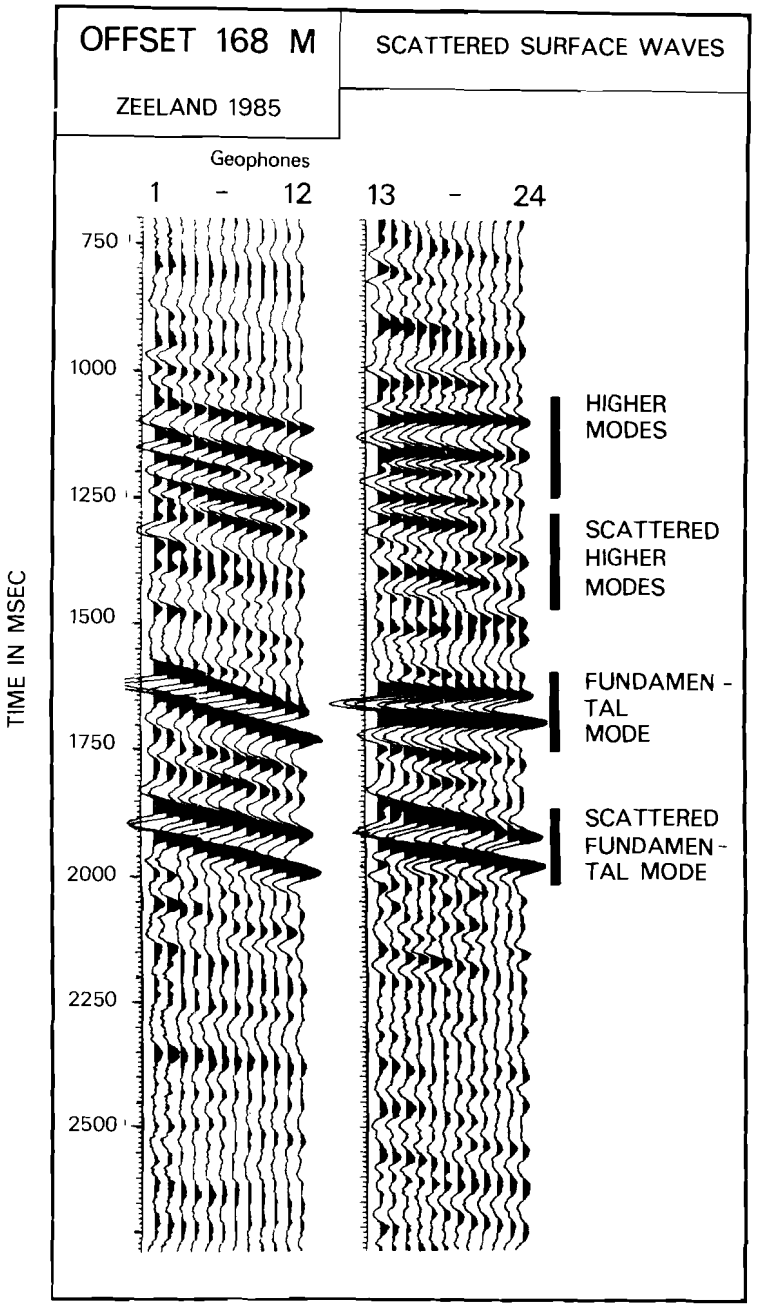

Figure 5. Field record for a shotpoint 168 meters from the geophone array.

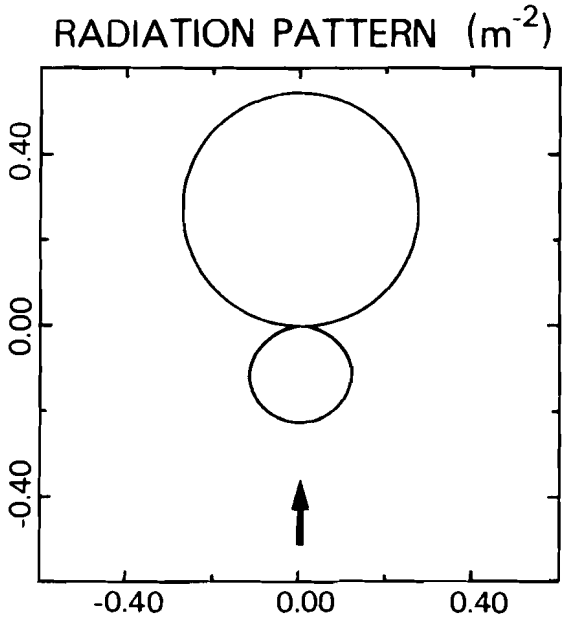

Figure 6. Radiation pattern for the basis function employed for the scattering of the fundamental Rayleigh mode to itself. The direction of the incoming wave is indicated by an arrow. The numbers indicate the scattering amplitude / m^2.

(The Love wave contribution to the data and the synthetic seismograms is zero, because a vertical force excites only Rayleigh waves, and vertical component geophones don't register Love waves.)

The sediments composing the tidal flat have a shear wave velocity of 100-300 m/sec (depending on depth), and a density of approximately 1500 kg/m^3. In the dam, shear wave velocities of several kilometers per second are possible, and the density can be as large as 2500 kg/m^3. It will be clear that the dam cannot be considered a "small perturbation", so that we cannot expect to obtain quantitatively correct information. However, the geometry of the scatterer isn't favourable to multiple scattering, which explains why this linear reconstruction technique can be employed.

As a basis function, a constant relative shear wave velocity perturbation of 500%, and a constant relative density perturbation of 25% was assumed down to a depth of 12 meters. The radiation pattern for fundamental mode Rayleigh wave scattering is shown in figure 6. Note that the radiation pattern has a node for a scattering angle of approximately 90 degrees.

The image reconstruction was performed with a straightforward numerical implementation of (4.4). The synthetic seismograms $s^{rs}(\mathbf{x},t)$ were computed in the frequency domain using (2.8), and then Fourier transformed. Imaging experiments were

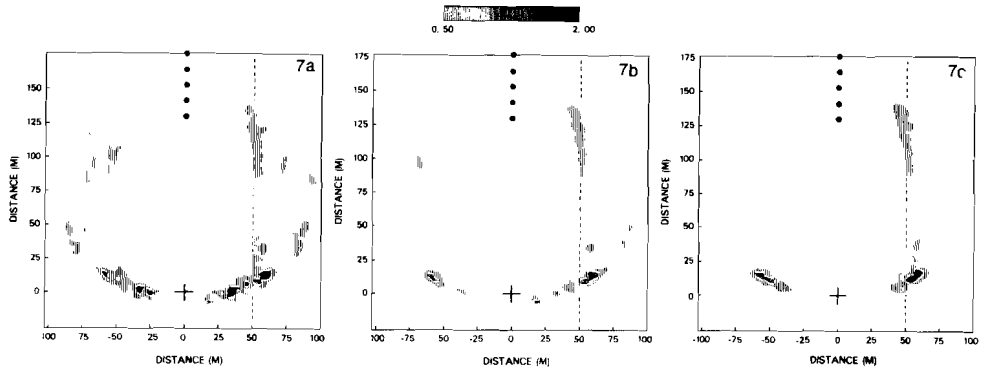

Figure 7a. Envelope of the reconstructed image $h(\mathbf{x})$ in the undamped case ($\sigma_u=0$), using only 4 geophones of the array. The true location of the edge of the dam is shown by the vertical dashed line. The shotpoints and the geophone array are marked with dots and a cross.
Figure 7b. As figure 7a, using only 8 geophones of the array.
Figure 7c. As figure 7c, using all 24 geophones of the array.

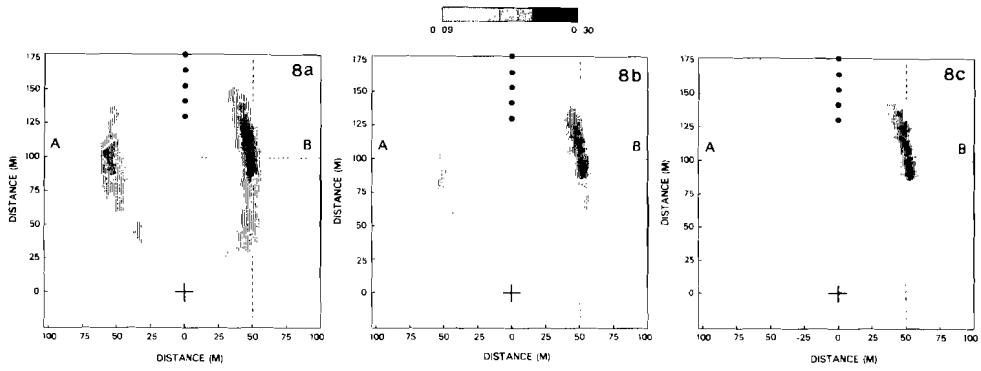

Figure 8a. Envelope of the reconstructed image $h(\mathbf{x})$ in the damped case ($\sigma_u\neq0$), using only 4 geophones of the array. The true location of the edge of the dam is shown by the vertical dashed line. The shotpoints and the geophone array are marked with dots and a cross.
Figure 8b. As figure 8a, using only 8 geophones of the array.
Figure 8c. As figure 8c, using all 24 geophones of the array.

performed for geophone spacings of 6 meters (using 4 geophones), 3 meters (using 8 geophones). and 1 meter (using all geophones). (The dominant wavelength of the fundamental Rayleigh mode is 6 m.) In all cases five shotpoints were used in the inversion. The reconstructed inhomogeneity is a highly oscillatory function of the space variables, since the reconstructed inhomogeneity $h(\mathbf{x})$ consists of the temporal correlation of two dispersed wavetrains. In the results presented here, the envelope of the function $h(\mathbf{x})$ is

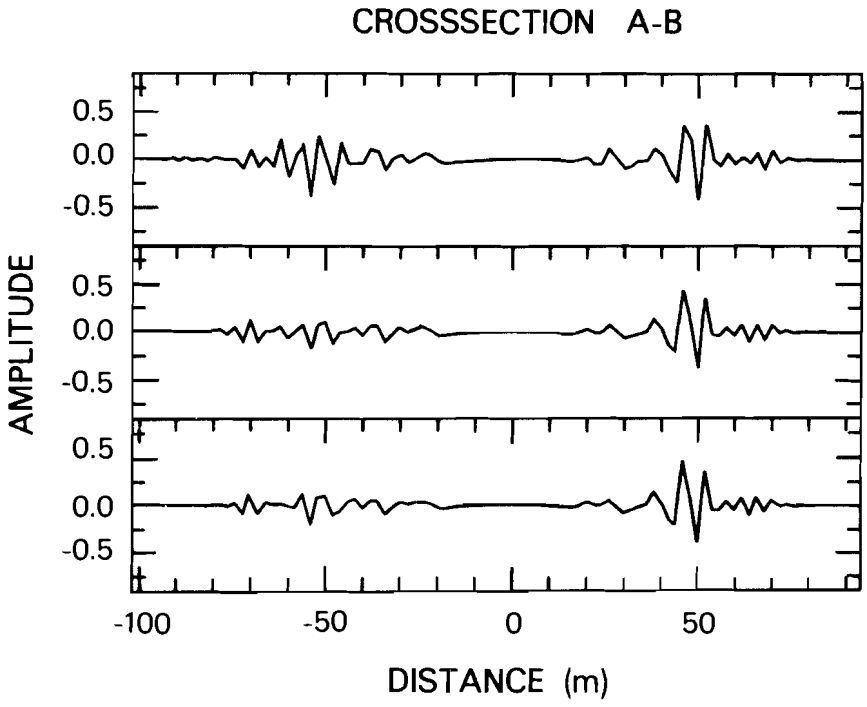

Figure 9. Cross sections of the reconstructed image $h(\mathbf{x})$ along the line AB for the solution in figure 8a (top panel), figure 8b (middle panel) and figure 8c (bottom panel).

therefore shown. In the figures 7a,b,c the reconstructed image is shown in the undamped case (σ_u=0) for different geophone spacings. The dam is not reconstructed very well, and the reconstructed heterogeneity is dominated by a sickle shaped body near the geophone array. This is caused by the fact that for the basis function employed here, the radiation pattern has a node near 90 degrees, see figure 6. Therefore, all the points near the circle with the source and the receiver as antipodal points produce a scattered wave $s^{rs}(\mathbf{x},t)$ with very small amplitude. Since the denominator in (4.4) goes faster to zero with $s^{rs}(\mathbf{x},t)$ than the numerator, this leads to an unrealistic inhomogeneity where these circles for different source receiver pairs overlap. This happens close to the geophone array. Taking more geophones into account gives some improvement, but the result isn't very good.

If the damping is nonzero ($\sigma_u \neq 0$), the results are considerably better, as can be seen in the figures 8abc. The sickle-shaped "ghost heterogeneity" has disappeared, and in all cases a clear image of the dam is visible at the correct location. In all cases a mirror image of the dam (at the left side of the shotpoint-geophone line) is visible, but if more source receiver pairs are taken into account this mirror image weakens. The reason for this is that only the geophones on the transverse leg of the array contribute to a determination between "left and right" for the incoming waves. Taking more geophones into account leads to a better determination of the direction of the incoming wave.

Note that with a geophone spacing comparable to the dominant wavelength (as in figure 8a), the inhomogeneity can still be reconstructed. This is fortunate, because in global seismology the station density is usually so small that the stations are more than a wavelength apart. Apparently, spatial aliasing effects don't affect the reconstruction strongly.

Cross sections of the field $h(\mathbf{x})$ along the line AB in figures 8abc are shown in figure 9 for the three geophone spacings employed. Note the oscillatory character of the reconstructed image, which is a by-product of the correlation technique used here. The image of the dam can clearly be seen at 50 meters. The mirror image of the dam is also visible, but it can be seen that using more geophones leads to a weakening of this mirror image. Unfortunately, it is not possible to determine the sign of the heterogeneity from figure 9. In reality, the inhomogeneity is certainly positive because both the shear wave velocity and the density are much higher in the dam than in the tidal flat. Due to the oscillatory character of the reconstructed image this cannot be determined from figure 9. This experiment has shown the feasibility of locating lateral heterogeneities in the Earth using scattered surface waves. Application of this technique to seismological data recorded with the NARS array (Dost et al., 1984) is currently in progress.

Acknowledgements. I am much indebted to Guust Nolet, both for proposing the field experiment as well as for his continuous interest and advice. Wout Brouwer helped developing the software for the data analysis. K. Helbig and Johan Tempels from the Department of Exploration Geophysics of the University of Utrecht kindly lent us their field equipment and provided technical assistance.

References

Aki, K., and P.G. Richards, *Quantitative Seismology, part I*, Freeman, San Francisco, 1980.

Backus, G.E., Geographical interpretation of measurements of average phase velocities over great circular and great semi circular paths, *Bull. seism. Soc. Am., 54*, 571-610, 1964.

Berkhout, A.J., *Seismic migration, imaging of acoustic energy by wave field extrapolation, B. Practical aspects*, Elsevier, Amsterdam, 1984.

Bleistein, N., and S.H. Gray, An extension of the Born inversion method to a depth dependent reference profile, *Geophys. Prosp., 33*, 999-1022, 1985.

Bleistein, N., J.K. Cohen, and F.G. Hagin, Computational and asymptotic aspects of velocity inversion, *Geophys., 50*, 1253-1265, 1985.

Butkov, E., *Mathematical Physics*, Addison-Wesley, Reading Ma., 1968.

Clayton, R.W., and R.H. Stolt, A Born-WKBJ inversion method for acoustic reflection data, *Geophys., 46*, 1559-1567, 1981.

Dahlen, F.A., The spectra of unresolved split normal mode multiplets, *Geophys. J. R. Astr. Soc., 58*, 1-33, 1979.

Doornenbal, J.B., and K. Helbig, High resolution reflection seismics on a tidal flat in the Dutch delta - Aquisition, Processing and Interpretation, *First Break, 9*, 9-20, 1983.

Dost, B., A. van Wettum, and G. Nolet, The NARS array, *Geol. Mijnbouw, 63*, 381-386, 1984.

Dziewonski, A.M., and A.L. Hales, Numerical analysis of dispersed seismic waves, in *Methods in computational physics, 11*, edited by B.A. Bolt, pp. 39-85, Academic Press,

New York, 1972.

Gabriels, P., R. Snieder, and G. Nolet, In situ measurements of shear velocity in sediments using higher mode Rayleigh waves, *Geophys. Prosp., 35*, 187-196, 1987.

Ikelle, L.T., J.P. Diet, and A. Tarantola, Linearized inversion of multioffset reflection data in the ω–k domain, *Geophys., 51*, 1266-1276, 1986.

Jordan, T.H., A procedure for estimating lateral variations from low frequency eigenspectra data, *Geophys. J. R. Astr. Soc., 52*, 441-455, 1978.

Kennett, B.L.N., Guided wave propagation in laterally varying media -I: Theoretical development, *Geophys. J. R. Astr. Soc., 79*, 235-255, 1984.

Montagner, J.P., Regional three-dimensional structures using long period surface waves, *Ann. Gephys., B4*, 283-294, 1986.

Nataf, H.C., I. Nakanishi, and D.L. Anderson, Measurements of mantle wave velocities and inversion for lateral heterogeneity and anisotropy 3. Inversion., *J. Geophys. Res., 91*, 7261-7308, 1986.

Nolet, G., The upper mantle under Western-Europe inferred from the dispersion of Rayleigh wave modes, *J. Geophys., 43*, 265-285, 1977.

Panza, G.F., S. Mueller, and G. Calcagnile, The gross features of the lithosphere-asthenosphere system from seismic surface waves and body waves, *Pure Appl. Geophys., 118*, 1209-1213, 1980.

Snieder, R., 3D Linearized scattering of surface waves and a formalism for surface wave holography, *Geophys. J. R. Astr. Soc., 84*, 581-605, 1986a.

Snieder, R., The influence of topography on the propagation and scattering of surface waves, *Phys. Earth. Plan. Int., 44*, 226-241, 1986b.

Snieder, R., and G. Nolet, Linearized scattering of surface waves on a spherical Earth, *J. Geophys., 61*, 55-63, 1987.

Tarantola, A., Inversion of seismic reflection data in the acoustic approximation, *Geophys., 49*, 1259-1266, 1984a.

Tarantola, A., Linearized inversion of seismic reflection data, *Geophys. Prosp., 32*, 998-1015, 1984b.

Tarantola, A., The seismic reflection inverse problem, in *Inverse problems of acoustic and elastic waves*, edited by F. Santosa, Y.H. Pao, W.W. Symes and C. Holland, SIAM, Philadelphia, 1986c.

Tarantola, A., and B. Valette, Generalized nonlinear inverse problems solved using the least squares criterion, *Rev. Geophys. Space Phys., 20*, 219-232, 1982.

Woodhouse, J.H., and A.M. Dziewonski, Mapping the upper mantle: three dimensional modeling of the Earth structure by inversion of seismic waveform, *J. Geophys. Res., 89*, 5953-5986, 1984.

Chapter 5

The connection between ray theory and scattering theory

This chapter is published as:

Snieder, R., On the connection between ray theory and scattering theory for surface waves, in *Mathematical Geophysics, a survey of recent developments in seismology and geodynamics*, edited by Vlaar, N.J., Nolet, G., Wortel, M.J.R. and Cloetingh, S.A.P.L., pp. 77-83, Reidel, Dordrecht, 1987

Chapter 4

On the connection between ray theory and scattering theory for surface waves

Roel Snieder

A proof is presented of the first order equivalence of ray theory for surface waves, and surface wave scattering theory, for the case of smooth lateral heterogeneity.

1. Introduction

Recently, a formalism was developed for linearized three dimensional surface wave scattering by buried heterogeneities (Snieder, 1986a), or by surface topography (Snieder, 1986bc). In this theory the Born approximation is used, a plane geometry is assumed, and the far field limit is used throughout. These simplifications lead to a scattering formalism which is simple enough to allow mathematical manipulations, and provides an efficient method for computing synthetic seismograms for scattered surface waves.

The resulting expression for the scattered surface waves contains an integral over the inhomogeneity. By using a stationary phase approximation for this integral one selects (at least for a smooth medium) the ray geometrical solution from this scattering integral. In this way, the first order ray geometrical effects (focussing, ray bending and phase shifting) can be determined by computing simple great circle integrals. This allows for an efficient scheme for computing synthetic seismograms in a smoothly varying medium. Furthermore, the fact that ray geometrical effects are contained in the scattering integral has consequences for the way we analyze surface wave data.

2. Scattering theory for surface waves

Suppose that the total displacement field in a laterally heterogeneous medium is decomposed as follows:

N.J. Vlaar, G. Nolet, M.J.R. Wortel & S.A.P.L. Cloetingh (eds), Mathematical Geophysics, 77-83.

$$\mathbf{u} = \mathbf{u}^0 + \mathbf{u}^1 \ , \tag{2.1}$$

where $\mathbf{u}^0$ is the displacement in a laterally homogeneous reference medium, and $\mathbf{u}^1$ describes the effect of the lateral heterogeneities. Using a dyadic decomposition of the Green's function, the wavefield $\mathbf{u}^0$ excited by a point force $\mathbf{f}$ in $\mathbf{r}_s$ is given by (Snieder, 1986a):

$$\mathbf{u}^0(\mathbf{r}) = \sum_{\nu} \mathbf{p}^{\nu}(z,\phi) \frac{\exp i(k_{\nu}X + \frac{\pi}{4})}{(\frac{\pi}{2}k_{\nu}X)^{1/2}} (\mathbf{p}^{\nu *}(z_s,\phi)\cdot\mathbf{f}) \ . \tag{2.2}$$

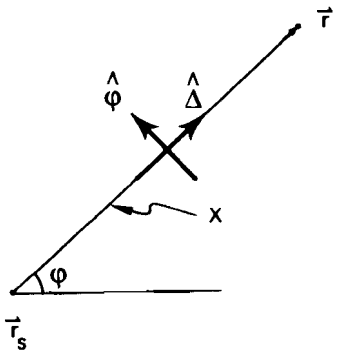

Figure 1. Definition of the geometric variables for the direct wave $\mathbf{u}^0$.

(See figure 1 for the definition of the geometric variables.) The $\mathbf{p}^{\nu}$ vectors are the polarization vectors, the Greek indices indicate mode numbers. These are for Love waves

$$\mathbf{p}^{\nu}(z,\phi) = l_1^{\nu}(z)\hat{\boldsymbol{\phi}} \ , \tag{2.3}$$

and for Rayleigh waves

$$\mathbf{p}^{\nu}(z,\phi) = r_1^{\nu}(z)\hat{\boldsymbol{\Delta}} + ir_2^{\nu}(z)\hat{\mathbf{z}} \ . \tag{2.4}$$

In these expressions l_1^{ν}, r_1^{ν} and r_2^{ν} are the surface wave eigenfunctions as defined in Aki and Richards (1980), normalized as in Snieder (1986a).

Reading (2.2) from right to left one follows the life history of the direct wave $\mathbf{u}^0$. At the source the wave field is excited, the excitation is given by the projection of the point force $\mathbf{f}$ on the polarization vector $\mathbf{p}^{\nu}(z_s,\phi)$. (In Snieder, 1986a, the extension to a moment tensor excitation is shown.) After this, the wave travels to the receiver, experiencing a phase shift and a geometrical spreading. Finally, the oscillation at the receiver is given by the polarization vector $\mathbf{p}^{\nu}(z,\phi)$. A summation over modes (index ν) superposes the contributions of different modes.

The distortion of the wavefield ($\mathbf{u}^1$) can be expressed in a similar way (Snieder, 1986a):

$$\mathbf{u}^1(\mathbf{r}) = \sum_{\sigma,\nu} \iint \mathbf{p}^{\sigma}(z,\phi_2) \frac{\exp i(k_\sigma X_2 + \frac{\pi}{4})}{(\frac{\pi}{2} k_\sigma X_2)^{1/2}} V^{\sigma\nu}(x_o, y_o) \frac{\exp i(k_\nu X_1 + \frac{\pi}{4})}{(\frac{\pi}{2} k_\nu X_1)^{1/2}} (\mathbf{p}^{\nu *}(z_s,\phi_1)\cdot\mathbf{f})\, dx_o\, dy_o \tag{2.5}$$

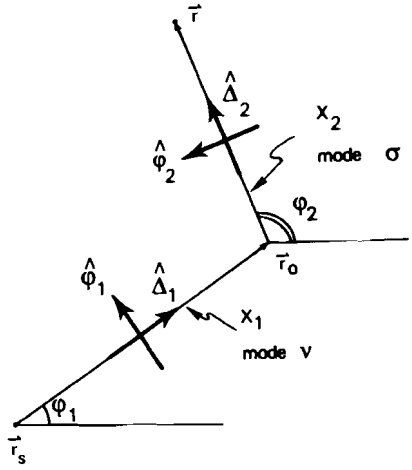

Figure 2 Definition of the geometric variables for the wave distortion $\mathbf{u}^1$.

(See figure 2 for the geometric variables.) In Snieder (1986a) a "single scattering interpretation" of this expression is presented. Note that we now have a double sum over modes (σ,ν), and that mode conversion and scattering is described by the interaction terms $V^{\sigma\nu}$. For buried scatterers the interaction terms are simple depth integrals containing the heterogeneity and the surface wave eigenfunctions (Snieder, 1986a). For perturbations in the surface topography the interaction terms contain the topography height and the surface wave eigenfunctions at the surface (Snieder, 1986b).

In Snieder (1986b) it is shown with a simple renormalization technique that the interaction terms for unconverted waves and forward scattering are closely related to the phase speed perturbations:

$$\left[\frac{\delta c}{c}\right]^{\nu} = \frac{-2}{k_\nu^2} V^{\nu\nu}(forward) \; . \tag{2.6}$$

3. The relation with ray theory

Now consider a smooth medium, i.e., let us assume that the horizontal scale at which the heterogeneity varies is much larger than the wavelength under consideration. In that case the surface wave modes decouple (Bretherton, 1968; Woodhouse, 1974). We shall therefore consider one mode, and drop the index ν. We take a coordinate system as shown in figure 3. The expression for the wave distortion can be written as

$$\mathbf{u}^1(s_r, n=0) = \iint \mathbf{R}(s,n)\, V(s,n)\, e^{ik(X_1+X_2)}\, ds dn \; , \tag{3.1}$$

with

$$\mathbf{R} = i\,\mathbf{p}_{receiver}\,(\mathbf{p}^{*}_{source}\cdot\mathbf{f})\,/\,\frac{\pi}{2}k(X_1X_2)^{1/2}\ . \tag{3.2}$$

In general, the phase in (3.1) is rapidly fluctuating except near the "great circle" (n=0) where

$$X_1 + X_2 \approx s_r + \tfrac{1}{2}\left[\frac{1}{s} + \frac{1}{s_r - s}\right] n^2\ . \tag{3.3}$$

If the heterogeneity (V) is smooth, the n-integral in (3.1) can be solved with the stationary phase approximation. Only a zone around the great circle contributes to the n-integral, the width of this zone is determined by the condition that the phase change (with n) should be less than π. This leads to the width of the Fresnel zone

$$|n| < \left[\frac{2\pi}{k}\,\frac{s(s_r - s)}{s_r}\right]^{1/2}\ . \tag{3.4}$$

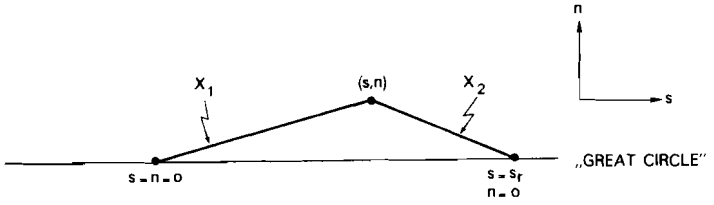

Figure 3 Definition of the geometric variables used in the stationary phase evaluation of (3.1).

This means that

$$\left[\frac{n}{s}\right]^2 < 2\pi\,\frac{s_r - s}{s_r}\,\frac{1}{ks} \ll 1\ , \tag{3.5}$$

because of the far field assumption. A similar relation holds for $(n/(s_r - s))^2$.

The fact that only small n-values contribute to the scattering integral (3.1) allows a Taylor expansion of the terms **R** and V in the transverse coordinate n. If one just assumes the great circle values for these functions (setting n=0) one obtains the traditional great circle theorem (Jordan, 1978; Dahlen, 1979) in a flat geometry. Focussing and ray bending effects are retrieved, if second order expansions are made in the transverse coordinate n.

The interaction terms for unconverted waves have the following form (Snieder, 1986ab):

$$V = V^{(0)} + V^{(1)}\cos\phi + V^{(2)}\cos 2\phi\ , \tag{3.6}$$

where ϕ is the scattering angle. Ignoring terms of relative order $1/ks_r$, the cosines can be replaced by 1. Using (2.6), the interaction term can then be expanded as

$$V(s,n) = -\tfrac{1}{2}k^2 \left[(\frac{\delta c}{c})(s,0) + n\partial_n(\frac{\delta c}{c})(s,0) + \tfrac{1}{2}n^2\partial_{nn}(\frac{\delta c}{c})(s,0) \right] . \qquad (3.7)$$

Likewise, the polarization vectors at the source and the receiver are in the far field limit given by:

$$\mathbf{p}_s = \mathbf{p}_s^0 - \frac{n}{s}\mathbf{q}_s^0 , \qquad (3.8.a)$$

$$\mathbf{p}_r = \mathbf{p}_r^0 + \frac{n}{s_r - s}\mathbf{q}_r^0 . \qquad (3.8.b)$$

In these expressions $\mathbf{p}^0$ is the polarization vector for propagation along the great circle, while $\mathbf{q}^0$ is the rotated polarization vector:

$$\mathbf{q}^0 = \hat{\mathbf{z}} \times \mathbf{p}^0 \qquad (3.10)$$

Inserting (3.7),(3.8ab) and (3.3) in (3.1), using the stationary phase approximation for the n-integral, and adding the reference wavefield $\mathbf{u}^0$, one obtains for the total wavefield

$$\mathbf{u} = \frac{\exp i(ks_r + \frac{\pi}{4})}{(\frac{\pi}{2}ks_r)^{1/2}} \left[(1 + i\Phi - \frac{F}{2})\mathbf{p}_r^0(\mathbf{p}_s^{0*}\cdot\mathbf{f}) + D_r\mathbf{q}_r^0(\mathbf{p}_s^{0*}\cdot\mathbf{f}) + D_s\mathbf{p}_r^0(\mathbf{q}_s^{0*}\cdot\mathbf{f}) \right] . \qquad (3.10)$$

In these expressions Φ, D_s, D_r and F are great circle integrals:

$$\Phi = -k\int_0^{s_r} (\frac{\delta c}{c})\, ds \qquad (3.11.a)$$

$$D_s = -\int_0^{s_r} \frac{s_r - s}{s_r}\partial_n(\frac{\delta c}{c})\, ds \qquad (3.11.b)$$

$$D_r = \int_0^{s_r} \frac{s}{s_r}\partial_n(\frac{\delta c}{c})\, ds \qquad (3.11.c)$$

$$F = -\int_0^{s_r} \frac{s(s_r - s)}{s_r}\partial_{nn}(\frac{\delta c}{c})\, ds , \qquad (3.11.d)$$

where the phase velocity and it's derivatives are to be evaluated at the great circle (n=0).

Up to first order in the heterogeneity, (3.10) can be rewritten as:

$$\mathbf{u} = (\mathbf{p}_r^0 + D_r\mathbf{q}_r^0)\frac{\exp i(kX + \Phi + \frac{\pi}{4})}{(\frac{\pi}{2}ks_r(1+F))^{1/2}}((\mathbf{p}_s^{0*} + D_s\mathbf{q}_s^{0*})\cdot\mathbf{F}) . \qquad (3.12)$$

Note the similarity between this expression, and the expression for the direct wave in the laterally homogeneous medium (2.2). The only difference is the great circle integrals appearing in (3.12). The phase integral Φ is just the phase shift due to the phase velocity perturbation at the great circle. (In Snieder (1986b) arguments are presented why it is

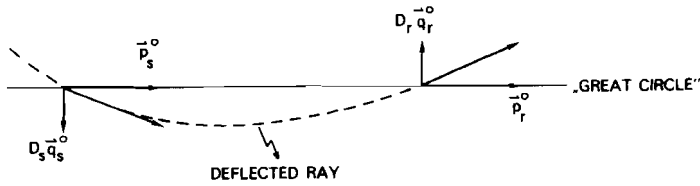

Figure 4 The relation between the ray deflection and the perturbation of the polarization vectors, for the horizontal component of the Rayleigh wave polarization vectors.

actually better to use $e^{i\Phi}$ instead of $1+i\Phi$.) The surface wave polarization vectors $\mathbf{p}_s^0$ and $\mathbf{p}_r^0$ are perturbed by the deflection integrals D_s and D_r. These integrals simply describe the ray bending effects, leading to an apparent rotation of the source and the receiver. As an example, this is shown in figure 4 for the horizontal component of the Rayleigh wave polarization vector. Finally, the focussing integral F describes the focussing due to the transverse curvature of the velocity profile.

The results (3.11) and (3.12) can also be obtained by applying perturbation theory to the ray tracing equations, as showed by Woodhouse and Wong (1986). For a straight reference ray their theory leads to the same expressions. Romanowicz (1987) derived a similar result in a spherical geometry using normal mode theory.

It is instructive to compare the order of magnitude of the terms (3.11.a-d) with the terms that have been ignored in the derivation. Suppose the velocity varies on a horizontal scale L, a simple scale analysis then shows that

$$\Phi : F : D_{rs} : N \approx 1 : \frac{1}{ks_r}\left[\frac{s_r}{L}\right]^2 : \frac{1}{ks_r}\left[\frac{s_r}{L}\right] : \frac{1}{ks_r} \ , \qquad (3.13)$$

where 'N' stands for the terms that have been neglected in the calculation. Note that the phase term is larger than the other terms by a relative factor ks_r, but that for the focussing and deflection terms this factor is reduced by the cumulative effect of the transverse velocity derivatives (the s_r/L terms). As a numerical example, consider a wavelength of 100 km, an epicentral distance s_r of 2000 km, and a horizontal length scale L of the velocity perturbation of 400 km. In that case

$$\Phi : F : D_{rs} : N \approx 1 : 0.21 : 0.04 : 0.01 \ ,$$

which means that the focussing term, and possibly the deflection terms, can be significant.

4. Discussion

The importance of the derivation presented here, is that it shows that ray geometrical effects like ray bending and focussing are contained within the expression for surface wave

scattering (2.5). This has consequences for the way we deal with surface wave data.

Up to this point, it was customary to (implicitly) divide the lateral heterogeneity in a smooth part and a rough part. The smooth part gives rise to ray geometrical effects, and formed the basis for the measurement of the dispersive properties of surface waves. The rough part of the heterogeneity generates scattered and diffracted surface waves, thus producing the surface wave coda. This part of the signal is usually regarded as noise, and is filtered out.

The separation between the smooth part of the heterogeneity and the rough part is highly artificial, and is not really necessary. The derivation in the previous section showed that both the ray geometrical effects, and the scattering effects are described by the same expression for the wave distortion (2.5), provided these effects are small. Since (2.5) constitutes a linearized relation between the inhomogeneities and the distortion of the wavefield, this expression can be used to invert for the inhomogeneities in the earth. As has been shown by Spakman (1986), extremely large noisy linear systems can be inverted sucessfully. This makes it possible to use a large data set of "surface wave residuals" for a reconstruction of the heterogeneities in the earth, incorporating ray geometrical effects and scattering effects in a unified way.

References

Aki, K. and Richards, P.G., 1980. *Quantitative Seismology* , **1** , Freeman,San Francisco.

Bretherton, F.B., 1968. Propagation in slowly varying waveguides, *Proc. Roy. Soc.*, **A302** , 555-576.

Dahlen, F.A., 1979. The spectra of unresolved split normal mode multiplets, *Geophys. J. R. Astr. Soc.*, **58** , 1-33.

Jordan, T.H., 1978. A procedure for estimating lateral variations from low frequency eigenspectra data, *Geophys. J. R. Astr. Soc.*, **52** , 441-455.

Romanowicz, B., 1987. Multiplet-multiplet coupling due to lateral heterogeneity: asymptotic effects on the amplitude and frequency of the Earth's normal modes, *Geophys. J. R. Astr. Soc.*, in press.

Snieder, R., 1986a. 3D Linearized scattering of surface waves and a formalism for surface wave holography, *Geophys. J. R. Astr. Soc.*, **84** , 581-605.

Snieder, R., 1986b. The influence of topography on the propagation and scattering of surface waves, *Phys. Earth Plan. Int.*, **44** , 226-241.

Snieder, R., 1986c. Phase speed perturbations and three-dimensional scattering effects of surface waves due to topography, *Bull. Seismol. Soc. Am.*, **76** , 1385-1392.

Spakman, W., 1986. Subduction beneath Eurasia in connection with the Mesozoic Thethys, *Geologie en Mijnbouw*, **65** , 145-154.

Woodhouse, J.H., 1974. Surface waves in a laterally varying layered structure, *Geophys. J. R. Astr. Soc.*, **37** , 461-490.

Woodhouse, J.H. and Wong, Y.K., 1986. Amplitude, phase and path anomalies of mantle waves, *Geophys. J. R. Astr. Soc.*, **87** , 753-774.

ROEL SNIEDER, Department of Theoretical Geophysics, University of Utrecht, PO Box 80.021, 3508 TA Utrecht, The Netherlands.

Chapter 6

Surface wave scattering on a spherical Earth

This chapter is published as:

Snieder, R., and G. Nolet, Linearized scattering of surface waves on a spherical Earth, *J. Geophys.*, *61*, 55-63, 1987.

Journal of Geophysics

Linearized scattering of surface waves on a spherical Earth

Rœl Snieder and Guust Nolet
Department of Theoretical Geophysics, University of Utrecht, Budapestlaan 4, P.O. Box 80.021, 3508 TA Utrecht, The Netherlands

Abstract. Recently, a formalism for three-dimensional surface-wave scattering in a plane geometry was derived. Since teleseismic surface-wave data are generally recorded at epicentral distances large enough to be influenced by the sphericity of the Earth, it is necessary to find the effects of a spherical geometry on surface-wave scattering. The theory of surface-wave scattering relies heavily on a dyadic decomposition of the Green's function, and a new derivation is given for the (dyadic) Green's function of a spherically symmetric Earth. This new derivation employs Poisson's sum formula and is more rigorous than previous derivations. Using the dyadic Green's function, a relation is established with the scattering theory in a flat geometry. This finally leads to a linearized formalism for three-dimensional surface-wave scattering on a sphere. Even for shallow surface waves the effects of sphericity are important and necessitate a modification of the propagator terms in the expression for the scattered surface waves.

Key words: Seismology – Normal modes – Surface waves – Scattering – Inversion

Introduction

Mapping the lateral heterogeneities in the Earth is a major task of modern seismology. This problem has been attacked with two types of methods. The first method utilizes the great circle theorem for surface waves (Backus, 1964; Jordan, 1978; Dahlen, 1979a). This theorem states that if the heterogeneity varies smoothly in the horizontal direction, the surface wave is only influenced by the Earth's structure on the source-receiver great circle. By combining the information of many source-receiver great circles an image of the Earth can in principle be obtained (e.g. Woodhouse and Dziewonski, 1984; Montagner, 1986; Nataf et al., 1986). The second method consists of the tomographic inversion of large data sets of body-wave delay times. This can be done on a global scale (Dziewonski, 1984), on a continental scale (Spakman, 1986) or on a more local scale (Nercessian et al., 1984).

None of these methods is able to cope with true body-wave or surface-wave scattering, so that a large part of the seismic signal is not used. Scattering of body waves has been treated by several authors in the Born approximation (Hudson and Heritage, 1982; Malin and Phinney, 1985; Wu and Aki, 1985). However, up to this point none of these techniques could cope with a layered reference medium, and they have not yet been used for systematic inversions in global seismology.

Apart from scattering body waves, lateral heterogeneities also scatter surface waves and give rise to the coupling of normal modes of a laterally homogeneous Earth. That surface-wave scattering occurs in reality is shown by the observations of Levshin and Berteussen (1979) and Bungum and Capon (1974). Scattering of surface waves is caused by sharp lateral inhomogeneities, and therefore scattered surface waves can provide valuable information on these heterogeneities. These heterogeneities may be located far from the plane of the source-receiver great circle. Unlike other types of waves, scattered surface waves enable us to investigate upper mantle heterogeneities even in regions devoid of adequate seismic instrumentation such as oceans, continental margins and large parts of the continents. It is therefore important to develop a workable method for the interpretation of these waves which, so far, by necessity have been regarded as 'noise'.

Kennett (1984) devised an exact theory for the effects of lateral inhomogeneities on surface waves in two dimensions. This theory employs invariant embedding and therefore relies heavily on the fact that surface waves in two dimensions propagate in only one horizontal direction. At this point there is no exact theory for surface-wave scattering in three dimensions. Snieder (1986a) developed a perturbation theory for the scattering of surface waves in a flat geometry, for buried inhomogeneities. He showed how different modes are coupled, and how this gives rise to surface-wave scattering. As an example, a "great circle theorem" in a flat geometry was derived, and it was shown that Snell's law holds for the reflection of surface waves by a vertical interface between two media. Furthermore, an inversion procedure was presented for the reconstruction of the medium from scattered surface-wave data. In Snieder (1986b) a similar theory is presented for surface-wave scattering by surface topography, and it is shown there that the restriction that the inhomogeneity should be buried is not necessary.

One limitation of the theory presented by Snieder (1986a, b) is that the theory is formulated for a flat geometry. This paper serves to show how the theory for a flat geometry can be generalized for a spherical geometry. It is shown here that even for shallow surface waves the theory has to be modified, since the propagator terms are affected by the sphericity.

Paradoxically, the major part of this paper is devoted to a spherically symmetric Earth. The reason for this is that in order to give an efficient derivation of the scattering

Offprint requests to: R. Snieder

effects of lateral heterogeneities, it is necessary to have a simple dyadic representation of the Green's function of a laterally homogeneous Earth. In principle, this problem is already solved. Gilbert and Dziewonski (1975) and Vlaar (1976) present the response of a layered Earth, while Ben-Menahem and Singh (1968) give a dyadic representation of the Green's function of a homogeneous sphere. However, none of these theories provides an expression for the Green's function which is convenient for analytical work, and which also has a simple physical interpretation. It is for this reason that a new derivation is given in this paper, leading to a simpler dyadic representation of the Green's function.

In order to do this, the response of the Earth is written as a sum of normal modes. The far-field limit of the Green's function and its gradient is derived in the following two sections. It is shown in the Appendix how the sum of all normal modes can be reduced to a sum over radial mode numbers only. Then a theory is derived for the scattering by lateral heterogeneities. In the subsequent section it is shown that the scattering coefficients on the sphere are similar to the scattering coefficients in a flat geometry.

In order to be able to derive this theory, several restrictive assumptions have to be made. It is assumed throughout this paper that:

1. The heterogeneity is weak enough that a linearization in the heterogeneity can be performed.
2. The modes which are excited have a horizontal wavelength small compared to the circumference of the Earth.
3. The far-field limit can be used, i.e. the scatterer is several wavelengths removed from both the source and the receiver.

One word about the notation in this paper. The summation convention is used both for vector and tensor indices. Latin indices are used for vector components, while a Greek index is used for the radial mode number of surface waves. (For normal modes we retain the conventional "n".) The dot product in this paper is defined by

$$[\mathbf{A}\cdot\mathbf{B}]=A_i^*B_i \tag{1}$$

and the double contraction by

$$[\mathbf{C}:\mathbf{D}]=C_{ij}^*D_{ji}. \tag{2}$$

The response of a radially symmetric Earth in terms of its normal modes

The equation of motion for the excitation of an elastic inhomogeneous sphere by a point force $\mathbf{F}$ oscillating with frequency ω is given by:

$$L_{ij}s_j=F_i \tag{3}$$

where,

$$L_{ij}=-\delta_{ij}\rho\omega^2-\partial_n(c_{inmj}\partial_m) \tag{4}$$

and c_{inmj} is the elasticity tensor.

In subsequent sections an expression is derived for the wave which is scattered by lateral heterogeneities. This expression contains the Green's function of a reference model, for which a spherically symmetric Earth is taken. For the moment we will restrict ourselves, therefore, to the excitation of a radially symmetric non-rotating Earth.

The response can conveniently be expressed as a sum over normal modes $\mathbf{s}^{nlm}$ (n, l and m are the conventional quantum numbers of the modes). According to Gilbert and Dziewonski (1975) or Vlaar (1976), the response to this point force is:

$$\mathbf{s}(\mathbf{r})=\sum_{n,l,m}\frac{\omega_{nl}^2}{\omega_{nl}^2-\omega^2}\,\mathbf{s}^{nlm}(\mathbf{r})\,[\mathbf{s}^{nlm}(\mathbf{r}_s)\cdot\mathbf{F}]. \tag{5}$$

If a small amount of damping (α_{nl}) is introduced this can be written as:

$$\mathbf{s}(\mathbf{r})=\sum_{n,l,m}\frac{-i}{\omega}\,\omega_{nl}^2\,C_{nl}(\omega)\,\mathbf{s}^{nlm}(\mathbf{r})\,[\mathbf{s}^{nlm}(\mathbf{r}_s)\cdot\mathbf{F}] \tag{6}$$

with

$$C_{nl}(\omega)=\tfrac{1}{2}\,(i(\omega-\omega_{nl})-\alpha_{nl})^{-1}+\tfrac{1}{2}\,(i(\omega+\omega_{nl})-\alpha_{nl})^{-1}. \tag{7}$$

For the moment we shall assume the source to be located at the pole. Furthermore, we shall restrict ourselves to the far-field response of the Earth. This means that the receiver is assumed to be located at such a colatitude that:

$$\sin\theta\gg\frac{m}{(l+\frac{1}{2})}. \tag{8}$$

Furthermore, we will only consider modes with a horizontal wavelength much smaller than the circumference of the Earth, i.e.

$$l\gg 1. \tag{9}$$

A point force or a point moment tensor only excites modes with

$$|m|\leqq 2 \tag{10}$$

so that (8) is satisfied several wavelengths from the source.

As shown by Dahlen (1979a), the toroidal (T) and spheroidal (S) modes in the far field, for $m\geqq 0$, behave as:

$$\mathbf{s}_T^{nlm}(\mathbf{r})=\frac{(l+\frac{1}{2})}{\pi(\sin\theta)^{\frac{1}{2}}}\,\hat{\boldsymbol{\phi}}\,W_{nl}(r)\sin\left[(l+\tfrac{1}{2})\,\theta+\left(\frac{m}{2}-\frac{1}{4}\right)\pi\right]e^{im\phi}, \tag{11}$$

$$\mathbf{s}_S^{nlm}(\mathbf{r})=\frac{1}{\pi(\sin\theta)^{\frac{1}{2}}}\left\{\hat{\mathbf{r}}\,U_{nl}(r)\cos\left[(l+\tfrac{1}{2})\,\theta+\left(\frac{m}{2}-\frac{1}{4}\right)\pi\right]\right.$$
$$\left.-\hat{\boldsymbol{\theta}}(l+\tfrac{1}{2})\,V_{nl}(r)\sin\left[(l+\tfrac{1}{2})\,\theta+\left(\frac{m}{2}-\frac{1}{4}\right)\pi\right]\right\}e^{im\phi}. \tag{12}$$

$\hat{\mathbf{r}}$, $\hat{\boldsymbol{\theta}}$ and $\hat{\boldsymbol{\phi}}$ are unit vectors pointing in the direction of increasing r, θ and ϕ. W, U and V are the radial eigenfunctions defined in Dahlen (1979a). For negative m, the modes follow from the symmetry properties of the spherical harmonics, which leads to:

$$\mathbf{s}^{n,l,-m}=(-1)^m(\mathbf{s}^{n,l,m})^*. \tag{13}$$

The bilinear formula (6) also requires the normal modes at the source position (the pole). As shown by Ben-Menahem and Singh (1968), the normal modes close to the pole behave as:

$$\mathbf{s}_T^{nlm}(\mathbf{r})=\left(\frac{l+\frac{1}{2}}{2\pi}\right)^{\frac{1}{2}}(l+\tfrac{1}{2})\,W_{nl}(r)\,\frac{\hat{\boldsymbol{\phi}}-im\hat{\boldsymbol{\theta}}}{2}\,(\delta_{m,1}-\delta_{m,-1})\,e^{im\phi}, \tag{14}$$

$$\mathbf{s}_S^{nlm}(\mathbf{r}) = \left(\frac{l+\frac{1}{2}}{2\pi}\right)^{\frac{1}{2}} \left(\hat{\mathbf{r}}\, U_{nl}(r)\, \delta_{m,0} - (l+\tfrac{1}{2})\, V_{nl}(r) \frac{(\hat{\theta} + im\hat{\phi})}{2} (\delta_{m,1} - \delta_{m,-1}) \right) e^{im\Phi}. \quad (15)$$

The m-summation in the modal sum can now be performed analytically by inserting Eqs. (11), (12), (14) and (15) in Eq. (6). For spheroidal modes this leads to:

$$\begin{aligned} \mathbf{s}_S(r, \theta, \phi) = \sum_{n,l} \frac{-i}{\omega} C_{nl}(\omega) \frac{\omega_{nl}^2}{\pi (\sin\theta)^{\frac{1}{2}}} \left(\frac{l+\frac{1}{2}}{2\pi}\right)^{\frac{1}{2}} \\ \cdot \left\{ \left[\hat{\mathbf{r}}\, U_{nl}(r) \cos\left[(l+\tfrac{1}{2})\theta - \frac{\pi}{4}\right] + \hat{\theta}(l+\tfrac{1}{2})\, V_{nl}(r) \right. \right. \\ \cdot \cos\left[(l+\tfrac{1}{2})\theta + \frac{\pi}{4}\right] \Big] [\hat{\mathbf{r}}_s \cdot \mathbf{F}]\, U_{nl}(r_s) \\ + \left[-\hat{\mathbf{r}}\, U_{nl}(r) \cos\left[(l+\tfrac{1}{2})\theta + \frac{\pi}{4}\right] + \hat{\theta}(l+\tfrac{1}{2})\, V_{nl}(r) \right. \\ \left. \left. \cdot \cos\left[(l+\tfrac{1}{2})\theta - \frac{\pi}{4}\right] \right] [\hat{\theta}_s \cdot \mathbf{F}]\, (l+\tfrac{1}{2})\, V_{nl}(r_s) \right\}. \quad (16) \end{aligned}$$

The l-summation can be converted to an integral by means of Poisson's summation formula. This integral can be evaluated with a contour integration; this procedure is described in the Appendix. For the first orbit this yields, after some rearrangement, the following result for the sum of the spheroidal modes:

$$\mathbf{s}_S(r, \theta, \phi) = \sum_{\nu} \left(\frac{l_\nu + \frac{1}{2}}{2\pi}\right)^{\frac{1}{2}} \frac{\omega}{2u_g^\nu} [\hat{\theta}(l_\nu + \tfrac{1}{2})\, V_\nu(r) - i\hat{\mathbf{r}}\, U_\nu(r)] \cdot \frac{\exp i\left[(l_\nu + \frac{1}{2})\theta + \frac{\pi}{4}\right]}{(\sin\theta)^{\frac{1}{2}}} [(\hat{\theta}_s (l_\nu + \tfrac{1}{2})\, V_\nu(r_s) - i\hat{\mathbf{r}}_s\, U_\nu(r_s)) \cdot \mathbf{F}]. \quad (17)$$

In this expression ν is the radial mode number, and u_g^ν is the angular group velocity of the ν-th mode. l_ν is related to the horizontal wavenumber (k_ν) of the surface-wave mode ν through the relation $k_\nu a = (l_\nu + \frac{1}{2})$, where a is the Earth's radius. The horizontal wavenumber (k_ν) depends continuously on frequency, therefore l_ν is not necessarily an integer.

For toroidal modes a similar result can be derived in the same way. These modes give the following contribution to the displacement:

$$\mathbf{s}_T(r, \theta, \phi) = \sum_{\nu} \left(\frac{l_\nu + \frac{1}{2}}{2\pi}\right)^{\frac{1}{2}} \frac{\omega}{2u_g^\nu} (l_\nu + \tfrac{1}{2})^2 \hat{\phi}\, W_\nu(r) \cdot \frac{\exp i\left[(l_\nu + \frac{1}{2})\theta + \frac{\pi}{4}\right]}{(\sin\theta)^{\frac{1}{2}}} W_\nu(r_s) [\hat{\phi}_s \cdot \mathbf{F}]. \quad (18)$$

The expressions (17) and (18) for the spheroidal and toroidal mode displacements depend only on the epicentral distance and the source-receiver direction. This means that the choice of the pole position is irrelevant. In order to make this more explicit we shall denote the epicentral distance by Δ, the unit vector along the source-receiver great circle by $\hat{\Delta}$, and the horizontal unit vector perpendicular to this great circle by $\hat{\phi}$, see Fig. 1.

The spheroidal and toroidal mode contributions to the displacement can both be accommodated in the following expression:

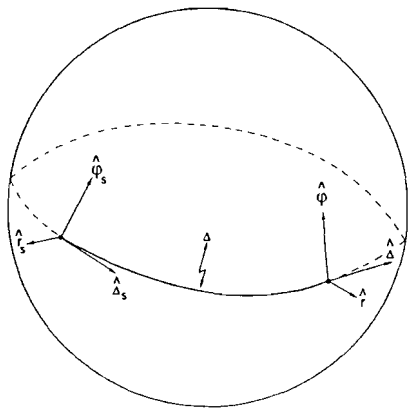

Fig. 1. Definition of the geometric variables for the direct wave

$$\mathbf{s}(\mathbf{r}) = \sum_{\nu} \left(\frac{l_\nu + \frac{1}{2}}{2\pi}\right)^{\frac{1}{2}} \frac{\omega}{2u_g^\nu} \mathbf{p}^\nu(\mathbf{r}, \Phi) \cdot \frac{\exp i\left[(l_\nu + \frac{1}{2})\Delta + \frac{\pi}{4}\right]}{(\sin\Delta)^{\frac{1}{2}}} [\mathbf{p}^\nu(r_s, \Phi) \cdot \mathbf{F}]. \quad (19)$$

The modal summation now includes both the toroidal and the spheroidal modes, and both types of modes are treated in an unified way. The $\mathbf{p}$ vectors are called the polarization vectors (Snieder, 1986a) since they describe the direction of oscillation of every mode. For spheroidal modes the polarization vector is:

$$\mathbf{p}^\nu(\mathbf{r}, \Phi) = (l_\nu + \tfrac{1}{2})\, V_\nu(r)\, \hat{\Delta} - i U_\nu(r)\, \hat{\mathbf{r}}. \quad (20)$$

While for toroidal modes:

$$\mathbf{p}^\nu(\mathbf{r}, \Phi) = -(l_\nu + \tfrac{1}{2})\, W_\nu(r)\, \hat{\phi}. \quad (21)$$

In these expressions Φ denotes the source-receiver great circle. Note that for toroidal modes the polarization vector is purely transverse, while for spheroidal modes the polarization vector has components both in the epicentral direction and the vertical direction which are 90° out of phase.

Up to this point the normalization of Dahlen (1979a) has been used implicitly, that is:

$$2\omega^2 I_1^\nu = 1. \quad (22)$$

[In Dahlen (1979a) this expression is used with the normal-mode eigenfrequency (ω_ν) instead of the frequency of excitation (ω). However, as shown in the Appendix, the dominant contribution to the contour integral comes from the point $\omega = \omega_\nu$, so that ω and ω_ν can freely be exchanged after the surface-wave limit is taken.] The integral I_1^ν for spheroidal modes is:

$$I_1^\nu = \tfrac{1}{2} \int \rho(r) (U_\nu^2(r) + l_\nu(l_\nu + 1)\, V_\nu^2(r))\, r^2\, dr. \quad (23a)$$

While for toroidal modes:

$$I_1^\nu = \tfrac{1}{2} \int \rho(r)\, l_\nu(l_\nu + 1)\, W_\nu^2(r)\, r^2\, dr. \quad (23b)$$

Inserting Eq. (22) in Eq. (19) yields:

$$\mathbf{s}(\mathbf{r})=\sum_{\nu}\left(\frac{l_\nu+\frac{1}{2}}{2\pi}\right)^{\frac{1}{2}}\frac{1}{4\omega u_g^\nu I_1^\nu}\,\mathbf{p}^\nu(\mathbf{r},\Phi)\cdot\frac{\exp i\left[(l_\nu+\frac{1}{2})\,\Delta+\frac{\pi}{4}\right]}{(\sin\Delta)^{\frac{1}{2}}}\,[\mathbf{p}^\nu(\mathbf{r}_s,\Phi)\cdot\mathbf{F}]. \tag{24}$$

The presence of the normalization integral I_1^ν in Eq. (24) makes it possible to renormalize the eigenfunctions U, V and W in the polarization vectors. For convenience we impose the following normalization:

$$I_1^\nu=\left(\frac{l_\nu+\frac{1}{2}}{2\pi}\right)^{\frac{1}{2}}\Big/4\omega u_g^\nu \tag{25}$$

which leads to

$$\mathbf{s}(\mathbf{r})=\sum_{\nu}\mathbf{p}^\nu(\mathbf{r},\Phi)\frac{\exp i\left[(l_\nu+\frac{1}{2})\,\Delta+\frac{\pi}{4}\right]}{(\sin\Delta)^{\frac{1}{2}}}\,[\mathbf{p}^\nu(\mathbf{r}_s,\Phi)\cdot\mathbf{F}]. \tag{26}$$

So that the Green's function for the displacement at $\mathbf{r}_1$ due to a point force at $\mathbf{r}_2$ has a very simple form:

$$G_{ij}(\mathbf{r}_1,\mathbf{r}_2)=\sum_{\nu}p_i^\nu(\mathbf{r}_1,\Phi)\frac{\exp i\left[(l_\nu+\frac{1}{2})\,\Delta+\frac{\pi}{4}\right]}{(\sin\Delta)^{\frac{1}{2}}}\,p_j^{\nu*}(\mathbf{r}_2,\Phi). \tag{27}$$

This is a similar dyadic expansion of the Green's function to that in Snieder (1986a). Apart from the geometrical spreading factor, the Green's function has the same form on the sphere as in a flat geometry if the higher orbits are neglected. This can be seen by using the correspondence

$$\begin{aligned}&\omega=k_\nu c_\nu,\quad k_\nu=(l_\nu+\tfrac{1}{2})/r,\quad U_g^\nu=u_g^\nu r,\\ &l_1^\nu(z)\leftrightarrow-(l_\nu+\tfrac{1}{2})\,W_\nu(r),\quad r_1^\nu(z)\leftrightarrow(l_\nu+\tfrac{1}{2})\,V_\nu(r),\\ &r_2^\nu(z)\leftrightarrow U_\nu(r),\qquad \frac{\partial}{\partial z}\leftrightarrow-\frac{\partial}{\partial r},\end{aligned} \tag{28}$$

so that

$$G_{ij}(\mathbf{r}_1,\mathbf{r}_2)=\left(\frac{\Delta}{\sin\Delta}\right)^{\frac{1}{2}}\sum_{\nu}\frac{1}{8c_\nu U_g^\nu I_1^\nu}\,p_i^\nu(\mathbf{r}_1,\Phi)\cdot\frac{\exp i\left(k_\nu r\Delta+\frac{\pi}{4}\right)}{\left(\frac{\pi}{2}k_\nu r\Delta\right)^{\frac{1}{2}}}\,p_j^{\nu*}(\mathbf{r}_2,\Phi). \tag{29}$$

Apart from the $(\Delta/\sin\Delta)^{\frac{1}{2}}$ term, this is expression (3) of Snieder (1986a). It reflects the well-known travelling-wave character of the Earth's normal modes for large angular quantum number l.

Expression (29) only takes the first orbit into account, but higher orbits can easily be included by adding similar terms to (29). The phase factors for the polar phase shift are given by Dahlen (1979a). For brevity we will neglect the contribution of the higher orbits.

The gradient of the Green's function and the excitation by a moment tensor

In the derivation of the scattered wave, the gradient of the Green's function is needed. For the moment let us once more assume that $\mathbf{r}_2$ in Eq. (27) is located at the pole. The expression for the gradient of the Green's function is somewhat more complicated in spherical coordinates than in Cartesian coordinates due to the affine terms in the derivative (Butkov, 1968). However, for the far-field Green's function the vertical derivatives and the derivative in the epicentral direction are of relative order $(l+\frac{1}{2})/r$, while the azimuthal derivative and the affine terms are of relative order $1/r$ and $\cot\theta/r$. This means that under the restrictions (8) and (9) the gradient tensor is given by:

$$\nabla\mathbf{f}=\hat{\mathbf{r}}\hat{\mathbf{r}}\,\partial_r f_r+\hat{\mathbf{r}}\hat{\boldsymbol{\theta}}\,\partial_r f_\theta+\hat{\mathbf{r}}\hat{\boldsymbol{\phi}}\,\partial_r f_\phi+\hat{\boldsymbol{\theta}}\hat{\mathbf{r}}\,\frac{1}{r}\,\partial_\theta f_r+\hat{\boldsymbol{\theta}}\hat{\boldsymbol{\theta}}\,\frac{1}{r}\,\partial_\theta f_\theta+\hat{\boldsymbol{\theta}}\hat{\boldsymbol{\phi}}\,\frac{1}{r}\,\partial_\theta f_\phi. \tag{30}$$

If this expression is used, the far-field $\mathbf{r}_1$ gradient of the Green's function takes the following form if one resubstitutes $\tilde{\Delta}=\tilde{\theta}$:

$$\nabla^{(1)}G_{ij}(\hat{\mathbf{r}}_1,\mathbf{r}_2)=\sum_{\nu}\left(\hat{\mathbf{r}}\,\partial_r p_i^\nu+i\frac{(l_\nu+\frac{1}{2})}{r}\,\tilde{\Delta}p_i^\nu\right)(\mathbf{r}_1)\cdot\frac{\exp i\left[(l_\nu+\frac{1}{2})\,\Delta+\frac{\pi}{4}\right]}{(\sin\Delta)^{\frac{1}{2}}}\,p_j^{\nu*}(\mathbf{r}_2). \tag{31a}$$

The gradient with respect to the $\mathbf{r}_2$ coordinates follows by complex conjugation:

$$\nabla^{(2)}G_{ij}(\mathbf{r}_1,\mathbf{r}_2)=\sum_{\nu}p_i^\nu(\mathbf{r}_1)\frac{\exp i\left[(l_\nu+\frac{1}{2})\,\Delta+\frac{\pi}{4}\right]}{(\sin\Delta)^{\frac{1}{2}}}\cdot\left(\hat{\mathbf{r}}\,\partial_r p_j^{\nu*}-i\frac{(l_\nu+\frac{1}{2})}{r}\,\tilde{\Delta}p_j^{\nu*}\right)(\mathbf{r}_2). \tag{31b}$$

These expressions can be used to determine the response to an excitation by a moment tensor. The response to a single couple follows by adding the response to a point force $\mathbf{F}$ at $\mathbf{r}_s+\boldsymbol{\delta}$ to a point force $-\mathbf{F}$ at $\mathbf{r}_s-\boldsymbol{\delta}$ and Taylor-expanding the result in $\boldsymbol{\delta}$. If the directions of $\mathbf{F}$ and $\boldsymbol{\delta}$ are interchanged and the results are added, the response to a double couple couple is obtained. Taking the limit $\delta\to0$ while keeping $F\delta$ constant and adding these results yields the following response to a moment tensor:

$$\mathbf{s}(\mathbf{r})=\sum_{\nu}\mathbf{p}^\nu(\mathbf{r})\frac{\exp i\left[(l_\nu+\frac{1}{2})\,\Delta+\frac{\pi}{4}\right]}{(\sin\Delta)^{\frac{1}{2}}}\,[\mathbf{E}^\nu:\mathbf{M}], \tag{32}$$

where the moment tensor is

$$\mathbf{M}=2(\boldsymbol{\delta}\mathbf{F}+\mathbf{F}\boldsymbol{\delta}) \tag{33}$$

and the excitation tensor ($\mathbf{E}$) is

$$\mathbf{E}^\nu=\left(\hat{\mathbf{r}}\,\partial_r+i\frac{(l_\nu+\frac{1}{2})}{r}\,\tilde{\Delta}\right)\mathbf{p}^\nu. \tag{34}$$

This means that the response to a moment tensor can, everywhere in this paper, be obtained by making the following substitution:

$$[\mathbf{p}\cdot\mathbf{F}]\to[\mathbf{E}:\mathbf{M}]. \tag{35}$$

In can be shown that apart from terms of relative order $1/l$, the excitation term $[\mathbf{E}:\mathbf{M}]$ is equivalent to the "Σ-expressions" of Dahlen (1979 b). The excitation terms of Dahlen (1979 b) can be written in the form $[\mathbf{E}:\mathbf{M}]$ by considering them in a coordinate system with the *θ-axis* along the source-receiver great circle. This particular choice of the coordinate system does not affect the excitation, since the double contraction is invariant under rotations. In this derivation, terms like $U(r)/r$ have been neglected because $|\partial_r U|$ is of the order $|(l+\frac{1}{2})U/r| \gg |U/r|$. This is consistent with the assumptions (8)–(10).

The response of a laterally inhomogeneous Earth

The previous sections dealt with a dyadic formulation for the response of a spherically symmetric Earth to a point force or moment tensor excitation. This section features a perturbation theory to treat the effect of lateral heterogeneities. Suppose that the density and the elasticity tensor have the following form:

$$\begin{aligned}\rho(r,\theta,\phi) &= \rho^0(r) + \varepsilon\,\rho^1(r,\theta,\phi)\\ \mathbf{c}(r,\theta,\phi) &= \mathbf{c}^0(r) + \varepsilon\,\mathbf{c}^1(r,\theta,\phi).\end{aligned} \tag{36}$$

The density ρ^0 and elasticity tensor $\mathbf{c}^0$ define a radially symmetric reference medium which is perturbed by the lateral heterogeneities ρ^1 and $\mathbf{c}^1$. The parameter ε is introduced to indicate that the perturbation is small, and facilitates a systematic perturbation approach.

The equation of motion is given by Eqs. (3) and (4). If the decomposition (36) is used, the differential operator L can be written as:

$$L = L^0 + \varepsilon L^1. \tag{37}$$

The displacement can be expressed as a perturbation series in ε:

$$\mathbf{s} = \mathbf{s}^0 + \varepsilon\mathbf{s}^1 + O(\varepsilon^2). \tag{38}$$

In this way the displacement field is divided into a direct wave ($\mathbf{s}^0$) and a scattered wave [the $O(\varepsilon)$ terms of $\mathbf{s}$]. Inserting Eqs. (37) and (38) in Eq. (3), and taking the terms proportional to ε^0 and ε^1 together gives:

$$L^0\mathbf{s}^0 = \mathbf{F} \tag{39}$$

$$L^0\mathbf{s}^1 = -L^1\mathbf{s}^0. \tag{40}$$

The direct wave can be expressed in the Green's function of the spherically symmetric reference medium. For a point force excitation at $\mathbf{r}_s$ one finds:

$$s_i^0(\mathbf{r}) = G_{ij}(\mathbf{r},\mathbf{r}_s)\,F_j(\mathbf{r}_s). \tag{41}$$

Hudson (1977) showed that in the absence of topography variations Eq. (40) is solved by:

$$\begin{aligned}s_i^1(\mathbf{r}) = \{&\int G_{ij}(\mathbf{r},\mathbf{r}')\,\rho^1(\mathbf{r}')\,\omega^2\,G_{jl}(\mathbf{r}',\mathbf{r}_s)\,d^3r'\\ &-\int[\partial_m G_{ij}(\mathbf{r},\mathbf{r}')]\,c^1_{jmnk}(\mathbf{r}')\,[\partial_n G_{kl}(\mathbf{r}',\mathbf{r}_s)]\,d^3r'\}\,F_l(\mathbf{r}_s).\end{aligned} \tag{42}$$

This expression is hard to interpret due to the presence of the gradient of the Green's function. If the dyadic form of the Green's function (27) and its gradient (31) is inserted in Eq. (42), and if an isotropic medium is assumed, the scattered wave takes after quite a bit of algebra, the following form:

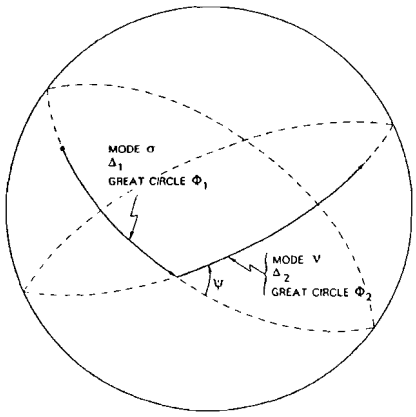

Fig. 2. Definition of the geometric variables for the scattered wave

$$\begin{aligned}\mathbf{s}^1(\mathbf{r}) = \sum_{\nu,\sigma}\int\int\mathbf{p}^\nu(\mathbf{r},\Phi_2)\,&\frac{\exp i\left[(l_\nu+\frac{1}{2})\,\Delta_2+\frac{\pi}{4}\right]}{(\sin\Delta_2)^{\frac{1}{2}}}\,V^{\nu\sigma}(\theta',\phi')\\ \cdot&\frac{\exp i\left[(l_\sigma+\frac{1}{2})\,\Delta_1+\frac{\pi}{4}\right]}{(\sin\Delta_1)^{\frac{1}{2}}}\,[\mathbf{p}^\sigma(\mathbf{r}_s,\Phi_1)\cdot\mathbf{F}]\,\sin\theta'\,d\theta'\,d\phi'.\end{aligned} \tag{43}$$

In this expression Δ_1 is the epicentral distance between the source and the scatterer, while Φ_1 denotes the source-scatterer great circle. Δ_2 is the epicentral distance between the scatterer and the receiver, and Φ_2 denotes the scatterer-receiver great circle. See Fig. 2 for the definition of variables. Note that the scattered wave is expressed as an integral over the horizontal extent of the heterogeneity. The depth dependence of the inhomogeneity is contained in the $V^{\nu\sigma}$ term. The coefficients $V^{\nu\sigma}$ are related to the perturbations in the density (ρ^1) and in the Lamé parameters (λ^1 and μ^1):

$$\begin{aligned}V^{\nu\sigma} = &\int\rho^1\,\omega^2\,[\mathbf{p}^\nu(\Phi_2)\cdot\mathbf{p}^\sigma(\Phi_1)]\,r^2\,dr\\ &-\int\lambda^1\left(\left(i[\partial_r\mathbf{p}^\nu(\Phi_2)\cdot\hat{\mathbf{r}}]+\frac{(l_\nu+\frac{1}{2})}{r}[\mathbf{p}^\nu(\Phi_2)\cdot\hat{\Delta}_2]\right)\right.\\ &\left.\cdot\left(-i[\hat{\mathbf{r}}\cdot\partial_r\mathbf{p}^\sigma(\Phi_1)]+\frac{(l_\sigma+\frac{1}{2})}{r}[\hat{\Delta}_1\cdot\mathbf{p}^\sigma(\Phi_1)]\right)\right)r^2\,dr\\ &-\int\mu^1\left[[\partial_r\mathbf{p}^\nu(\Phi_2)\cdot\hat{\mathbf{r}}]\,[\hat{\mathbf{r}}\cdot\partial_r\mathbf{p}^\sigma(\Phi_1)]\right.\\ &-i\frac{(l_\nu+\frac{1}{2})}{r}[\mathbf{p}^\nu(\Phi_2)\cdot\hat{\mathbf{r}}]\,[\hat{\Delta}_2\cdot\partial_r\mathbf{p}^\sigma(\Phi_1)]\\ &+i\frac{(l_\sigma+\frac{1}{2})}{r}[\partial_r\mathbf{p}^\nu(\Phi_2)\cdot\hat{\Delta}_1]\,[\hat{\mathbf{r}}\cdot\mathbf{p}^\sigma(\Phi_1)]\\ &\left.+\frac{(l_\nu+\frac{1}{2})(l_\sigma+\frac{1}{2})}{r^2}[\mathbf{p}^\nu(\Phi_2)\cdot\hat{\Delta}_1]\,[\hat{\Delta}_2\cdot\mathbf{p}^\sigma(\Phi_1)]\right]r^2\,dr\\ &-\int\mu^1\left([\partial_r\mathbf{p}^\nu(\Phi_2)\cdot\partial_r\mathbf{p}^\sigma(\Phi_1)]\right.\\ &\left.+\frac{(l_\nu+\frac{1}{2})(l_\sigma+\frac{1}{2})}{r^2}[\hat{\Delta}_2\cdot\hat{\Delta}_1]\,[\mathbf{p}^\nu(\Phi_2)\cdot\mathbf{p}^\sigma(\Phi_1)]\right)r^2\,dr.\end{aligned} \tag{44}$$

The expressions (43) and (44) can be interpreted in a simple way, despite their complicated form. Reading Eq. (43) from right to left one follows the "life history" of the scattered wave. At the source, mode σ is excited. The excitation is described by the projection of the force on the polarization vector of mode σ. The wave then travels from the source to the scatterer, the phase shift and the geometrical spreading being described by the term

$$\exp i\left[(l_\sigma+\tfrac{1}{2})\,\Delta_1+\frac{\pi}{4}\right]\Big/(\sin\Delta_1)^{\frac{1}{2}}.$$

After this, scattering occurs at (θ', ϕ'). This is described by the term $V^{\nu\sigma}$, which will be called the interaction matrix. The scattering also involves mode conversion to mode ν since a summation over all modes ν and σ is performed in Eq. (43). The wave then travels to the receiver, which is described by another propagator term. Finally, at the receiver the direction of the displacement oscillation is given by the polarization vector $\mathbf{p}^\nu$.

The expression for the scattered wave (43) closely resembles the expression given by Woodhouse and Girnius (1982) for elastic waves on a laterally inhomogeneous elastic sphere. Both their results and Eq. (43) express the scattered wave as an integral over the horizontal extent of the heterogeneity. However, Woodhouse and Girnius present their result in the time domain which, in the Born approximation, leads to a divergence for large times. The formalism presented here does not have this problem, thus making it possible to consider scattered waves with shorther periods. Furthermore, their formalism does not handle interactions between modes, which are fully taken care of in the theory presented here.

Equations (43) and (44) are obtained for a point force. Since the expressions are linear in the excitation, a more general excitation can be treated by integrating over the source coordinate $\mathbf{r}_s$. Excitation by a moment tensor can be incorporated with the substitution (35). It is shown in Snieder (1986b) how topography variations can be treated within the same formalism.

Analysis of the interaction matrix

The most interesting part of Eq. (43) is of course the interaction matrix $V^{\nu\sigma}$, because this matrix determines how the modes interact with each other. Unfortunately, Eq. (44) is not easy to interpret because this expression is extremely complicated. However, comparing Eq. (44) with the interaction matrix in a flat geometry [see (27) of Snieder (1986a)], using the correspondence (28), one finds that these expressions are equivalent. (The only difference is that here the depth integral is absorbed in the interaction terms.) The interaction terms are analysed in great detail in Snieder (1986a). It is shown there that even though $V^{\nu\sigma}$ depends on the polarization vectors of the incoming and the outgoing waves, $V^{\nu\sigma}$ depends in a very simple way on the scattering angle ψ defined by:

$$\cos\psi=[\Delta_2\cdot\Delta_1]_{\text{scatterer}} \tag{45}$$

(see Fig. 2). As in Snieder (1986a), the interaction matrix takes a simple form if analysed for toroidal and spheroidal modes separately:

$$\begin{aligned}V_{TT}^{\nu\sigma}=&(l_\nu+\tfrac{1}{2})(l_\sigma+\tfrac{1}{2})\int\big(W^\nu W^\sigma\rho^1\omega^2\\&-(\partial_r W^\nu)(\partial_r W^\sigma)\mu^1\big)r^2\,dr\cos\Psi\\&-(l_\nu+\tfrac{1}{2})^2(l_\sigma+\tfrac{1}{2})^2\int W^\nu W^\sigma\mu^1\quad dr\cos 2\psi,\end{aligned}\tag{46}$$

$$\begin{aligned}V_{ST}^{\nu\sigma}=&(l_\nu+\tfrac{1}{2})(l_\sigma+\tfrac{1}{2})\int\Big(-V^\nu W^\sigma\rho^1\omega^2\\&+\Big(\frac{1}{r}U^\nu+\partial_r V^\nu\Big)(\partial_r W^\sigma)\mu^1\Big)r^2\,dr\sin\Psi\\&+(l_\nu+\tfrac{1}{2})^2(l_\sigma+\tfrac{1}{2})^2\int V^\nu W^\sigma\mu^1\quad dr\sin 2\psi,\end{aligned}\tag{47}$$

$$V_{TS}^{\nu\sigma}=-V_{ST}^{\nu\sigma},\tag{48}$$

$$\begin{aligned}V_{SS}^{\nu\sigma}=&\int\Big\{U^\nu U^\sigma\rho^1\omega^2\\&-\Big(\frac{(l_\nu+\frac{1}{2})^2}{r}V^\nu-\partial_r U^\nu\Big)\Big(\frac{(l_\sigma+\frac{1}{2})^2}{r}V^\sigma-\partial_r U^\sigma\Big)\lambda^1\\&-\Big(\frac{(l_\nu+\frac{1}{2})^2(l_\sigma+\frac{1}{2})^2}{r^2}V^\nu V^\sigma+2(\partial_r U^\nu)(\partial_r U^\sigma)\Big)\mu^1\Big\}r^2\,dr\\&+(l_\nu+\tfrac{1}{2})(l_\sigma+\tfrac{1}{2})\int\Big(V^\nu V^\sigma\rho^1\omega^2\\&-\Big(\frac{U^\nu}{r}+\partial_r V^\nu\Big)\Big(\frac{U^\sigma}{r}+\partial_r V^\sigma\Big)\mu^1\Big)r^2\,dr\cos\Psi\\&-(l_\nu+\tfrac{1}{2})^2(l_\sigma+\tfrac{1}{2})^2\int V^\nu V^\sigma\mu^1\quad dr\cos 2\psi.\end{aligned}\tag{49}$$

$V_{TT}^{\nu\sigma}$ describes the coupling between the toroidal mode ν and the toroidal mode σ, $V_{TS}^{\nu\sigma}$ describes the conversion from the spheroidal mode σ to the toroidal mode ν, etc. Snieder (1986a) gives calculations of these terms for a flat Earth structure. It is shown there that the interaction terms are, in general, a strong function of frequency. Since for high l the modes of a spherical Earth are not dramatically different from the modes in a flat Earth structure, this conclusion remains valid in the spherical case.

Discussion, general inversion with surface waves

The scattering theory developed in the previous sections makes it possible to calculate the surface waves scattered by lateral inhomogeneities in a spherical earth. It is shown in Snieder (1986a) how this theory can be modified for the situation that the scatterers are not embedded in a laterally homogeneous medium, but in a reference medium with smooth lateral heterogeneities. The effect of surface perturbations on surface waves (Snieder, 1986b) can be taken into account in the same fashion as in the previous derivation.

In general, the (unknown) heterogeneities will have a wide range of horizontal spatial scales. Inhomogeneities with a horizontal scale of the order of the horizontal wavelength are efficient scatterers. This can be described with the theory of the two previous sections. Heterogeneities which vary on a horizontal scale much larger than the horizontal wavelength do not give rise to scattering, but they do affect the propagation of the surface waves. The great circle theorem (Jordan, 1978; Dahlen, 1979a) can be used for this type of heterogeneity either with linearized inver-

sions using dispersion data (Nolet, 1977), or with a waveform fitting technique which can be either linearized (Lerner-Lam and Jordan, 1983) or nonlinear (Nolet et al., 1986).

It would be desirable to have an inversion scheme with can cope with all the scales of the heterogeneity. This algorithm should be able to handle both the scattering effects of the small-scale inhomogeneities and the effects of the large-scale heterogeneity on the propagation of surface waves. This can, in principle, be achieved along the following lines.

Let us designate the data (which consist of a large set of seismograms) by "d". The lateral heterogeneity can be expanded in a set of basis functions (which might be functions defining a cell model), so that the heterogeneity can be represented by a model vector "m" of expansion coefficients. The lateral heterogeneity "m" is superposed on a laterally homogeneous background model "M". Furthermore, we shall use "s" to designate the synthetic seismograms for this model:

$$s = s(m). \tag{50}$$

The relation between the model perturbation and the changes in the synthetic seismograms is, in general, strongly nonlinear because small perturbations in the wavenumber k_v are multiplied by the epicentral distance $r\Delta$. However, this nonlinearity is only important in modelling the propagation effects on surface waves. We can hopefully treat the scattering amplitudes in a linearized way with the single scattering theory presented in this paper. In that case the synthetic seismograms can be written [using Eqs. (38), (41) and (43)] symbolically as:

$$s = g_0 F + g_{\text{out}} V g_{\text{in}} F. \tag{51}$$

In this expression F denotes the excitation, while g_0, g_{in} and g_{out} denote the propagator terms and polarization vectors for the direct surface wave, the surface wave propagating to the scatterer and the scattered surface wave, respectively. The interaction terms V are given in Eq. (49). Since we assumed that the scattering is linear, the interaction terms can be written as:

$$V(m) = \frac{\partial V}{\partial m} m. \tag{52}$$

The synthetic seismograms then depend on the model in the following way:

$$s(m) = g_0(m) F + g_{\text{out}}(m) \frac{\partial V}{\partial m} m g_{\text{in}}(m) F. \tag{53}$$

The inversion can now proceed by fitting the synthetic seismograms to the data. This can be done by minimizing the misfit (S):

$$S = \| s(m) - d \| + \gamma \| m \|. \tag{54}$$

A regularization parameter γ is added to ensure stability, $\| . \|$ denotes a suitable measure of the misfit. The inversion can therefore be treated as a (nonlinear) optimization problem. These problems can be solved iteratively.

However, these iterative schemes need the gradient of the synthetic seismograms with respect to the model parameters. This gradient can be determined from Eq. (53) by varying the model by a small amount δm, and linearizing the change δs in δm:

$$\delta s(m) = \left(\frac{\partial g_0}{\partial m} F + g_{\text{out}} \frac{\partial V}{\partial m} g_{\text{in}} F \right) \delta m. \tag{55}$$

(Here we tacitly assumed that terms of the order $m \delta m$ in the scattering term can be ignored, this is consistent with the Born approximation.) The derivatives $\partial V / \partial m$ can be obtained from Eq. (49) analytically, so that only the derivatives of the propagator $\partial g_0 / \partial m$ of the direct-wave term have to be determined. These derivatives can be obtained by direct calculation of the Frechet derivatives using ray tracing (Babich et al., 1976) or Gaussian beams (Yomogida and Aki, 1985). A faster, but less accurate way to estimate the derivatives is to combine the great circle theorem with results from WKB theory, as in Nolet et al. (1986).

In principle, it should therefore be possible to invert for heterogeneities with a large range of horizontal spatial scales. The price one has to pay is that the number of unknowns is extremely large. The cell size (or the minimum wavelength of the basis functions in which the heterogeneity is expanded) has to be smaller than the wavelength of the scattered waves. This means that several thousands of unknowns have to be determined for an inversion on a continental scale, requiring a huge data set. With the continuing growth in power of even moderate machines, this is no computational problem. However, if insufficient data are available, widely different models may give an equally reasonable fit to the data. A broad-band digital seismic network with a density that matches the length scale of the lithospheric heterogeneities, as proposed in the ORFEUS (Nolet et al., 1985) and PASSCAL (1984) proposals, is necessary to make this type of inversion feasible.

References

Aki, K., Richards, P.G.: Quantitative seismology, volume 1. San Francisco: Freeman 1980

Babich, V.M., Chikhachev, B.A., Yanovskaya, T.B.: Surface waves in a vertically inhomogeneous elastic halfspace with a weak horizontal inhomogeneity. Izv. Phys. Earth **12**, 242–245, 1976

Backus, G.E.: Geographical interpretation of measurements of average phase velocities of surface waves over great circular and great semi circular paths. Bull. Seism. Soc. Am. **54**, 571–610, 1964

Ben-Menahem, A., Sing, S.J.: Eigenvector dyads with applications to geophysical theory. Geophys. J. R. Astron. Soc. **16**, 417–452, 1968

Bungum, H., Capon, J.: Coda pattern and multipathing propagation of Rayleigh waves at NORSAR. Phys Earth Planet. Inter. 9, 111–127, 1974

Butkov, E.: Mathematical physics. Reading Ma.: Addison-Wesley 1968

Dahlen, F.A.: The spectra of unresolved split normal mode multiplets. Geophys. J. R. Astron. Soc. **58**, 1–33, 1979a

Dahlen, F.A.: Exact and asymptotic synthetic multiplet spectra on an ellipsoidal Earth. Geophys. J. R. Astron. Soc. 59, 19–42, 1979b

Dziewonski, A.M.: Mapping the lower mantle: determination of lateral heterogeneity in P velocity up to degree and order 6. J. Geophys. Res. **89**, 5929–5952, 1984

Gilbert, F., Dziewonski, A.M.: An application of normal mode theory to the retrieval of structure parameters and source mechanism from seismic spectra. Phil. Trans. Roy. Soc. Lon. **A278**, 187–269, 1975

Hudson, J.A.: Scattered waves in the coda of P.J. Geophys. **43**, 359–374, 1977

Hudson, J.A., Heritage, J.R.: The use of the Born approximation in seismic scattering problems. Geophys. J. R. Astron Soc. **66**, 221–240, 1982

Jordan, T.H.: A procedure for estimating lateral variations from low frequency eigenspectra data. Geophys. J. R. Astron. Soc. **52**, 441–455, 1978

Kennett, B.L.N.: Guided wave propagation in laterally varying media – I. Theoretical development. Geophys. J. R. Astron. Soc. 79, 235–255, 1984

Lerner-Lam, A.L., Jordan, T.H.: Earth structure from fundamental and higher-mode waveform analysis. Geophys. J. R. Astron. Soc. **75**, 759–797, 1983

Levshin, A., Berteussen, K.A.: Anomalous propagation of surface waves in the Barentz Sea as inferred from NORSAR recordings. Geophys. J. R. Astron. Soc. **56**, 97–118, 1979

Malin, P.E., Phinney, R.A.: On the relative scattering of *P*- and *S*-waves. Geophys. J. R. Astron. Soc. **80**, 603–618, 1985

Montagner, J.P.: Regional three-dimensional structures using long-period surface waves. Ann. Géophys. **B4**, 283–294, 1986

Nataf, H.C., Nakanishi, I., Anderson, D.L.: Measurements of mantle wave velocities and inversion for lateral heterogeneities and anisotropy 3. Inversion. J. Geophys. Res. **91**, 7261–7308, 1986

Nercessian, A., Hirn, A., Tarantola, A.: Three dimensional prospecting of the Mont-Dore volcano, France. Geophys. J.R. Astron. Soc. **76**, 307–315, 1984

Nolet, G.: Higher modes and the determination of upper mantle structure. PhD-thesis, University of Utrecht, 1976

Nolet, G.: The upper mantle under Western Europe inferred from the dispersion of Rayleigh modes. J. Geophys. **43**, 265–285, 1977

Nolet, G., Romanovicz, B., Kind, R., Wielandt, E.: ORFEUS, Observatories and Research Facilities for European Seismology, 1985

Nolet, G., Trier, J. van, Huisman, R.: A formalism for nonlinear inversion of seismic surface waves. Geophys. Res. Lett. **13**, 26–29, 1986

PASSCAL, Program for Array of the Continental Lithosphere. Issued by the Incorporated Research Institute for Seismology, 1984

Snieder, R.: 3-D Linearized scattering of surface waves and a formalism for surface wave holography. Geophys. J. R. Astron. Soc. **84**, 581–605, 1986a

Snieder, R.: The influence of topography on the propagation and scattering of surface waves. Phys. Earth Planet. Inter. **44**, 226–241, 1986b

Spakman, W.: Subduction beneath Eurasia in connection with the Mesozoic Thethys. Geol. Mijnbouw **65**, 145–154, 1986

Vlaar, N.: On the excitation of the Earth's seismic normal modes. Pure Appl. Geophys. **114**, 863–875, 1976

Woodhouse, J.H., Dziewonski, A.M.: Mapping the upper mantle: three-dimensional modeling of the Earth structure by inversion of seismic waveforms. J. Geophys. Res. **89**, 5953–5986, 1984

Woodhouse, J.H., Girnius, T.P.: Surface waves and free oscillations in a regionalized Earth model. Geophys. J. R. Astron. Soc. **68**, 653–673, 1982

Wu, R., Aki, K.: Scattering characteristics of elastic waves by an heterogeneity. Geophysics **50**, 582–595, 1985

Yomogida, K., Aki, K.: Total waveform synthesis of surface waves in laterally heterogeneous Earth by Gaussian beam method. J. Geophys. Res. **90**, 7665–7688, 1985

Received September 15, 1986; revised version December 9, 1986
Accepted December 12, 1986

Appendix
The evaluation of the sum of normal modes

The sum of normal modes (16) can be evaluated by simple summation over l, but for high frequencies this summation becomes rather expensive. A modified approach to the calculation of the Green's function for surface waves in a spherical Earth was given by Nolet (1976), using the FFT, and by Lerner-Lam and Jordan (1983) using the Filon quadrature algorithm. Here we describe the FFT method.

This philosophy of the FFT method is to extend the l-summation from $l=0$ to ∞ to a summation from $l=-\infty$ to ∞, after which Poisson's sum formula and a contour integration make it possible to evaluate this sum. Now first consider the sum

$$S_+(\theta)=\sum_{l=0}^{\infty} b_+(l)\cos\left[(l+\tfrac{1}{2})\theta+\frac{\pi}{4}\right] \tag{56}$$

and assume that under the transformation

$$l\to -l-1 \tag{57}$$

the b_+ coefficients behave as follows:

$$b_+(-l-1)=ib_+(l) \qquad (l<0). \tag{58}$$

By expanding the cosine in Eq. (56) in two exponentials, and making the substitution (57) for l in the term with the negative exponent, one finds with Eq. (58) that

$$S_+(\theta)=\sum_{l=-\infty}^{\infty} \tfrac{1}{2} b_+(l)\exp i\left[(l+\tfrac{1}{2})\theta+\frac{\pi}{4}\right]. \tag{59}$$

Likewise, if S_- is defined by

$$S_-(\theta)=\sum_{l=0}^{\infty} b_-(l)\cos\left[(l+\tfrac{1}{2})\theta-\frac{\pi}{4}\right] \tag{60}$$

and if b_- has the following symmetry property

$$b_-(-l-1)=-ib_-(l) \qquad (l<0), \tag{61}$$

then S_- satisfies:

$$S_-(\theta)=\sum_{l=-\infty}^{\infty} \tfrac{1}{2} b_-(l)\exp i\left[(l+\tfrac{1}{2})\theta-\frac{\pi}{4}\right]. \tag{62}$$

These results can be used to evaluate the modal sum (16). In order to do this, the symmetry properties of the l-dependent coefficients in Eq. (16) under the transformation (57) have to be determined. It is shown in Aki and Richards (1980) that the spheroidal modes depend only on $l(l+1)$. This quantity is invariant under the substitution (57), and therefore C_{nl}, ω_{nl}, U_{nl} and V_{nl} are invariant under this transformation. [A similar result holds for toroidal modes, which depend on l only through the combination $(l-1)(l+2)$. This quantity also does not change under (57).] Apart from terms which are invariant under (57), the coefficients of the $\cos[(l+\frac{1}{2})-\pi/4]$ terms in Eq. (16) are proportional to $(l+\frac{1}{2})^{\frac{1}{2}}$ or $(l+\frac{1}{2})^{\frac{3}{2}}$. Likewise, the $\cos[(l+\frac{1}{2})+\pi/4]$ coefficients in Eq. (16) are proportional to $(l+\frac{1}{2})^{\frac{3}{2}}$.

The square root in these expressions has to defined with some care. In the subsequent derivation we want to do a contour integration with the variable $\xi=l+\frac{1}{2}$. We want to avoid a branch cut in the complex upper plane, so that we take the branch cut for the square root in the lower plane. This means that for $(l+\frac{1}{2})<0$

$$(l+\tfrac{1}{2})^{\frac{1}{2}}=+i[-(l+\tfrac{1}{2})]^{\frac{1}{2}}$$

and therefore

$$[-(l+\tfrac{1}{2})]^{\frac{1}{2}} = -i(l+\tfrac{1}{2})^{\frac{1}{2}} \quad [(l+\tfrac{1}{2})<0]. \tag{63}$$

This means that the l-dependent coefficients of the $\cos[(l+\frac{1}{2})-\pi/4]$ term in Eq. (16) satisfy Eq. (61), while the coefficients of the $\cos[(l+\frac{1}{2})+\pi/4]$ term satisfy Eq. (58). Using Eqs. (59) and (62) we can write Eq. (16) then as:

$$s_S = \tfrac{1}{2}\sum_n \sum_{l=-\infty}^{\infty} A_{nl}(r,\theta)\, C_{nl}(\omega)\, e^{i[(l+\frac{1}{2})\theta+\frac{\pi}{4}]} \tag{64}$$

with

$$A_{nl}(r,\theta) = \frac{-1}{\omega}\,\frac{\omega_{nl}^2}{\pi(\sin\theta)^{\frac{1}{2}}}\left(\frac{l+\frac{1}{2}}{2\pi}\right)^{\frac{1}{2}} (\hat{\mathbf{r}}\, U_{nl}(r) + i\hat{\boldsymbol{\theta}}(l+\tfrac{1}{2})\, V_{nl}(r))$$
$$\cdot[(-i\hat{\mathbf{r}}\, U_{nl}(r_s) + \hat{\boldsymbol{\theta}}(l+\tfrac{1}{2})\, V_{nl}(r_s))\cdot \mathbf{F}]. \tag{65}$$

Application of Poisson's sum formula leads to:

$$s_S = \tfrac{1}{2}\sum_{j,n}(-1)^j \int_{-\infty}^{\infty} A_n(r,\theta,\xi)\, C_n(\omega,\xi)\, e^{i(\xi\theta+\frac{\pi}{4}+2\pi\xi j)}\, d\xi. \tag{66}$$

If we restrict ourselves to the direct arriving wave ($j=0$) this reduces to:

$$s_S = \tfrac{1}{2}\sum_n \int_{-\infty}^{\infty} A_n(r,\theta,\xi)\, C_n(\omega,\xi)\, e^{i(\xi\theta+\frac{\pi}{4})}\, d\xi. \tag{67}$$

For one value of ω, say ω_0, the function $C_n(\omega_0,\xi)$ is sharply peaked around ξ_n, where $\omega_n(\xi_n)=\omega_0$. Thus, the integral may be approximated by:

$$s_S(\omega_0) = \tfrac{1}{2}\sum_n A_n(r,\theta,\xi_n)\, D_n(\omega_0) \tag{68}$$

where

$$D_n(\omega_0) = \int_{-\infty}^{\infty} e^{i(\xi\theta+\frac{\pi}{4})}\, C_n(\omega_0,\xi)\, d\xi. \tag{69}$$

Because of Eq. (7), the integrand in Eq. (69) has two poles, one in the first quadrant and one in the third quadrant. Since the integral (69) is only needed for $\theta>0$, the contour should be closed in the upper half plane so that only the pole in the first quadrant gives a contribution. This contribution can easily be evaluated by a Taylor expansion around $\xi_n>0$:

$$\omega(\xi) = \omega_0 + (\xi-\xi_n)\, u_g^n + \ldots$$

where $u_g^n = \dfrac{d\omega}{d\xi}$ is the angular group velocity of mode n (in radians per second), evaluated in ξ_n. The pole is located in

$$\xi_n' = \xi_n + i\alpha(\xi_n)/u_g^n, \tag{70}$$

which gives a residue

$$2\pi i\ \mathrm{Res}\,(\xi=\xi_n') = \frac{-\pi}{u_g^n}\exp[i\xi_n - \alpha(\xi_n)/u_g^n]\,\theta. \tag{71}$$

We then find

$$D_n(\omega_0) = \frac{-\pi}{\omega}\exp[i\xi_n - \alpha(\xi_n)/u_g^n]\,\theta, \tag{72}$$

which gives for the contribution of the spheroidal modes

$$s_S(\mathbf{r},\omega) = -\sum_n A_n(r,\theta,\xi_n)\,\frac{\pi}{2u_g^n}\exp[i\xi_n - \alpha(\xi_n)/u_g^n]\,\theta. \tag{73}$$

This finally proves Eq. (17).

For toroidal modes, the derivation is completely analogous. The derivation can also be applied directly to the excitation by a moment tensor given by the "Σ-expressions" of Dahlen (1979b). In the normal-mode sum of Dahlen, two types of terms can be seen to occur after using relations like $\sin(x+\pi/4)=\cos(x-\pi/4)$. The first kind of term is proportional to

$$(l+\tfrac{1}{2})^{\frac{1}{2}}(l+\tfrac{1}{2})^{\text{odd number}}\cos\left[(l+\tfrac{1}{2})\,\theta+\frac{\pi}{4}\right],$$

while the second type of term is proportional to

$$(l+\tfrac{1}{2})^{\frac{1}{2}}(l+\tfrac{1}{2})^{\text{even number}}\cos\left[(l+\tfrac{1}{2})\,\theta-\frac{\pi}{4}\right].$$

Therefore, the coefficients of the cosine terms satisfy Eqs. (58) and (61) and the same derivation can be used to evaluate the l-summation.

The evaluation of the l-summation, as it is presented here, leads to the same results as in Dahlen (1979a). However, Dahlen makes three approximations which are not needed. Firstly, Dahlen ignores the pole in the third quadrant. Secondly, he extends the lower bound of the ξ-integration from 0 to $-\infty$. Thirdly, he ignores the incoming wave term. This incoming wave term could only be ignored because Dahlen also ignored the pole in the third quadrant. The derivation presented here gives a more rigorous proof of his result.

Chapter 7

Surface wave scattering derived from normal mode interactions

Abstract

Lateral heterogeneities in the Earth produce a coupling of the normal modes of a laterally homogeneous Earth model, and lead to mode interactions for surface waves. Traditionally, this problem was treated by expanding the heterogeneity in spherical harmonics, and was thereby reduced to a complicated algebraic problem requiring the use of Wigner 3j-symbols and generalized spherical harmonics. However, due to the global character of this theory, the resulting equations are not convenient for obtaining physical insight into the problem, and are cumbersome to manipulate. In this paper, the effects of lateral heterogeneity in density, bulk modulus, shear modulus, interface displacements and gravitation are treated without a global expansion in spherical harmonics. Using a simple operator formalism, the coupling coefficients between the Earth's normal modes can be expressed by an integral over the horizontal extent of the inhomogeneity. The integrand can be expressed by a set of 17 local frequencies of interaction, and some simple geometrical variables. The mode coupling depends in a simple way on the scattering angle, even for modes with such a long period that the concept of scattering is meaningless. Apart from the restrictions of first order perturbation theory, there are no other restrictions, specifically, it is not necessary to assume a far field limit. From the expression for normal mode coupling, a theory for surface wave scattering and conversion is derived. This leads to a complete set of local surface wave interaction coefficients, where the effects of sphericity are fully taken into account. The surface wave polarization vectors and excitation tensor are derived from the source and receiver operators. The resulting theory for normal mode interactions and surface wave scattering leads to an efficient method for generating synthetic seismograms in laterally inhomogeneous media, and is simple enough to allow extensive mathematical manipulation of the resulting equations. The effects of anisotropy are treated in the sequel of this paper.

This chapter is published as:

Snieder, R., and B. Romanowicz, A new formalism for the effect of lateral heterogeneity on normal modes and surface waves -I: Isotropic perturbations, perturbations of interfaces and gravitational perturbations, *Geophys. J. R. Astron. Soc., in press,* 1987

1) Introduction.

The relation between lateral heterogeneities in the Earth and long period or broadband seismological data is of continued interest to seismologists. This is because the problem is mathematically appealing, but also because inferences can be made on the nature of the lateral inhomogeneities in the Earth using seismological data.

The theory for the effect of lateral inhomogeneities on the eigenfrequencies of the Earth is studied extensively by Luh (1973, 1974), Dahlen (1974) or Woodhouse and Dahlen (1978). The coupling between modes of different multiplets is discussed in Woodhouse (1980). In Woodhouse (1983) a waveform fitting routine is used to obtain a low order spectral model for the inhomogeneities in the Earth. In all these theories the effect of the lateral heterogeneity is treated by expanding the inhomogeneity in spherical harmonics. Apart from eigenfrequency data or waveform data, path averaged surface wave velocities have also been used to determine the lateral inhomogeneity in the Earth. The great circle theorem (Backus, 1964; Jordan, 1978; Dahlen, 1979) provides a theoretical justification for this procedure, provided the heterogeneity is sufficiently smooth. Interestingly, both Backus (1964), Jordan (1978) and Dahlen (1979) expressed the inhomogeneity in spherical harmonics in order to derive the great circle theorem. Woodhouse and Girnius (1982) discussed the effects from inhomogeneities away form the great circle on the self interaction of surface waves. They derived this in a roundabout way by resumming the spherical harmonics expansion of the inhomogeneity.

It therefore appears as if a global expansion of the heterogeneity in spherical harmonics is the traditional route to take. This may be useful if one is interested in heterogeneities which are extremely smooth. This is the case for the effects of rotation and ellipticity as in Dahlen (1968, 1969), but it is also convenient if one desires to find only a low order spectral model of the Earth's inhomogeneities, e.g. Woodhouse and Dziewonski (1984).

However, we have the impression that the expansion of the heterogeneity in spherical harmonics has been complicating the mathematics of the theory unnecessarily. Also, for some practical problems it may be inconvenient to expand the inhomogeneity in spherical harmonics. For example, surface waves are most efficiently scattered by "sharp" inhomogeneities with large horizontal gradients. An extremely large number of spherical harmonics may be needed to express such an inhomogeneity accurately. It has been shown by Romanowicz (1987) using GEOSCOPE data, that low order spectral models tend to underestimate the horizontal gradient of the lateral heterogeneity. An expansion of the heterogeneity in spherical harmonics has the additional problem that it is a global method, and that it is unsuitable for studying the heterogeneity on a local (continental) scale. It is therefore desirable to formulate a local theory for surface wave scattering and normal mode interactions, which can accommodata sharp lateral heterogeneities in an efficient way.

It has been shown by Snieder (1986ab) that surface wave scattering and mode conversions in a flat geometry can be described as a simple integral over the horizontal extend of the heterogeneity. In Snieder and Nolet (1987) similar results are derived to leading order in l for a spherical geometry. In Romanowicz (1987) a rigorous proof is given of a "minor arc theorem" instead of a "great circle theorem". This was achieved by expressing the effects of the inhomogeneity as an integral over the horizontal extend of the inhomogeneity, and by solving this integral in the stationary phase approximation.

In this paper we present a unified first order theory for the effects of lateral heterogeneity which takes both normal mode interactions and surface wave scattering (and conversion) into

account. This theory constitutes a synthesis of the first order theory for normal mode interactions of Woodhouse (1980, 1983) or Tanimoto (1984), the surface wave scattering theory of Snieder and Nolet (1987), and the operator formalism of Romanowicz and Roult (1986) and Romanowicz (1987). In the derivations no use is made of an expansion of the heterogeneity in spherical harmonics, nor is it necessary to invoke the generalized spherical harmonics of Phinney and Burridge (1973).

The theory leads to a set of interaction coefficients which both describe normal mode interactions, as well as surface wave scattering. These interaction coefficients are valid both in the far field as in the near field. The effects of sphericity are fully taken into account. The perturbations in the density and elastic constants are considered, as well as the effects of displacements of internal interfaces and surface topography. Furthermore, the effects of gravitation are fully taken care of. In a following paper the effects of anisotropy are considered (Romanowicz and Snieder, 1987).

The fact that the normal mode and surface wave interactions are described by an integral over the inhomogeneity leads to an efficient method for solving both the forward and the inverse problem. With present day computers, large scale inversions can be performed for detailed structures on a continental scale. At this point, inversions are performed for the structure under Europe and the Mediterranean, using surface wave data recorded by the NARS array.

The formalism presented in this paper uses the Born approximation, so that the heterogeneity has to be sufficiently weak. The validity of this approximation can be evaluated in the same way as in Hudson and Heritage (1982). However, this entails making estimates of scattering integrals with oscillatory integrands, these estimates may be unnecessarily conservative. We take the pragmatic point of view, that the Born approximation can be used whenever the differences between the wavefield in the laterally heterogeneous Earth model (the data), and the synthetics for the radially symmetric reference Earth model are sufficiently small. In practice this puts a lower limit, dependent on the Earth's structure, on the periods that can be analized with linear theory. Apart from finite difference or finite element computations, only the theory of Kennett (1984a) can handle nonlinear effects of sharp lateral heterogeneities on surface waves. However, his theory deals with surface wave propagation in only two dimensions, which restricts the application to plane surface waves that impinge perpendicularly on a structure varying in only one horizontal direction (Kennett, 1984b).

In section 2 the operator formalism is reintroduced. With this formalism the interaction coefficients are derived in section 3. These interaction coefficients are briefly discussed in section 4. As shown in section 5, the source and receiver effects turn out to be simple. Finally, the link with surface wave scattering theory is established in section 6.

2) The operator formalism.

Lateral inhomogeneity produces a coupling between the eigenmodes $|K,m>$ and $|K',m'>$ of a radially symmetric Earth model. (The index $K=q,n,l$ designates the multiplet of kind q (toroidal, $q=T$, or spheroidal, $q=S$), radial mode number n, and angular mode number l, while m is the azimuthal mode number.) Starting from the general matrix element $Z^{mm'}_{KK'}$ for

the interaction between modes as given by Woodhouse (1980) equation (A1), we shall restrict our attention to the contribution due to lateral inhomogeneity in the case of an isotropic perturbation to the Earth model. This is described by perturbations $\delta\rho(r,\theta,\phi)$, $\delta\phi(r,\theta,\phi)$, $\delta\kappa(r,\theta,\phi)$ and $\delta\mu(r,\theta,\phi)$ in density, gravitational potential, bulk and shear moduli respectively, and a perturbation $h(\theta,\phi)$ of each discontinuity of the model. The notations will be those of Woodhouse (1980).

The displacement **s** corresponding to the mode $|K,m>$ in the reference SNREI model can be written in a general spherical coordinate system $(\hat{\mathbf{r}},\hat{\boldsymbol{\theta}},\hat{\boldsymbol{\phi}})$ as follows:

$$\mathbf{s}_{nlm}(r,\theta,\phi) = \mathbf{D}_{nl} Y_l^m(\theta,\phi) \ . \tag{1}$$

$$\mathbf{D}_{nl} \equiv U_{nl}(r)\hat{\mathbf{r}} + V_{nl}(r)\nabla_1 - W_{nl}(r)\hat{\mathbf{r}}\times\nabla_1 \tag{2}$$

where U, V and W are the vertical eigenfunctions in the notation of Gilbert and Dziewonski (1975). Y_l^m are spherical harmonics normalized as in Edmonds (1960), and ∇_1 is the gradient operator on the unit sphere. The vertical eigenfunctions are normalized according to:

$$\omega^2 \int_0^a \rho(r)\,(U^2 + l(l+1)V^2)\,r^2 dr = 1 \qquad \omega^2 \int_0^a \rho(r)\,l(l+1)W^2\,r^2 dr = 1 \tag{3}$$

Analogously to the displacement operator $\mathbf{D}_{nl}$, we define the strain operator by

$$\mathbf{e} = \tfrac{1}{2}\,(\nabla\mathbf{D} + (\nabla\mathbf{D})^T) \tag{4}$$

We wish to evaluate the effect of model perturbations on the long period seismogram, as expressed by normal mode summation in the framework of first order perturbation theory. Equation (11) of Tanimoto (1984) for the perturbation in the displacement field excited by a step function excitation can be written in the notation of Romanowicz (1987) as

$$s^1(t) = \sum_{\substack{KK',mm' \\ \omega_K=\omega_{K'}}} \omega_K^4 R_K^m \left[\frac{t}{2\omega_K^3} \sin\omega_K t\,(H_{KK'}^{mm'} - \omega_K^2 P_{KK'}^{mm'}) + \frac{1}{\omega_K^4} \cos\omega_K t\, H_{KK'}^{mm'} \right] S_{K'}^{m'} \tag{5}$$

$$- \sum_{\substack{KK',mm' \\ \omega_K\neq\omega_{K'}}} \frac{\omega_K^2\omega_{K'}^2}{\omega_K^2-\omega_{K'}^2} R_K^m \left[\frac{1}{\omega_K^2} \cos\omega_K t\,(H_{KK'}^{mm'} - \omega_K^2 P_{KK'}^{mm'}) - \frac{1}{\omega_{K'}^2} \cos\omega_{K'} t\,(H_{KK'}^{mm'} - \omega_{K'}^2 P_{KK'}^{mm'}) \right] S_{K'}^{m'}$$

(In this expression we left out the static part of the displacement field.) The factor $\omega_K^2\omega_{K'}^2$ is due to the difference in the normalization of Tanimoto (1984) and our normalization (3). H is the splitting matrix while P denotes the density matrix. Note that there is a sign difference in the definition of H in Tanimoto (1984), and in Woodhouse (1980) or Romanowicz (1987), hence the different sign of H in our equation (5) and in equation (11) of Tanimoto (1984).

Ignoring terms of relative order $1/\omega_K t$, equation (5) can be written as

$$s^1(t) = \sum_{\substack{KK' \\ \omega_K=\omega_{K'}}} \omega_K^4 \frac{A_{KK'}(\omega_K^2)}{2\omega_K^3} t \sin \omega_K t \tag{6}$$

$$- \sum_{\substack{KK' \\ \omega_K\neq\omega_{K'}}} \frac{\omega_K^2\omega_{K'}^2}{\omega_K^2-\omega_{K'}^2}\left[\frac{A_{KK'}(\omega_K^2)}{\omega_K^2}\cos\omega_K t - \frac{A_{KK'}(\omega_{K'}^2)}{\omega_{K'}^2}\cos\omega_{K'} t\right]$$

, with $A_{KK'}$ given by

$$A_{KK'}(\omega^2) = \sum_{mm'} R_{K'}^{m'} Z_{K'K}^{m'm}(\omega^2) S_K^m \qquad , \qquad Z_{K'K}^{m'm}(\omega^2) = H_{K'K}^{m'm} - \omega^2 P_{K'K}^{m'm} \tag{7}$$

S_K^m and $R_{K'}^{m'}$ are source and receiver functions respectively which can be written using an operator formalism (Romanowicz and Roult, 1986) as:

$$S_K^m = \mathbf{e}_S : \mathbf{M}\left[Y_l^{m*}(\theta_S,\phi_S)\right] \tag{8}$$

$$R_{K'}^{m'} = \mathbf{v}\cdot\mathbf{D}_R\left[Y_{l'}^{m'}(\theta_R,\phi_R)\right]$$

where $\mathbf{D}_R$ is the displacement operator at the receiver, $\mathbf{e}_S$ the strain operator at the source, and $\mathbf{v}$ indicates the component of the ground motion that is considered. Here (θ_S,ϕ_S) and (θ_R,ϕ_R) are the colatitude and longitude of the epicenter and the receiver respectively. Indices R and S affected to operators indicate that the differentiations included in them must be applied to the receiver and source coordinates respectively.

The interaction term $Z_{K'K}^{m'm}$ in equation (A1) of Woodhouse (1980) can symbolically be written using an operator notation as

$$Z_{K'K}^{m'm} = \sum_{i,j}\int_V \delta x_{ij}^V \, Op_i^V\left[Y_l^m(\theta,\phi)\right] \, Op_j^V\left[Y_{l'}^{m'*}(\theta,\phi)\right] dV \tag{9}$$

$$+ \sum_{i,j}\int_\Sigma \delta x_{ij}^\Sigma \, Op_i^\Sigma\left[Y_l^m(\theta,\phi)\right] \, Op_j^\Sigma\left[Y_{l'}^{m'*}(\theta,\phi)\right] d\Sigma$$

where Op_i^V and Op_i^Σ are linear combinations of differential operators acting on the coordinates (θ,ϕ) of the running point of the sphere, the coefficients being functions of the variable r alone, and δx_{ij}^V and δx_{ij}^Σ represent the different perturbations to the Earth model ($\delta\kappa$, $\delta\rho$, etc.) . The interaction terms consist of a volume integral $\int_V$ over the volume of the heterogeneity, and of surface integrals $\int_\Sigma$ over all displaced interfaces. The important point to note is that these operators do not themselves depend on the azimuthal orders m and m'. For example, the term corresponding to the perturbation $\delta\kappa$ in bulk modulus is:

$$\int_V \delta\kappa\,(\nabla\cdot\mathbf{s})\,(\nabla\cdot\mathbf{s}'^*)\,dV = \int_V \delta\kappa\left[\nabla\cdot\mathbf{D}Y_l^m(\theta,\phi)\right]\left[\nabla\cdot\mathbf{D}Y_{l'}^{m'}(\theta,\phi)^*\right] dV$$

, where we define

$$Op_1^V = Op_2^V = \nabla\cdot\mathbf{D} \quad , \quad \delta x_{12} = \delta\kappa$$

and for example

$$Op_1^V\left[Y_l^m(\theta,\phi)\right] = \left[\frac{2U - l(l+1)V}{r} + \partial_r U\right] Y_l^m(\theta,\phi)$$

Since none of the operators involved depends on the azimuthal orders m and m', we can rewrite expression (7) as:

$$A_{KK'} = (\mathbf{v}.\mathbf{D})_R\,(\mathbf{e}:\mathbf{M})_S \left\{ \sum_{i,j} \int_V \delta x_{ij}^V\, Op_i^V \left[\sum_m Y_l^{m*}(\theta_S,\phi_S) Y_l^m(\theta,\phi) \right] Op_j^V \left[\sum_{m'} Y_{l'}^{m'*}(\theta,\phi) Y_{l'}^{m'}(\theta_R,\phi_R) \right] dV \right.$$

$$\left. + \sum_{i,j} \int_\Sigma \delta x_{ij}^\Sigma\, Op_i^\Sigma \left[\sum_m Y_l^{m*}(\theta_S,\phi_S) Y_l^m(\theta,\phi) \right] Op_j^\Sigma \left[\sum_{m'} Y_{l'}^{m'*}(\theta,\phi) Y_{l'}^{m'}(\theta_R,\phi_R) \right] d\Sigma \right\} \tag{10}$$

Using the addition theorem for spherical harmonics (Edmonds, 1960) this can also be written as

$$A_{KK'} = (\mathbf{v}\cdot\mathbf{D})_R\,(\mathbf{e}:\mathbf{M})_S f_l f_{l'}\, C_{KK'} \tag{11}$$

with

$$C_{KK'} = \sum_{i,j} \int_V \delta x_{ij}^V\, Op_i^V \left[X_l^0(\lambda) \right] Op_j^V \left[X_{l'}^0(\lambda') \right] dV + \sum_{i,j} \int_\Sigma \delta x_{ij}^\Sigma\, Op_i^\Sigma \left[X_l^0(\lambda) \right] Op_j^\Sigma \left[X_{l'}^0(\lambda') \right] d\Sigma \tag{12}$$

where the angles λ and λ' are defined to be the angular distances between the source (θ_S,ϕ_S) and the running point of integration (θ,ϕ), and between the receiver (θ_R,ϕ_R) and (θ,ϕ) respectively, as shown in figure 1. The functions X_l^m are defined by

$$Y_l^m(\theta,\phi) = X_l^m(\theta) e^{im\phi} \quad . \tag{13}$$

In equations (10) and (12) we keep in mind that the operators inside the integration sign in (12) act on the running coordinates (θ,ϕ), while $(\mathbf{e}:\mathbf{M})_S$ and $(\mathbf{v}\cdot\mathbf{D})_R$ in (11) act on (θ_S,ϕ_S) and (θ_R,ϕ_R) respectively. In equation (11) we use

$$f_l = \left[\frac{2l+1}{4\pi}\right]^{1/2} \quad . \tag{14}$$

Throughout this paper we use unprimed variables for the modes and geometric variables associated with the source and the running point on the sphere, while the corresponding primed variables are associated with the receiver and the running point on the sphere (figure 1).

We shall first focus our attention on the evaluation of $C_{KK'}$ in equation (12), the application of the source and receiver operators in (11) being then straightforward, as we shall see.

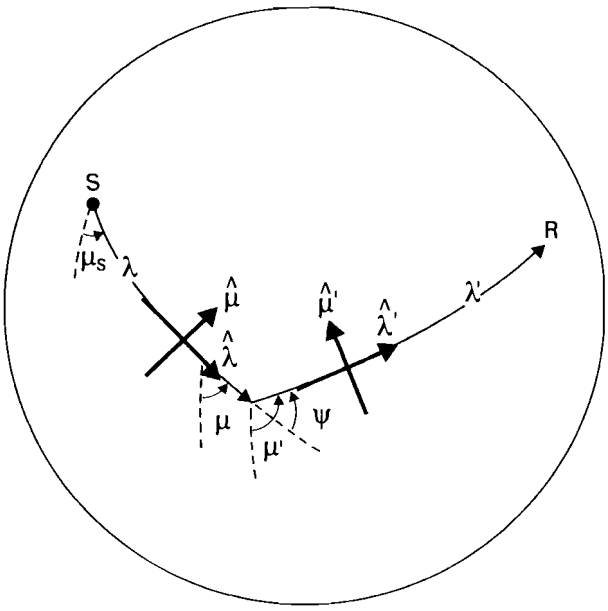

Figure 1 - Definition of the geometric variables.

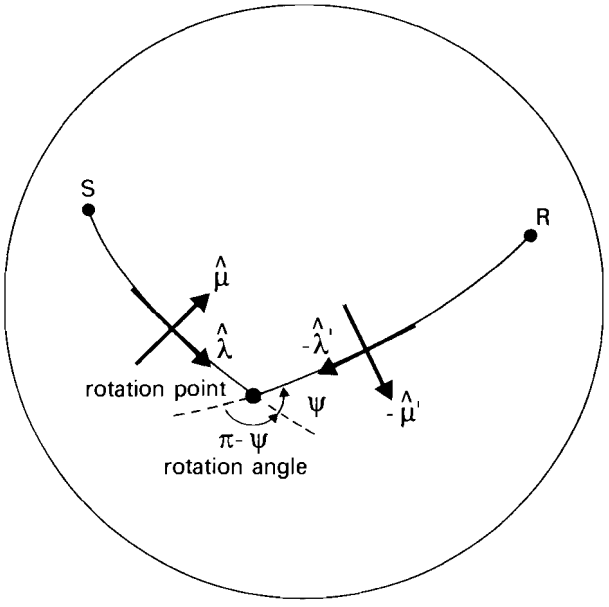

Figure 2. Definition of the coordinate systems (r,λ,μ) and $(r,-\lambda',-\mu')$, and the rotation $\mathbf{R}_{\pi-\Psi}$.

3) The coupling coefficients between modes and their relation with geometric variables

In order to obtain explicit expressions for the coupling between the Earth's normal modes, it is necessary to use an explicit expression for the operators Op_i^V and Op_i^Σ in equation (12). The factors δx_{ij}^V and δx_{ij}^Σ and the operators Op_i^V and Op_i^Σ denote the operations to be performed on $Y_l^0(\lambda,\mu)$ and $Y_l^0(\lambda',\mu')$ to obtain the coupling coefficients. Using equation (A1) of Woodhouse (1980) we find that:

$$
\begin{aligned}
C_{KK'} = & \int \Big[\delta\kappa(\nabla\cdot\mathbf{s})(\nabla\cdot\mathbf{s}') + 2\delta\mu\Gamma:\Gamma' + \delta\rho\Big[\mathbf{s}\cdot\nabla\Phi_1' + \mathbf{s}'\cdot\nabla\Phi_1 + 8\pi G\rho s_r s_r' + g_o\Lambda - \omega^2(\mathbf{s}\cdot\mathbf{s}') \Big] \Big] dV \\
& + \tfrac{1}{2}\int \rho \Bigg\{ \Bigg[-\frac{2}{r}(\nabla_1\cdot\mathbf{s}_H)s_r' - \frac{2}{r}(\nabla_1\cdot\mathbf{s}_H')s_r - 4s_r s_r' \Bigg] \delta\dot\phi + \Big[s_r\mathbf{s}_H' + s_r'\mathbf{s}_H \Big]\cdot\frac{1}{r}\nabla_1\delta\dot\phi \\
& \quad + \Bigg[-\Big(\frac{2}{r}(\nabla_1\cdot\mathbf{s}_H) + \dot s_r\Big)\mathbf{s}_H' - \Big(\frac{2}{r}(\nabla_1\cdot\mathbf{s}_H') + \dot s_r'\Big)\mathbf{s}_H + s_r\dot{\mathbf{s}}_H' + s_r'\dot{\mathbf{s}}_H - \frac{1}{r}s_r\mathbf{s}_H' - \frac{1}{r}s_r'\mathbf{s}_H \Bigg]\cdot\frac{1}{r}\nabla_1\delta\phi \\
& \quad - \frac{2}{r^2}s_r s_r'\nabla_1^2(\delta\phi) \Bigg\} dV \\
& - \int_\Sigma h \Big[\kappa(\nabla\cdot\mathbf{s})(\nabla\cdot\mathbf{s}') + 2\mu\Gamma:\Gamma + \rho\,(\mathbf{s}\cdot\nabla\Phi_1' + \mathbf{s}'\cdot\nabla\Phi_1 + 8\pi G\rho s_r s_r' + g_o\Lambda - \omega_o^2(\mathbf{s}\cdot\mathbf{s}')) \\
& \quad - \kappa(\nabla\cdot\mathbf{s})\dot s_r' - \kappa(\nabla\cdot\mathbf{s}')\dot s_r - 2\mu\Gamma:\hat{\mathbf{r}}\dot{\mathbf{s}}' - 2\mu\Gamma':\hat{\mathbf{r}}\dot{\mathbf{s}} \Big]_-^+ d\Sigma \qquad (15) \\
& - \int_\Sigma \nabla_\Sigma h\cdot\Big[\kappa(\nabla\cdot\mathbf{s})\mathbf{s}' + \kappa(\nabla\cdot\mathbf{s}')\mathbf{s} + 2\mu\Gamma_{rr}\mathbf{s}' + 2\mu\Gamma'_{rr}\mathbf{s} \Big]_-^+ d\Sigma
\end{aligned}
$$

Unless stated otherwise, the notation of Woodhouse (1980) is followed. Note that the gravitational perturbation terms differ from the expression given in Woodhouse (1980). The reason for this is that we have applied an integration by parts to these terms. The details of this rearrangement are given in appendix A. In this paper κ, μ and ρ are the elastic moduli and the density of the spherically symmetric reference model. $\mathbf{s}$ is used for the displacement field while Φ_1 denotes the change in the gravitational potential of the modes. A dot is used to denote the radial derivative: $\dot{\mathbf{s}} \equiv \frac{\partial \mathbf{s}}{\partial r}$. The subscript H denotes the horizontal components, while the subscript r denotes the vertical component. The quantities Γ and Λ are related to the strain ($\mathbf{e}$) and the displacement through the relations

$$\Gamma = \mathbf{e} - \frac{1}{3}(\nabla\cdot\mathbf{s})\mathbf{I} \qquad (16)$$

, and

$$\Lambda = \tfrac{1}{2}\left[\mathbf{s}\cdot\nabla s_r' + \mathbf{s}'\cdot\nabla s_r - s_r\nabla\cdot\mathbf{s}' - s_r'\nabla\cdot\mathbf{s} - \frac{4}{r}s_r s_r' \right]. \qquad (17)$$

As in Woodhouse (1980), the notation $\Big[\ldots\ldots \Big]_-^+$ refers to the difference between the quantity

between brackets above and below the interface.

It can be seen from expression (12) that only the m=0 component of the modes need to be taken into account, since only the functions $X_l^0(\lambda)$ and $X_{l'}^0(\lambda')$ occur in equation (12). Therefore, the displacement fields which are to be used in (12) are the m=0 displacement fields with a dependence on the horizontal coordinates through terms $X_l^0(\lambda)$ and $X_{l'}^0(\lambda')$. The fact that we only need to consider the m=0 component of the displacement field, implies that all variables in equation (12) are real, therefore the complex conjugations used in Woodhouse (1980) have been suppressed.

The m=0 displacement fields **s** and **s'** follow by applying the displacement operator (**D**) of equation (2) to $X_l^0(\lambda)$ and $X_{l'}^0(\lambda')$. The gradient in this operator acts on the running point on the sphere. This leads to

$$\mathbf{s}_{nl}(r,\lambda) = \hat{\mathbf{r}}U_{nl}(r)X_l^0(\lambda) + \hat{\boldsymbol{\lambda}}V_{nl}(r)\partial_\lambda X_l^0(\lambda) - \hat{\boldsymbol{\mu}}W_{nl}(r)\partial_\lambda X_l^0(\lambda) \tag{18a}$$

, and

$$\mathbf{s}'_{n'l'}(r,\lambda') = \hat{\mathbf{r}}U_{n'l'}(r)X_{l'}^0(\lambda') - \hat{\boldsymbol{\lambda}}'V_{n'l'}(r)\partial_{\lambda'}X_{l'}^0(\lambda') + \hat{\boldsymbol{\mu}}'W_{n'l'}(r)\partial_{\lambda'}X_{l'}^0(\lambda') \tag{18b}$$

The convention is used that both toroidal and spheroidal eigenfunctions are used simultaneously in one expression, but that for toroidal modes U=V=Φ_1=0, and for spheroidal modes W=0. The different signs of the horizontal displacements in equation (18a) and (18b) are due to the fact that at the running point on the sphere, $\nabla_1 X_l^m(\lambda)$ points in the $\hat{\boldsymbol{\lambda}}$ direction, whereas $\nabla_1 X_{l'}^m(\lambda')$ points in the $-\hat{\boldsymbol{\lambda}}'$ direction, as in figure 1.

In equation (15) the strain field enters through the Γ terms (16) in the mode coupling. Since we only need to know the strain field for m=0 modes with a horizontal dependence $X_l^0(\lambda)$ or $X_{l'}^0(\lambda')$, it is convenient to use spherical coordinates system with their pole either at the source or the receiver, see figure 2. Using expression (8.36) of Aki and Richards (1980), one finds in (r,λ,μ) coordinates:

$$e_{rr} = \dot{U}X_l^0 \quad , \quad e_{\lambda\lambda} = \frac{V}{r}\partial_\lambda^2 X_l^0 + \frac{U}{r}X_l^0 \quad , \quad e_{\mu\mu} = \frac{U}{r}X_l^0 + \frac{V}{r}\,cot\,\lambda\,X_l^0$$

$$e_{\lambda\mu} = \frac{-W}{2r}\left[\partial_\lambda^2 X_l^0 - cot\,\lambda\,X_l^0\right] \quad , \quad e_{r\mu} = -\tfrac{1}{2}Z\partial_\lambda X_l^0 \quad , \quad e_{r\lambda} = \tfrac{1}{2}X\partial_\lambda X_l^0 \tag{19}$$

A similar expression holds for e' in $(r,-\lambda',-\mu')$ coordinates. The eigenfunctions Z and X are defined by

$$X = \dot{V} + \frac{1}{r}(U-V) \tag{20a}$$

$$Z = \dot{W} - \frac{1}{r}W \quad , \tag{20b}$$

furthermore we shall use

$$F = \frac{1}{r}(2U-LV) \quad , \tag{20c}$$

and

$$L=l(l+1). \tag{20d}$$

For toroidal modes $X=F=0$, while for spheroidal modes $Z=0$.

It can be seen that equation (15) consists essentially of four kind of terms. 1) terms which only contain scalars. These terms contain either the divergence or the vertical component of the displacement field. 2) terms containing dot products between vectors associated with the modes, such as $\delta\rho\omega^2 \mathbf{s}_H \cdot \mathbf{s}_H'$ or $\delta\rho \mathbf{s} \cdot \nabla\Phi_1'$. 3) dot products between modal vectors and the gradient of the inhomogeneity, such as $\frac{1}{r} s_r' \mathbf{s}_H \cdot \nabla_1 \delta\phi$ or $\kappa(\nabla\cdot\mathbf{s})\mathbf{s}'\cdot\nabla_\Sigma h$. 4) contractions between strain tensors, because Γ contains the strain tensor. These four types of terms should be treated in a different way.

The scalar terms are easily found using

$$s_r = UX_l^0 \quad \text{and} \quad \nabla\cdot\mathbf{s} = (\dot{U}+F)X_l^0 . \tag{21}$$

These terms do not contain any dependence on the azimuths μ and μ'. Therefore these terms lead to an isotropic interaction between the modes. This isotropic interaction in only non-zero if both modes s and s′ are spheroidal.

The vector terms containing dot products between modal vectors can be analyzed using simple geometrical relations such as

$$(\hat{\boldsymbol{\lambda}}\cdot\hat{\boldsymbol{\lambda}}') = (\hat{\boldsymbol{\mu}}\cdot\hat{\boldsymbol{\mu}}') = \cos\Psi \tag{22a}$$

$$-(\hat{\boldsymbol{\lambda}}\cdot\hat{\boldsymbol{\mu}}') = (\hat{\boldsymbol{\mu}}\cdot\hat{\boldsymbol{\lambda}}') = \sin\Psi \tag{22b}$$

, where Ψ is the scattering angle defined in figure 1. For example, using equation (18a),we can rewrite

$$\delta\rho \mathbf{s}_H \cdot \nabla_1\Phi_1' = \delta\rho\left[\hat{\boldsymbol{\lambda}}V - \hat{\boldsymbol{\mu}}W\right]\cdot(-\hat{\boldsymbol{\lambda}}')\Phi_1'(\partial_\lambda X_l^0)(\partial_{\lambda'}X_{l'}^0)$$

$$= -\delta\rho\left[V\Phi_1'\cos\Psi - W\Phi_1'\sin\Psi\right](\partial_\lambda X_l^0)(\partial_{\lambda'}X_{l'}^0)$$

These vector products lead to a cos Ψ or sin Ψ dependence of the scattering angle.

In order to analyze the vector terms containing dot products between modal vectors and the gradient of the heterogeneity, we introduce for a scalar ξ the slope vector defined by

$$\mathbf{S}_\xi \equiv \frac{1}{r}\nabla_1\xi \tag{23}$$

, where ξ is either the interface displacement h, the perturbation in the gravitational potential $\delta\phi$, or its vertical derivative $\delta\dot{\phi}$. The azimuth of the slope vector is denoted by ϕ_ξ (see figure 3), while S_ξ is used to denote the magnitude of the slope vector. (Note that the slope vectors $\mathbf{S}_{\delta\phi}$ and $\mathbf{S}_{\delta\dot{\phi}}$ are not necessarily aligned.) With this definition, the mode coupling due to the horizontal gradients of h, $\delta\phi$ and $\delta\dot{\phi}$ can readily be computed. For example

$$\kappa\nabla h\cdot\mathbf{s}(\nabla\cdot\mathbf{s}') = \kappa S_h \hat{\mathbf{S}}_h\cdot\left[\hat{\boldsymbol{\lambda}}V\partial_\lambda X_l^0 - \hat{\boldsymbol{\mu}}W\partial_\lambda X_l^0\right](\dot{U}'+F')X_{l'}^0 = \kappa S_h\left[V\cos(\mu-\phi_h) + W\sin(\mu-\phi_h)\right](\partial_\lambda X_l^0)X_{l'}^0$$

The terms containing contractions of the strain tensor can be analyzed using equation (19), which gives a simple expression for the strain tensor e in (r,λ,μ) coordinates, and for e′ in

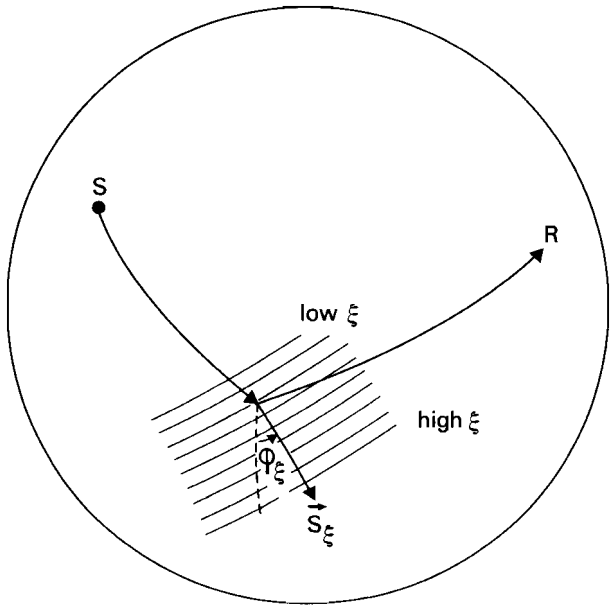

Figure 3 - Definition of the slope vector $\mathbf{S}_\xi$ and the slope azimuth ϕ_ξ.

$(r,-\lambda',-\mu')$

coordinates. However, except for the special case $\Psi=\pi$, these coordinate systems are different. A contraction between these tensors can only be performed after the coordinate system $(r,-\lambda',-\mu')$ has been rotated around a vertical axis through the running point on the sphere over $\pi-\Psi$, so that the coordinate systems are aligned, see figure 2. In $(r,-\lambda',-\mu')$ coordinates the rotation matrix is given by

$$\mathbf{R}_{\pi-\Psi} = \begin{bmatrix} 1 & 0 & 0 \\ 0 & -\cos\Psi & -\sin\Psi \\ 0 & \sin\Psi & -\cos\Psi \end{bmatrix} \tag{24}$$

The matrix multiplication $\mathbf{R}_{\pi-\Psi}^{-1}\mathbf{e}'\mathbf{R}_{\pi-\Psi}$ aligns the two coordinate systems so that, using expression (19) and its equivalent with the primed variables, the contraction of the strain tensor can be performed. The $e_{r\lambda}$ and $e_{r\mu}$ components lead to a $\cos\Psi$ and $\sin\Psi$ dependence of the scattering angle. The other components lead either to an isotropic interaction (only for spheroidal modes), and $\sin 2\Psi$ or $\cos 2\Psi$ interactions.

After some algebra one finds using the recurrence relations for X_l^m (Edmonds, 1960) that

$$A_{KK'} = (\mathbf{v}\cdot\mathbf{D})_R\,(\mathbf{e}:\mathbf{M})_S\,f_l f_{l'}\,\frac{2}{\sqrt{\omega_K\,\omega_{K'}}}\left\{\int_\Omega f^{\Psi}_{KK'}(\lambda,\mu)\,d\Omega + \int_\Omega f^{\mu\mu'}_{KK'}(\lambda,\mu)\,d\Omega\right\} \tag{25}$$

, where

$$f^{\Psi}_{KK'}(\lambda,\mu) = \delta\omega^0_{KK'}(\lambda,\mu)\,X_l^0(\lambda)X_{l'}^0(\lambda') - \left\{\delta\omega^1_{KK'}(\lambda,\mu)\,\cos\Psi + \delta\omega^2_{KK'}(\lambda,\mu)\,\sin\Psi\right\}a_l a_{l'} X_l^1(\lambda)X_{l'}^1(\lambda')$$

$$+\left\{\delta\omega^3_{KK'}(\lambda,\mu)\,\cos 2\Psi + \delta\omega^4_{KK'}(\lambda,\mu)\,\sin 2\Psi\right\}b_l b_{l'} X_l^2(\lambda)X_{l'}^2(\lambda') \tag{26}$$

, and

$$\begin{aligned} f^{\mu\mu'}_{KK'}(\lambda,\mu) = \Big\{ & -\delta\omega^5_{KK'}(\lambda,\mu)\,\cos(\mu'-\phi_h) - \delta\omega^6_{KK'}(\lambda,\mu)\,\sin(\mu'-\phi_h) \\ & - \delta\omega^9_{KK'}(\lambda,\mu)\,\cos(\mu'-\phi_{\delta\phi}) - \delta\omega^{10}_{KK'}(\lambda,\mu)\,\sin(\mu'-\phi_{\delta\phi}) \\ & - \delta\omega^{13}_{KK'}(\lambda,\mu)\,\cos(\mu'-\phi_{\delta\dot\phi}) - \delta\omega^{14}_{KK'}(\lambda,\mu)\,\sin(\mu'-\phi_{\delta\dot\phi})\Big\}a_{l'}X_l^0(\lambda)X_{l'}^1(\lambda') \\ + \Big\{ & \delta\omega^7_{KK'}(\lambda,\mu)\,\cos(\mu-\phi_h) + \delta\omega^8_{KK'}(\lambda,\mu)\,\sin(\mu-\phi_h) \\ & + \delta\omega^{11}_{KK'}(\lambda,\mu)\,\cos(\mu-\phi_{\delta\phi}) + \delta\omega^{12}_{KK'}(\lambda,\mu)\,\sin(\mu-\phi_{\delta\phi}) \\ & + \delta\omega^{15}_{KK'}(\lambda,\mu)\,\cos(\mu-\phi_{\delta\dot\phi}) + \delta\omega^{16}_{KK'}(\lambda,\mu)\,\sin(\mu-\phi_{\delta\dot\phi})\Big\}a_l X_l^1(\lambda)X_{l'}^0(\lambda') \end{aligned} \tag{27}$$

The mode coupling is now described by a set of local frequencies of interaction $\delta\omega^i_{KK'}$ (i=0,16), which are shown in appendix B. The parameters a_l and b_l are defined by

$$a_l=\sqrt{l\,(l+1)} \quad \text{and} \quad b_l=\sqrt{(l+2)(l+1)l\,(l-1)}\ . \tag{28}$$

4) Some remarks on the coupling coefficients $A_{KK'}$

Equation (25) constitutes a simple expression where the coupling between normal modes is expressed in an integral over the horizontal extend of the inhomogeneity. Apart from the local frequencies of interaction $\delta\omega^i$, the integrand in the expressions (26) and (27) only contain simple geometrical terms which can easily be computed.

The local frequencies $\delta\omega^i$ (i=0,16) of appendix B consist of two parts. One part contains the depth integral of the modes K and K' and the inhomogeneity. The second part consists of the jump in the product of the modes K and K' and the parameters of the SNREI reference medium across the internal and external interfaces. Once the modes are computed, it is simple to compute the $\delta\omega^i$.

It can be seen from appendix B and equation (26) that the perturbation in the density and the elastic parameters lead to a dependence of the mode interaction on the scattering angle Ψ proportional to cos Ψ, sin Ψ, cos 2Ψ or sin 2Ψ, while the spheroidal-spheroidal mode interactions also have an isotropic component. Using equation (27) it follows that the interactions due to the gradient of the interfaces and the gravitational potential depends in a more complicated way on azimuth through terms containing cos $(\mu-\phi_\xi)$, sin $(\mu-\phi_\xi)$, cos $(\mu'-\phi_\xi)$ or sin $(\mu'-\phi_\xi)$, where ξ is either the perturbations in the interfaces, the perturbation in the gravitational potential, or the vertical derivative of the latter.

In general, the mode conversions between toroidal and spheroidal depend on the sine of some angle (Ψ, $\mu-\phi_\xi$, etc.), while the interactions between equal kind of modes depends on the cosine of these angles. In the absence of horizontal gradient terms (hence when $\delta\omega^5$ through $\delta\omega^{16}$ are zero) there is no conversion between spheroidal and toroidal modes in the the forward and backward direction (where sin $m\Psi = 0$). However, the gradient terms in equation (27) may produce spheroidal-toroidal mode coupling in the forward and backward direction, because terms like sin $(\mu-\phi_h)$ are not necessarily zero in the forward and backward direction. These terms produce the strongest coupling between toroidal and spheroidal modes in the forward and backward direction if the gradient is perpendicular to the path of propagation.

Note that the gradient of the interface displacement enters explicitly in the local frequencies $\delta\omega^5$ through $\delta\omega^8$. This contrasts the observation of Snieder (1986b) who found that (in first order perturbation theory) surface waves are influenced by surface topography, but not by the gradient of the surface topography. The reason for this discrepancy is that the local frequencies $\delta\omega^5$ through $\delta\omega^8$ are proportional to the tractions τ_{rr} or τ_{rr}'. These terms vanish at the surface, so that to first order the gradient of the surface topography does not contribute.

5) Incorporation of source and receiver effects.

To obtain the complete expression for $A_{KK'}$ in equation (25), we need only to apply the operators $(\mathbf{e}:\mathbf{M})_S$ and $(\mathbf{v}\cdot\mathbf{D})_R$. We shall analyze these operators in the same way as in Romanowicz and Roult (1986) and Romanowicz (1987). Let us first consider the receiver effects, these are described by the operator $(\mathbf{v}\cdot\mathbf{D})_R$. It can be seen that $f_{KK'}^{\Psi}$ and $f_{KK'}^{\mu\mu'}$ in equations (26) and (27) can be written as

$$f_{KK'}^{\Psi}(\lambda,\mu) = S_{KK'}^{\Psi(0)}(\lambda,\mu)\, X_l^0(\lambda)X_{l'}^0(\lambda') - S_{KK'}^{\Psi(1)}(\lambda,\mu)\cos(\mu'-\phi^{\Psi})\, a_l a_{l'} X_l^1(\lambda)X_{l'}^1(\lambda') + S_{KK'}^{\Psi(2)}(\lambda,\mu)\cos 2(\mu'-\phi^{\Psi})\, b_l b_{l'} X_l^2(\lambda)X_{l'}^2(\lambda') \quad (29)$$

$$f_{KK'}^{\mu\mu'}(\lambda,\mu) = S_{KK'}^{\mu\mu'(0)}(\lambda,\mu)\, a_l X_l^1(\lambda)X_{l'}^0(\lambda') - S_{KK'}^{\mu\mu'(1)}(\lambda,\mu)\cos(\mu'-\phi^{\mu\mu'})\, a_{l'} X_l^0(\lambda)X_{l'}^1(\lambda') . \quad (30)$$

Therefore, the receiver operator should be applied to a sum of terms, each containing a factor

$$\eta(\lambda',\mu') = \cos m(\mu'-\phi_{max})\, X_l^m(\lambda') \qquad (m=0,1,2)\,. \tag{31}$$

Applying the displacement operator (2) to these factors shows that we can obtain the vertical component by making in equations (29) and (30) the following replacement

$$\cos m(\mu'-\phi_{max})\, X_l^m(\lambda') \longrightarrow U(a) X_l^m(\lambda') \cos m(\mu'-\phi_{max})\,. \tag{32a}$$

Similarly, the radial component follows by replacing

$$\cos m(\mu'-\phi_{max})\, X_l^m(\lambda') \longrightarrow V(a)\partial_{\lambda'} X_l^m(\lambda') \cos m(\mu'-\phi_{max}) - W(a)\frac{m}{\sin\lambda'} X_l^m(\lambda') \sin m(\mu'-\phi_{max})\,, \tag{32b}$$

while for the transverse component we should replace

$$\cos m(\mu'-\phi_{max})\, X_l^m(\lambda') \longrightarrow -W(a)\partial_{\lambda'} X_l^m(\lambda') \cos m(\mu'-\phi_{max}) - V(a)\frac{m}{\sin\lambda'} X_l^m(\lambda') \sin m(\mu'-\phi_{max})\,. \tag{32c}$$

In order to incorporate the source effects we should analyze terms of the form $(\mathbf{e}:\mathbf{M})_S X_l^m(\lambda)$ for $m=0,1,2$. As an example we show how to deal with the $m=2$ component. Using the recurrence relations for the X_l^m (Edmonds, 1960) one can show that

$$(\mathbf{e}:\mathbf{M})_S\; b_l X_l^2(\lambda) = (\mathbf{e}:\mathbf{M})_S \left[2\frac{\partial^2}{\partial\lambda^2} + l(l+1) \right] X_l^0(\lambda)\,.$$

The strain operator is essentially a differentiator. Since differentiations commute we therefore have

$$(\mathbf{e}:\mathbf{M})_S\; b_l X_l^2(\lambda) = \left[2\frac{\partial^2}{\partial\lambda^2} + l(l+1) \right] (\mathbf{e}:\mathbf{M})_S X_l^0(\lambda)\,. \tag{33}$$

In a similar way we find for the $m=1$ contribution

$$(\mathbf{e}:\mathbf{M})_S\; a_l X_l^1(\lambda) = \frac{\partial}{\partial\lambda} (\mathbf{e}:\mathbf{M})_S X_l^0(\lambda)\,. \tag{34}$$

The effect of the source operator $(\mathbf{e}:\mathbf{M})_S$ follows from expression (2.1.18) and the tables (2.1.22) and (2.1.23) in Gilbert and Dziewonski (1975). Using this result one finds

$$(\mathbf{e}:\mathbf{M})_s X_l^0(\lambda) = C_0 X_l^0(\lambda) + C_1 X_l^1(\lambda) + C_2 X_l^2(\lambda)\,. \tag{35}$$

The excitation coefficients C_0, C_1 and C_2 are given by

$$C_0 = \left[M_{rr}\dot{U}(r_s) + \tfrac{1}{2}(M_{\theta\theta}+M_{\phi\phi})F(r_s) \right]$$

$$C_1 = -a_l \left[M_{r\theta}\left[X(r_s)\cos\mu_s - Z(r_s)\sin\mu_s \right] + M_{r\phi}\left[X(r_s)\sin\mu_s + Z(r_s)\cos\mu_s \right] \right] \tag{36}$$

$$C_2 = b_l \frac{1}{r}\Big[\tfrac{1}{2}(M_{\theta\theta}-M_{\phi\phi})\Big[V(r_s)\cos 2\mu_s + W(r_s)\sin 2\mu_s\Big] + M_{\theta\phi}\Big[V(r_s)\sin 2\mu_s - W(r_s)\cos 2\mu_s\Big]\Big]$$

,μ_s is the source azimuth taken counterclockwise from south as shown in figure 1, and r_s denotes the radius of the source position.

To summarize, the source effects can be incorporated by making the following replacements in equations (26) and (27) (or (29) and (30)):

$$X_l^0(\lambda) \longrightarrow C_0 X_l^0(\lambda) + C_1 X_l^1(\lambda) + C_2 X_l^2(\lambda) \tag{37a}$$

$$a_l X_l^1(\lambda) \longrightarrow \frac{\partial}{\partial\lambda}\Big[C_0 X_l^0(\lambda) + C_1 X_l^1(\lambda) + C_2 X_l^2(\lambda)\Big] \tag{37b}$$

$$b_l X_l^2(\lambda) \longrightarrow \Big[2\frac{\partial^2}{\partial\lambda^2} + l(l+1)\Big]\Big[C_0 X_l^0(\lambda) + C_1 X_l^1(\lambda) + C_2 X_l^2(\lambda)\Big] \tag{37c}$$

6) Correspondence with propagating waves.

In order to take the surface wave limit, we consider the perturbation in the displacement in the frequency domain, using the Fourier transform convention of Aki and Richards (1980): $s(\omega) \equiv \int s(t)\exp i\omega t\, dt$. The perturbation in the displacement field excited by a step function excitation follows from the equations (5) and (10) of Tanimoto (1984), by making the substitution $p \rightarrow -i\omega$. Adding a factor $\omega_K^2\omega_{K'}^2$ due to the difference in normalization, changing the sign of H because of the difference in the definition of H in this paper and in Tanimoto (1984), and rearranging terms one finds that in the notation of equation (6)

$$s^1(\omega) = \sum_{KK',mm'} \frac{-i\omega_K\omega_{K'}}{4\omega}\Big[\frac{1}{\omega-\omega_K} - \frac{1}{\omega+\omega_K}\Big]\Big[\frac{1}{\omega-\omega_{K'}} - \frac{1}{\omega+\omega_{K'}}\Big] R_{K'}^{m'}\Big[H_{K'K}^{m'm} - \omega^2 P_{K'K}^{m'm}\Big] S_K^m \,. \tag{38}$$

If a small amount of damping (α) is applied, the term $1/(\omega-\omega_K)$ has a pole at $\omega_K = \omega + i\alpha$, while the term $1/(\omega+\omega_K)$ has a pole at $\omega_K = -\omega - i\alpha$. In the following derivation only the poles in the upper half plane contribute, and we therefore drop the contribution of the $1/(\omega+\omega_K)$ term. Likewise, the $1/(\omega+\omega_{K'})$ term also doesn't contribute, so that this term can also be discarded. Using the definition (7), expression (38) can be written as

$$s^1(\omega) = \sum_{KK'} \frac{-i\omega_K\omega_{K'}}{4\omega(\omega-\omega_K)(\omega-\omega_{K'})} A_{KK'}(\omega^2) \tag{39}$$

, with $A_{KK'}$ defined in equation (7). $A_{KK'}$ can be eliminated using expression (25). The summation over K and K' implies a summation over all pairs of mode branches, as well as a summation over all angular quantum numbers l and l' within each mode branch. We shall restrict our attention to the contribution of one pair of mode branches. Dropping the operators $(\mathbf{e}:\mathbf{M})_S$ and $(\mathbf{v}\cdot\mathbf{D})_R$ in equation (25), as well as the integration over the sphere, which we shall implicitly assume, we can write

$$s^1(\omega) = \sum_{l,l'} \frac{-i\,\omega_l \omega_{l'}}{4\omega(\omega-\omega_l)(\omega-\omega_{l'})} f_l f_{l'} \frac{2}{\sqrt{\omega_l \omega_{l'}}} \delta\omega^0_{ll'} X_l^0(\lambda) X_{l'}^0(\lambda') \tag{40}$$

It is understood that ω_l is the eigenfrequency of multiplet l belonging to mode branch K, and $\omega_{l'}$ is the eigenfrequency of multiplet l' on mode branch K' in the reference SNREI Earth model. $\delta\omega^0_{ll'}$ is the local frequency of interaction between multiplets l and l', as given in appendix B. We have only written the first term in the definition of f^{Ψ} in equation (26), extension of the derivation which follows to the other local frequencies of interaction in equations (26) and (27) is straightforward.

If the inhomogeneity is sufficiently far away from the source and the receiver and their antipodes ($\sin\lambda \gg 1/l$ and $\sin\lambda' \gg 1/l'$), then $X_l^0(\lambda)$ and $X_{l'}^0(\lambda')$ can be replaced by their asymptotic expansion (Edmonds, 1960).

$$s^1(\omega) = \sum_{l,l'} \frac{-i\,\omega_l \omega_{l'} f_l f_{l'} \delta\omega^0_{ll'}}{4\omega(\omega-\omega_l)(\omega-\omega_{l'})} \frac{2}{\sqrt{\omega_l \omega_{l'}}} \frac{\cos\left((l+\tfrac{1}{2})\lambda-\frac{\pi}{4}\right)\cos\left((l'+\tfrac{1}{2})\lambda'-\frac{\pi}{4}\right)}{\pi^2\sqrt{\sin\lambda\,\sin\lambda'}} \tag{41}$$

Using Poisson's sum formula both for l and l', and a contour integration in the upper half plane, the sum over l and l' can be performed. This procedure is shown in detail in Snieder and Nolet (1987). In their derivation the symmetry properties of the coefficients of the cosines under the parity transformation

$$l \longrightarrow -l-1 \tag{42}$$

play a crucial role. Since the $\delta\omega^i$ depend only on the eigenfunctions U, V, W and Φ_1 and the product $l(l+1)$, these terms are invariant under the transformation (42), see Snieder and Nolet (1987) for details. Therefore, the coefficients of the cosines in equation (41) satisfy the requirement (A6) of Snieder and Nolet (1987).

Using the derivation in the appendix of Snieder and Nolet (1987), equation (41) leads to the following contribution of the mode branches K and K'

$$s^1_{KK'}(\omega) = \frac{-i\,\omega f_l f_{l'} a^2}{4U_K U_{K'}} \frac{2}{\omega} \delta\omega^0_{ll'} \frac{e^{i\left((l+\frac{1}{2})\lambda+\frac{\pi}{4}\right)}\; e^{i\left((l'+\frac{1}{2})\lambda'+\frac{\pi}{4}\right)}}{\sqrt{\sin\lambda\,\sin\lambda'}}\,. \tag{43}$$

In this expression U_K and $U_{K'}$ are the group velocities of the modes under consideration at the Earth's surface. The contour integration in the derivation only gives a contribution at the poles of the sum in equation (41), where

$$\omega_{qnl} = \omega_{q'n'l'} = \omega\,. \tag{44}$$

In this expression it is made explicit that the eigenfrequencies depend both on the radial modes number (n), the angular mode number (l) and the kind of modes ($q=S$ or $q=T$). Note that only

resonant modes are coupled by the inhomogeneity. For a given mode branch (where n and q or n' and q' are specified) the values of l and l' which are to be used in equation (43) follow from the condition (44).

So far, we have only considered terms depending on the local frequency $\delta\omega^0_{KK'}$ and have not applied the source and receiver operators. The same derivation holds for the remaining terms in equations (26) and (27), only we need to consider asymptotic expansions of $a_l a_{l'} X_l^1(\lambda) X_{l'}^1(\lambda')$, $b_l b_{l'} X_l^2(\lambda) X_{l'}^2(\lambda')$, $a_{l'} X_l^0(\lambda) X_{l'}^1(\lambda')$ or $a_l X_l^1(\lambda) X_{l'}^0(\lambda')$. Compared with the outgoing wave expansion of X_l^0, each term $a_l X_l^1$ produces an extra factor $i(l+\frac{1}{2})$, while each term $b_l X_l^2$ leads to an extra factor $-(l+\frac{1}{2})^2$.

In the surface wave limit, the source and receiver operators can be rewritten in a concise way. In the asymptotic expansion of the X_l^m it is assumed that $\sin\lambda \gg m/(l+\frac{1}{2})$, and a similar far field condition holds for the primed coordinates. Under this restriction, the directivity of the radiation pattern leads in the computation of the displacement to terms of relative order $1/l$, and can be neglected. In this approximation, application of the receiver operator $(\mathbf{v}\cdot\mathbf{D})_R$, as in equations (32a-c), amounts to a multiplication with a factor $i(\mathbf{v}\cdot\mathbf{p}')$. The polarization vector $\mathbf{p}'$ is defined by

$$\mathbf{p}' = (l'+\tfrac{1}{2})(V'\hat{\boldsymbol{\lambda}}' - W'\hat{\boldsymbol{\mu}}') - iU'\hat{\mathbf{r}} \ . \tag{45}$$

For the source effects the substitutions (37a-c) should be used. In the far field, each differentiation $\frac{\partial}{\partial\lambda}$ of the outgoing wave component of X_l^m produces an extra factor $i(l+\frac{1}{2})$. Apart from the effects of the differentiations, we should also analyze the term $C_0X_l^0(\lambda)+C_1X_l^1(\lambda)+C_2X_l^2(\lambda)$ which occur in (37a-c). Using the asymptotic outgoing wave expansion for the X_l^m we should replace

$$C_0X_l^0(\lambda)+C_1X_l^1(\lambda)+C_2X_l^2(\lambda) \longrightarrow \frac{1}{2\pi i\sqrt{\sin\lambda}}(C_0+iC_1-C_2)\exp i((l+\tfrac{1}{2})\lambda+\frac{\pi}{4}) \ .$$

The source effects are therefore contained in the factor $(C_0+iC_1-C_2)$. Using expression (36), with the definition (45) one finds that

$$C_0+iC_1-C_2 = -i\mathbf{E}^*:\mathbf{M} \ , \tag{46}$$

where the excitation tensor $\mathbf{E}$ is given by

$$\mathbf{E} = \left[\hat{\mathbf{r}}(\partial_r - \frac{1}{r}) + i\frac{l+\frac{1}{2}}{r}\hat{\boldsymbol{\lambda}}\right]\mathbf{p} - \frac{iU}{r}\mathbf{I} \ . \tag{47}$$

(This can most easily be seen by rotating $\hat{\boldsymbol{\lambda}}$ and $\mathbf{p}$ from the (r,λ,μ) frame to the fixed (r,θ,ϕ) system in which the moment tensor is defined.) The polarization vector is defined by the unprimed equivalent of equation (45), where the modes are to be evaluated at the source depth. Therefore, the source effects are incorporated by a multiplication with $-i\mathbf{E}^*:\mathbf{M}$.

To summarize, the displacement spectrum of the perturbed wave can be written as the following double sum over all mode branches K and K'

$$s^1(\omega) = \sum_{KK'} \frac{-1}{i\omega} \int_{\Omega} (\mathbf{E}^* : \mathbf{M}) \frac{\exp i(k_K(\omega)d + \frac{\pi}{4})}{(\sin \frac{d}{a})^{1/2}} V_{KK'} \frac{\exp i(k'_{K'}(\omega)d' + \frac{\pi}{4})}{(\sin \frac{d'}{a})^{1/2}} (\mathbf{p}_{K'} \cdot \mathbf{v})\, d\Omega \quad (48)$$

, where we defined the epicentral distance and wavenumber

$$d = a\lambda \quad , \quad k_K(\omega) = (l+1/2)/a \quad . \quad (49)$$

In these expression l and l' are defined by the condition (44), so that only one mode on each mode branch contributes to equation (48). The interaction coefficients $V_{KK'}$ are given by

$$\begin{aligned} V_{KK'} = \frac{-\omega^2 a^2 f_l f_{l'}}{4U_K(\omega)U_{K'}(\omega)} \frac{2}{\omega} \Big\{ & \delta\omega^0_{KK'} + (l+1/2)(l'+1/2)\delta\omega^1_{KK'} \cos\Psi + (l+1/2)(l'+1/2)\delta\omega^2_{KK'} \sin\Psi \\ & + (l+1/2)^2(l'+1/2)^2\delta\omega^3_{KK'} \cos 2\Psi + (l+1/2)^2(l'+1/2)^2\delta\omega^4_{KK'} \sin 2\Psi \\ & - i(l'+1/2)\delta\omega^5_{KK'} \cos(\mu'-\phi_h) - i(l'+1/2)\delta\omega^6_{KK'} \sin(\mu'-\phi_h) \\ & - i(l'+1/2)\delta\omega^9_{KK'} \cos(\mu'-\phi_{\delta\phi}) - i(l'+1/2)\delta\omega^{10}_{KK'} \sin(\mu'-\phi_{\delta\phi}) \\ & - i(l'+1/2)\delta\omega^{13}_{KK'} \cos(\mu'-\phi_{\delta\dot{\phi}}) - i(l'+1/2)\delta\omega^{14}_{KK'} \sin(\mu'-\phi_{\delta\dot{\phi}}) \\ & + i(l+1/2)\delta\omega^7_{KK'} \cos(\mu-\phi_h) + i(l+1/2)\delta\omega^8_{KK'} \sin(\mu-\phi_h) \\ & + i(l+1/2)\delta\omega^{11}_{KK'} \cos(\mu-\phi_{\delta\phi}) + i(l+1/2)\delta\omega^{12}_{KK'} \sin(\mu-\phi_{\delta\phi}) \\ & + i(l+1/2)\delta\omega^{15}_{KK'} \cos(\mu-\phi_{\delta\dot{\phi}}) + i(l+1/2)\delta\omega^{16}_{KK'} \sin(\mu-\phi_{\delta\dot{\phi}}) \Big\} \end{aligned} \quad (50)$$

The local frequencies $\delta\omega^i$ are given in appendix B.

Expression (48) can be interpreted in the same way as in Snieder (1986a). At the source mode K is excited, this is described by the excitation tensor $\mathbf{E}$. Surface wave mode K then travels to the point of interaction, this is described by the term $\exp i(kd+\pi/4)/(\sin d/a)^{1/2}$. The interaction coefficients $V_{KK'}$ describe the scattering and mode conversion effects from mode K to mode K'. After this, modes K' travels to the receiver, thus producing another propagator factor $\exp i(k'd'+\pi/4)/(\sin d'/a)^{1/2}$. Finally the oscillation at the receiver is described by the

polarization vector $\mathbf{p}'$. An integration over the horizontal extend of the heterogeneity and a summation over all incoming (K) and outgoing modes (K') completes the expression for the perturbed surface wave.

7) Discussion and a comparison with previous results.

The theory presented in Woodhouse (1980) and Woodhouse (1983), and the theory presented here are equivalent formulations of the same first order theory for normal mode interactions. Woodhouse (1980) expresses the heterogeneity in spherical harmonics, so that the integration over the sphere can be performed analytically, thus producing an algebraic system of equations for the mode interactions. In Woodhouse (1983) the normal modes are expressed in a fixed (arbitrary) reference frame, whereas in our theory the modes are expressed in coordinate systems fixed to the source and the receiver, which allows for a simple scattering interpretation of the normal mode interactions. The fact that Woodhouse (1983) expresses the interacting normal modes in the same reference frame precludes taking the surface wave limit directly from his results.

There is a close analogy between equation (25) with the local frequencies $\delta\omega^i$ (i=0,16) of appendix B, and the coupling terms given in equations (A36) through (A42) of Woodhouse (1980) for an inhomogeneity of the form $Y_{l'}^{m''}(\theta,\phi)$. These expressions can be compared using the correspondence

$$B_{l'l''l}^{(m)+} \longleftrightarrow (-1)^m \left[\frac{(l+m)!(l'+m)!}{(l-m)!(l'-m)!}\right]^{1/2} X_l^m(\lambda) X_{l'}^m(\lambda') \cos m\Psi \quad (m=0,1,2)$$

$$B_{l'l''l}^{(m)-} \longleftrightarrow (-1)^{m+1} \left[\frac{(l+m)!(l'+m)!}{(l-m)!(l'-m)!}\right]^{1/2} X_l^m(\lambda) X_{l'}^m(\lambda') \sin m\Psi \quad (m=1,2)$$

$$l''(l''+1) B_{l'l''l}^{(0)+} \longleftrightarrow X_l^0(\lambda) X_{l'}^0(\lambda') \frac{-1}{r^2} \nabla_1^2$$

$$B_{l'll''}^{(1)+} \longleftrightarrow -a_{l'} S_\xi X_l^0(\lambda) X_{l'}^1(\lambda') \cos(\mu'-\phi_\xi) \qquad (51)$$

$$iB_{l'll''}^{(1)-} \longleftrightarrow -a_{l'} S_\xi X_l^0(\lambda) X_{l'}^1(\lambda') \sin(\mu'-\phi_\xi)$$

$$B_{ll'l''}^{(1)+} \longleftrightarrow a_l S_\xi X_l^1(\lambda) X_{l'}^0(\lambda') \cos(\mu-\phi_\xi)$$

$$-iB_{ll'l''}^{(1)-} \longleftrightarrow a_l S_\xi X_l^1(\lambda) X_{l'}^0(\lambda') \sin(\mu-\phi_\xi)$$

In our theory we avoid an expansion of the heterogeneity in spherical harmonics, so that an integral over the inhomogeneity is present in the final result (25). It depends on the application which formulation is more useful. If one wants to restrict oneself to smooth inhomogeneities on a global scale, the formulation of Woodhouse (1980,1983) is preferable. For sharp localized inhomogeneities the theory presented here is more useful since it allows for an

efficient local representation of such an heterogeneity. For this type of heterogeneity a very large number of terms is needed if one wants to express the inhomogeneity in spherical harmonics. This expansion in spherical harmonics leads then to a global theory, whereas we know that some problems have a local character. As an example, think of the scattering of surface waves by a continental margin, as observed by Levshin and Berteussen (1979) or Bungum and Capon (1974).

The theory of this paper is related in a curious way to the results of Woodhouse and Girnius (1982). They used a spherical harmonics expansion for the inhomogeneity, but by applying a partial integration reexpressed this result in a local integral over the inhomogeneity. This integral contains a kernel given by $Y_l^m(\theta_r,\phi_r)\left[(\nabla_1^2)^i Y_l^{m*}(\theta,\phi)Y_l^{m'}(\theta,\phi)\right] Y_l^{m'*}(\theta_s,\phi_s)$ for $(i=0,1,2)$. As shown in Romanowicz (1987), this expression can be reduced to $(\nabla_1^2)^i\left[X_l^0(\lambda)X_l^0(\lambda')\right]$, where we used the notation of figure 1. It is possible to show the identities

$$\nabla_1^2\left[X_l^0(\lambda)X_{l'}^0(\lambda')\right] = -\left[l(l+1)+l'(l'+1)\right]X_l^0(\lambda)X_{l'}^0(\lambda') - 2a_l a_{l'}X_l^1(\lambda)X_{l'}^1(\lambda')\cos\Psi \qquad (52)$$

, and

$$\begin{aligned}\nabla_1^4\left[X_l^0(\lambda)X_{l'}^0(\lambda')\right] = &\left[\left[l(l+1)+l'(l'+1)\right]^2 + 2l(l+1)l'(l'+1)\right]X_l^0(\lambda)X_{l'}^0(\lambda') \\ &- 4\left[l(l+1)+l'(l'+1)-1\right]a_l a_{l'}X_l^1(\lambda)X_{l'}^1(\lambda')\cos\Psi \\ &+ 2b_l b_{l'}X_l^2(\lambda)X_{l'}^2(\lambda')\cos 2\Psi\end{aligned} \qquad (53)$$

, with a_l and b_l defined in equation (28) Therefore, the results which are derived in this paper with geometrical methods can also be obtained using the algebraic results (52) and (53). This can only be done from the theory of Woodhouse and Girnius (1982) for the case of unconverted modes, since they did not address the problem of mode conversions. Romanowicz (1987) pointed out that the formalism of Woodhouse and Girnius (1982) can be generalized for the interactions between different modes of equal kind. However, it is not clear to us how the sin Ψ and sin 2Ψ interaction terms for the coupling between toroidal and spheroidal modes can be derived in a way similar to the equations (52) and (53).

The break up into local frequencies $\delta\omega_{KK'}^i$ in this paper can be compared to that of Woodhouse and Girnius (1982) for the case of self interaction ($K=K'$), as needed for the calculation of the location parameter of Jordan (1978). Only $\delta\omega_{KK}^0=\delta\omega_K^0$ is equal in this paper and in Woodhouse and Girnius (1982), while $\delta\omega_{KK}^1$ and $\delta\omega_{KK}^3$ as defined in equation (26), are linear combinations of $\delta\omega_{KK}^0$, $\delta\omega_{KK}^1$, $\delta\omega_{KK}^2$ as defined in Woodhouse and Girnius (1982). This linear combination follows from the identities (52) and (53). The $\delta\omega_{KK'}^2$ and $\delta\omega_{KK'}^4$ terms in (26) have no equivalence in the results of Woodhouse and Girnius (1982), since these terms describe interactions between spheroidal and toroidal modes.

After the surface wave limit is taken, the theory of this paper is to leading order in l equivalent to the results of Snieder and Nolet (1987). They only took the leading order terms of the interaction terms into account, whereas in this paper no high l approximation is used in the derivation of the interaction terms. Note that also the excitation terms and displacement terms agree up to terms of relative order $1/l$. The reason for this is that even though we used a high l

approximation to derive (45) and (47), the effects of sphericity are fully taken into account, whereas Snieder and Nolet (1987) ignored subdominant contributions. The main discrepancy is the last term in the excitation tensor (47), which after a contraction with the moment tensor leads to a contribution $\frac{iU}{r_s}$ *tr* **M**. This term precludes a dyadic decomposition of the excitation tensor **E**, and is only nonzero for sources with an explosive component.

It can be seen by comparing equation (50) and appendix B with the corresponding results of Snieder and Nolet (1987), that the interaction terms in equation (50) of this paper and in equation (5.2) through (5.5) of Snieder and Nolet (1987) are (up to terms of relative order $1/l$) proportional, with a proportionality factor $\omega^2 f_l f_{l'} a^2/4U_K U_{K'}$. The reason for this discrepancy is that the eigenfunctions in Snieder and Nolet (1987) are normalized differently with a relative factor $\omega f_l a/2U_K$. Expression (48) differs with a factor $-1/i\,\omega$ from expression (4.8) from Snieder and Nolet (1987). However, equation (48) is the perturbation in the displacement in case of a step function excitation, whereas equation (4.8) of Snieder and Nolet (1987) is the perturbation in displacement for a general excitation $F(\omega)$. These results are reconciled if equation (48) is multiplied with $-i\,\omega$ to correct for the source spectrum of the step function excitation.

The results of Snieder and Nolet (1987) were derived using polarization vectors. However, the concept 'polarization vector' is only useful in the far field limit, where the direction of the particle motion is completely described by the wave path. It is therefore not surprising that the results of Snieder and Nolet (1987) are only valid in the far field. In this paper, polarization vectors have not been used in the derivation of the interaction coefficients. The interaction terms derived in expressions (26) and (27) are not only valid in the far field limit, because in section 2 no restriction was made for the epicentral distances λ and λ'. Interestingly, the local frequencies of interaction in appendix B are, apart from a trivial proportionality factor, to leading order in l equal to the far field interaction terms of Snieder and Nolet (1987). From this we conclude that near field effects only affect the propagator terms, but not the interaction terms.

The question of the far field restrictions is important, because in many applications the source and the receiver may be located on top of an inhomogeneity (or it's antipode), thus violating the far field conditions. Unfortunately, in taking the surface wave limit in section 5, an asymptotic expansion of the spherical harmonics is used which is only valid in the far field. Therefore, our surface wave results are only valid in the far field. Clearly, a new procedure is needed for the surface wave limit, which uniformly takes care of both the far field effects and the near field effects. (The special case where the source and receiver are antipodal is discussed in Romanowicz and Roult, 1988.)

Perturbations in low frequency seismograms due to lateral heterogeneity can be computed using normal mode summation using the equations (6), (25), (29) and (30), where the source and receiver effects are affected with the substitutions (37a-c) and (32a-c). Perturbations in surface wave seismograms follow from the expressions (48) and (50).

Numerically, it is much simpler to compute equation (25), than the corresponding expression (40) from Woodhouse (1983), or expression (4.5) from Woodhouse and Girnius (1982) for the self interaction of modes. The reason for this is that in the latter formulations a double sum over modes Y_l^m has to be performed for all $0 \le m \le l$, whereas for equation (27) of this paper one only needs to compute X_l^m for $m=0,1,2$, and some simple geometrical variables on a sphere.

The theory presented in this paper leads to a formalism for normal modes interactions without using an expansion of the inhomogeneity in spherical harmonics, and without using generalized spherical harmonics. The simplicity of the final results allows for analytical manipulation (along the lines of Romanowicz (1987), Snieder (1986a) or Snieder (1987)), and leads to an efficient algorithm for the generation of synthetic seismograms in a laterally heterogeneous Earth.

References

Aki, K., and P.G. Richards, *Quantitative seismology, part 1*, Freeman, San Francisco, 1980.

Backus, G.E., Geographical interpretation of measurements of average phase velocities over great circular and great semi circular paths, *Bull. seism. Soc. Am., 54*, 571-610, 1964.

Bungum, H., and J. Capon, Coda pattern and multipathing propagation of Rayleigh waves at NORSAR, *Phys. Earth Plan. Int., 9*, 111-127, 1974.

Dahlen, F.A., The normal modes of a rotating elliptical Earth, *Geophys. J. R. astr. Soc., 16*, 329-367, 1968.

Dahlen, F.A., The normal modes of a rotating elliptical Earth-II. Near resonance multiplet coupling, *Geophys. J. R. astr. Soc., 18*, 397-406, 1969.

Dahlen, F.A., Inference of the lateral heterogeneity of the Earth from the eigenfrequency spectrum: a linear inverse problem, *Geophys. J. R. astr. Soc., 38*, 143-167, 1974.

Dahlen, F.A., The spectra of unresolved split normal mode multiplets, *Geophys. J. R. astr. Soc., 58*, 1-33, 1979.

Edmonds, A.R., *Angular mechanics in Quantum Mechanics*, Princeton University Press, Princeton, 1960.

Gilbert, F., and A. Dziewonski, An application of normal mode theory to the retrieval of structural parameters and source mechanisms from seismic spectra, *Phil. Trans. R. Soc. London, A278*, 187-269, 1975.

Hudson, J.A., and J.R. Heritage, The use of the Born approximation in seismic scattering problems, *Geophys. J. R. astr. Soc., 66*, 221-240, 1982.

Jordan, T.H., A procedure for estimating lateral variations from low frequency eigenspectra data, *Geophys. J. R. astr. Soc., 52*, 441-455, 1978.

Kennett, B.L.N., Guided wave propagation in laterally varying media -I. Theoretical development., *Geophys. J. R. astr. Soc., 79*, 235-255, 1984a.

Kennett, B.L.N., Guided wave propagation in laterally varying media -II. Lg waves in north western Europe., *Geophys. J. R. astr. Soc., 79*, 257-267, 1984b.

Levshin, A., and K.A. Berteussen, Anomalous propagation of surface waves in the Barentz Sea as inferred from NORSAR recordings, *Geophys. J. R. astr. Soc., 56*, 97-118, 1979.

Luh, P.C., Free oscillations of the laterally inhomogeneous Earth: Quasi degenerate multiplet coupling, *Geophys. J. R. astr. Soc., 32*, 187-207, 1973.

Luh, P.C., Normal modes of a rotating self gravitating inhomogeneous Earth, *Geophys. J. R. astr. Soc., 38*, 187-224, 1974.

Phinney, R.A., and R. Burridge, Representation of the elastic-gravitational excitation of a spherical earth model by generalized spherical harmonics, *Geophys. J. R. asrt. Soc., 34*, 451-487, 1973.

Romanowics, B., and G. Roult, First order asymptotics for the eigenfrequencies of the Earth and application to the retrieval of large scale variations of structure, *Geophys. J. R. astr. Soc., 87,* 209-239, 1986.

Romanowicz, B., Multiplet-multiplet coupling due to lateral heterogeneity: asymptotic effects on the amplitude and frequency of the Earth's normal modes, *Geophys. J. R. astr. Soc.,* 1987. , in press.

Romanowicz, B., and G. Roult, Asymptotic approxmations for normal modes and surface waves in the vicinity of the antipode; constraints on global Earth models, *(in preparation),* 1988.

Romanowicz, B., and R. Snieder, A new formalism for the effect of lateral heterogeneity on normal modes and surface waves - II: General anisotropic perturbations, *submitted to Geophys. J. R. astr. Soc.,* 1987.

Snieder, R., 3D Linearized scattering of surface waves and a formalism for surface wave holography, *Geophys. J. R. astr. Soc., 84,* 581-605, 1986a.

Snieder, R., The influence of topography on the propagation and scattering of surface waves, *Phys. Earth. Plan. Int., 44,* 226-241, 1986b.

Snieder, R., On the connection between ray theory and scattering theory for surface waves, in *Mathematical Geophysics, a survey of recent developments in seismology and geodynamics,* edited by Vlaar, N.J., Nolet, G., Wortel, M.J.R. and Cloetingh, S.A.P.L., pp. 77-83, Reidel, Dordrecht, 1987.

Snieder, R., and G. Nolet, Linearized scattering of surface waves on a spherical Earth, *J. Geophys., 61,* 55-63, 1987.

Tanimoto, T., A simple derivation of the formula to calculate long-period seismograms in a heterogeneous earth by normal mode summation, *Geophys. J. R. astr. Soc., 77,* 275-278, 1984.

Woodhouse, J.H., The coupling and attenuation of nearly resonant multiplets in the Earth's free oscillation spectrum, *Geophys. J. R. astr. Soc., 61,* 261-283, 1980.

Woodhouse, J.H., The joint inversion of seismic waveforms for lateral variations in Earth structure and earthquake source parameters, in *Earthquakes: Observation, Theory and Interpretation, Proc. Int. School Phys. Enrico Fermi, 85,* edited by H. Kanamori and E. Boschi, pp. 366-397, 1983.

Woodhouse, J.H., and F.A. Dahlen, The effect of a general aspherical perturbation on the free oscillations of the Earth, *Geophys. J. R. astr. Soc., 53,* 335-354, 1978.

Woodhouse, J.H., and A.M. Dziewonski, Mapping the upper mantle: Three dimensional modeling of the Earth structure by inversion of seismic waveforms, *J. geophys. Res., 89,* 5923-5986, 1984.

Woodhouse, J.H., and T.P. Girnius, Surface waves and free oscillations in a regionalized Earth model, *Geophys. J. R. astr. Soc., 68,* 653-673, 1982.

Appendix A, a rearrangement of the normal mode interaction terms due to the gravitational potential

According to equation (A1) of Woodhouse (1980), the normal mode interaction due to the perturbation in the gravitational potential $\delta\phi$ is given by

$$<K',m'\,|\,Z_{\delta\phi}\,|\,K,m> = \tfrac{1}{2}\int_V \rho\Big[\mathbf{s}\cdot\nabla(\mathbf{s}'\cdot\nabla\delta\phi) + \mathbf{s}'\cdot\nabla(\mathbf{s}\cdot\nabla\delta\phi) - (\mathbf{s}\cdot\nabla\delta\phi)(\nabla\cdot\mathbf{s}') - (\mathbf{s}'\cdot\nabla\delta\phi)(\nabla\cdot\mathbf{s})\Big]\,dV. \tag{A1}$$

Let us consider the term

$$I \equiv \int_V \rho\mathbf{s}\cdot\nabla(\mathbf{s}'\cdot\nabla\delta\phi)\,dV\ . \tag{A2}$$

This integral can be split in a radial integral and an integral over the unit sphere. Since the density ρ of the SNREI reference model is radially symmetric, we have

$$I = \int_0^a \rho\left[\int_\Omega \mathbf{s}\cdot\nabla(\mathbf{s}'\cdot\nabla\delta\phi)\,d\Omega\right] r^2 dr \tag{A3}$$

, where Ω denotes the unit sphere.

Decompose $\mathbf{s}$ in a horizontal component and a vertical component, and apply an integration by parts to the term with the horizontal component, this leads to

$$\int_\Omega \mathbf{s}\cdot\nabla(\mathbf{s}'\cdot\nabla\delta\phi)d\Omega = \frac{1}{r}\int_\Omega \mathbf{s}_H\cdot\nabla_1(\mathbf{s}'\cdot\nabla\delta\phi)d\Omega + \int_\Omega s_r\partial_r(\mathbf{s}'\cdot\nabla\delta\phi)d\Omega$$

$$= \frac{-1}{r}\int_\Omega (\nabla_1\cdot\mathbf{s}_H)(\mathbf{s}'\cdot\nabla\delta\phi)d\Omega + \int_\Omega s_r\partial_r(\mathbf{s}'\cdot\nabla\delta\phi)d\Omega \tag{A4}$$

Using the decomposition $\nabla = \frac{1}{r}\nabla_1 + \hat{\mathbf{r}}\partial_r$ and differentiation with respect to r gives

$$\partial_r(\mathbf{s}'\cdot\nabla\delta\phi) = \frac{1}{r}\dot{\mathbf{s}}_H'\cdot\nabla_1\delta\phi + \frac{1}{r}\mathbf{s}_H'\cdot\nabla_1\dot{\delta\phi} - \frac{1}{r^2}\mathbf{s}_H'\cdot\nabla_1\delta\phi + \dot{s}_r'\dot{\delta\phi} + s_r'\ddot{\delta\phi}\ . \tag{A5}$$

The $\ddot{\delta\phi}$ term can be eliminated using

$$\ddot{\delta\phi} = \frac{\partial^2}{\partial r^2}\delta\phi = \frac{1}{r^2}\frac{\partial}{\partial r}\left[r^2\frac{\partial\delta\phi}{\partial r}\right] - \frac{2}{r}\dot{\delta\phi} = \left[\nabla^2 - \frac{1}{r^2}\nabla_1^2\right]\delta\phi - \frac{2}{r}\dot{\delta\phi} \tag{A6}$$

, and the field equation for the perturbation in the gravitational potential

$$\nabla^2\delta\phi = 4\pi G\,\delta\rho \tag{A7}$$

, so that

$$\ddot{\delta\phi} = 4\pi G\,\delta\rho - \frac{1}{r^2}\nabla_1^2\delta\phi - \frac{2}{r}\dot{\delta\phi}\ . \tag{A8}$$

The first term on the right hand side of equation (A8) is absorbed in the $\delta\rho$ term of equation (15), leading to a factor $8\pi G\,\rho s_r s_{r'}$ instead of the factor $4\pi G\,\rho s_r s_{r'}$ in equation (A1) of Woodhouse (1980). Inserting (A4) through (A7) in equation (A1) leads to the gravitational perturbation term in equation (15).

Appendix B, the local frequencies of interaction $\delta\omega^i$.

$$\delta\omega^0 = \frac{\sqrt{\omega\omega'}}{2}\int_0^a \Big\{ (\delta\kappa - \frac{2}{3}\delta\mu)(\dot{U}+F)(\dot{U}'+F') + \delta\mu(FF'+2\dot{U}\dot{U}')$$

$$+ \delta\rho(U\dot{\Phi}_1'+\dot{\Phi}_1U'+8\pi GUU'-\tfrac{1}{2}g(UF'+FU'+\frac{4}{r}UU')-\omega^2UU')$$

$$- \rho UU'(\frac{1}{r^2}\nabla_1^2\delta\phi) - \rho(UF'+FU')\delta\dot{\phi}\Big\} r^2dr$$

$$- \frac{\sqrt{\omega\omega'}}{2}\sum hr^2\Big[(\kappa - \frac{2}{3}\mu)(\dot{U}+F)(\dot{U}'+F') + \mu(FF'+2\dot{U}\dot{U}')$$

$$+ \rho(U\dot{\Phi}_1'+\dot{\Phi}_1U'+8\pi GUU'-\tfrac{1}{2}g(UF'+FU'+\frac{4}{r}UU')-\omega^2UU')$$

$$- (\kappa - \frac{2}{3}\mu)(2\dot{U}\dot{U}'+\dot{U}F'+F\dot{U}')-4\mu\dot{U}\dot{U}'\Big]_-^+$$

$$\delta\omega^1 = \frac{\sqrt{\omega\omega'}}{2}\int_0^a \Big\{ \delta\mu(XX'+ZZ')+\delta\rho\,(V\Phi_1'+\Phi_1V'+\frac{1}{2r}g(UV'+VU')-\omega^2(VV'+WW'))\Big\} r^2dr$$

$$- \frac{\sqrt{\omega\omega'}}{2}\sum hr^2\Big[\mu(XX'+ZZ')+\rho\,(V\Phi_1'+\Phi_1V'+\frac{1}{2r}g(UV'+VU')-\omega^2(VV'+WW'))$$

$$-\mu(\dot{V}X'+\dot{W}Z'+X\dot{V}'+Z\dot{W}')\Big]_-^+$$

$$\delta\omega^2 = \frac{\sqrt{\omega\omega'}}{2}\int_0^a \Big\{ +\delta\mu(XZ'-ZX')+\delta\rho\,(W\Phi_1'-\Phi_1W'+\frac{1}{2r}g(UW'-WU')-\omega^2(VW'-WV'))\Big\} r^2dr$$

$$- \frac{\sqrt{\omega\omega'}}{2}\sum hr^2\Big[+\mu(XZ'-ZX')+\rho\,(W\Phi_1'-\Phi_1W'+\frac{1}{2r}g(UW'-WU')-\omega^2(VW'-WV'))$$

$$-\mu(\dot{V}X'-\dot{W}X'-Z\dot{V}'+X\dot{W}')\Big]_-^+$$

$$\delta\omega^3 = \frac{\sqrt{\omega\omega'}}{2}\int_0^a \delta\mu(VV'+WW')\,dr - \frac{\sqrt{\omega\omega'}}{2}\sum h\Big[\mu(VV'+WW')\Big]_-^+$$

$$\delta\omega^4 = \frac{\sqrt{\omega\omega'}}{2}\int_0^a \delta\mu(VW'-WV')\,dr - \frac{\sqrt{\omega\omega'}}{2}\sum h\Big[\mu(VW'-WV')\Big]_-^+$$

$$\delta\omega^5 = -\frac{\sqrt{\omega\omega'}}{2}\sum r\,S_h\left[\left((\kappa-\frac{2}{3}\mu)(\dot{U}+F)+2\mu\dot{U}\right)V'\right]_-^+$$

$$\delta\omega^6 = -\frac{\sqrt{\omega\omega'}}{2}\sum r\,S_h\left[\left((\kappa-\frac{2}{3}\mu)(\dot{U}+F)+2\mu\dot{U}\right)W'\right]_-^+$$

$$\delta\omega^7 = -\frac{\sqrt{\omega\omega'}}{2}\sum r\,S_h\left[V\left((\kappa-\frac{2}{3}\mu)(\dot{U}'+F')+2\mu\dot{U}'\right)\right]_-^+$$

$$\delta\omega^8 = -\frac{\sqrt{\omega\omega'}}{2}\sum r\,S_h\left[W\left((\kappa-\frac{2}{3}\mu)(\dot{U}'+F')+2\mu\dot{U}'\right)\right]_-^+$$

$$\delta\omega^9 = \frac{\sqrt{\omega\omega'}}{4}\int_0^a \rho S_{\delta\phi}\left(U\dot{V}'+\frac{UV'}{r}-\dot{U}V'-2FV'\right)r^2dr$$

$$\delta\omega^{10} = \frac{\sqrt{\omega\omega'}}{4}\int_0^a \rho S_{\delta\phi}\left(U\dot{W}'+\frac{UW'}{r}-\dot{U}W'-2FW'\right)r^2dr$$

$$\delta\omega^{11} = \frac{\sqrt{\omega\omega'}}{4}\int_0^a \rho S_{\delta\phi}\left(\dot{V}U'+\frac{VU'}{r}-V\dot{U}'-2VF'\right)r^2dr$$

$$\delta\omega^{12} = \frac{\sqrt{\omega\omega'}}{4}\int_0^a \rho S_{\delta\phi}\left(\dot{W}U'+\frac{WU'}{r}-W\dot{U}'-2WF'\right)r^2dr$$

$$\delta\omega^{13} = \frac{\sqrt{\omega\omega'}}{4}\int_0^a \rho S_{\delta\dot{\phi}}\,UV'\,r^2dr$$

$$\delta\omega^{14} = \frac{\sqrt{\omega\omega'}}{4}\int_0^a \rho S_{\delta\dot{\phi}}\,UW'\,r^2dr$$

$$\delta\omega^{15} = \frac{\sqrt{\omega\omega'}}{4}\int_0^a \rho S_{\delta\dot{\phi}}\,VU'\,r^2dr$$

$$\delta\omega^{16} = \frac{\sqrt{\omega\omega'}}{4}\int_0^a \rho S_{\delta\dot{\phi}}\,WU'\,r^2dr$$

Chapter 8

Theory and numerical examples of waveform inversions of surface wave data

1) Introduction.

Standard surface wave analysis proceeds by extracting path averaged group or phase velocities from surface wave data using dispersion analysis. If sufficient data are available, these path averaged dispersion data can be used to determine the local phase or group velocity. Mathematically, this approach relies on the great circle theorem (Backus, 1964; Jordan, 1978; Dahlen, 1979), or more accurately on the minor arc theorem (Romanowicz, 1987). These theorems state that surface waves are only influenced by the integral of the phase or group velocity over the source receiver great circle (or minor arc). This is justified if the lateral heterogeneity is smooth on a scale of a wavelength of the surface waves under consideration.

In practice, this condition may not be satisfied. For example, a 30 s. Rayleigh wave has a wavelength of approximately 120 km. In continents the lateral variation on this scale can be considerable, so that the use of the great circle (minor arc) theorem and the related dispersion measurements are not justified. Surprisingly, this well known fact is widely ignored and in some cases dispersion analysis is used over structures which have the same length scale as the surface waves e.g. Panza et al. (1980), Calcagnile and Scarpa (1985). If the structure is not smooth on a scale of a wavelength, surface wave scattering and multipathing may occur. This is documented for reflection of surface waves at a continental margin by Levshin and Berteussen (1979) and Bungum and Capon (1974). Linearized scattering theory can be used to describe these effects. This theory is developed both for a flat geometry (Snieder, 1986ab), and for a spherical geometry (Snieder and Nolet, 1987).

Scattered surface waves must to some degree be responsible for the generation of the surface wave coda, and it would be fruitful to extract this information from the surface wave coda. In Snieder (1986a) a holographic inversion scheme is presented for the surface wave coda, reminiscent of migration procedures in exploration seismics. This inversion method has been applied successfully to image the surface wave reflections from a concrete dam on a tidal flat (Snieder, 1987a). In order to achieve this, several severe approximations have been used, and it is desirable to give waveform inversion for surface data a firmer theoretical basis. This paper serves to provide a rigorous waveform fitting method for surface waves, based on surface wave scattering theory. This inversion is set up as a huge matrix problem, and it is shown how solutions can be found iteratively.

This chapter is submitted for publication as:

Snieder, R., Large scale waveform inversions of surface waves for lateral heterogeneity -I: Theory and numerical examples, *submitted to J. Geophys. Res.*, 1988.

There is, however, more to be gained from surface wave scattering theory than an analysis of the surface wave coda. Surface wave scattering theory can also be used to describe the distortion of the direct wave due to lateral heterogeneity (Snieder, 1987b). This allows not only for accurate forward modelling of the direct surface wave in the presence of lateral heterogeneity, but also for a waveform inversion of the direct surface wave train. In this way both amplitude and phase information can be used.

A waveform inversion of surface wave data was first attempted by Lerner-Lam and Jordan (1983), who linearly fitted fitted higher mode surface waves with a laterally homogeneous model. Nolet et al. (1986a) extended this method to incorporate nonlinear effects and lateral inhomogeneity. However, they only used the phase information of the surface waves. Yomogida and Aki (1987) used the Rytov field to fit both the amplitude and phase of fundamental mode Rayleigh wave data. The starting point of Yomogida and Aki (1987) is the 2D wave equation. One can argue that their method lacks rigor, because it is not clear that surface waves satisfy the 2D wave equation. Tanimoto (1987) determined a global model for the S-velocity in terms of spherical harmonics up to order 8 using long period higher mode waveforms. In computing the synthetics he used the great circle theorem to compute the phase shift, and he ignored focusing effects. Because of the low order of his spectral expansion ($l \leq 8$), ray theory could be used for this inversion. This means that up to this point, all waveform inversions for surface waves relied either on ray theory, or on the 2D wave equation.

In this paper it is shown how linear scattering theory can be used for waveform fitting of the direct surface wave by the reconstruction of a 2D phase velocity field. The derivation uses the full equations of elasticity, and neither uses ray theory nor the 2D wave equation. Specifically, there is no need to assume any smoothness properties of the medium. In fact, in section 7 a numerical example is shown of the distortion of the direct surface wave by a structure with sharp edges. A restriction of this inversion method is that small scattering angles are assumed. This can in practice be realized by time windowing the data.

In section 2 of this paper some elements of surface wave scattering theory are revisited. The isotropic approximation, which allows the determination of phase velocities from scattering theory, is introduced in section 3. The following section features a method to invert the resulting scattering integral. Due to the extremely large size of the resulting matrix equation this is not without problems, and in section 5 several tricks are shown to make these computations feasible on systems as small as a super mini computer. Unfortunately, the surface wave inversion problem is in reality nonlinear, and the assumption of linearity is only justified for reference models which are sufficiently close to the real Earth. It is therefore advantageous to perform a nonlinear inversion (using ray theory) first (section 6), in order to find a smooth reference model for the subsequent linear inversion. (This linear inversion is in this paper referred to as "Born inversion".) In section 7, it is shown that a more or less realistic distribution of scatterers produces a realistic looking coda, but also that sharp lateral heterogeneity may severely distort the direct surface wave. Examples of inversions for a point scatterer and for ray geometrical effects (phase shifting and focusing) are presented in the last two sections. Application of this technique to surface wave data recorded with the NARS array are presented in part II of this paper (Snieder, 1988).

Throughout this paper the limitations of surface wave scattering are assumed (Snieder and Nolet, 1987), i.e. it is assumed that the heterogeneity is weak, and that the far field limit can be used. In order to transcend these limitations a considerable amount of theoretical work remains to be done. For reasons of simplicity, only vertical component fundamental mode data

are assumed, but this restriction is not crucial. Note that this does not mean that the fundamental Love wave need not be considered, because in general a double couple source excites Love waves, which may be converted by the heterogeneity to Rayleigh waves.

2) Surface wave scattering theory.

A dyadic decomposition of the surface wave Green's function (Snieder, 1986a; Snieder and Nolet, 1987) has allowed compact expressions for both the direct and the scattered surface waves. In this section, elements of surface wave scattering theory are briefly presented. Throughout this paper a spherical geometry is assumed, and computations are performed to leading order of ka, where k is the wavenumber and a the circumference of the Earth. As shown in Snieder and Nolet (1987), the unperturbed surface wave excited by a moment tensor $\mathbf{M}$ can be written as a sum over surface wave modes (with index ν):

$$\mathbf{u}^0(r,\theta,\phi) = \sum_\nu \mathbf{p}^\nu(r,\mu_R)\, \frac{e^{i(k_\nu a \Delta + \frac{\pi}{4})}}{\sqrt{\sin\Delta}}\, (\mathbf{E}^{\nu *}(r_S,\mu_S):\mathbf{M}) \ . \tag{1}$$

In this expression μ_S and μ_R are the azimuths of the source receiver minor arc at the source and receiver respectively counted anticlockwise from south, while Δ is the epicentral distance. In this paper, we shall only be concerned with the fundamental modes, so that the (Greek) mode indices are usually omitted. The polarization vector $\mathbf{p}$ is for Love waves given by

$$\mathbf{p}_L = -(l+\tfrac{1}{2})\, W(r)\, \hat{\boldsymbol{\phi}} \ , \tag{2a}$$

and for Rayleigh waves by

$$\mathbf{p}_R = (l+\tfrac{1}{2})\, V(r)\, \hat{\boldsymbol{\Delta}} - iU(r)\hat{\mathbf{r}} \ , \tag{2b}$$

where $\hat{\mathbf{r}}$, $\hat{\boldsymbol{\Delta}}$ and $\hat{\boldsymbol{\phi}}$ are unit vectors in the vertical, radial and transverse direction respectively. The eigenfunctions U, V and W of the Earth's normal modes are defined in Gilbert and Dziewonski (1975). The eigenfunctions are assumed to be normalized as in Snieder and Nolet (1987):

$$\tfrac{1}{2}\int \rho(r)\left[U^2(r) + l(l+1)V^2(r)\right] r^2 dr = \tfrac{1}{2}\int \rho(r)\, l(l+1)W^2(r)\, r^2 dr = \left[\frac{l+\frac{1}{2}}{2\pi}\right]^{\frac{1}{2}} / 4\omega u_g \tag{3}$$

The angular quantum number l is related to the wavenumber by the relation $ka = l+\frac{1}{2}$, and u_g is the angular group velocity of the mode under consideration. The excitation tensor $\mathbf{E}$ in equation (1) can be expressed in the polarization vector at the source

$$\mathbf{E}(r_S,\mu_S) = \left[\hat{\mathbf{r}}\partial_r + i\frac{(l+\frac{1}{2})}{r}\hat{\boldsymbol{\Delta}}_S\right] \mathbf{p}(r_S,\mu_S) \ . \tag{4}$$

The perturbation of the wavefield due to the lateral heterogeneity can be expressed as a double sum over incoming (σ) and scattered (ν) surface waves modes (Snieder and Nolet, 1987)

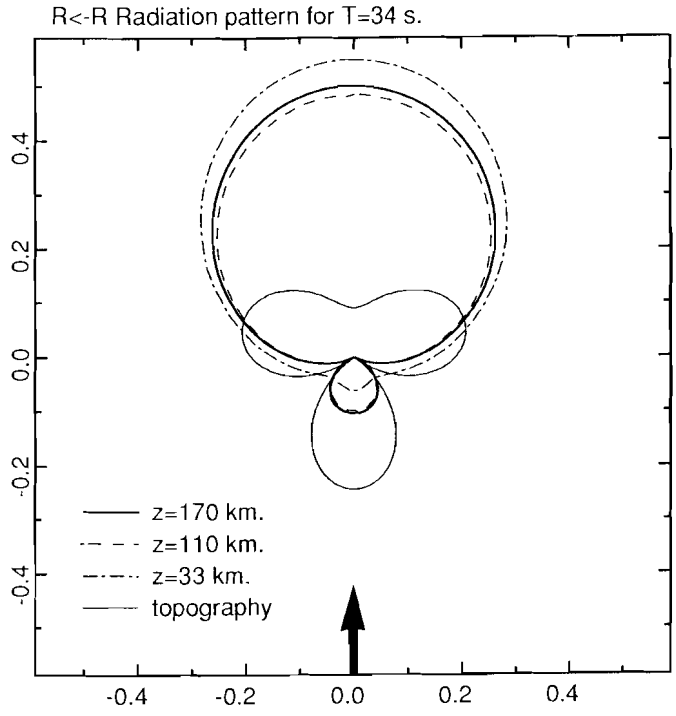

Figure 1a. Radiation pattern for the interaction of the fundamental Rayleigh mode with itself for surface topography (3 km.) and for S-velocity perturbations extending down to 170 km. ($\delta\beta/\beta$=4%), 110 km. ($\delta\beta/\beta$=4%) and 33 km. ($\delta\beta/\beta$=12%). The effective size of the scatterer is $100\times100 km^2$. The direction of the incoming wave is shown by an arrow.

$$\mathbf{u}^1(r,\theta,\phi) = \sum_{\nu,\sigma} \iint \mathbf{p}^{\nu}(r,\mu_R') \frac{e^{i(k_\nu a \Delta_2 + \frac{\pi}{4})}}{(sin\ \Delta_2)^{1/2}} \tilde{V}^{\nu\sigma}(\theta',\phi') \frac{e^{i(k_\sigma a \Delta_1 + \frac{\pi}{4})}}{(sin\ \Delta_1)^{1/2}} (\mathbf{E}^{\sigma *}(r_S,\mu_S').\mathbf{M})\, d\Omega' \ . \tag{5}$$

The surface wave distortion is expressed a scattering integral over the horizontal extend of the heterogeneity (θ',ϕ'). The minor arc from the source to the heterogeneity (θ',ϕ') defines the azimuth μ_S' at the source and the angular distance Δ_1, while the minor arc from (θ',ϕ') to the receiver defines the azimuth μ_R' at the receiver and the angular distance Δ_2. The interaction matrix $\tilde{V}^{\nu\sigma}$ describes the coupling between the modes ν and σ. For isotropic perturbations in the density $\delta\rho$ and the Lamé parameters $\delta\lambda$ and $\delta\mu$ the interaction matrix depends only on frequency and the scattering angle Ψ defined by

$$\Psi = \mu_{out} - \mu_{in} \ . \tag{6}$$

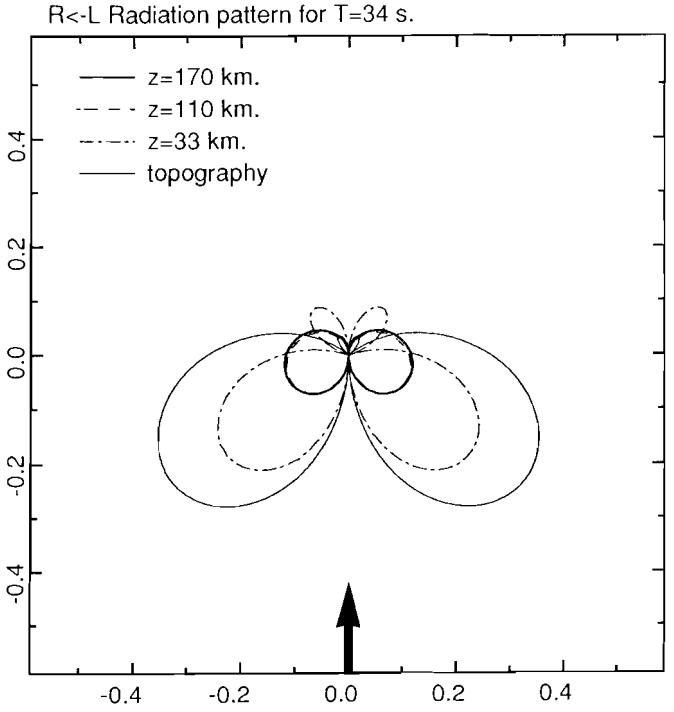

Figure 1b. Radiation pattern for the conversion from the fundamental Love mode to the fundamental Rayleigh mode. Conventions as in figure 1a.

(μ_{out} and μ_{in} are the azimuths of the incoming and scattered wave at the scatterer.) Extensions for perturbations of interfaces and gravitational effects are given in Snieder and Romanowicz (1987), while the effects of anisotropy are discussed in Romanowicz and Snieder (1987).

For perturbations in the density and the Lamé parameters the interaction terms are depth integrals containing the heterogeneity and the modes under consideration (Snieder and Nolet, 1987). For example, the Love wave to Rayleigh wave conversion ($R \leftarrow L$) is given by

$$\tilde{V}_{RL} = (l_R+\tfrac{1}{2})(l_L+\tfrac{1}{2}) \int \left[-V_R W_L \delta\rho\omega^2 + (\frac{1}{r}U_R + \partial_r V_R)(\partial_r W_L)\delta\mu \right] r^2 dr \sin\psi$$

$$+ (l_R+\tfrac{1}{2})^2(l_L+\tfrac{1}{2})^2 \int V_R W_L \delta\mu \, dr \sin 2\psi \ . \qquad (7)$$

For Love-Love wave interactions (LL) or Rayleigh-Rayleigh wave interactions (RR) a similar dependence on the scattering angle exists

$$\tilde{V}_{RR \text{ or } LL} = \tilde{V}^{(0)}_{RR} + \tilde{V}^{(1)}_{RR \text{ or } LL} \cos\Psi + \tilde{V}^{(2)}_{RR \text{ or } LL} \cos 2\Psi \ . \qquad (8)$$

In the figures 1a and 1b the radiation patterns are shown for interactions of the fundamental Rayleigh wave with itself, and for conversion from the fundamental Love wave to the fundamental Rayleigh wave. These radiation patterns are shown for surface topography (Snieder, 1986b; Snieder and Romanowicz, 1987), and for a constant relative perturbation in the S-velocity $\delta\beta/\beta$ down to different depths with an unperturbed density ($\delta\rho=0$). The perturbations in the Lamé parameters are equal.

In Snieder (1986b) it is shown that the interaction terms for forward scattering and unconverted waves are proportional to the perturbation of the phase velocity δc. Using the normalization (3), equation (9.3) of Snieder (1986b) can be written as

$$\frac{\delta c}{c} = \left[\frac{2\pi}{l+\frac{1}{2}}\right]^{\frac{1}{2}} \frac{1}{(l+\frac{1}{2})} \tilde{V}^{unconverted}(\Psi=0) \ . \tag{9}$$

Up to this point, it has been assumed that the real Earth can be treated as a radially symmetric reference model (producing a seismogram $\mathbf{u}^0$), with superposed lateral inhomogeneities (leading to the seismogram distortion $\mathbf{u}^1$). However, as shown in Snieder (1986a), the theory can also be formulated for a smoothly varying reference model, with embedded heterogeneities. (Smooth means that the lateral variation is small on scale of one horizontal wavelength.) In that case the phase terms and the geometrical spreading terms of the propagators follow from ray theory (Snieder, 1986a). Solving the ray tracing equations is a cumbersome affair, and as long as the inhomogeneity of the reference medium is sufficiently weak, the ray geometrical effects can be expressed as simple line integrals over the minor arc under consideration (Woodhouse and Wong, 1987; Romanowicz, 1987). Using these results, the propagator terms $\exp i(ka\Delta+\pi/4)/\sqrt{\sin\Delta}$ in the expressions (1) and (5) should for the case of a smooth reference medium be replaced by

$$ka\Delta \longrightarrow ka\left[\Delta - \int_0^\Delta \frac{\delta c}{c}\, d\Delta'\right] \tag{10a}$$

$$\sin\Delta \longrightarrow \sin\Delta - \int_0^\Delta \sin\Delta' \sin(\Delta-\Delta')\, \partial_{nn}\left(\frac{\delta c}{c}\right) d\Delta' \ . \tag{10b}$$

The azimuth terms in the polarization vectors and the scattering angle should be replaced by

$$\mu_S \longrightarrow \mu_S - \frac{1}{\sin\Delta} \int_0^\Delta \sin(\Delta-\Delta')\, \partial_n\left(\frac{\delta c}{c}\right) d\Delta' \tag{10c}$$

$$\mu_R \longrightarrow \mu_R + \frac{1}{\sin\Delta} \int_0^\Delta \sin\Delta'\, \partial_n\left(\frac{\delta c}{c}\right) d\Delta' \ , \tag{10d}$$

with similar expressions for the azimuths of the incoming and outgoing wave at the scatterer. In these expressions $\delta c/c$ is the relative phase velocity perturbation of the reference medium, while ∂_n and ∂_{nn} are the first and second angular derivatives in the transverse direction.

One should be careful giving $\mathbf{u}^1$ the interpretation of the scattered surface wave, because $\mathbf{u}^1$ describes all perturbations of the wavefield due to the perturbations superposed on the reference medium. If there are abrupt lateral variations, this leads to surface wave scattering.

However, in the case of a smoother perturbation on the reference model, $\mathbf{u}^1$ describes the change in the direct wave due to these inhomogeneities. For example, it is shown explicitly in Snieder (1987b) that the "scattering integral" (5) describes the ray geometrical effects on the direct wave due to smooth lateral heterogeneity.

3) The isotropic approximation.

The surface wave scattering formalism, as presented in the previous section, establishes a linear relation between the lateral heterogeneity and the perturbations of the surface wave field. In principle, a 3D inversion could therefore be formulated as a huge system of linear equations, by discretizing both the scattering integral over the heterogeneity (5) and the depth integrals in the interaction terms (7). Unfortunately, the simplicity of this approach is elusive. An inversion using the surface wave scattering integral (5) should take care of the following effects.

[1] The inhomogeneities should be located at their correct horizontal position.

[2] The depth distribution of the heterogeneity should be determined.

[3] The contributions from the different inhomogeneities $\delta\rho$, $\delta\lambda$ and $\delta\mu$ should be unravelled.

It is difficult those achieve these goals, since the heterogeneity acts on the wavefield only through the interaction terms $\tilde{V}^{\nu\sigma}$. This means that it is only possible to retrieve certain depth integrals of the heterogeneity. Information for different frequencies, and possibly different modes, is needed for the reconstruction of the depth dependence of the inhomogeneity. The contribution of the different types of inhomogeneity ($\delta\rho$,$\delta\lambda$,$\delta\mu$) can only be retrieved by using information of different scattering angles.

It will be clear that a complete 3D reconstruction of the heterogeneity is hard to realize with a finite set of band limited, noise contaminated data. With present data sets there are two realistic approaches. One can parameterize the depth dependence and the different contributions of $\delta\rho$, $\delta\lambda$ and $\delta\mu$ in a finite set of basis functions. This reduces the degrees of freedom of the heterogeneity, which facilitates a well behaved inversion. This approach has been taken in a field experiment where surface waves on a tidal flat were reflected by a concrete dam (Snieder, 1987a). In this test example, the depth dependence of the heterogeneity was prescribed, and an accurate reconstruction of the location of the dam was realized using the surface wave coda.

Alternatively, one can make the "isotropic approximation". It follows from expression (8) that the $R \leftarrow R$ radiation pattern is stationary with respect to the scattering angle for near forward directions. This can be verified in figure 1a for several different inhomogeneities. Furthermore, it follows from equation (7) that the $R \leftarrow L$ conversion vanishes in the forward direction. From figure 1b it can be seen that for the shown examples the $R \leftarrow L$ conversion is small for near forward directions. This means that (at least for the fundamental modes) for near forward directions one can make the "isotropic approximation". This means that

$$\tilde{V}_{RL} \approx 0 \ , \tag{11}$$

$$\tilde{V}_{RR} \approx \tilde{V}_{RR}^{(0)} + \tilde{V}_{RR}^{(1)} + \tilde{V}_{RR}^{(2)} = - \left[\frac{l+½}{2\pi} \right]^{½} (l+½) \frac{\delta c}{c} \ . \tag{12}$$

These expressions are extremely useful, because they make it possible to retrieve the phase velocity perturbation from scattering theory. This allows a two stage inversion of surface wave data. In the first step, the scattering theory is used to find the phase velocity perturbation using the expressions (5), (11) and (12). Once these local phase velocities are computed, a standard linear inversion can be used to determine the depth dependence of the heterogeneity (Nolet, 1981). The catch is that this approach forces us to use information for small scattering angles only. In practice, this can easily be achieved by time windowing the seismograms, and only using the information contained in the direct wave. Note that there are no smoothness restrictions on the heterogeneity, so that it is in principle possible to reconstruct a 2D phase velocity field without doing any dispersion measurements. In this way, the conditions for the validity of the great circle theorem need not be fulfilled.

4) Inversion of the scattering integral.

The linear relation (5) between the perturbation of the wavefield, and the perturbation of the medium can be written as

$$\mathbf{u}^1 = \sum_{\nu,\sigma} \iint \mathbf{p}^{\nu} g_{\nu}(\Delta_2) \frac{\partial \tilde{V}^{\nu\sigma}}{\partial m} \cdot m(\theta',\phi') \, g_{\sigma}(\Delta_1) \, (\mathbf{E}^{\sigma *} : \mathbf{M}) \, d\Omega' \ , \tag{13}$$

with the propagators defined by

$$g_{\nu}(\Delta) = \frac{e^{i(k_{\nu} a \Delta + \frac{\pi}{4})}}{\sqrt{\sin \Delta}} \ , \tag{14}$$

or its equivalent for a smoothly varying reference medium (10). The model parameter m designates either the heterogeneity ($\delta\rho$,$\delta\lambda$,$\delta\mu$) parameterized in some suitable form, or the phase velocity perturbation $\delta c/c$ if the isotropic approximation is used. The difference between the recorded surface wave data and the synthetics for the reference model ($\mathbf{u}^0$) can for all events, stations, and frequency components be arranged in one (huge) vector $\mathbf{d}$ of data residuals. Likewise, the model parameters can, after a discretization in cells of the surface integral (13) (and possibly also of the depth integrals in the interaction terms), be arranged in one model vector $\mathbf{m}$. (Of course, one does not have to expand the heterogeneity in cells,other parameterizations can also be used.) In that case, equation (13) can be written as a matrix equation

$$d_i = \sum_j G_{ij} m_j \ , \tag{15}$$

where G_{ij} is the spectral component of the synthetic seismogram for event-station pair "i" at

frequency ω_i, due to a unit perturbation of model parameter "j".

In general, the matrix **G** is extremely large. The reason for this is that the integrand in the original scattering equation (13) is rapidly oscillating with the position of the inhomogeneity. This means that in order to discretize (13) accurately, a cell size much smaller than a wavelength is needed. For an inversion on a continental scale for surface waves with a wavelength of say 100 km., several thousands of cells are needed. Fortunately, extremely large systems of linear equations can be solved iteratively in the least squares sense (Van der Sluis and Van der Vorst, 1987), so that a brute force inversion of **G** need not be performed. The least squares solution minimizes the misfit $|\mathbf{d}-\mathbf{G}\mathbf{m}|^2$, so that one performs in fact a least squares waveform fit of the data residual **d** to the synthetics **Gm**.

In the inversions presented in this paper, and in part II, the algorithm LSQR of Paige and Saunders (1982ab) is used to solve equation (15) iteratively in the least squares sense. LSQR performs the inversion by doing suitable matrix multiplications with **G** and $\mathbf{G}^T$. (In the language of modern optimization schemes (Tarantola and Valette, 1982), one would say that one only needs to solve the forward problem.) There is no need to store the matrix in memory, in fact, one only needs to supply LSQR with a subroutine to do a multiplication with one row of **G** or $\mathbf{G}^T$. As an additional advantage, LSQR has convenient "built in" regularization properties (Van der Sluis and Van der Vorst, 1987). The stability of LSQR is confirmed by Spakman and Nolet (1987), who applied LSQR to a tomographic inversion of an extremely large set of P-wave delay times, and who made a comparison with other iterative solvers of linear equations.

The inversion with LSQR has some interesting similarities with migration methods in exploration seismics. The first iteration of LSQR yields a solution proportional to $\mathbf{G}^T\mathbf{d}$, higher iterations perform corrections to the misfit (Van der Sluis and Van der Vorst, 1987). It is shown in detail in Snieder(1987a) that the contraction $\mathbf{G}^T\mathbf{d}$ amounts to a holographic reconstruction of the heterogeneity. This means that the waves propagating away from the sources (the illumination) are correlated with the surface wave residuals which have backpropagated from the receivers into the medium. For one source-receiver pair this leads to an ellipsoidal contribution to the reconstructed image. By summing over all source-receiver pairs (which is implicit in the product $\mathbf{G}^T\mathbf{d}$) an image is constructed. It is shown by Tarantola (1984ab) that this procedure is similar to Kirchoff migration as used in exploration seismics. Just as with these techniques, the surface wave reconstructions using the method of this paper will contain "smiles" (Berkhout, 1984) if insufficient data are used.

It may be advantageous to impose an a-priori smoothness constraint on the solution. This can be achieved by solving of equation (15) the equation

$$\mathbf{G}\mathbf{S}\tilde{\mathbf{m}} = \mathbf{d} \ , \tag{16}$$

where **S** is a prescribed smoothing matrix. This yields the solution

$$\mathbf{m} = \mathbf{S}\tilde{\mathbf{m}} \ , \tag{17}$$

which incorporates the smoothness criterion imposed by **S**.

5) Practical implementation of solving the matrix equation

Solving the linear system (15) or (16) is not entirely straightforward, because the matrix may be extremely large. For example, discretizing the continent of Europe (with a size of say $3500 \times 3500 km^2$) in cells of $35 \times 35 km^2$ (which is 1/4 of the wavelength of a 30 s. fundamental mode Rayleigh wave), leads to a model of 10,000 cells. For the data set used in paper II, there are approximately 2,500 spectral components of surface wave data to be fitted. This means that storing this matrix on disc required 100 Mbyte of disc space, which is impractical (if not impossible on many machines). As mentioned before, LSQR does not need the whole matrix at once, but only needs access to the rows of **G** and $\mathbf{G}^T$. In principle, the matrix can therefore be computed during the inversion. However, due to the large number of trigoniometric operations required for the computation of the synthetics this leads to prohibitive CPU times.

If we restrict ourselves to vertical component data for the fundamental mode only, the elements of the matrix **G** have the form

$$G = A_R e^{i\phi_R} + A_L e^{i\phi_L} \quad . \tag{18}$$

The first term in this expression describes the scattering of the fundamental Rayleigh mode to itself, while the second term describes the conversion from the fundamental Love mode to the fundamental Rayleigh mode. The terms ϕ_R and ϕ_L are the phase terms of the propagators (14), while the complex amplitudes A_R and A_L contain the remaining terms.

Due to the phase terms, the matrix G_{ij} (which is the synthetic for data point i due to a unit perturbation of model parameter j) is an oscillatory function of the position of the inhomogeneity, and hence of the index j. This oscillatory character makes it impossible to use some interpolation scheme to compute G_{ij}. However, the phase functions ϕ_R, ϕ_L and the complex amplitudes A_R, A_L **are** smooth functions of the location of the inhomogeneity. This makes it possible to store these terms at selected grid points, and to compute values at intermediate points by interpolation during the inversion. One could call this procedure "Filon matrix multiplication".

This procedure can be simplified even further by using the fact that the the wavenumbers of the fundamental Rayleigh wave and the fundamental Love wave usually are not too different (hence $\phi_R \approx \phi_L$). If equation (18) is written as

$$G = Z\, e^{i\phi_R} \quad , \tag{19}$$

with

$$Z = A_R + A_L\, e^{i(\phi_L - \phi_R)} \quad , \tag{20}$$

one only needs to store Z and ϕ_R at selected gridpoints.

The functions Z and ϕ_R are in general also a smooth function of frequency, so that the matrix only needs to be stored at certain selected frequencies. The value of the matrix elements for intermediate frequencies can also be computed by interpolation. This interpolation with respect to frequency can be performed with a simple linear interpolation. For the interpolation with respect to the location of the inhomogeneity it is better to use a quadratic scheme. The reason for this is that the phase ϕ_R has a minimum on the minor arc between the source and the receiver. It is especially at this location that accuracy is required if the isotropic approximation is used, because in that case the requirement of a small scattering angle confines the solution to the vicinity of the minor arc. A linear interpolation scheme for the horizontal coordinates is not

able to reproduce such a minimum, and is thus unsuitable.

In the inversions shown in part II of this paper for the structure under Europe and the Mediterranean, an area of $3500\times3500 km^2$ is investigated. Storing the matrix on a 15×15 grid, and interpolating in between produced accurate results. (Halving the grid distance for the interpolation did not change the solution.) In the period range from 30 s. to 100 s., only 15 frequencies were sufficient to achieve an accurate interpolation with respect to frequency. (Doubling the number of frequency points for the interpolation did not change the solutions.) In this way, only 2 Mbyte of disc space was needed to store the interpolation coefficients for the matrix **G**.

The edges of the domain of inversion require special attention. Artificial reflections may be generated at the edge of the domain of inversion if this domain is truncated abruptly (Wielandt, personal communication). This problem can be circumvented by tapering the matrix **G** near the edges of the domain. In the inversions used in this study, a linear taper was applied to **G** near the edges of the domain over a length of 254 km.

The theory formulated here is strictly only valid in the far field (Snieder and Nolet, 1987). It can be seen from equation (14) that the theory becomes singular in the near field. Due to the lack of a better theory, this problem is ignored in this study. The singularity was removed by replacing the $\sin\Delta$ term in the propagator (14) by a constant ($\sin\Delta_o$), whenever $\Delta<\Delta_o$. A value of 2.7 degrees was adopted for Δ_o.

The data fit (16) is performed in the frequency domain, whereas surface wave data are recorded in the time domain. After applying some taper, these data can be transformed to the frequency domain. In case one uses the isotropic approximation a time window is needed to extract only the direct wave. In general, the data are therefore in the time domain multiplied with some nonnegative time window $w(t)$. Of course, the matrix elements, which are the spectral components of the inhomogeneity in each cell, should incorporate the effects of this time window. A multiplicative window in the time domain acts as a convolution in the frequency domain, which complicates the inversion. However, it is shown in appendix A that if the time window $w(t)$ is nonnegative and sufficiently broad, that due to the surface wave character of the signal this filter acts in the frequency domain as a simple multiplication with $w(L/U(\omega))$. In this expression, L is the distance covered by the surface wave, and $U(\omega)$ is the group velocity of the mode under consideration.

6) Waveform fitting by nonlinear optimization.

The theory presented here establishes an inversion scheme in case a linear relation exists between the inhomogeneity and the deviation between the recorded surface waves and the synthetics for the reference model. In practice, this relation may suffer from nonlinearities. The main culprit for this effect is that small changes in the wavenumber are multiplied in the exponent by a large epicentral distance so that $\exp i(k+\delta k)L \simeq (1+i\delta kL)\exp ikL$ may be a poor approximation.

It is therefore desirable to perform first a nonlinear inversion in order to find a smooth reference model for the Born inversion. This nonlinear inversion can be achieved by minimizing the penalty function

$$F = \sum_{r,s} \int \left[u^{rs}(t) - s^{rs}(m,t) \right]^2 dt + \gamma \iint |\nabla_1 m|^2 \, d\Omega \tag{21}$$

with respect to the model parameters m. In this expression $u^{rs}(t)$ is the surface wave seismogram for source s and receiver r, while $s^{rs}(t)$ is the corresponding synthetic for model m. The last term serves to select the smoothest possible solution by minimizing the horizontal gradient $|\nabla_1 m|$.

As shown in Nolet et al. (1986a), the minimization of F in (21) can be achieved efficiently using conjugate gradients. In this kind of inversion one only needs to solve the forward problem repeatedly (Nolet et al., 1986a), and most of the computer time is spend computing the gradient of the penalty function with respect to the model parameters. It is therefore crucial to have a fast method for computing this gradient. (In this study, the forward problem is solved using the line integrals (10) in order to incorporate ray geometrical effects. Bicubic splines are useful for representing the lateral phase velocity variations, because they ensure continuity of the phase velocity with its first and second derivatives. In this approach, the model parameters m are the phase velocities at some selected grid points.)

The gradient of the misfit $M = \int \left[u(t) - s(m,t) \right]^2 dt$ for one source receiver pair can for bandlimited data be estimated analytically. It is shown in appendix B that if the synthetic consists of a sum of modes

$$S(m,\omega) = \sum_\nu S_\nu(m,\omega) = \sum_\nu A_\nu e^{i\phi_\nu} \ , \tag{22}$$

the gradient of the misfit can be approximated by

$$\frac{\partial M}{\partial m} = -2 \sum_\nu \left\{ \frac{1}{c_\nu^2} \int \frac{\partial c_\nu}{\partial m} \, dx \, B_1^\nu + \frac{1}{A_\nu} \frac{\partial A_\nu}{\partial m} B_2^\nu \right\} \ . \tag{23}$$

In this expression

$$B_1^\nu = \int \dot{s}_\nu(m,t) \left[u(t) - s(m,t) \right] dt \ , \tag{24}$$

$$B_2^\nu = \int s_\nu(m,t) \left[u(t) - s(m,t) \right] dt \ , \tag{25}$$

and $\int .....dx$ denotes the integral over the minor arc from the source to the receiver. The virtue of this approach is that the correlations B_1^ν and B_2^ν have to be computed only once, and that the derivatives of **all** model parameters follow from these correlations. Note the similarity between expression (24) and the correlation functions used by Lerner-Lam and Jordan (1983) (the "bccfs") in their linear inversion of surface wave data.

7) A numerical example of scattered surface waves.

In order to see whether the scattering theory presented here is useful for inversion, it is instructive to study synthetic seismograms for some artificial distribution of scatterers. Figure 2

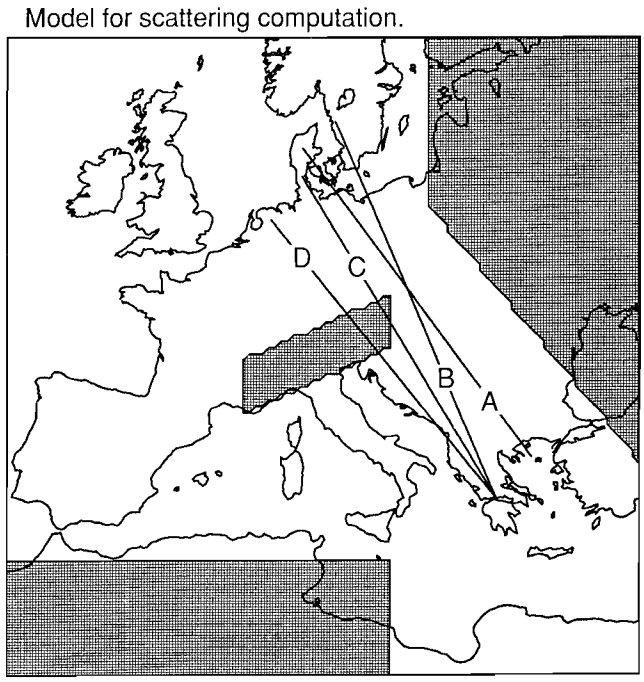

Figure 2. Horizontal extend of the heterogeneity used in the example of the scattering computation. The inhomogeneity extends down to 170 km. with $\delta\beta/\beta=10\%$, $\delta\rho=0$ and $\delta\lambda=\delta\mu$.

shows a fictitious distribution of scatterers which forms an extremely crude model of structures as the Alps, the Tornquist-Teisseyre zone, and the edge of north Africa. The inhomogeneity consists of a constant S-velocity perturbation of 10% down to a depth of 170 km., while the density is unperturbed. Equal perturbations of the Lamé parameters are assumed. Synthetics are computed with a brute force integration of equation (5). In order to satisfy the criterion of linearity, only periods larger than 30 s. are considered (see part II of this paper).

Figure 3 shows the synthetic seismogram for the laterally homogeneous reference model, the model with the inhomogeneity, and data recorded at station NE02 of the NARS network (Dost et al., 1984; Nolet et al, 1986b). Observe the realistic looking coda in the synthetics for the model with the scatterers. Of course, one cannot speak of a fit of the recorded surface wave data for this simple minded model, but the coda in the data and in the synthetics are at least of the same nature.

In figure 4 the synthetics are shown for paths which propagate with different lengths through the central block which mimics the Alps. For path B, which does not propagate through the heterogeneity, only the coda is affected, while for the paths C and D the direct wave is substantially distorted. For path D, the inhomogeneity induces both a forward time shift as well as an amplitude increase. Physically this happens because the scattered waves arrive almost simultaneously with the direct wave (forward scattering). The resulting

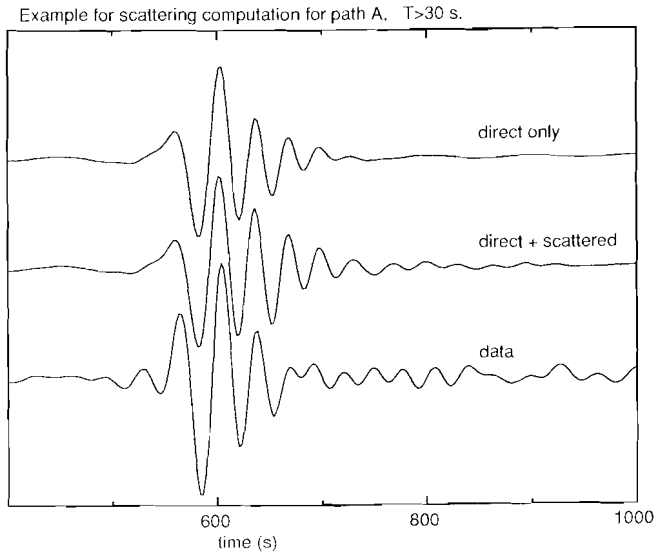

Figure 3. Seismograms for path A of figure 2. The top seismogram is for the laterally homogeneous reference medium, the middle seismogram for the medium with the heterogeneity, and the bottom seismogram shows data.

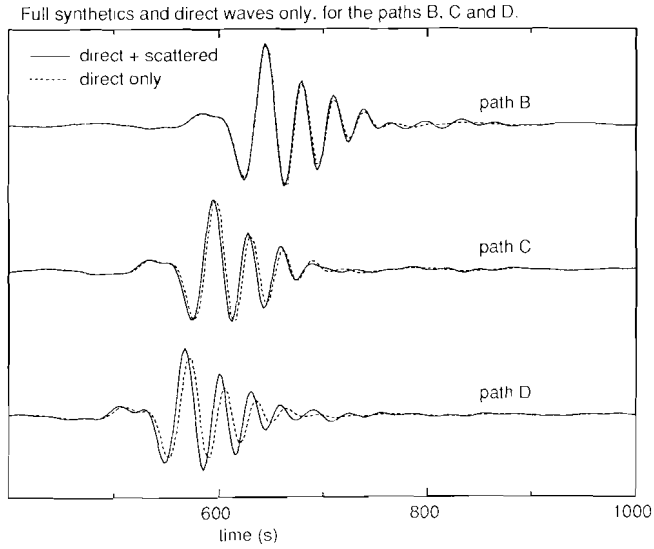

Figure 4. Synthetic seismograms for the laterally homogeneous reference medium, and the medium with the inhomogeneity for the paths B, C and D of figure 2.

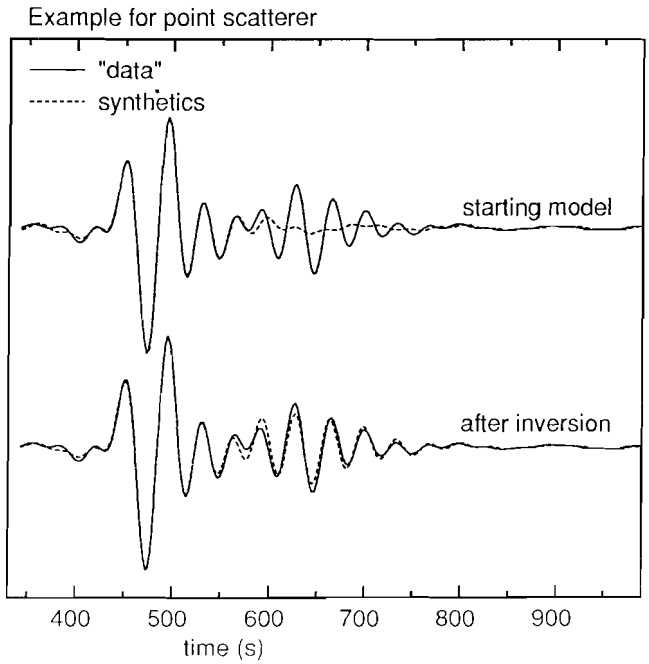

Figure 5. Waveform fit before and after Born inversion for a synthetic seismogram generated with the point scatterer of figure 6.

interference leads to a distortion of the arriving wave train. This example shows that non-smooth structures may lead to a distortion of the direct surface wave. It is not clear if a standard dispersion analysis (which assumes ray theory) gives correct results when applied to seismogram D.

8) Inversion for a point scatterer.

In order to see how the inversion for the surface wave coda operates, an example is shown where one point scatterer influences one seismogram. This point scatterer has the same depth structure as in the example of section 6, but has an effective strength of $\frac{\delta\beta}{\beta}\times area = 70\times 70 km^2$. The synthetics for the laterally homogeneous reference medium, and the (synthetic) data for the medium with the scatterer are shown in the top seismograms of figure 5. The point scatterer has generated a wave packet which arrives after the direct wave between 600 s. and 700 s. The Born inversion is applied to these data for a model of 100×100 cells. After three iterations the model shown in figure 6 is produced. (The correct depth dependence of the heterogeneity is prescribed.) The corresponding synthetics are shown in the

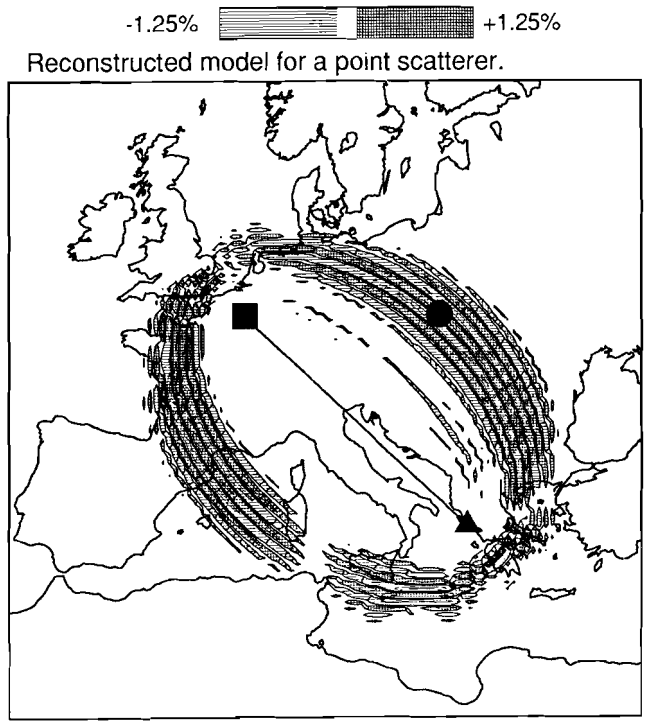

Figure 6. Model reconstructed by Born inversion of the top (solid) seismogram of figure 5. The triangle marks the source, the square marks the receiver and the circle gives the true location of the point scatterer.

bottom seismograms of figure 5. The "data" for this point scatterer have been fitted quite well.

The resulting model (figure 6) bears of course no resemblance to the original point scatterer, because it consists of an ellipsoidal band of positive and negative anomalies. With one source and one receiver it is impossible to determine the true location of the heterogeneity on this ellipse. By using more sources and receivers, an image is constructed by the superposition of these ellipses.

As mentioned in section 4, the result of the first iteration of the Born inversion is proportional to $\mathbf{G}^T\mathbf{d}$, which can be interpreted as the temporal correlation between the excited wavefield, and the backpropagated data residuals (Snieder, 1987a). Since surface wave trains consist of oscillating wave packets, this correlation also has an oscillatory nature, which produces the alternation of positive and negative anomalies in figure 6. The "holes" in these ellipses are caused by the nodes in the radiation pattern of the source (a double couple), and in the radiation pattern of the scatterers (the thick solid line in the figures 1a and 1b).

The strength of the reconstructed inhomogeneity is of the order of 1%, whereas the synthetic "data" have been computed for a point inhomogeneity of 100% with an effective area of $70\times70km^2$. The reconstructed heterogeneity is spread out over a much larger area, which

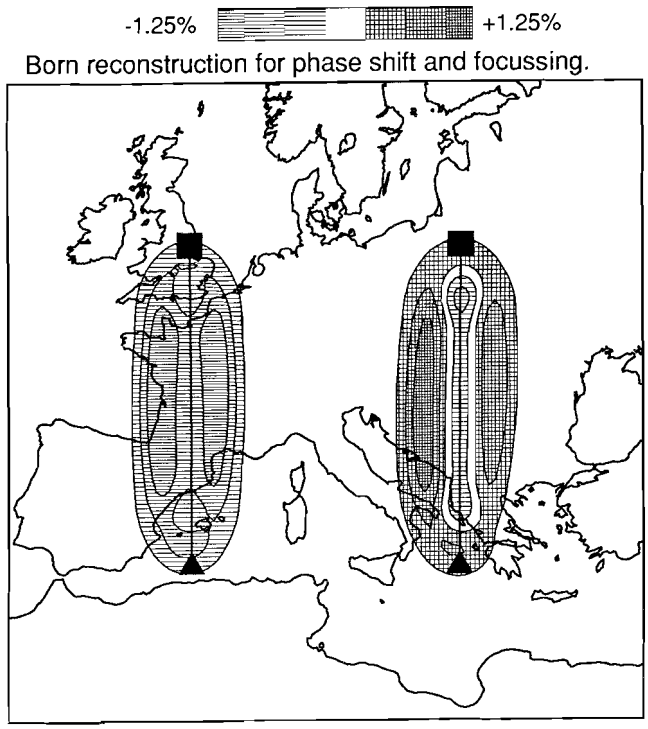

Figure 7. Model reconstructed by Born inversion for ray geometrical effects. The triangles indicate the sources, the squares mark the receivers.

explains the weakened reconstructed image. Suppose the heterogeneity is spread out over zone of $2000\times300km^2$, which is about the right size (see figure 6). This would lead to a weakening of the reconstructed image of $70\times70km^2/2000\times300km^2 \approx 1\%$, which is of the order of magnitude of the reconstruction in figure 6.

9) Inversion for ray geometrical effects.

In this section it is shown how the Born inversion takes ray geometrical effects such as focusing and phase shifting into account. Synthetics have been computed for the two source receiver pairs shown in figure 7, assuming a double couple source for the excitation. The seismogram for the right wave path has been multiplied with 1.4, and the seismogram for the left wave path has been shifted backward in time over 4 s. (which is roughly 1% of the travel time).

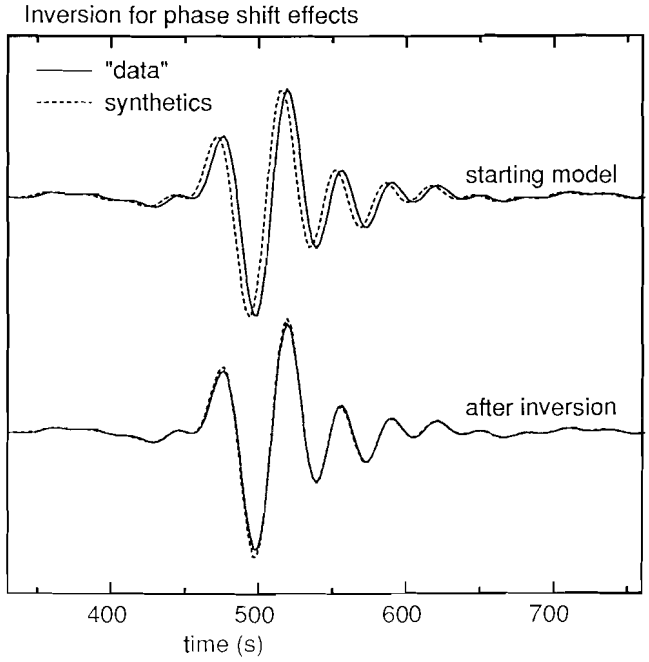

Figure 8. Waveform fit before and after Born inversion for the left wavepath in figure 7, where the phase is shifted.

These seismograms have been inverted simultaneously with the Born inversion using the isotropic approximation. In this inversion a smoothness criterion is imposed because in contrast to the scattering example of the previous section, no sharp heterogeneities are needed to generate the perturbations of the wave field. The domain shown in figure 7 consists of 100×100 cells of $35\times35 km^2$. The smoothing matrix that is used is given by

$$S_{i_\phi i_\theta, j_\phi j_\theta} = \alpha^{|i_\phi - j_\phi|}\, \alpha^{|i_\theta - j_\theta|} \quad \text{if} \quad |i_\phi - j_\phi| \le N \quad \text{and} \quad |i_\theta - j_\theta| \le N \tag{26}$$

$$S_{i_\phi i_\theta, j_\phi j_\theta} = 0 \qquad \textit{elsewhere} \ ,$$

where i_ϕ, i_θ etc. denote the cell indices in the horizontal directions. In this example the values α=0.66 and N=4 are adopted.

The resulting model after 3 iterations is shown in figure 7. Note that because the isotropic approximation is used, this figure displays the phase velocity perturbation $\delta c / c$. In figure 8 the waveform fit for the left wave path in shown. (This is the time shifted seismogram.) The phase shift is correctly taken into account. This is realized by a negative phase velocity anomaly in the first Fresnel zone of the left wave path in figure 7. This negative phase velocity anomaly is not distributed evenly over the first Fresnel zone of the left wavepath, there are phase velocity minima slightly away from the source receiver minor arc. If these minima were

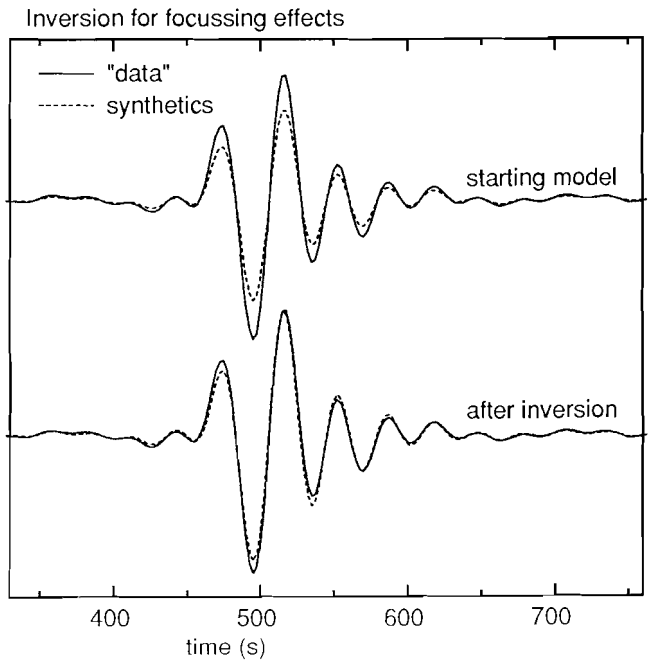

Figure 9. Waveform fit before and after Born inversion for the right wavepath in figure 7, where the amplitude is increased.

absent, the resulting concave transverse phase velocity profile would produce an anomalously large amplitude due to focusing. Because of the phase velocity minima adjacent to the source receiver minor arc, the transverse phase velocity profile is actually convex at the minor arc. This produces defocusing of surface wave energy, which compensates the amplitude increase due to refraction at the edge of the Fresnel zone.

The seismograms for the right wave path are shown in figure 9. The synthetic data are 40% too strong for the laterally homogeneous reference model, this is almost completely taken care of in the inversion. Physically, this is achieved by a negative phase velocity anomaly on the source receiver line, and an anomalously high phase velocity just away from this line. This phase velocity pattern leads to focusing of surface wave energy, so that the large amplitude is fitted. This confirms not only that surface wave scattering theory can account for ray geometrical effects (Snieder, 1987b), but also that these ray geometrical effects are taken care of in the Born inversion. The asymmetry of the phase velocity pattern in figure 7 around the wave paths is due to the the asymmetry in the radiation pattern of the double couple source.

There are approximately 10 cells between the maxima in the strips of high phase velocities for the right wave path in figure 7. The focusing produced by this structure is achieved by the transverse curvature of the phase velocity. Increasing the cell size (which is computationally advantageous) leads to a representation of this curvature with only a few cells, which may produce unacceptable inaccuracies.

10) Conclusion.

Large scale inversion of the surface wave coda can in principle be performed using an iterative solver of a large system of linear equations. For this kind of inversion the depth dependence of the heterogeneity should be prescribed, or be parameterized in a limited number of basis functions. Alternatively, the isotropic approximation can be used, which leads to a waveform fit of the direct surface wave due to a laterally heterogeneous phase velocity field. These phase velocities, determined for different frequency bands, can be inverted locally to a depth distribution of the heterogeneity.

The Born inversions shown in this paper are performed iteratively using LSQR. Although LSQR is originally designed for sparse matrices, and the matrix for surface wave scattering is not sparse, good results are obtained in inversions of synthetic data. In practice, three iterations proved to be sufficient both for an inversion for the surface wave coda, and of the direct wave. A similar conclusion was drawn by Gauthier et al. (1986), who used an iterative scheme for fitting waveforms in an exploration geophysics setting.

In hindsight, the success of linear waveform inversions in a few number of iterations is not so surprising. It has been argued by Tarantola (1984ab) that the standard Kirchoff migration methods in exploration seismics is equivalent to the first (steepest descent) step of an iterative optimization scheme. Analogously, the first step of the iterative matrix solver used here amounts to a holographic inversion (Snieder, 1987a) analogously to Kirchoff migration. These one step migration methods have been extremely successful in oil exploration, and there is no principal reason why a similar scheme cannot be used in global seismology. Applications of this technique to surface wave data recorded by the NARS array are shown in part II of this paper (Snieder, 1988)

References.

Backus, G.E., Geographical interpretation of measurements of average phase velocities over great circular and great semi circular paths, *Bull. seism. Soc. Am., 54*, 571-610, 1964.

Berkhout, A.J., *Seismic migration, imaging of acoustic energy by wave field extrapolation, B. Practical aspects*, Elsevier, Amsterdam, 1984.

Bungum, H., and J. Capon, Coda pattern and multipathing propagation of Rayleigh waves at NORSAR, *Phys. Earth Plan. Int., 9*, 111-127, 1974.

Butkov, E., *Mathematical Physics*, Addison-Wesley, Reading Ma., 1968.

Calcagnile, G., and R. Scarpa, Deep structure of the European-Mediterranean area from seismological data, *Tectonophys., 118*, 93-111, 1985.

Dahlen, F.A., The spectra of unresolved split normal mode multiplets, *Geophys. J. R. Astr. Soc., 58*, 1-33, 1979.

Dost, B., A. van Wettum, and G. Nolet, The NARS array, *Geol. Mijnbouw, 63*, 381-386, 1984.

Gauthier, O., J. Virieux, and A. Tatantola, Two-dimensional nonlinear inversion of seismic waveforms: Numerical results, *Geophys., 51*, 1387-1403, 1986.

Gilbert, F., and A. Dziewonski, An application of normal mode theory to the retrieval of structural parameters and source mechanisms from seismic spectra, *Phil. Trans. R. Soc. London, A278*, 187-269, 1975.

Jordan, T.H., A procedure for estimating lateral variations from low frequency eigenspectra data, *Geophys. J. R. Astr. Soc., 52,* 441-455, 1978.

Lerner-Lam, A.L., and T.J. Jordan, Earth structure from fundamental and higher-mode waveform analysis, *Geophys. J. R. Astron. Soc., 75,* 759-797, 1983.

Levshin, A., and K.A. Berteussen, Anomalous propagation of surface waves in the Barentz Sea as inferred from NORSAR recordings, *Geophys. J. R. Astr. Soc., 56,* 97-118, 1979.

Nolet, G., Linearized inversion of (teleseismic) data, in *The solution of the inverse problem in geophysical interpretation,* edited by R. Cassinis, Plenum-Press, New York, 1981.

Nolet, G., J. van Trier, and R. Huisman, A formalism for nonlinear inversion of seismic surface waves, *Geophys. Res. Lett., 13,* 26-29, 1986a.

Nolet, G., B. Dost, and H. Paulssen, Intermediate wavelength seismology and the NARS experiment, *Ann. Geophys., B4,* 305-314, 1986b.

Paige, C.G., and M.A. Saunders, LSQR: An algorithm for sparse linear equations and sparse least squares, *ACM Trans. Math. Software, 8,* 43-71, 1982a.

Paige, C.G., and M.A. Saunders, LSQR: Sparse linear equations and least squares problems, *ACM Trans. Math. Software, 8,* 195-209, 1982b.

Panza, G.F., S. Mueller, and G. Calcagnile, The gross features of the lithosphere-asthenosphere system from seismic surface waves and body waves, *Pure Appl. Geophys., 118,* 1209-1213, 1980.

Romanowicz, B., Multiplet-multiplet coupling due to lateral heterogeneity: asymptotic effects on the amplitude and frequency of the Earth's normal modes, *Geophys. J. R. Astr. Soc., 90,* 75-100, 1987.

Romanowicz, B., and R. Snieder, A new formalism for the effect of lateral heterogeneity on normal modes and surface waves - II: General anisotropic perturbations, *submitted to Geophys. J. R. Astr. Soc.,* 1987.

Sluis, A. van der, and H.A. van der Vorst, Numerical solution of large, sparse linear algebraic systems arising from tomographic problems, in *Seismic tomography, with applications in global seismology and exploration geophysics,* edited by G. Nolet, pp. 49-83, Reidel, Dordrecht, 1987.

Snieder, R., 3D Linearized scattering of surface waves and a formalism for surface wave holography, *Geophys. J. R. Astr. Soc., 84,* 581-605, 1986a.

Snieder, R., The influence of topography on the propagation and scattering of surface waves, *Phys. Earth. Plan. Int., 44,* 226-241, 1986b.

Snieder, R., Surface wave holography, in *Seismic tomography, with applications in global seismology and exploration geophysics,* edited by G. Nolet, pp. 323-337, Reidel, Dordrecht, 1987a.

Snieder, R., On the connection between ray theory and scattering theory for surface waves, in *Mathematical Geophysics, a survey of recent developments in seismology and geodynamics,* edited by Vlaar, N.J., Nolet, G., Wortel, M.J.R. and Cloetingh, S.A.P.L., pp. 77-83, Reidel, Dordrecht, 1987b.

Snieder, R., Large scale waveform inversions of surface waves for lateral heterogeneity -II: Application to surface waves in Europe and the Mediterranean, *submitted to J. Geophys. Res.,* 1988.

Snieder, R., and G. Nolet, Linearized scattering of surface waves on a spherical Earth, *J. Geophys., 61,* 55-63, 1987.

Snieder, R., and B. Romanowicz, A new formalism for the effect of lateral heterogeneity on normal modes and surface waves -I: Isotropic perturbations, perturbations of interfaces and gravitational perturbations, *Geophys. J. R. Astron. Soc., in press,* 1987.

Spakman, W., and G. Nolet, Imaging algorithms, accuracy and resolution in delay time tomography, in *Mathematical Geophysics, a survey of recent developments in seismology and geodynamics*, edited by Vlaar, N.J., Nolet, G., Wortel, M.J.R. and Cloetingh, S.A.P.L., Reidel, Dordrecht, 1987.

Tanimoto, T., The three-dimensional shear wave velocity structure in the mantle by overtone waveform inversion -I: Radial seismogram inversion, *Geophys. J. R. Astron. Soc., 89*, 713-740, 1987.

Tarantola, A., Inversion of seismic reflection data in the acoustic approximation, *Geophys., 49*, 1259-1266, 1984a.

Tarantola, A., Linearized inversion of seismic reflection data, *Geophys. Prosp., 32*, 998-1015, 1984b.

Tarantola, A., and B. Valette, Generalized nonlinear inverse problems solved using the least squares criterion, *Rev. Geophys. Space Phys., 20*, 219-232, 1982.

Woodhouse, J.H., and Y.K. Wong, Amplitude, phase and path anomalies of mantle waves, *Geophys. J. R. Astr. Soc., 87*, 753-774, 1986.

Yomogida, K., and K. Aki, Amplitude and phase data inversion for phase velocity anomalies in the Pacific Ocean basin, *Geophys. J. R. Astron. Soc., 88*, 161-204, 1987.

Appendix A, the effect of the time window function on the spectrum of surface waves.

Suppose that a surface wave seismogram $s(t)$ is multiplied with some nonnegative window function $w(t)$ to give a windowed seismogram $f(t)$

$$f(t) = w(t)s(t) \ . \tag{A1}$$

In the frequency domain the application of this window leads to a convolution

$$F(\omega) = \int W(\omega')S(\omega-\omega')\, d\omega' \ . \tag{A2}$$

Since $w(t)$ is nonnegative, $|W(\omega)|$ attains its maximum for $\omega=0$, this can be seen by making the following estimates:

$$|W(\omega)| = \left| \int w(t)e^{i\omega t} dt \right| \leq \int |w(t)e^{i\omega t}|\, dt = \int w(t)dt = |W(\omega=0)| \ . \tag{A3}$$

If the time window has a length T in the time domain, its frequency spectrum will have a width of the order π/T in the frequency domain. From this we conclude that long nonnegative time windows, have a spectrum is peaked around $\omega=0$.

Now assume that the surface wave spectrum consists of one mode (extensions to multimode signals is straightforward):

$$S(\omega) = A(\omega)e^{ik(\omega)L} \ , \tag{A4}$$

where L is the epicentral distance. Substituting in (A2) gives

$$F(\omega) = \int W(\omega')A(\omega-\omega')e^{ik(\omega-\omega')L}\, d\omega' \ . \tag{A5}$$

$W(\omega)$ is a function peaked around $\omega=0$, so that the main contribution to the ω'-integral comes from the point $\omega'=0$. Usually, the complex amplitude $A(\omega)$ is a smooth function of frequency,

so that one can approximate for small ω'

$$A(\omega-\omega') \approx A(\omega) \ . \tag{A6}$$

The phase term can be analyzed with a simple Taylor expansion

$$k(\omega-\omega')L \approx k(\omega)L - \frac{L\omega'}{U(\omega)} \ , \tag{A7}$$

where $U(\omega)$ is the group velocity of the surface wave mode. Inserting (A6) and (A7) in (A5) gives

$$F(\omega) \approx A(\omega) e^{ik(\omega)L} \int W(\omega') e^{-iL\omega'/U(\omega)} \, d\omega' \ . \tag{A8}$$

With (A4) and the definition of the Fourier transform this leads to

$$F(\omega) \approx S(\omega) \, w(L/U(\omega)) \ . \tag{A9}$$

Appendix B, analytical estimation of the gradient $\partial M/\partial m$.

The misfit between the data $d(t)$ and the surface wave synthetics $s(m,t)$ for model m is in the L_2 norm defined by

$$M \equiv \int \Big[d(t) - s(m,t) \Big]^2 dt \ . \tag{B1}$$

Using Parseval's theorem (Butkov, 1968), the misfit has the same form in the frequency domain

$$M = \int | \, D(\omega) - S(m,\omega) \, |^2 \, d\omega \ . \tag{B2}$$

In general, the model m consists of many parameters. The derivative of the misfit with respect to one of these parameters is

$$\frac{\partial M}{\partial m} = -2 \, \mathrm{Re} \left\{ \frac{\partial S(m,\omega)}{\partial m} (D^*(\omega) - S^*(m,\omega)) \, d\omega \right\} \ . \tag{B3}$$

Let the surface wave seismogram be given by a superposition of modes ν with complex amplitude A_ν and phase ϕ_ν

$$S(m,\omega) = \sum_\nu S_\nu(m,\omega) = \sum_\nu A_\nu(m,\omega) e^{i\phi_\nu(m,\omega)} \ , \tag{B4}$$

so that

$$\frac{\partial S}{\partial m} = \sum_\nu \left[\frac{1}{A_\nu} \frac{\partial A_\nu}{\partial m} + i \frac{\partial \phi_\nu}{\partial m} \right] S_\nu \ . \tag{B5}$$

According to equation (2.10), the phase of the surface waves is in a laterally heterogeneous medium

$$\phi(\omega) = \int_0^L k(\omega,x)\, dx \quad , \tag{B6}$$

where $k(\omega,x)$ is the local wavenumber. Differentiation with respect to the model parameter m gives

$$\frac{\partial \phi}{\partial m} = \int_0^L \frac{\partial k}{\partial m}\, dx = -\frac{\omega}{c^2} \int_0^L \frac{\partial c}{\partial m}\, dx \quad . \tag{B7}$$

Inserting this in (B5) gives

$$\frac{\partial M}{\partial m} = -2\,\mathrm{Re}\left\{ \sum_\nu \int \frac{1}{A_\nu} \frac{\partial A_\nu}{\partial m} S_\nu(m,\omega)\left[D^*(\omega) - S^*(m,\omega) \right] d\omega \right\} \tag{B8}$$

$$+2\,\mathrm{Re}\left\{ \sum_\nu \int \frac{i\omega}{c_\nu^2} \left[\int_0^L \frac{\partial c_\nu}{\partial m} dx \right] S_\nu^*(m,\omega)\left[D^*(\omega) - S^*(m,\omega) \right] d\omega \right\} \quad .$$

When one is attempting to find phase velocities by nonlinear optimization, one will usually work with bandpassed data for which $c(\omega)$ can be assumed to be independent of frequency. In that case, the phase velocity term and the amplitude term can be taken out of the frequency integral. Applying Parseval's theorem once more to the resulting expression gives

$$\frac{\partial M}{\partial m} \approx -2 \sum_\nu \frac{1}{c_\nu^2} \left[\int \frac{\partial c_\nu}{\partial m} dx \right] \int \dot{s}_\nu(m,t)\left[d(t) - s(m,t) \right] dt \tag{B9}$$

$$-2 \sum_\nu \frac{1}{A_\nu} \frac{\partial A_\nu}{\partial m} \int s_\nu(m,t)\left[d(t) - s(m,t) \right] dt \quad ,$$

which proves equation (23).

Chapter 9

Waveform inversions of surface wave data recorded with the NARS array

1) Introduction.

One of the main tasks of modern seismology is to map the lateral heterogeneity in the Earth. Low order spectral models of lateral heterogeneity have been constructed using P-wave delay times (Dziewonski, 1984), surface wave dispersion data (Nataf et al., 1986) or surface waveforms (Woodhouse and Dziewonski, 1984; Tanimoto, 1987). These studies produced extremely smooth Earth models, because of the low order expansion of the heterogeneity in spherical harmonics. However, recent large scale tomographic inversion of P-wave delay times have shown that lateral heterogeneity exists down to depths of at least 500 km. on a horizontal scale of a few hundred kilometers (Spakman, 1986ab).

Lateral variations in the P-velocity on this scale can be analyzed accurately using delay time tomography. In principle, tomographic inversions could also be applied to S-wave delay times. In practice, this is not so simple, because the presence of the low velocity layer renders the S-wave tomography problem highly nonlinear. In fact, it is shown by Chapman (1987) that the tomographic inversion problem is ill-posed if a low velocity layer is present. The fact that the low velocity layer exhibits strong lateral variations (York and Helmberger, 1973; Souriau, 1981; Paulssen, 1987) poses an additional complication.

One could use surface wave data instead, because Love waves and Rayleigh waves are strongly influenced by the S-velocity. However, fundamental mode surface wave data (which are most easily measured and identified) that penetrate as deep as 200 km., have a horizontal wavelength of the order of 300 km. This means that lateral heterogeneities on a scale of a few hundred kilometers are no longer smooth on a scale of a wavelength of these waves. Therefore ray theory, which forms the basis of all dispersion measurements, cannot be used in that case. Up to this point, this fact has been consequently ignored.

The breakdown of ray theory means that scattering and multipathing effects can be important. In the companion paper of this article (Snieder, 1988; this paper is referred to as "paper I"), linear surface wave scattering is presented. It is shown in paper I how this theory can be used to map the lateral variations of the S-velocity in the Earth. With this method, the complete waveform of surface wave data can be inverted, so that not only the phase but also the amplitude can be used for inversion. Unfortunately, there is at this point only linear theory for surface wave scattering in three dimensions (Snieder, 1986ab; Snieder and Nolet, 1987;

This chapter is submitted for publication as:

Snieder, R., Large scale waveform inversions of surface waves for lateral heterogeneity -II: Application to surface waves in Europe and the Mediterranean, *submitted to J. Geophys. Res.*, 1988.

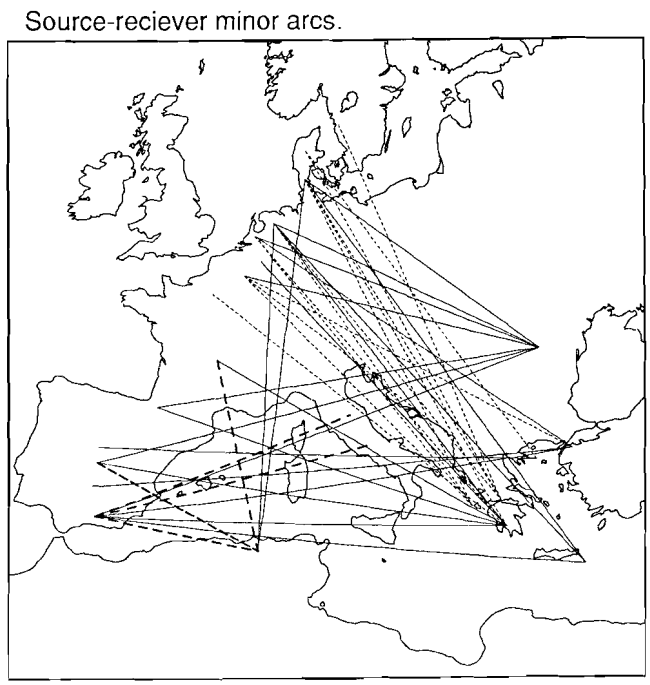

Figure 1. Source-receiver minor arcs for the seismograms used in the inversions. The different line styles are defined in section 2.

Snieder and Romanowicz, 1987; Romanowicz and Snieder, 1987) which limits the applicability of this method. Large scale inversion of both the phase and the amplitude of surface wave data has also been performed by Yomogida and Aki (1987), who applied a scattering formalism to the Rytov field of surface waves. However, their method is based on the assumption that surface waves satisfy the 2D wave equation, which has never been shown (and which is probably not true).

In this paper large scale waveform inversions using linear scattering theory, as presented in paper I, are applied to surface wave data recorded with the NARS array (Dost et al, 1984; Nolet et al., 1986) for events in southern Europe. The inversions with linear scattering theory, which will be called the "Born inversion", are applied both to the surface wave coda and to the direct surface wave. Details of the inversion method with numerical examples are shown in paper I.

The Born inversion is first applied to the surface wave coda. To this end the nature of the surface wave coda is investigated in section 2, and the conditions for the validity of the Born approximation for the surface wave coda is established. In inversions of the complete waveform, parameters like the source mechanism, station amplification etc. should be specified correctly. The procedures that are followed in this study are reported in section 3. As shown in paper I, it may be advantageous to perform a nonlinear inversion first for a smooth reference model, in order to render the problem more linear. The results of this nonlinear inversion are

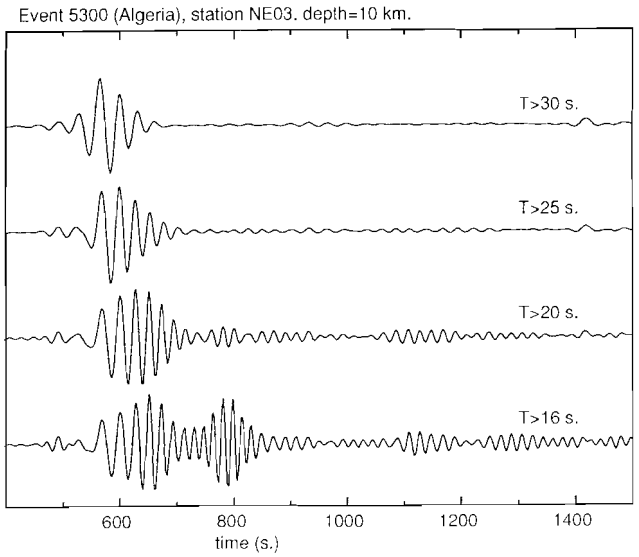

Figure 2. Low passed seismograms for an Algerian event recorded in NE03 (Danmark).

shown in section 4. The next section features waveform inversions of the surface wave coda, while in section 6 the Born inversions of the direct wave are shown. The reliability of these results is investigated in section 7, where a resolution analysis is presented. A two layer model of the S-velocity under Europe and the Mediterranean is finally presented in section 8.

2) The nature of the surface wave coda.

Before proceeding with the inversion, it is instructive to study the surface wave coda in some more detail. In this study surface wave data recorded by the NARS array (Dost et al., 1984; Nolet et al., 1986) are used for shallow events around the Mediterranean and a deeper event in Rumania. Figure 1 shows the source receiver minor arcs for the seismograms used in this study. Because the inversion is linear, it is important to establish first the conditions for the validity of the Born approximation for the surface wave coda.

In figure 2 a seismogram is shown for an event in Algeria recorded at station NE03 in Danmark, low passed at several different periods. For the seismogram low passed at 16 s., the coda has approximately the same strength as the direct wave. This means that the Born approximation cannot be used to describe the surface wave coda at these periods. However, for periods larger than 20 s. the coda is much weaker than the direct wave, which justifies the Born approximation for these periods. Low passed seismograms recorded in the same station for a Greek event at approximately the same depth are shown in figure 3. For this event in the

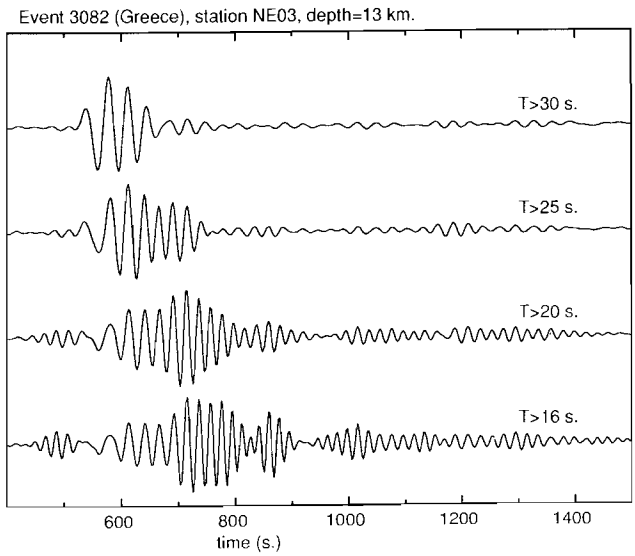

Figure 3. Low passed seismograms for a Greek event recorded in NE03 (Danmark).

seismogram lowpassed at 25 s., there is still an appreciable secondary wavetrain (around 700 s.) just after the arrival of the direct wave, and the Born approximation for the surface wave coda is therefore only justified for periods larger than 30 s. (This is confirmed later by figure 4b.) Therefore, only periods larger than 30 s. have been used in the inversions presented in this paper. It is verified that for all recorded seismograms low pass filtering at 30 s. leads to a coda level which is low enough to justify the Born approximation.

This condition for the validity of the Born approximation may be overconservative. In a field experiment, surface waves reflected from a concrete dam on a tidal flat have been used successfully to reconstruct the location of this dam using Born inversion (Snieder, 1987). Due to the very large contrast posed by this dam, the direct surface wave and the reflected surface wave had approximately the same strength, and Born inversion was strictly not justified. Nevertheless an accurate reconstruction of the location of this dam was achieved. The reason for this discrepancy is that the geometry of the heterogeneity precluded multiple scattering. In such a situation, linear inversion gives at least qualitatively good results.

The examples shown in the figures 2 and 3 show that the coda level is very different for the different wave paths. This is verified by dividing the seismograms in two groups. One group consists of seismograms for with wave paths through the western Mediterranean (the dashed lines in figure 1), while the other group is for the wave paths through eastern and central Europe (the dotted lines in figure 1). For each group the spectrum of the direct surface wave is determined, as well as the spectra of the coda (defined by group velocities between 1.6 and 2.9 km./s.), and the spectrum of the signal before the arrival of the direct wave. The spectrum of the signal before the arrival of the direct wave is considered to give an estimate of the background noise level. From an academic point of view this is acceptable, because body

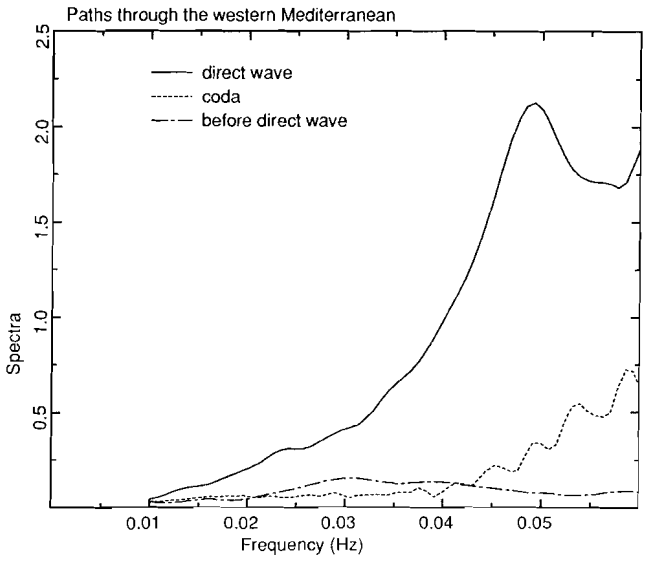

Figure 4a. Spectra of the direct wave, surface wave coda and background noise for wave paths through the western Mediterranean.

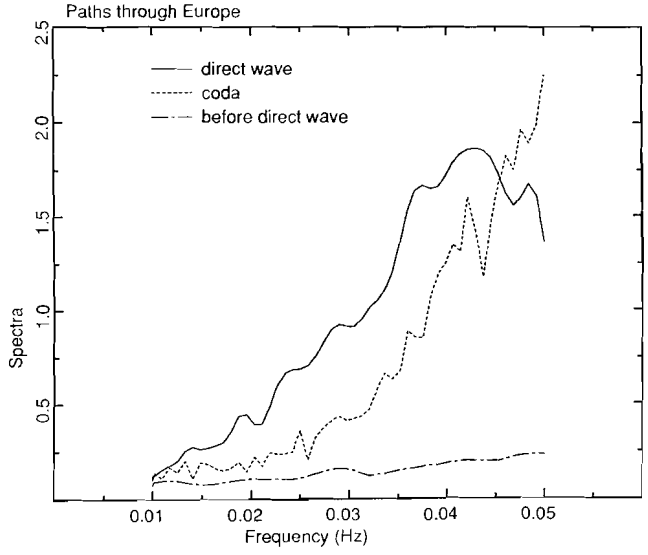

Figure 4b. Spectra of the direct wave, surface wave coda and background noise for wave paths through eastern and central Europe.

waves and higher mode surface waves are noise for our purposes. On the other hand, this procedure may give an overestimate of the background noise.

The spectra for the paths through the Mediterranean is shown in figure 4a Note that the average coda level is much weaker than the strength of the direct surface wave, even for periods as short as 16 s. (0.06 Hz). For periods larger than 25 s. (0.04 Hz) the noise level has about the same strength as the coda level. The means that inversions using the surface wave coda for these periods can only give meaningful results if there is an abundance of data, which leads to a system of linear equations which is sufficiently overdetermined to average out the contaminating influence of noise. For the wave paths through eastern and central Europe (figure 4b) the situation is different. For all frequencies, the coda level lies above the noise level, although for periods longer than 50 s. (0.02 Hz) this difference is marginal. For these seismograms, the coda energy increases rapidly as a function of frequency, for periods shorter than 22 s. (0.045 Hz) the coda spectrum is even higher than the spectrum of the direct wave. This means that there is only a relatively narrow frequency band where the Born approximation is valid, and where the coda stands out well above the noise level.

The fact that the coda level for the paths through eastern and central Europe increases more rapidly as a function of frequency than for the paths through the western Mediterranean has implications for the depth of the heterogeneities that generate the coda. In order to quantify this notion, a normalized coda level can be defined by subtracting a constant noise level from the coda spectrum, and by division by the spectrum of the direct wave. This normalized coda level is approximately equal to the interaction coefficients, see the equations (1) and (5) of paper I. (One should be a bit careful with this identification, because an organized distribution of scatterers leads to extra frequency dependent factors, see Snieder (1986a) for an example of scattering of surface waves by a quarter space.)

The normalized coda level are in the figures 5a and 5b compared with the interaction terms for different heterogeneities. (In this example, the absolute value of the interaction terms is averaged over all scattering angles.) These inhomogeneities have a constant relative shear wave velocity perturbation down to the indicated depth, while the density is unperturbed, furthermore $\delta\lambda=\delta\mu$. For the wave paths through eastern and central Europe, these curves in figure 5b can only be compared with the interaction terms for periods longer than 30 s., because the condition of linearity breaks down for shorter periods. All shown heterogeneities fit the normalized coda level within the accuracy of the measurements. Also, it follows from the figures 1ab of paper I that these heterogeneities have approximately the same radiation pattern. This means that for these wave paths, it is virtually impossible to determine the depth of the heterogeneity from the surface wave coda. For the paths through the western Mediterranean this situation is different, because it can be seen from figure 5a that a shallow heterogeneity (or topography) fits the normalized coda spectrum better than a deeper inhomogeneity. This is an indication that the lateral heterogeneity in eastern and central Europe is present at greater depths than in the western Mediterranean.

3) Procedures for the inversion of surface wave seismograms.

In order to perform waveform fits of surface wave data, several parameters and procedures need to be specified. All inversions presented in this paper have been performed with the model shown in figure 6. This model is equal to the M7 model of Nolet (1977), except that the S-velocity in the top 170 km. is 2% lower than in the M7 model. This compensates for the

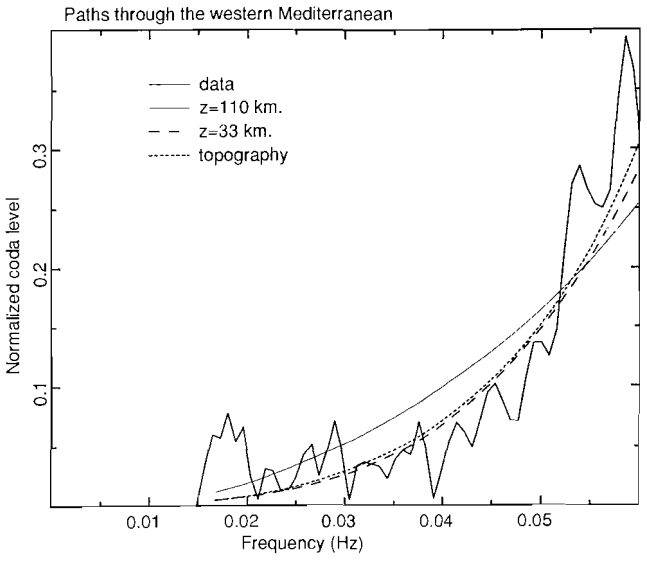

Figure 5a. Normalized coda level for the wave paths through the western Mediterranean, and the (normalized) integrated radiation for different inhomogeneities as defined in section 3.

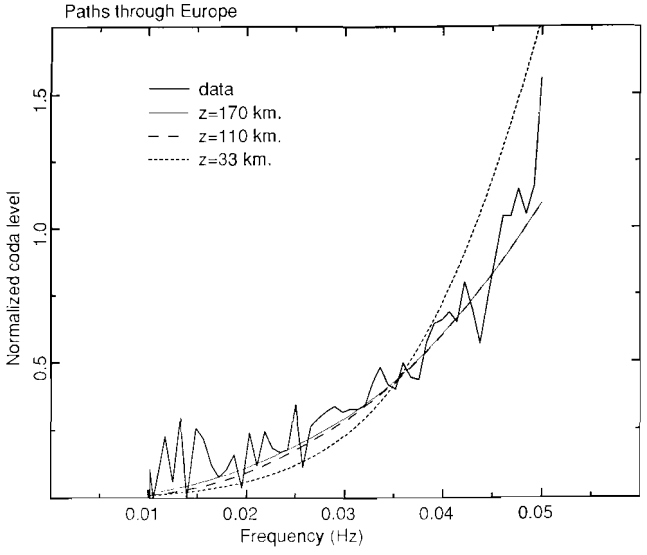

Figure 5b. Normalized coda level for the wave paths through eastern and central Europe, and the (normalized) integrated radiation for different inhomogeneities as defined in section 3.

fact that the M7 model is for the Scandinavian shield which has an anomalously high S-velocity. The anelastic damping of the PREM model (Dziewonski and Anderson, 1981) is assumed, this damping is not varied in the inversions.

For the source mechanisms, the event location, depth, and centroid moment tensor solutions, as reported in the ISC bulletins are used, whenever available. For the remaining events, the source parameters from the PDE bulletins are used. For the Rumania event, the source mechanism as determined from GEOSCOPE data (Romanowicz, personal communication) is employed. No inversion for the source mechanism is performed, because the NARS stations provide only a limited azimuthal coverage, which means that the source mechanisms are poorly constrained by the data. The source strength is usually rather inaccurate, this parameter determined by fitting the envelopes of the synthetics to the data envelopes. The events used in this study are in general rather weak (ms≈5-6), so that the reported source mechanisms are not always reliable. All seismograms with a strong difference in waveshape between the data and the (initial) synthetics have not been used in the inversion. Surface wave recordings that triggered on the surface wave have also been discarded.

The station magnifications are not included in the inversions presented here. The station magnification includes not only the instrumental magnification, but also the magnification effects of the local environment of the station. As a check, the inversions presented here have also been performed with a simultaneous inversion for the station amplifications. Even though this produced station magnifications as large as 10%, the results in the models for lateral heterogeneity was minimal.

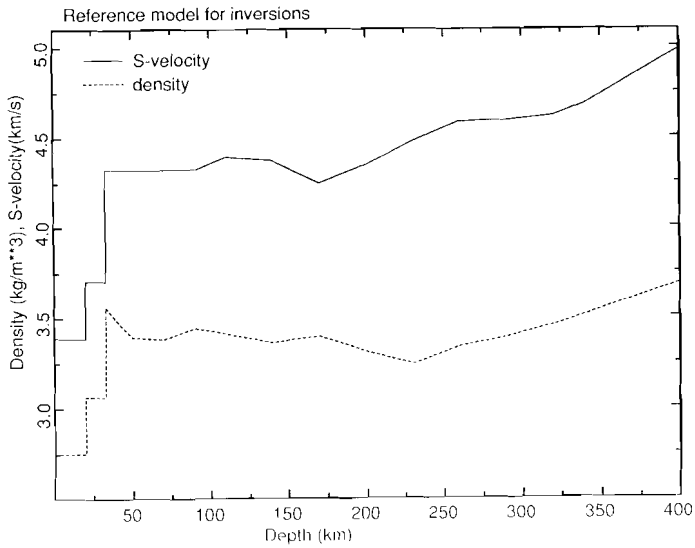

Figure 6. Starting model for the inversions.

In paper I, the waveform inversion is formulated as the least squares solution of a large matrix equation. The rows and columns of this matrix can be scaled at will (Van der Sluis and Van der Vorst, 1987). It has been shown by Tanimoto (1987) that it is important that each seismogram gets more or less the same weight in the inversion. Similarly, the different frequency components within each seismogram should have a comparable weight. For the shallow events used here, the low frequencies are not excited very well. In order to compensate for this, data and synthetics are scaled in the frequency domain with a factor $1/\omega$. In the inversions for the surface wave coda, a scaling with $M_o/\sqrt{\sin\Delta}$ is applied, where M_o is the strength of the moment tensor, and Δ the epicentral distance. This factor corrects for the different strengths and geometrical spreading factors of the different events. In the inversion for the direct wave, the seismograms are scaled in such a way that maximum amplitude in the time domain is equalized.

Lastly, in the Born inversions both for the coda and the direct wave, each seismogram is scaled with a factor $1/\sqrt{1+\frac{E}{<E>}}$. In this expression, E is the energy of the data residual of the seismogram under consideration, while $<E>$ denotes the average of this quantity for all seismograms. This weight factor ensures that the seismograms with appreciable misfits get more or less the same weight in the inversion, so that the contaminating influence of outliers is reduced. In the meantime, seismograms with a good initial fit have a low weight in the inversion, this prevents that a small amount of spurious noise in these seismograms gets an excessive weight in the inversion.

4) Nonlinear inversion of the direct wave.

As mentioned in paper I, it is advantageous to perform a nonlinear inversion of the direct wave first, because this renders the Born inversion more linear. For this inversion, the procedures described in paper I are used for determining the phase velocity perturbation of a smooth reference model. In this inversion, the phase velocity is determined on a rectangular grid of 12×12 points in the domain shown in figure 1, and is interpolated at intermediate locations using bicubic splines. The relative phase velocity perturbation $\delta c/c$ is assumed to be constant in the period bands 30-40 s., 40-60 s. and 60-100 s.

In figure 7a the phase velocity perturbation for periods between 60 s. and 100 s. is shown for the unconstrained case, i.e. $\gamma=0$ in equation (21) of paper I. Note that the phase velocity perturbations are not confined to the vicinity of the source receiver paths. This is an artifact of the bicubic spline parameterization, which has an oscillatory nature near places where the interpolated function changes rapidly. These artifacts can be removed by switching on the regularization parameter γ in expression (21) of paper I. The constrained solution ($\gamma>0$) is shown in figure 7b. This regularization goes at the expense of the waveform fit, and it is subjective how much regularization one wants to impose on these solution. However, in this study the nonlinear inversion for a smooth reference model is only the first step in the complete waveform inversion, so that there is no need to obtain the maximum information from this nonlinear inversion. For periods larger than 30 s., the resulting reference models for the employed value of γ (see for example figure 7b) produce a waveform fit which are sufficiently good to

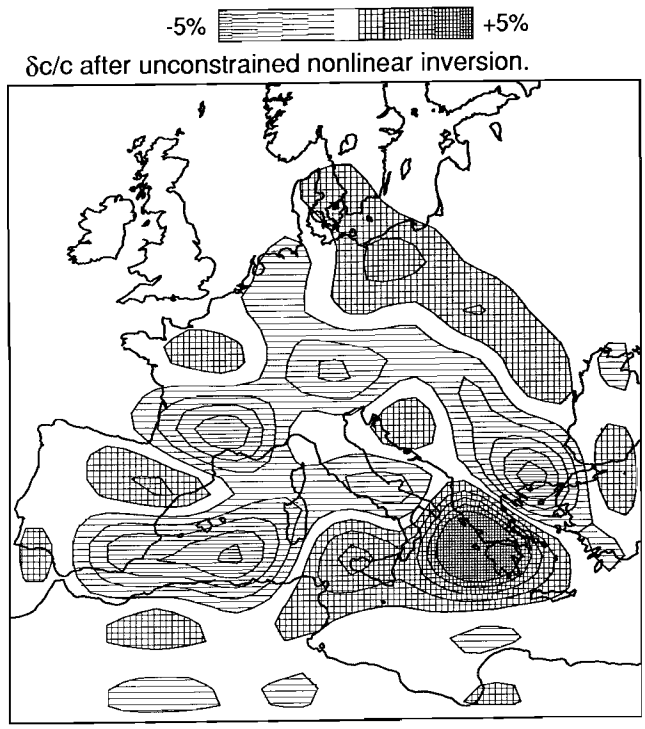

Figure 7a. Relative phase velocity perturbation ($\delta c/c$) for periods between 60-100 s. determined from unconstrained nonlinear waveform fitting (γ=0).

warrant a linear inversion for the remaining data residual. (This means that the phase shift between the data and synthetics is at the most 45 degrees, and that the amplitude mismatch is not larger than 30%.) These reference models for the phase velocity perturbations are used in the subsequent Born inversions. Waveform fits of the nonlinear inversion are presented in section 6.

5) Born inversion of the surface wave coda.

The Born inversion can be applied both for inversion of the direct surface wave, as well as for the coda. In this section the waveform inversion of the surface wave coda is discussed. The surface wave coda is extracted from the full seismogram with a time window that allows group velocities between 1.74 km./s. and 2.90 km./s. At both ends this window is tapered with a cosine taper over a length of 100 s.

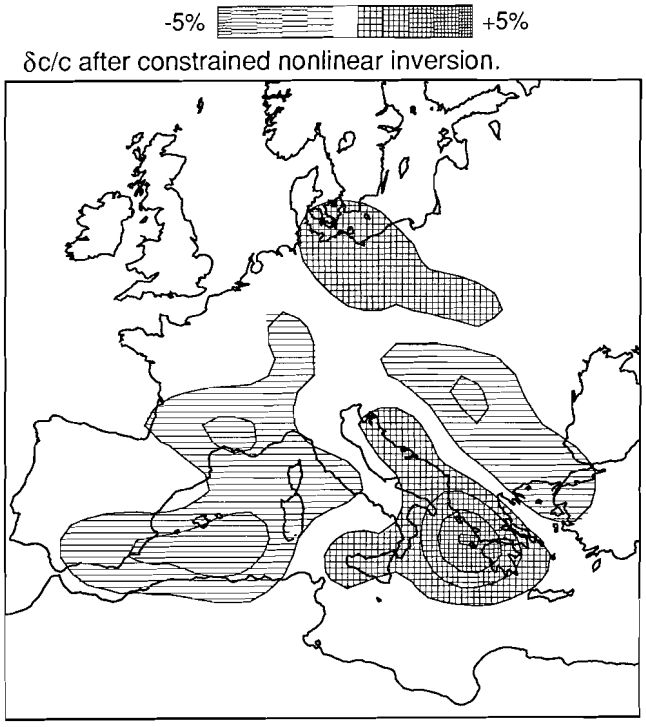

Figure 7b. Relative phase velocity perturbation ($\delta c/c$) for periods between 60-100 s. determined from constrained nonlinear waveform fitting ($\gamma>0.$).

In this inversion, the depth dependence of the heterogeneity is prescribed to consist of a constant relative S-velocity perturbation $\delta\beta/\beta$ down to a depth of 170 km., while the density is unperturbed. The perturbations on the Lamé parameters are equal. In the inversion, a model of 100×100 cells is determined (with a cell size of $35\times35 km^2$), so that 10,000 unknowns are determined in the inversion. The 42 seismograms produce 2520 data points, where the real and imaginary parts of each spectral component are counted as independent variables. This means that the resulting system of linear equations is underdetermined. Increasing the cell size has the disadvantage that the scattering integral (5) of paper I is not discretized accurately. Imposing a smoothness constraint also is no option, since scattered surface waves are most sensitive to abrupt lateral changes of the heterogeneity. As argued in section 2, it is difficult to obtain a good depth resolution for this kind of inversion. This, and the consideration that for a fixed depth dependence of the heterogeneity the resulting system of linear equation is already underdetermined, makes it unjustifiable to perform an inversion with more degrees of freedom with respect to the depth dependence of the heterogeneity.

The result of the Born inversion of the surface wave coda for periods between 30-100 s. is shown in figure 8. For this inversion three iterations have been performed, according to the results of paper I this is sufficient to image the heterogeneity. The reconstructed model has a

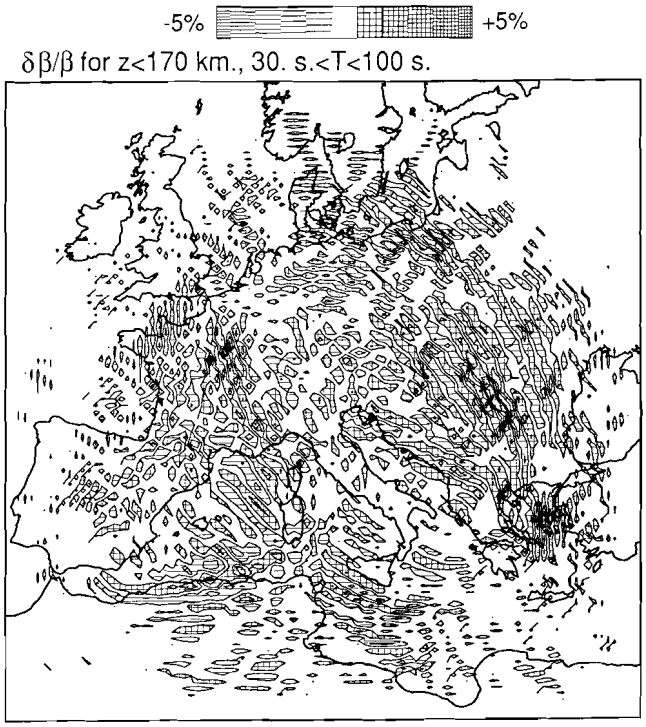

Figure 8. Relative S-velocity perturbation ($\delta\beta/\beta$) from the inversion of the surface wave coda. The heterogeneity extends down to a depth of 170 km.

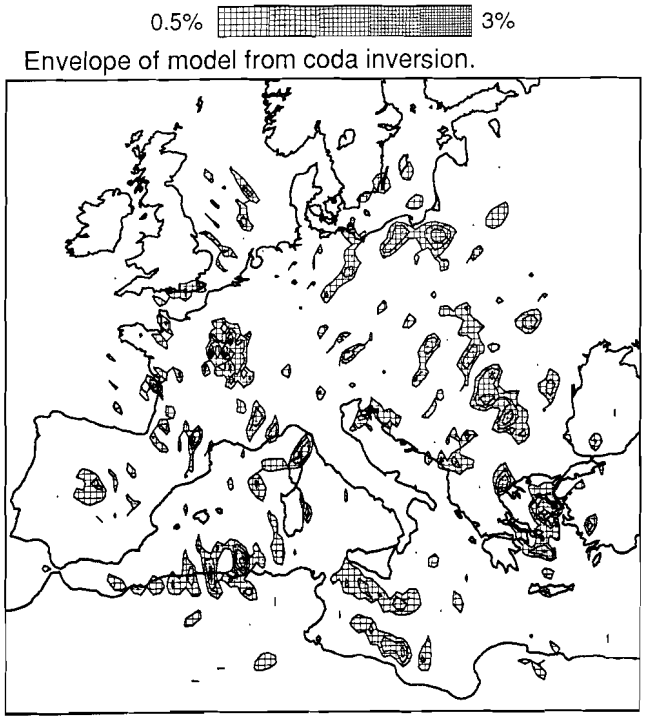

Figure 9. Filtered envelope of the model in figure 8.

messy appearance, and is dominated by ellipsoidal structures. These structures are reminiscent of the "smiles" that occur in improperly migrated sections in exploration seismics (Berkhout, 1984). Note the oscillatory nature of the solution, which is a consequence of the fact that this image is reconstructed essentially with a correlation method (paper I). The direction of this ellipsoidal stripes is determined by the geometry of the events and the stations, it does not necessarily reflect the structure of the inhomogeneity.

This directivity and the oscillations in the reconstructed model can be removed by envelope filtering. Subtracting a smoothed version of this envelope from the envelope itself enhances the the contrasts in the final solution. The result of this procedure is shown in figure 9. One should always be careful in applying this kind of image processing techniques, because it may introduce an unwanted degree of subjectivity in the resulting patterns. On the other hand, these methods may help to extract some order out of an apparent chaos. Unfortunately, in the resulting model (figure 9) this goal is only partly reached. Some of the heterogeneities could be related to familiar geological structures such as the Tornquist-Tesseyre zone, and the northern edge of the African continent, while other heterogeneities appear to be distributed at random.

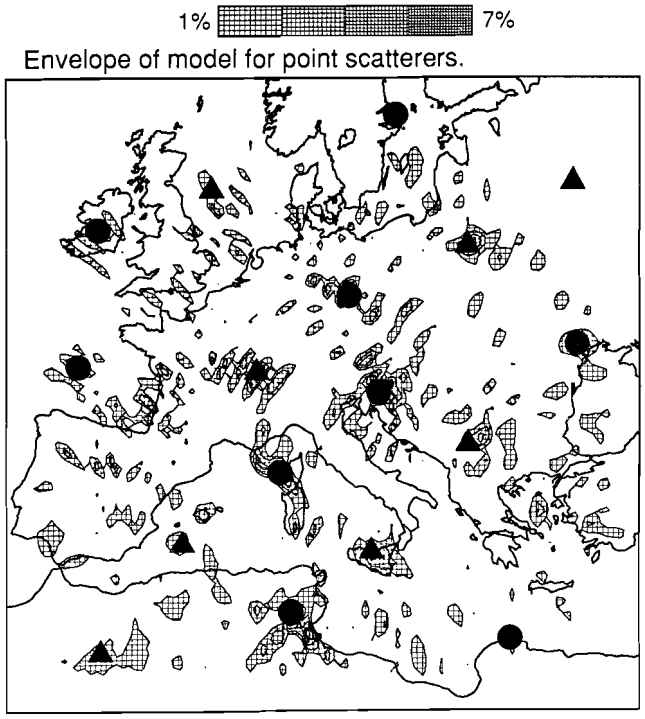

Figure 10. Filtered envelope of the model determined from a waveform inversion of synthetics computed for positive (circles) and negative (triangles) point scatterers with $\delta\beta/\beta$ constant down to a depth of 170 km.

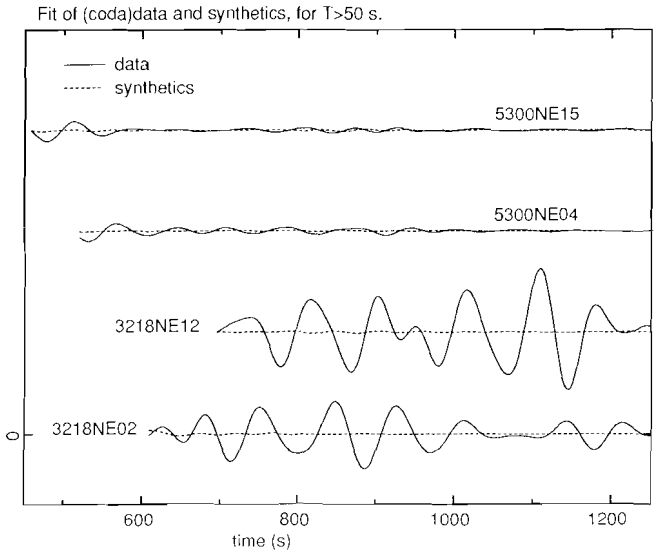

Figure 11a. Examples of the waveform fit of the surface wave coda, low passed at a corner period of 50 s.

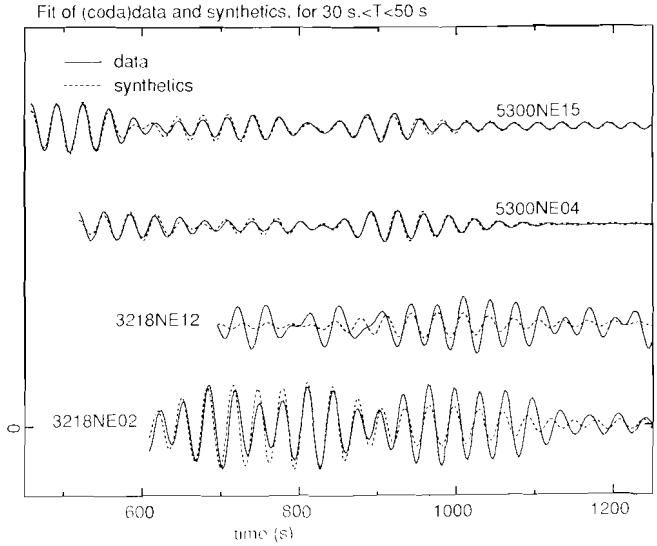

Figure 11b. Examples of the waveform fit of the surface wave coda, high passed at a corner period of 50 s.

In order to establish the significance of these results, the same inversion is performed with synthetic data for a model consisting of 9 positive and 8 negative point scatterers. The

envelope of the resulting model is shown in figure 10. The heterogeneity is reconstructed near most point scatterers, but also in areas away from these point scatterers (Spain, southwest France, Aegean sea, etc.). This means that even if the data were noise free, there are insufficient data to constrain the resulting model. For noise corrupted data this effect is aggravated.

Nevertheless a reasonable good fit of the surface wave coda is achieved, with a variance reduction of 25%. The resulting waveform fits of the surface wave coda are shown in the figures 11a and 11b both low passed and high passed at a corner period of 50 s. For periods larger than 50 s. (figure 11a) the waveform fit is poor. This is consistent with the results of section 2 where it was argued that the coda level does not stand out very well above the noise level. However, for the higher frequencies (periods from 30-50 s., see figure 11b) a reasonable waveform fit is obtained. Most of the beats in the surface wave coda are reproduced in the synthetics. It should be remembered that the seismograms in these figures only show the surface wave coda. In order to see these data in their proper perspective, a fit of the coda (bandpassed for periods between 30 s. and 50 s.) is shown in figure 12 together with the direct wave. Unfortunately, the fact that good waveform fits are achieved, does not establish the reliability of the resulting models, because the linear system of equations is underdetermined.

Inversions for heterogeneities which extend to a depth different than 170 km. produce almost the same model, only the strengths of these heterogeneities differs from the model shown in figure 8. An inversion for data bandpassed between 30-40 s. gives virtually the same result as figure 8, which confirms that for longer periods the surface wave coda contains a large noise component, and not much scattered surface waves.

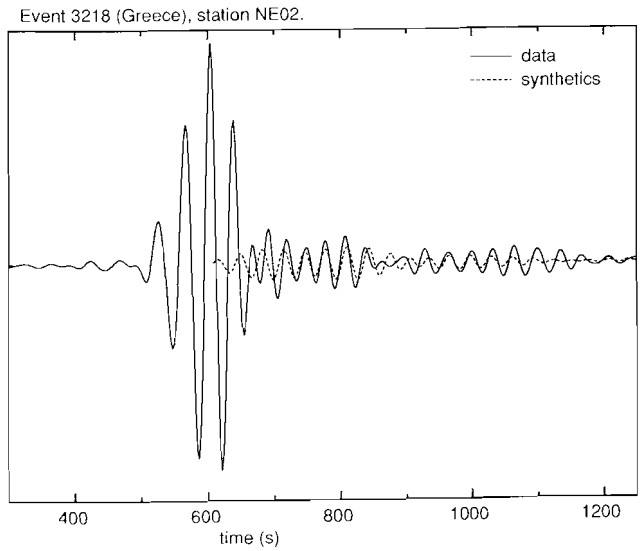

Figure 12. Full waveform fit of the surface wave coda, low passed at a corner period of 50 s.

These results do not imply that mapping lateral heterogeneity using the surface wave coda is impossible. In fact, it has been shown in a controlled field experiment that successful imaging of the surface wave coda is possible (Snieder, 1987a). However, the surface wave coda data at our disposal are currently too sparse to produce an accurate reconstruction of the lateral heterogeneity. This is exacerbated by the fact that the noise level in the surface wave coda is relatively high, which can only be compensated with a redundant data set. Large networks of digital seismic stations, as formulated in the ORFEUS (Nolet et al., 1985) and PASSCAL proposals, are necessary to achieve this goal. Alternatively, the Born inversion of the surface wave coda might be used in regional studies where one wishes to study tectonic features such as continental margins, or the boundaries of major geological formations. A system of portable digital seismographs would be very useful for this kind of investigations.

6) Born inversion of the direct surface wave.

Linear scattering theory can also be used to describe the distortion of the direct wave (Snieder, 1987b). This distortion can either be due to ray geometrical effects, or to multipathing effects that are not accounted for by ray theory. In the Born inversion presented in this section, the isotropic approximation is used (paper I). This means that the relative phase velocity perturbations are retrieved from the linear waveform inversion of the direct wave. This quantity is assumed to be constant within the frequency bands employed (30-40 s., 40-60 s. and 60-100 s.). A separate Born inversion is performed for each of these frequency bands, so that the phase velocity perturbation is determined independently for each frequency band. In order to justify the isotropic approximation (paper I), a time window is used to extract the direct wave from the complete seismograms.

The Born inversions presented here are performed for a model of 100×100 cells with a cell size of $35\times35 km^2$. In the Born inversion of the surface wave coda in the previous section, no a-priori smoothness constraint was imposed, because scattered surface waves are most efficiently generated by sharp lateral heterogeneities. This led to an underdetermined system of linear equations. For the Born inversion of the direct wave, the available data set also produces an underdetermined system of linear equations. One alternative would be to increase the cell size, but according to the example of figure 7 in paper I, rather small cells are needed to produce the required focusing/defocusing. Instead of this, the smoothing operator of equation (26) in paper I is used in this inversion to constrain the solution. In these inversions, the values $\alpha=0.66$ and $N=4$ are used, which implies an effective correlation length of 140 km. The Born inversions are performed in three iterations (see also paper I), it has been checked that more iterations don't change the resulting models very much.

The phase velocity perturbation for the three frequency bands are shown in the figures 13abc. The phase velocities are the result of both the nonlinear inversion for the smooth reference medium, and the subsequent Born inversion. See figure 7b as an example of the contribution of the nonlinear inversion for the smooth reference medium, to the phase velocity model of figure 13c.

Note that the resulting phase velocity patterns vary considerably on a scale of one horizontal wavelength. This means that ray theory cannot be used to model the effects of these

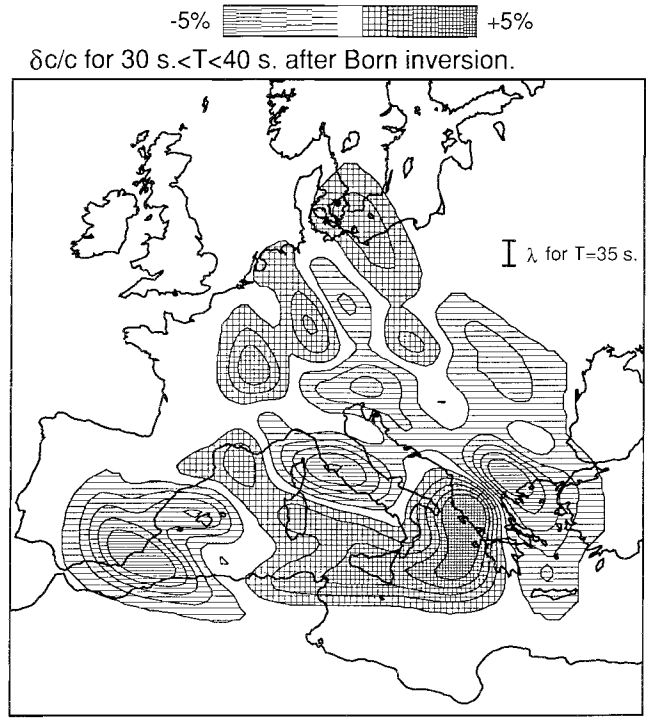

Figure 13a. Relative phase velocity perturbation $(\delta c/c)$ for periods between 30-40 s. as determined from nonlinear waveform inversion plus a subsequent Born inversion.

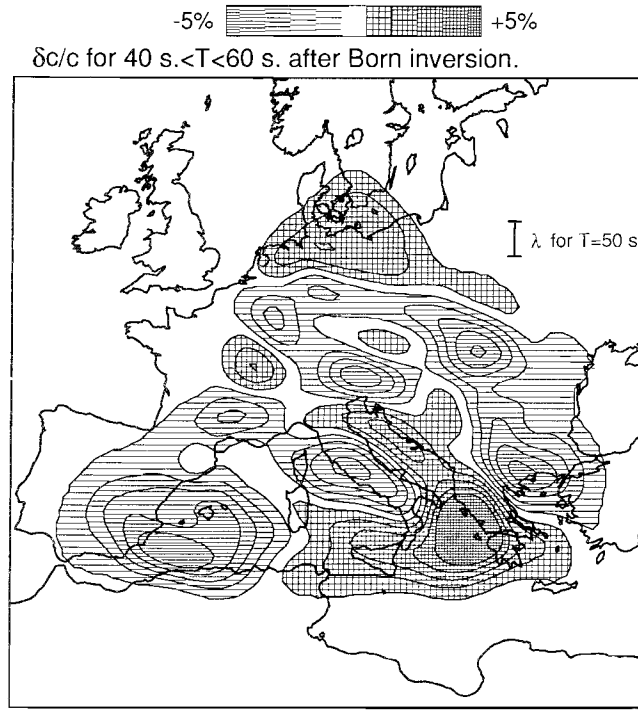

Figure 13b. As figure 13a, but for periods between 40-60 s.

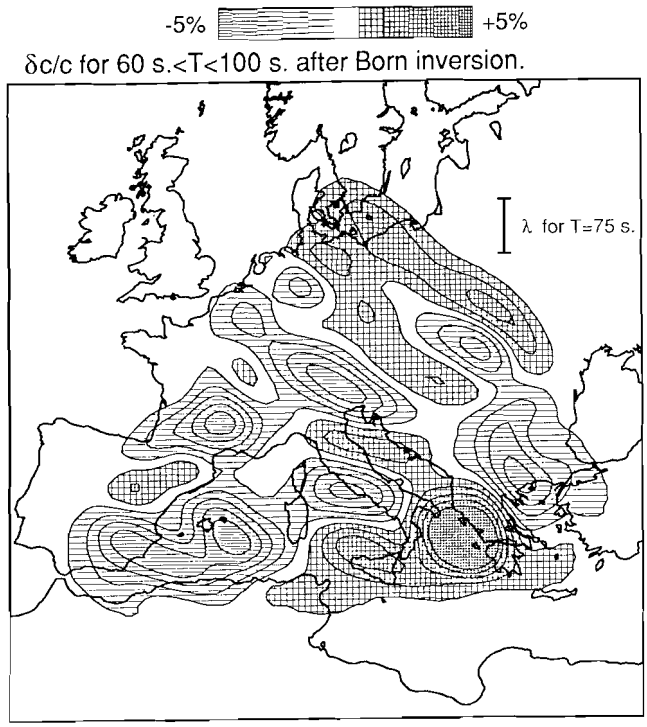

Figure 13c. As figure 13a, but for periods between 60-100 s.

heterogeneities, while surface wave scattering theory takes effects such as multipathing into account. Surprisingly, figure 13c for the phase velocity determined from Born inversion is not too different from figure 7a for the unconstrained nonlinear inversion using ray theory. The smaller scale features of figure 13c are absent in figure 7a because the spline interpolation does not allow these small scale features (nor does ray theory). Nevertheless, the overall pattern in these figures is the same. Apparently, ray theory is rather robust to violations of the requirement that the heterogeneity is smooth. This may explain the success of dispersion measurements in situations where ray theory is not justified. Most of the information on the S-velocity structure under Europe in the crust and upper mantle is determined from surface wave dispersion measurements. For example, Panza et al. (1982) delineate a heterogeneity between Corsica and northern Italy with a scale of approximately 250 km., from anomalously low Rayleigh wave phase velocities between 40-60 s. Their results are therefore inconsistent with the (ray) theory they employed. Nevertheless, this low phase velocity anomaly is also visible in figure 13b, which is constructed using surface wave scattering theory.

Waveform fits after the nonlinear inversion for the smooth reference model, and after the subsequent Born inversion (the "final fit") are shown in the figures 14 to 19. In figure 14 results for station NE12 near Madrid are shown. The amplitude of the direct surface wave is changed considerably in the inversion. Note that the waveform fit has slightly deteriorated in the nonlinear inversion. The reason for this is that the 42 seismograms are inverted simultaneously, so

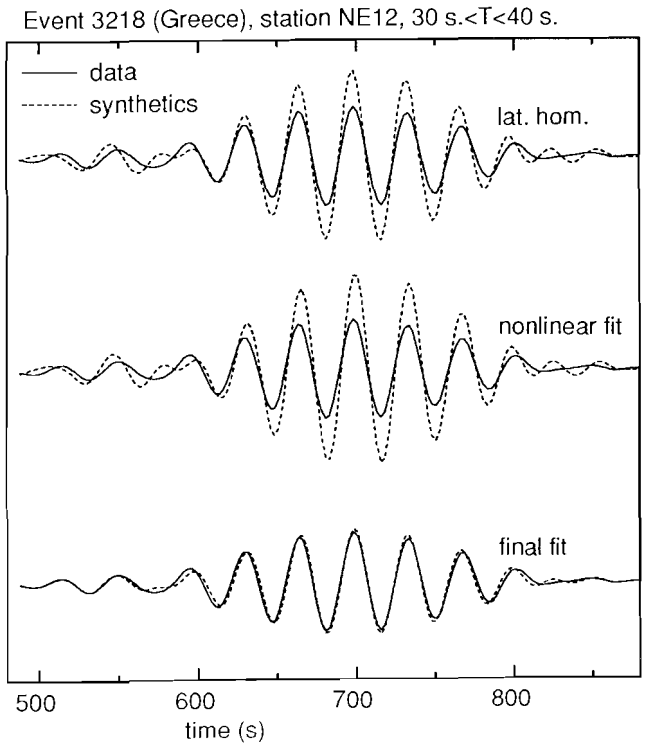

Figure 14. Waveform fit for periods between 30-40 s. for the laterally homogeneous starting model (top), after the nonlinear inversion for a smooth reference model (middle), and after Born inversion (bottom), for a Greek event recorded in NE12 (Spain).

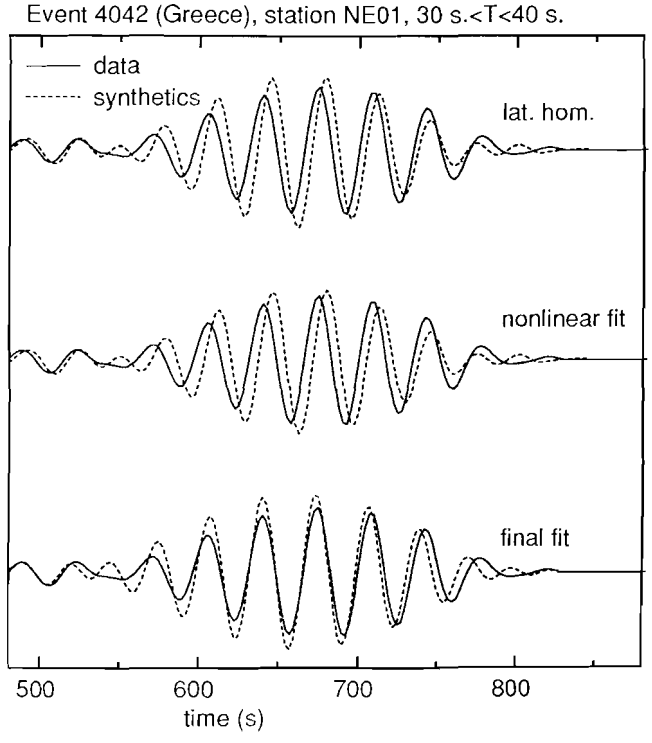

Figure 15. As figure 14, for a Greek event recorded in NE01 (Gothenborg) for periods between 30-40 s.

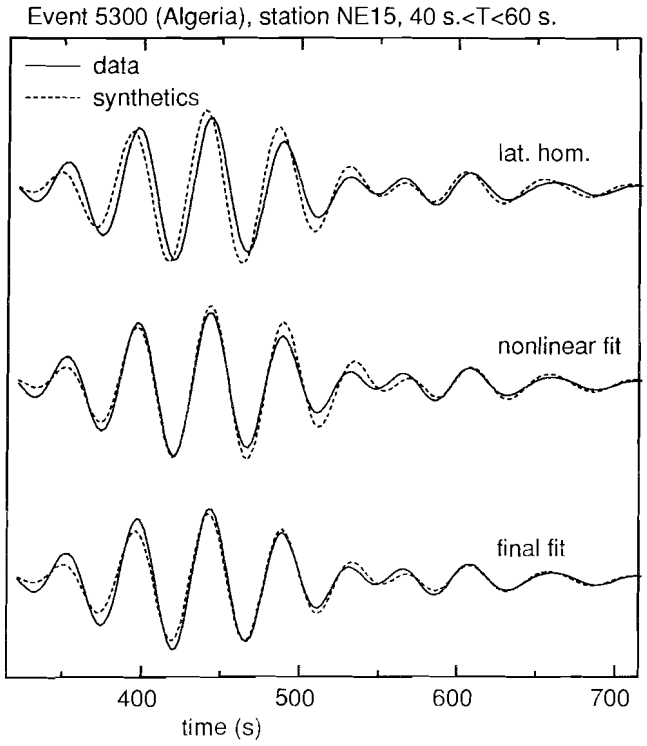

Figure 16. As figure 14 for an Algerian event recorded in NE15 (Netherlands) for periods between 40-60 s.

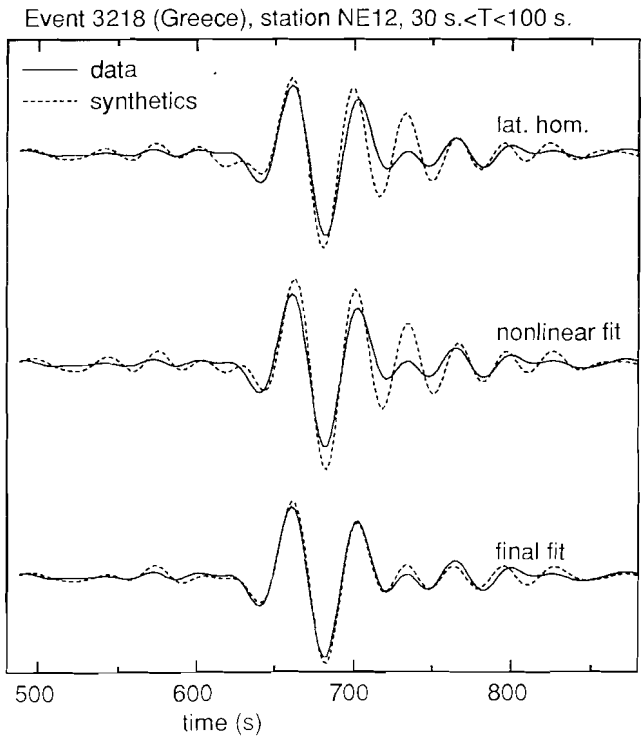

Figure 17. As figure 14 for the full bandwidth (30-100 s.).

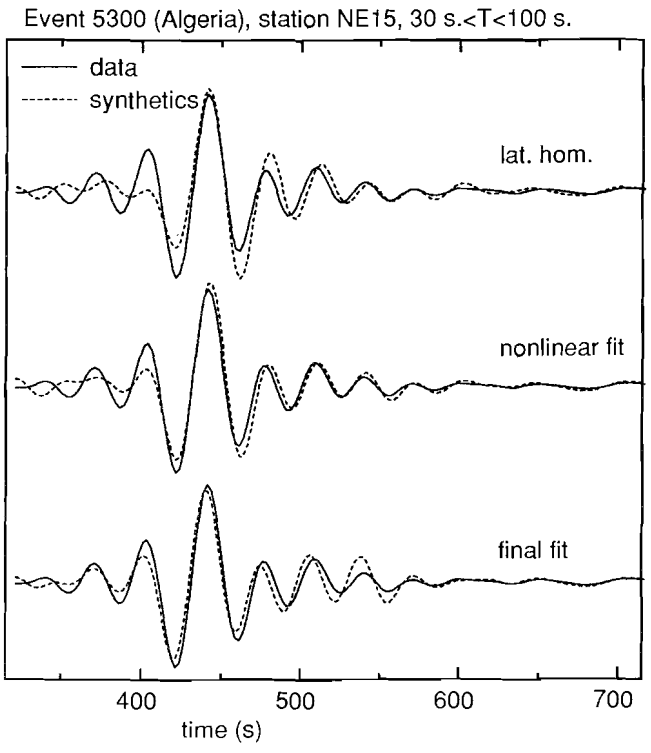

Figure 18. As figure 15 for the full bandwidth (30-100 s.)

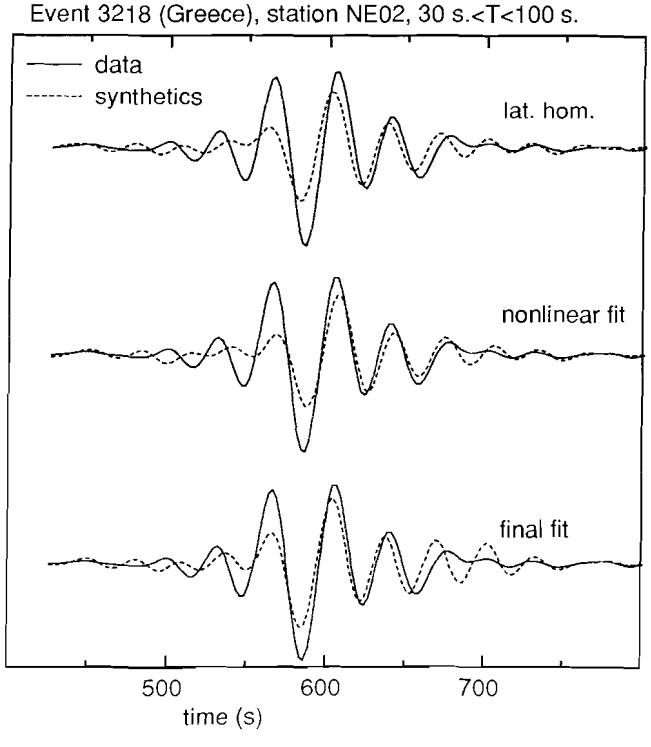

Figure 19. As figure 14 for a Greek event recorded in NE02 (Danmark) for the full bandwidth (30-100 s.).

that it is possible that the fit of one seismogram is improved at the expense of another seismogram. In figure 15, an example is shown for a seismogram recorded at NE01 (Gothenborg). For this seismogram, the amplitude is already quite good for the laterally homogeneous starting model, but the phase is adjusted in the Born inversion. In the preceding examples, the Born inversion realized the fit between data and synthetics. This is not the case for all seismograms. In figure 16 a seismogram for an event in Algeria recorded at NE15 (Netherlands) is shown. For this seismogram the nonlinear inversion performed most of the waveform fit.

By superposing the seismograms for the three frequency bands, seismograms for the full bandwidth (30-100 s.) can be constructed. Figure 17 displays the seismogram of figure 14, but now for the full employed bandwidth. The final fit between the data and the synthetic is extremely good. Note that the tail of the direct wave (around 725 s.) is fitted quite well after the Born inversion. For the recording of the Algerian event in NE15, the full bandwidth data are shown in figure 18. The trough in the waveform around 420 s. has been adjusted well in the nonlinear inversion, whereas the fit of the start of the signal (around 400 s.) is improved considerably in the subsequent Born inversion. Unfortunately, the improvement in the waveform fits is not for all seismograms as dramatic as in the preceding examples. Figure 19 features the waveform fit for a Greek event recorded at NE02 (Danmark). The phase of the signal is slightly improved in the nonlinear inversion, but the final waveform fit is not impressive.

period (s.)	nonlinear	Born	nonlinear + Born
30-40	15%	20%	31%
40-60	37%	27%	54%
60-100	21%	25%	41%

Table 1, variance reductions for the waveform inversions.

The quality of the waveform fits is expressed by the variance reductions shown in table 1. Both in the nonlinear inversion, and in the subsequent Born inversion the variance reduction is of the order of 25%, although this differs considerably between the different frequency bands. In the nonlinear inversion for the smooth reference medium, the solution is rather heavily constrained (compare the figures 7a and 7b) so that larger variance reductions could be achieved with the nonlinear inversion. The smallest variance reduction occurs in the period range from 30-40 s. This is not surprising, because these surface waves have the shallowest penetration depths, and are therefore most strongly subjected to lateral heterogeneity and therefore most difficult to fit. Surprisingly, the variance reduction for periods between 40-60 s. is larger than for 60-100 s. The reason for this might be that surface waves between 60-100 s. are influenced by the low velocity zone, which is reported to exhibit strong lateral variations (York and Helmberger, 1973; Paulssen, 1987). The total variance reduction is larger than the variance reduction obtained by Yomogida and Aki (1987) for surface waves which propagated through the Pacific. (They obtained a variance reduction of approximately 30%.) However, it is difficult to compare these results because on the one hand the paths of propagation of the surface waves they used are much longer than in this study, but on the other hand Europe and the Mediterranean is much more heterogeneous than the Pacific.

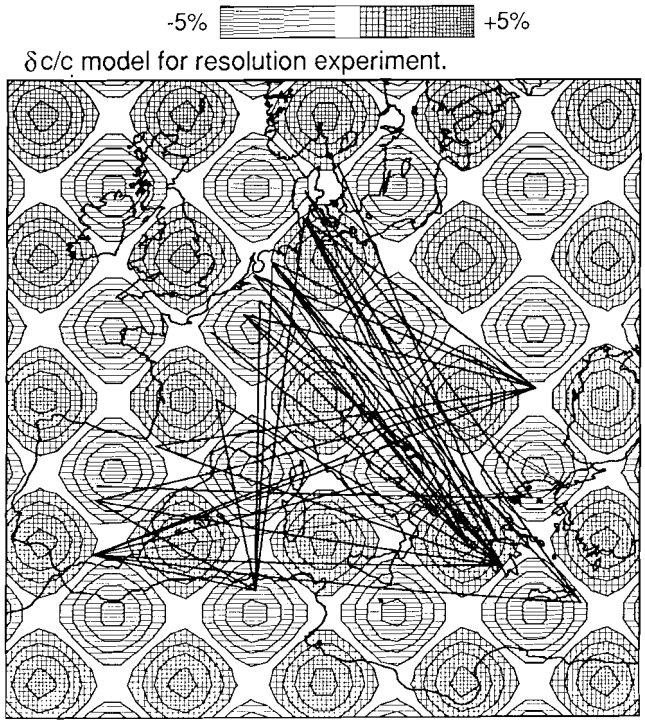

Figure 20. Synthetic model of the relative phase velocity perturbation ($\delta c/c$) for the resolution experiment of section 7. The source-receiver minor arcs are superposed.

7) A resolution analysis of the inversion for the direct wave.

Just as with the inversion for the surface wave coda, the quality of the waveform fit is no measure of the resolution of the inversion. In order to address this issue, synthetics have been computed using asymptotic ray theory (Woodhouse and Wong, 1987) for the phase velocity model shown in figure 20. For convenience the minor arcs of the used source-receiver pairs are also shown in this figure. The resulting synthetics have been subjected to the same two step inversion as the surface wave data from the previous section. As a representative example, the results for the period band between 60-100 s. are presented in this section. In figure 21 the model as derived in the nonlinear inversion for the smooth reference model is shown. The thin lines show the model of figure 20, in the ideal case the inversion would reproduce this model. Since only the direct wave is used in this inversion, the solution is only nonzero in the vicinity of the source-receiver minor arcs. Apart from the positive anomaly in the northern Adriatic, the heterogeneities are placed more or less at their correct location. The reconstructed model after the subsequent Born inversion is depicted in figure 22.

The strength of the model after Born inversion is closer to the true model than after the nonlinear inversion alone. However, the magnitude of the reconstructed heterogeneity is still much less than the magnitude of the input model. The physical reason for this is that the model

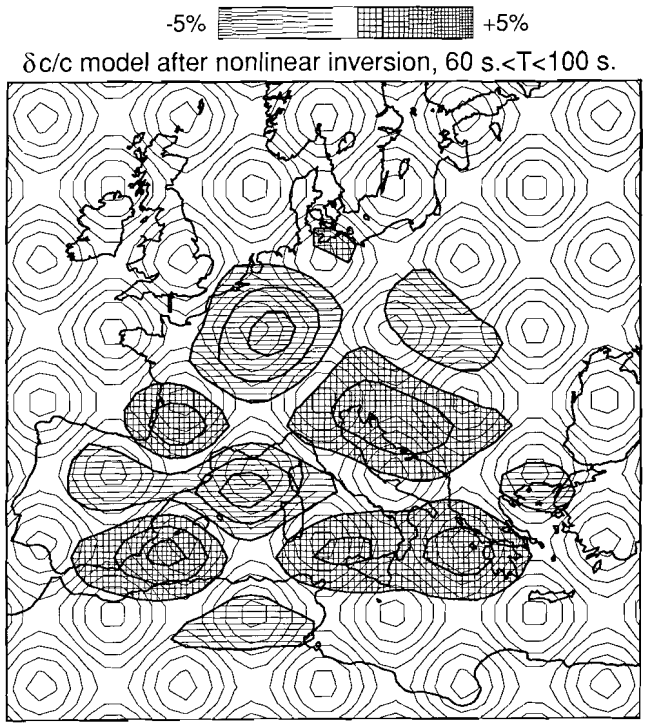

Figure 21. Reconstruction of the model of figure 20 after the constrained nonlinear inversion for periods between 60-100 s.

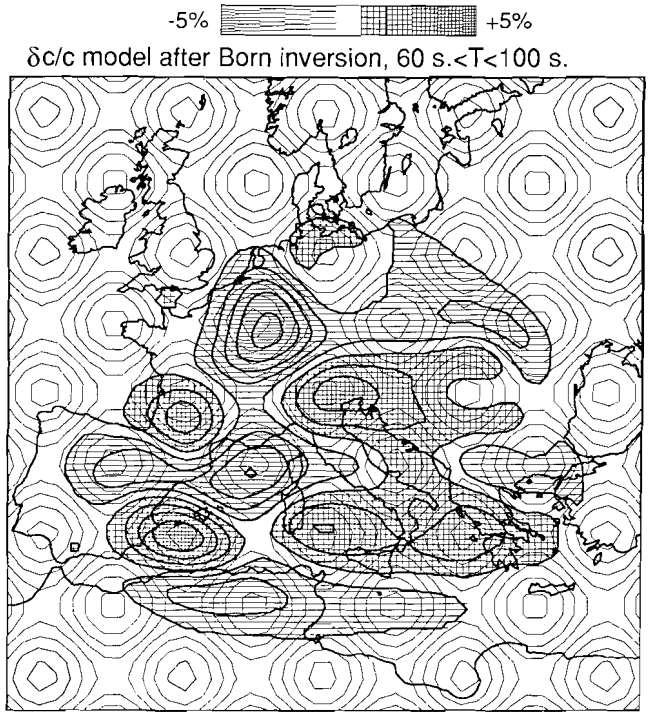

Figure 22. Reconstruction of the model of figure 20 after the constrained nonlinear inversion and the subsequent Born inversion for periods between 60-100 s.

used in this resolution test consists of alternating positive and negative anomalies. A smearing of these anomalies leads to a reduction of the magnitude of these anomalies. In the true Earth, an alternation between positive and negative phase velocity anomalies may also occur, so that the reconstructed models (figures 13abc) may underestimate the true phase velocity perturbations.

Surprisingly, the heterogeneities are better positioned after the Born inversion (figure 22) than after the nonlinear inversion alone (figure 21). The reason for this is that with the ray geometrical nonlinear inversion one basically measures certain path integrals over the source receiver minor arc (see equation (10a-d) of paper I), whereas in the Born inversion more complete wave information is used.

It follows from figure 22 that the east-west resolution in the southern Mediterranean is rather poor. This is due to the fact that there are no crossing ray in that region. A large portion of the wave paths runs in a bundle from Greece to north western Europe, and encounter a suite of positive and negative anomalies. This leads to a smearing of the solution under Germany and Danmark in the northwest-southeast direction, and a subsequent underestimate of the true inhomogeneity. A similar smearing in the northwest-southeast direction is visible in the northern Adriatic, this area also suffers from a lack of crossing ray paths. One of the most conspicuous features in the figures 13abc are the high phase velocities under Greece. This is no artifact of the inversion, because this feature is not present in the results from the resolution analysis (figure 22).

In conclusion, the reconstructed phase velocity models are meaningless outside the dotted line in the figures 24 and 25. In the area enclosed by this line, lateral smearing in the northwest-southeast direction occurs under Danmark, Germany and the northern Adriatic, while there is an east-west smearing in the southern Mediterranean.

8) A model for the S-velocity under Europe and the Mediterranean.

The phase velocity perturbations presented in section 6 can be converted to a depth model using the phase velocity information of the different frequency bands. However, these phase velocities are not only influenced by the composition of the crust and upper mantle, but also by the crustal thickness. The crustal thickness under Europe and the Mediterranean is known from refraction studies, and it is therefore possible to correct for the varying crustal thickness. The reference model shown in figure 6 has a crustal thickness of 33 km. By determining the phase velocity for the same model, but with a different crustal thickness, the following linear parameterization of the effect of crustal thickness on the fundamental Rayleigh mode phase velocity has been determined:

$$\frac{\delta c}{c} = \Gamma(z-33.)\ (\%)\ , \tag{1}$$

in this expression z is the crustal thickness in kilometers.

The parameter Γ is for the different frequency bands given by

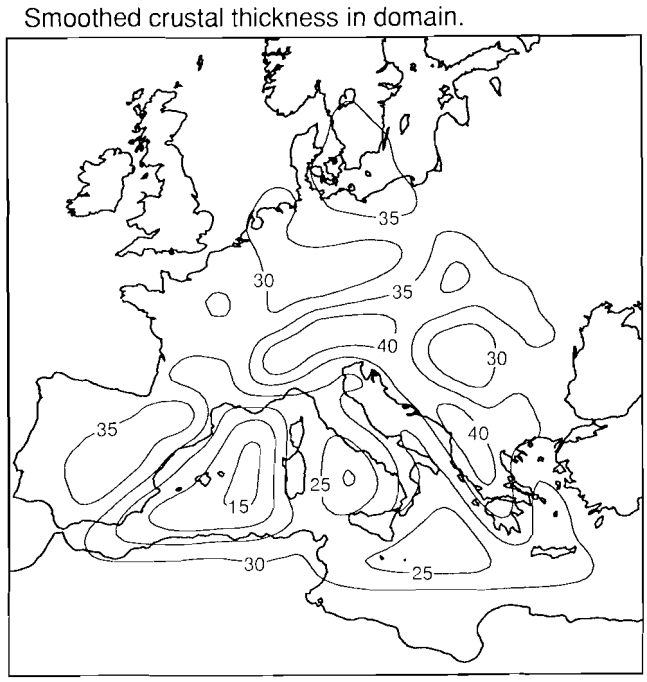

Figure 23. Smoothed crustal thickness used in the correction for the varying Moho depth.

$$\Gamma = -0.180\ (\%/km.) \quad \text{for} \quad 30\ s. < T < 40 s.$$
$$\Gamma = -0.113\ (\%/km.) \quad \text{for} \quad 40\ s. < T < 60 s. \qquad (2)$$
$$\Gamma = -0.076\ (\%/km.) \quad \text{for} \quad 60\ s. < T < 100 s.$$

The crustal thickness used in this study is adopted from Meissner (1986) and Stoko et al. (1987), and is shown in figure 23. In the area outside the dotted line in figures 24 and 25 the default value is assumed (33 km.). For consistency reasons, the same smoothing is applied to the crustal thickness, as for the reconstructions of shown in the figures 13abc. The variations in the crustal thickness are as large as 25 km. in the area of interest. For the shortest period band this leads to a phase velocity perturbation of 4.5%, which is of the same order of magnitude as the perturbations as determined from the Born inversion (figure 13a).

After correcting for the crustal thickness, a standard linear inversion (Nolet, 1981) leads to the S-velocity perturbations for depths between 0 km. and 100 km., and between 100 km. and 200 km. A simple resolution analysis shows that incorporating a third layer is unjustified. The resulting S-velocity perturbations are shown in the figures 24 and 25. The S-velocity models in these figures can be compared with maps of the S-velocity as compiled subjectively from a wide range of surface wave and body wave data (Panza et al., 1980; Calcagnile and Scarpa, 1985). In general, there is a correspondence of the large scale features. The velocity is

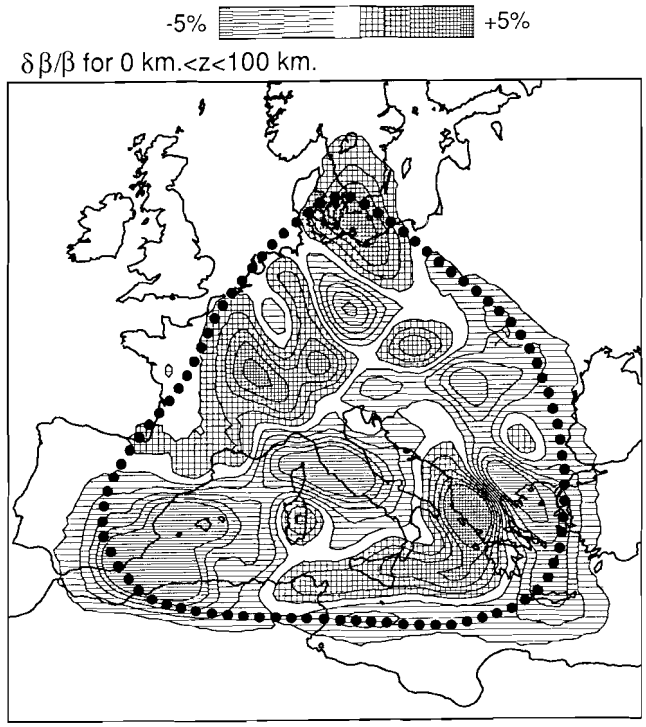

Figure 24. Relative S-velocity perturbation ($\delta\beta/\beta$) between the surface and a depth of 100 km.

high in the Scandinavian shield, which can be seen in the northern area of inversion of the figures 24 and 25. Under the western Mediterranean the velocity is low (Marillier and Mueller, 1985), whereas the Adriatic is characterized by a S-velocity higher than in the adjacent regions. This high velocity under the Adriatic is more pronounced in the lowest layer (figure 25), than in the top layer (figure 24). Note that the Alps do not show up in the figures 24 and 25, whereas Panza et al. (1980) and Calcagnile and Scarpa (1985) report large anomalies both in the western Alps and the eastern Alps. A reason for this discrepancy might be that the depth-averaged structure of the Apls deviates not very much from the rest of Europe, so that the surface waves are not perturbed strongly.

Early tomographic studies using P-wave delay times (Romanowicz, 1980; Hovland et al., 1981; Hovland and Husebey, 1982; Babuska and Plomerova, 1984) produced rather different results for the P-velocity under Europe. The only consistent feature of these studies are the low velocity in the Pannonian basin, and the high velocity under the Bohemian massif for the upper layer (0-100 km.). Both features can also be seen in figure 24. (In figure 23 the Pannonian basin shows up as a region with a thin crust, whereas the Bohemian massif can be identified by it's thick crust.) A more recent tomographic inversion with a much larger data produced more detailed results (Spakman, 1986ab). In his study the subduction of Africa under

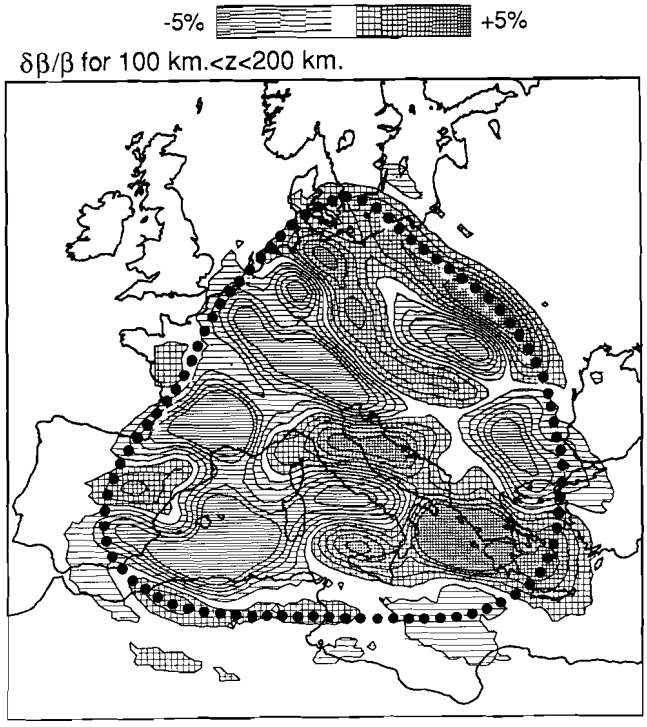

Figure 25. Relative S-velocity perturbation ($\delta\beta/\beta$) for depths between 100 km. and 200 km.

Europe has been imaged spectacularly. The subduction of Africa of the African slab under Europe can also be seen in figure 25 as a positive velocity anomaly in the deepest layer (100-200 km.) under the Adriatic and northern Italy. Panza et al. (1982) observed relatively low velocities in the lid between Corsica and Italy, the same anomaly is visible in figure 24.

In the figures 24 and 25 the Rhine Graben shows up as a zone of relatively low velocities extending towards the southeast from the Netherlands. Most wave paths in this region are in the southeast-northwest direction. This may explain why in the top layer (figure 24) only the northern part of the Rhine Graben can be seen, whereas the southern part of the Rhine Graben (which trends in the north-south direction) is not delineated. The variations in the S-velocity for the deepest layer (figure 25) reflects the lateral variations of the low velocity zone. It is noted by York and Helmberger (1973) and Paulssen (1987) that strong velocity variations of the low velocity zone exist, which is confirmed by figure 25. Under the Massif Central the positive anomaly in the top layer (figure 24), and the negative anomaly in the bottom layer (figure 25) indicates a pronounced low velocity zone, which is consistent with the results of Souriau (1981).

The feature which shows the power of the inversion method of this paper most spectacularly, is the high velocity anomaly in eastern Europe. (It is possible that this area of high

velocities extends further eastward, but this area is not sampled by the data.) From the waveform point of view, this anomaly is needed to produce the focusing needed to fit the amplitudes of seismograms recorded in the northern station of the NARS array. For this reason, this anomaly is located away from (but close to) the source receiver minor arcs. This zone of a high S-velocity closely marks the Tornquist-Tesseyre zone, the boundary between central Europe and the east European platform. Note that this transition zone is not visible in the upper layer of the S-velocity model (figure 24) This is consistent with the findings of Hurtig et al. (1979) who showed by fitting travel time curves, that below 100 km. the eastern European platform has higher P-velocities than central Europe. According to figure 25, this transition at depth between central Europe and the eastern European platform is very sharp.

9) Conclusion.

Linear inversion of a large set of surface wave data is feasible with present day computers. The Born inversion for the surface wave coda (using 42 seismograms) ran in roughly one night on a super mini computer. The inversion of the direct surface wave for the three frequency bands takes approximately the same time. The nonlinear inversion for the smooth reference model is comparatively fast, and takes about 3 hours for the three frequency bands. With the present growth in computer power, larger data sets can soon be inverted with the same method, possibly on a global scale.

Reasonable waveform fits of the surface wave coda can be obtained, leading to a variance reduction of approximately 25% for the surface wave coda. However, with the data set used in this study many artifacts are introduced in the inversion (the analogue of the smiles in exploration seismics). The fact that the surface wave coda contains a relatively large noise component is an extra complication. A larger (redundant) data set is needed to perform an accurate imaging of the inhomogeneity in the Earth using the surface wave coda. It would be interesting to set up controlled experiments to probe tectonic structures like continental margins or the Tornquist- Tesseyre zone with scattered surface waves.

Application of Born inversion to the direct surface waves leads to detailed S-velocity models on a scale comparable to the wavelength of the used surface waves. With the data set employed, a lateral resolution of approximately 300 km. can be achieved in some regions (Italy, France, Alps, Western Mediterranean), while in other areas smearing along the wave paths occurs (southern Mediterranean, north eastern Europe, the Adriatic). More data are needed to achieve a more evenly distributed resolution. Only a limited depth resolution can be obtained.

The fact that a model of the heterogeneity is constructed with a horizontal length scale comparable to the wavelength of the used surface waves, implies that scattering and multipathing effects are operative. This means that for this situation dispersion measurements are not justified. Nevertheless, the resulting model for the S-velocity bears close resemblance to the S-velocity models constructed by Panza et al. (1980) and Calcagnile and Scarpa (1985), which are largely based on surface wave dispersion measurements. Apparently, ray theory is relatively robust for structures that are not smooth on scale of a wavelength.

Linear waveform inversion is a powerful and rigorous method to fit surface wave data. Presently, the main limitation is imposed by the availability of high quality digital surface wave data. A network of seismometers, as described in the ORFEUS (Nolet et al., 1985) or PASSCAL proposals, will increase the resolution and reliability of the resulting models. A data distribution center like ODC (ORFEUS Data Center) provides access to digital seismological data at low costs. Born inversion for surface waves, applied to these data may help to construct accurate S-velocity models of the Earth.

References.

Babuska, V., J. Plomerova, and J. Silcny, Large-scale oriented structures in the subcrustal lithosphere of Central Europe, *Ann. Geophys., 2*, 649-662, 1984.

Berkhout, A.J., *Seismic migration, imaging of acoustic energy by wave field extrapolation, B. Practical aspects*, Elsevier, Amsterdam, 1984.

Calcagnile, G., and R. Scarpa, Deep structure of the European-Mediterranean area from seismological data, *Tectonophys., 118*, 93-111, 1985.

Chapman, C.H., The Radon transform and seismic tomography, in *Seismic tomography, with applications in global seismology and exploration geophysics*, edited by G. Nolet, pp. 99-108, Reidel, Dordrecht, 1987.

Dost, B., A. van Wettum, and G. Nolet, The NARS array, *Geol. Mijnbouw, 63*, 381-386, 1984.

Dziewonski, A.M., Mapping the lower mantle: determination of lateral heterogeneity in P velocity to degree and order 6, *J. Gephys. Res., 89*, 5929-5952, 1984.

Dziewonski, A.M., and D.L. Anderson, Preliminary Reference Earth Model, *Phys. Earth Plan. Int., 25*, 297-356, 1981.

Hovland, J., and E.S. Husebye, Upper mantle heterogeneities beneath eastern Europe, *Tectonophys., 90*, 137-151, 1982.

Hovland, J., D. Gubbins, and E.S. Husebye, Upper mantle heterogeneities beneath central Europe, *Geophys. J. R. Astr. Soc., 66*, 261-284, 1981.

Hurtig, E., S. Grassl, and R.P. Oesberg, Velocity variations in the upper mantle beneath central Europe and the east European platform, *Tectonophys., 56*, 133-144, 1979.

Marillier, F., and St. Mueller, The western Mediterranean region as an upper mantle transition zone between two lithospheric plates, *Tectonophys., 118*, 113-130, 1985.

Meissner, R., *The continental crust, a geophysical approach*, Academic Press, Orlando, 1986.

Nataf, H.C., I. Nakanishi, and D.L. Anderson, Measurements of mantle wave velocities and inversion for lateral heterogeneity and anisotropy 3. Inversion., *J. Geophys. Res., 91*, 7261-7308, 1986.

Nolet, G., The upper mantle under Western-Europe inferred from the dispersion of Rayleigh wave modes, *J. Geophys., 43*, 265-285, 1977.

Nolet, G., Linearized inversion of (teleseismic) data, in *The solution of the inverse problem in geophysical interpretation*, edited by R. Cassinis, Plenum-Press, New York, 1981.

Nolet, G., B. Romanowicz, R. Kind, and E. Wielandt, ORFEUS, Observatories and Research Facilities for European Seismology, 1985.

Nolet, G., B. Dost, and H. Paulssen, Intermediate wavelength seismology and the NARS experiment, *Ann. Geophys., B4*, 305-314, 1986.

Panza, G.F., S. Mueller, and G. Calcagnile, The gross features of the lithosphere-asthenosphere system from seismic surface waves and body waves, *Pure Appl. Geophys., 118,* 1209-1213, 1980.

Panza, G.F., St. Mueller, G. Calcagnile, and L. Knopoff, Delineation of the North Central Italian upper mantle anomaly, *Nature, 296,* 238-239, 1982.

PASSCAL, Program for Array Studies of the Continental Lithosphere, issued by the Incorporated Research Institute for Seismology, 1984.

Paulssen, H., Lateral heterogeneity of Europe's upper mantle as inferred from modelling of broad-band body waves, *Geophys. J. R. Astr. Soc., 91,* in press, 1987.

Romanowicz, B., A study of large-scale lateral variations of P velocity in the upper mantle beneath western Europe, *Geophys. J. R. Astr. Soc., 63,* 217-232, 1980.

Romanowicz, B., and R. Snieder, A new formalism for the effect of lateral heterogeneity on normal modes and surface waves - II: General anisotropic perturbations, *submitted to Geophys. J. R. Astr. Soc.,* 1987.

Sluis, A. van der, and H.A. van der Vorst, Numerical solution of large, sparse linear algebraic systems arising from tomographic problems, in *Seismic tomography, with applications in global seismology and exploration geophysics,* edited by G. Nolet, pp. 49-83, Reidel, Dordrecht, 1987.

Snieder, R., 3D Linearized scattering of surface waves and a formalism for surface wave holography, *Geophys. J. R. Astr. Soc., 84,* 581-605, 1986a.

Snieder, R., The influence of topography on the propagation and scattering of surface waves, *Phys. Earth. Plan. Int., 44,* 226-241, 1986b.

Snieder, R., Surface wave holography, in *Seismic tomography, with applications in global seismology and exploration geophysics,* edited by G. Nolet, pp. 323-337, Reidel, Dordrecht, 1987a.

Snieder, R., On the connection between ray theory and scattering theory for surface waves, in *Mathematical Geophysics, a survey of recent developments in seismology and geodynamics,* edited by Vlaar, N.J., Nolet, G., Wortel, M.J.R. and Cloetingh, S.A.P.L., pp. 77-83, Reidel, Dordrecht, 1987b.

Snieder, R., Large scale waveform inversions of surface waves for lateral heterogeneity -I: Theory and numerical examples, *submitted to J. Geophys. Res.,* 1988.

Snieder, R., and G. Nolet, Linearized scattering of surface waves on a spherical Earth, *J. Geophys., 61,* 55-63, 1987.

Snieder, R., and B. Romanowicz, A new formalism for the effect of lateral heterogeneity on normal modes and surface waves -I: Isotropic perturbations, perturbations of interfaces and gravitational perturbations, *Geophys. J. R. Astron. Soc., in press,* 1987.

Souriau, A., Le manteau superieur sous la France, *Bull. Soc. Geol. France, 23,* 65-81, 1981.

Spakman, W., Subduction beneath Europe in connection with the Mesozoic Tethys, *Geol. Mijnbouw, 65,* 145-154, 1986a.

Spakman, W., The upper mantle structure in the central European-Mediterranean region, *Proceedings of the third workshop on the European Geotraverse Project (EGT),* 1986b.

Stoko, D., E. Prelogovic, and B. Alinovic, Geological structure of the Earth's crust above the Moho discontinuity in Yugoslavia, *Geophys. J. R. Astr. Soc., 89,* 379-382, 1987.

Tanimoto, T., The three-dimensional shear wave velocity structure in the mantle by overtone waveform inversion -I: Radial seismogram inversion, *Geophys. J. R. Astron. Soc., 89,* 713-740, 1987.

Woodhouse, J.H., and A.M. Dziewonski, Mapping the upper mantle: three dimensional modeling of the Earth structure by inversion of seismic waveform, *J. Geophys. Res., 89,* 5953-

5986, 1984.
Woodhouse, J.H., and Y.K. Wong, Amplitude, phase and path anomalies of mantle waves, *Geophys. J. R. Astr. Soc., 87,* 753-774, 1986.
Yomogida, K., and K. Aki, Amplitude and phase data inversion for phase velocity anomalies in the Pacific Ocean basin, *Geophys. J. R. Astron. Soc., 88,* 161-204, 1987.
York, J.E., and D.V. Helmberger, Low-velocity zone variations in the Southwestern United States, *J. Geophys. Res., 78,* 1883-1886, 1973.

Chapter 10

Summary and conclusion

Scattering of surface waves in a three dimensional layered elastic medium with embedded heterogeneities is described in this thesis with the Born approximation. The dyadic decomposition of the surface wave Green's function provides the crucial element for an efficient application of Born theory to surface wave scattering. This is because the dyadic Green's function allows for an efficient bookkeeping of the different processes that contribute to the scattered surface wave: excitation, propagation, scattering (conversion), and oscillation. One can argue that the most crucial (and surprisingly also the simplest) expression in this thesis is equation (3) of chapter 2. The resulting surface wave scattering theory for buried heterogeneities in a flat geometry (chapter 2), can easily be extended to incorporate the effects of surface topography (chapter 3), and a spherical geometry (chapters 6 and 7).

In practice, the Born approximation imposes a lower limit on the periods that can be analyzed. This limit depends both on the properties of the heterogeneity and on the source receiver separation. An analysis of the surface wave coda recorded in stations of the NARS array shows that the surface wave coda level differs substantially for different regions. For paths through eastern and middle Europe, the Born approximation breaks down for periods shorter than 30 s., while for paths through the western Mediterranean periods as short as 20 s. can be analyzed with linear theory (chapter 8).

In exploration seismics, linear theory is usually used to establish a relation between the heterogeneity and the reflected waves, as well as for the inversion of these reflection data. It is therefore not surprising that the surface wave coda can in principle be used to map the heterogeneity in the Earth, with an inversion scheme which is reminiscent to Kirchoff migration as used in exploration seismics (chapter 2). In a simple field experiment the feasibility of such an inversion scheme is established (chapter 4). It is also possible to formulate the waveform inversion of surface wave data as a (huge) matrix problem. The least squares solution of these matrix equations can iteratively be constructed. These reconstructed models have the same characteristics as the models found with a simple holographic inversion (chapter 8).

Inversion of the surface wave coda recorded in stations of the NARS array produce chaotic models of scatterers which are difficult to interpret unambiguously. Apart from a lack of enough data to perform a good imaging, this inversion is hampered by an appreciable noise component in the surface wave coda. This noise level might be acceptable if the data set were redundant, so that this noise component can be averaged out. However, the 42 available seismograms lead to an underdetermined system of linear equations, which make it likely that the noise in the surface wave coda introduces

artifacts in the reconstructed model (chapter 9).

Born theory for surface waves describes the distortion of the wavefield due to the heterogeneity of the medium. This distortion consists of true surface wave scattering due to abrupt lateral inhomogeneities, as well as a distortion of the direct surface wave due to smooth variations of the heterogeneity. Up to first order, ray geometrical effects follow from linear scattering theory (chapter 5). Furthermore, the scattering coefficient for forward scattering of unconverted waves is proportional to the phase velocity perturbation of these waves (chapter 3). This makes it possible to reconstruct phase velocity fields for surface waves using a large scale linear waveform inversion of the direct surface wave (chapter 8).

This inversion is applied to the direct surface wave train recorded in stations of the NARS array. This results in detailed reconstructions of the phase velocity of the fundamental Rayleigh mode. In this inversion, a variance reduction of approximately 40% is achieved. By combining this information for different frequencies, detailed models of the S-velocity under Europe and the Mediterranean are reconstructed (chapter 9). With the present data set, the resolution of this model differs considerably from region to region. The only way to overcome this restriction is to use more data, which can be realized by employing dense networks of digital seismic stations.

There is still a considerable amount of research to be performed on scattering theory of elastic waves. Apart from the restriction of linearity, the theory presented in this thesis is only valid in the far field. This means that the inhomogeneity should be several wavelengths removed from the source and the receiver (and their antipodes). In practice, this is a troublesome limitation, because seismic stations are often located on top of heterogeneities, and earthquakes usually occur in heterogeneous areas such as subduction zones. The interaction terms are valid both in the far field and in the near field (chapter 7), so that in order to resolve the far field restriction, the propagator terms need to be investigated. Future theoretical research should also address the problem of conversions between surface waves and body waves. This issue is related to the near field problem, because in the near field the concepts of "surface waves" and "body waves" are poorly defined.

It would be interesting to use portable seismic stations for local investigations by recording scattered surface waves in the vicinity of strong lateral variations in the crust and upper mantle. In this way, it should be possible to probe tectonic features such as subduction zones using scattered surface waves. The waveform inversions of the direct surface waves, as presented in this thesis, can be applied to other regions of the Earth with a good coverage with digital seismic stations (e.g. Japan, the continental US), and possibly for lower frequencies on a global scale. In this way, large scale waveform inversions for both the phase and amplitude of surface wave data may dramatically increase our knowledge of the Earth's interior.

Acknowledgements

This thesis could not have been written without the help and support of others. Wim, Lammie and Mies helped and guided me whenever they could. I greatly appreciate it that Idske always respected my wanderlust, and that she always supported and encouraged me. My academic development could not have been possible without the lessons taught to me by many fine scientists. I especially want to mention Steve Fels and Jerry Mahlman (GFDL, Princeton), who showed me that enthusiasm and a critical frame of mind are indispensable trades for a good scientist. Guust Nolet has been a great example for me, because he showed me that theoretical and observational skills **can** be combined.

The help of Guust Nolet has been crucial for the completion of this thesis. He created a stimulating environment for seismological research both by his enthusiastic presence, and by taking care of the required hardware. His intuition put me invariably on the right track. Gordon Shudofsky has given me valuable advice in data handling. Despite the fact that I can be an impossible office mate he always maintained his kindness and interest. Working with Barbara Romanowicz was a pleasure, I appreciate it that she had the stamina to bring our long distance cooperation to a good end. NARS could not have been possible without the efforts of Bernard Dost and Arie van Wettum, who installed and maintained the array, often under difficult conditions. Hanneke Paulssen has been most helpful in handling the NARS data with all its complications. Wim Spakman kindly provided me with his tomography program, which formed the backbone of the linear waveform inversions, while his marvelous plotting program "P" facilitated a clear presentation of the results. Lastly, I want to thank all other colleagues who have helped me in some way, and who made these three years of research enjoyable.

The NARS project has been funded by AWON, the Earth Science branch of the Netherlands Organization for the Advancement of Pure Research (ZWO).

Samenvatting

Oppervlakte golven verstrooid aan heterogeniteiten ingebed in een drie dimensionaal gelaagd medium worden in dit proefschrift beschreven met behulp van de Born benadering. De dyadische ontwikkeling van de Greense functie is het cruciale element voor een efficiente boekhouding van de verschillende elementen die een bijdrage leveren aan de verstrooide oppervlakte golf: excitatie, propagatie, verstrooiing (conversie), en oscillatie. Men kan stellen dat vergelijking (3) van hoofdstuk 2 de meest cruciale (en verrassend genoeg ook de simpelste) uitdrukking is. De resulterende theorie voor oppervlakte golf verstrooiing aan interne heterogeniteiten in een vlakke geometrie (hoofdstuk 2), kan eenvoudig gegeneraliseerd worden voor de effecten van oppervlakte topografie (hoofdstuk 3), en voor een bolgeometrie (hoofdstuk 6 en 7).

In de praktijk stelt de Born benadering een ondergrens aan de perioden die geanaliseerd kunnen worden. Deze ondergrens hangt af van de eigenschappen van de heterogeniteit, en van de epicentrale afstand. Een analyse van de oppervlakte golf coda geregistreerd in de stations van het NARS netwerk toont aan dat de oppervlakte golf coda aanzienlijk verschilt voor verschillende regios. Voor golfpaden door oost- en midden Europa is de Born benadering niet geldig voor perioden korter dan 30 s., terwijl voor golfpaden door het westelijke Middenlandse Zee gebied deze ondergrens op 20 s. ligt (hoofdstuk 8).

In de exploratie seismologie wordt lineaire theorie meestal gebruikt zowel voor de relatie tussen de heterogeniteit en de gereflecteerde golven, als voor de inversie van deze reflectie data. Het is daarom niet verbazend dat de oppervlakte golf coda in principe gebruikt kan worden om de heterogeniteit in de Aarde te reconstrueren met een inversie methode die doet denken aan Kirchoff migratie zoals gebruikt wordt in de exploratie geofysica (hoofdstuk 2). In een simpel veld experiment is de haalbaarheid van een dergelijke inversie aangetoond (hoofdstuk 4). Het is tevens mogelijk om de golfvorm inversie van oppervlakte golf data te formuleren als een (zeer groot) matrix probleem. Met behulp van iteratieve technieken kan een kleinste kwadraten oplossing van dit probleem gevonden worden. De op deze wijze gereconstrueerde modellen hebben dezelfde karakteristieken als modellen bepaald met een eenvoudige holografische inversie (hoofdstuk 8).

Inversie van de oppervlakte golf coda geregistreerd in stations van het NARS netwerk leidt tot chaotische modellen voor de heterogeniteit die niet eenduidig te interpreteren zijn. Behalve een gebrek aan voldoende data voor een goede focussering, is een relatief hoog ruisniveau in de coda hiervan de oorzaak. Dit ruisniveau zou aanvaardbaar kunnen zijn voor een grote (overbepaalde) data collectie, zodat de ruis uitmiddelt in de inversie. De 42 gebruikte seismogrammen leidden echter tot een onderbepaald stelsel lineaire vergelijkingen, zodat het waarschijnelijk is dat ruis in de coda artefacten in het geronstrueerde model introduceert.

Born theorie voor oppervlakte golven beschrijft de vervorming van het golfveld ten gevolge van heterogeniteiten in het medium. Deze vervorming bestaat niet alleen uit echte oppervlakte golf verstrooiing ten gevolge van abrupte heterogeniteiten, maar ook uit een vervorming van de directe golf ten gevolge van gladde variaties van de inhomogeniteit. Tot op eerste orde volgen optisch geometrische effecten uit de lineaire verstrooiingstheorie (hoofdstuk 5). De verstrooiingscoefficient voor voorwaartse verstrooiing van ongeconverteerde golven is evenredig met de fasesnelheid verstoring van deze golven (hoofdstuk 3). Dit maakt het mogelijk om fasesnelheid verdelingen van oppervlakte golven te bepalen met behulp van een grootschalige lineaire golfvorm inversie van de directe oppervlakte golf (hoofdstuk 8).

Deze inversie is toegepast op de directe oppervlakte golf geregistreerd in stations van het NARS netwerk. Dit leidt tot gedetailleerde reconstructies van de fasesnelheid van de Rayleigh golf grondtoon. Door deze informatie voor verschillende frequenties te combineren zijn gedetailleerde modellen van de S-snelheid onder Europa en de Middenlandse Zee geconstrueerd (hoofdstuk 9). Met de huidige gegevens varieert de resolutie aanzienlijk van regio tot regio. Alleen met meer gegevens is hier verbetering in te brengen. Dit kan gerealiseerd worden met dichte netwerken van digitale seismische stations.

Er is nog veel onderzoek te doen op het gebied van verstrooiingstheorie voor elastische golven. Behalve de restrictie van lineariteit, is de theorie in dit proefschrift alleen geldig in het verre veld. Dit betekent dat de heterogeniteit zich op minstens enkele golflengten van de bron en de ontvanger (en hun antipolen) moet bevinden. In de praktijk is dit een complicerende factor, omdat seismische stations vaak boven heterogeniteiten staan, en omdat aardbevingen meestal in heterogene gebieden zoals subductie zones optreden. De verstrooiingscoefficienten zijn zowel in het verre- als het nabije veld geldig (hoofdstuk 7), zodat teneinde de verre veld restrictie op te lossen de propagator termen onderzocht moeten worden. Het theoretisch onderzoek moet tevens een beschrijving geven van de interacties tussen oppervlakte golven en ruimte golven. Dit probleem is gerelateerd aan de problemen met het nabije veld, aangezien in het nabije veld de concepten "oppervlakte golf" en "ruimte golf" slecht gedefinieerd zijn.

Het zou interressant zijn om draagbare seismische stations te gebruiken voor locale metingen van verstrooide oppervlakte golven in de nabijheid van sterke heterogeniteiten in de korst en bovenmantel. Op deze manier is het wellicht mogelijk om tectonische fenomenen zoals subductie zones of the Tornquist-Teisseyre zone te bemonsteren. De golfvorm inversies van de directe golf zoals gepresenteerd in dit proefschrift, kan tevens toegepast worden op andere gebieden met een goede bedekking met digitale seismische stations (bijv. Japan en de continentale V.S.), en wellicht voor lagere frequenties ook op een globale schaal. Op deze wijze kunnen grootschalige golfvorm inversies van oppervlakte golf gegevens op dramatische wijze onze kennis van het inwendige van de aarde vergroten.

CURRICULUM VITAE

May 20th 1958	Born in Leiden, Netherlands.
1970-1976	Atheneum-B, Oegstgeest, Netherlands.
1976-1982	Basic academic training; major, theoretical physics ; minors mathematics and exploration geophysics (drs. degree); University of Utrecht, Netherlands.
1982-1984	Research assistant at the Geophysical Fluid Dynamics Laboratory (Masters degree); Princeton University, USA.
1984-1987	Research assistant at the Department of geophysics; University of Utrecht, Netherlands.

BIBLIOGRAPHY

Snieder, R., 1985, The origin of the 100,000 year cycle in a simple ice age model, J. Geophys. Res., **90** , 5661-5664.

Snieder, R., 1986, 3D Linearized scattering of surface waves and a formalism for surface wave holography, Geophys. J. R. Astr. Soc., **84** , 581-605.

Snieder, R., 1986, The influence of topography on the propagation and scattering of surface waves, Phys. Earth Plan. Int., **44** , 226-241.

Snieder, R., 1986, Phase speed perturbations and three dimensional scattering effects of surface waves due to topography, Bull. Seism. Soc. Am., **76** , 1385-1392.

P. Gabriels, R. Snieder and G. Nolet, 1987, In situ measurements of shear-wave velocity in sediments using higher mode Rayleigh waves, Geophys. Prosp., **35** , 187-196.

Snieder, R. and G. Nolet, 1987, Linearized scattering of surface waves on a spherical Earth, J. Geophys., **61** , 55-63.

Snieder, R., 1987, On the connection between ray theory and scattering theory for surface waves, in "Mathematical Geophysics", ed. N.J. Vlaar, G. Nolet, M.J.R. Wortel and S.A.P.L. Cloetingh, Reidel, Dordrecht.

Snieder, R., 1987, Surface wave holography, in "Seismic tomography, with applications in global seismology and exploration geophysics", ed. G. Nolet, Reidel, Dordrecht, 387pp.

Snieder, R. and B. Romanowicz, 1987, A new formalism for the effect of lateral heterogeneity on normal modes and surface waves -I: Isotropic perturbations, perturbations of interfaces and gravitational perturbations, Geophys. J. R. Astr. Soc., in press.

Romanowicz B. and R. Snieder, 1987, A new formalism for the effect of lateral heterogeneity on normal modes and surface waves -II: General anisotropic perturbations ,Geophys. J. R. Astr. Soc., in press.

Snieder, R. and B. Romanowicz, A new formalism for normal mode interaction and surface waves scattering on an aspherical Earth, EOS, **68** , 358.

Snieder, R., 1988, Large scale waveform inversions of surface waves for lateral heterogeneity -I: Theory and numerical examples, submitted to J. Geophys. Res.

Snieder, R., 1988, Large scale waveform inversions of surface waves for lateral heterogeneity -II: Application to surface waves in Europe and the Mediterranean, submitted to J. Geophys. Res.